Wind Tunnel Seeding Systems for Laser Velocimeters

Compiled by
William W. Hunter, Jr.
and Cecil E. Nichols, Jr.
Langley Research Center

PREFACE

The principal motivating factor for convening the Workshop on the Development and Application of Wind Tunnel Seeding Systems for Laser Velocimeters was the necessity to achieve efficient operation and, most importantly, to insure accurate measurements with velocimeter techniques. The ultimate accuracy of particle scattering based laser velocimeter measurements of wind tunnel flow fields depends on the ability of the scattering particle to faithfully track the local flow field in which it is embedded. A complex relationship exists between the particle motion and the local flow field. This relationship is dependent on particle size, size distribution, shape, and density. To quantify the accuracy of the velocimeter measurements of the flow field, the researcher has to know the scattering particle characteristics. In order to obtain optimum velocimeter measurements, the researcher is striving to achieve control of the particle characteristics and to verify those characteristics at the measurement point. Additionally, the researcher is attempting to achieve maximum measurement efficiency through control of particle concentration and location in the flow field.

The above considerations have driven the laser velocimeter practitioners to develop a variety of seeding systems using a variety of seeding materials, which must be compatible with specific wind tunnel environments. This situation has created a great deal of activity without any apparent consensus on the "best" way to achieve the desired seeding goals of control of size, size distribution, and shape with a specific material density.

A second significant problem is to ascertain the scattering particle size at the point of measurement; i.e., in-situ measurement. This problem has also generated significant activity without the development or acceptance of the "best" way.

The goal of this workshop was to bring together those engineers and scientists who have conducted research and development efforts addressing the above seeding issues so that each could share experiences and insights with others of similar interest.

A list of attendees is included in this document. Grateful appreciation is expressed to the authors who shared their experiences and their views with the workshop participants, and to those who contributed to many useful exchanges of information.

CONTENTS

Orlando Amoroso
Spectron Development Laboratories
3303 Harbor Blvd., Suite G-3
Costa Mesa, CA 92626
Phone: (714) 549-3477

J. D. Trolinger
Spectron Development Laboratories
3303 Harbor Blvd., Suite G-3
Costa Mesa, CA 92626
Phone: (714) 549-3477

Jugal Agarwal
TSI, Inc.
P.O. Box 64394
St. Paul, MN 55164
Phone: (612) 485-0900

Stan Kaufman
TSI, Inc.
500 Cardigan Road
St. Paul, MN 55164
Phone: (612) 483-0900

Dr. M. S. Chandrasekhara
TSI, Inc.
500 Cardigan Road
St. Paul MN 55164
Phone: (612) 483-0900

A. Deepak
Science and Technology Corp.
101 Research Drive
Hampton, VA 23666
Phone: (804) 865-1894

Arnold S. Collier
Naval Surface Weapons Center
White Oak Laboratory
Silver Spring, MD 20903
Phone: (202) 394-1928

William J. Yanta
Naval Surface Weapons Center
White Oak Laboratory
Silver Spring, MD 20905
Phone: (202) 394-1928

H. Lee Seegmiller
NASA Ames Research Center
N-229-1
Moffett Field, CA 94035
Phone: (415) 694-6211

Timothy S. Smith
Naval Surface Weapons Center
New Hampshire Ave., White Oak
Silver Spring, MD 20910
Phone: (202) 394-3251

Roland Lee
APL/JHU
Johns Hopkins Road
Laurel, MD 20707
Phone: (202) 953-5000, ext. 4463

F. L. Crosswy
Calspan/AEDC
Arnold Air Force Station, TN 37389
Phone: (615) 454-7618

Fred L. Heltsley
Calspan Corporation/PC4
Arnold Engineering Development Center
Arnold Air Force Station, TN 37389
Phone: (615) 454-7364

Robert H. Nichols
AEDC/DOTR
MS 900
Arnold Air Force Station, TN 37389
Phone: (615) 454-6512

Terry Ng
U. of Notre Dame
Dep. of Aero. and Mech. Eng.
Notre Dame, IN 46556
Phone: (219) 239-5177

David Fry
Naval Ship R&D Center
Code 1542
Pethesda, MD 20084
Phone: (202) 227-1324

William Patrick
United Technologies Research Center
MS 17/Silver Lane
E. Hartford, CT 06108
Phone: (203) 727-7495

Richard J. Roback
United Technologies Research Center
Silver Lane, MS 16
E. Hartford, CT 06108
Phone: (203) 727-7181

Dr. Anthony E. Smart
Spectron Dev. Labs., Inc.
3303 Harbor Blvd., Suite G-3
Costa Mesa, CA 92626-1579
Phone: (714) 549-8477

Daniel M. Parobek
AFWAL/FIMN
Wright-Patterson AFB, OH 45433

Colin E. Hackett
Sandia National Labs - 8244
P.O. Box 969
Livermore, CA 94550
Phone: (415) 422-2172

George L. Seibert
USAF
AFWAL/FIMN
Wright-Patterson AFB, OH 45433
Phone: (513) 255-2809

Alexander Dybbs
Case Center for Complex Flow Measurements
Cae Western Reserve University
Cleveland, OH 44106
Phone: (216) 368-6448

Robert V. Edwards
Case Western Reserve University
Chemical Engineering Department
Cleveland, OH 44106
Phone: (216) 368-4151

Ken McAlister
Army Aeromechanics Lab.
Ames Research Center
Moffett Field, CA 94035
Phone: (415) 694-5892

Ronald K. Takahashi
Army Aeromechanics Lab.
Ames Research Center, MS 215-1
Moffett Field, CA 94035
Phone: (415) 694-5892

Warren Hingst
NASA Lewis Research Center
27000 Brookpark Road, MS 5-11
Cleveland, OH 44135
Phone: (419) 433-4000, ext. 4344

Randall Chriss
NASA Lewis Research Center
5503 E. Rowland
Toledo, OH 43613
Phone: (419) 474-7313

A. Robert Porro
NASA Lewis Research Center
27000 Brookpark Road, MS 5-11
Cleveland, OH 44135
Phone: (419) 433-4000, ext. 6823

John Greissing
NASA Lewis Research Center
27000 Brookpark Road, MS 4-8
Cleveland, OH 44135
Phone: (419) 433-4000, ext. 6140

Brooks A. Childers
NASA Langley Research Center
Mail Stop 236
Hampton, VA 23665
Phone: (804) 865-3234

John C. Hoppe
NASA Langley Research
Mail Stop 236
Hampton, VA 23665
Phone: (804) 865-3234

Peter F. Covell
NASA Langley Research Center
Mail Stop 170
Hampton, VA 23665
Phone (804) 865-4008

Warren C. Kelliher
NASA Langley Research Center
Mail Stop 416A
Hampton, VA 23665
Phone: (804) 865-3068

David E. Reubush
NASA Langley Research Center
Mail Stop 280
Hampton, VA 23665
Phone: (804) 865-2673

Jerome T. Foughner
NASA Langley Research Center
Mail Stop 285
Hampton, VA 23665
Phone: (804) 865-2961

Stewart L. Ocheltree
NASA Langley Research Center
Mail Stop 235A
Hampton, VA 23665
Phone: (804) 865-2791

James I. Clemmons
NASA Langley Research Center
Mail Stop 235A
Hampton, VA 23665
Phone: (804) 865-2791

Leonard M. Weinstein
NASA Langley Research Center
Mail Stop 163
Hampton, VA 23665
Phone: (804) 865-4546

Joe W. Elliott
NASA Langley Research Center
Mail Stop 286
Hampton, VA 23665
Phone: (804) 865-3611

Burt Northam
NASA Langley Research Center
Mail Stop 168
Hampton, VA 23665
Phone: (804) 865-2803

Richard Sailey
NASA Langley Research Center
Mail Stop 235A
Hampton, VA 23665
Phone: (804) 865-2791

Jag J. Singh
NASA Langley Research Center
Mail Stop 235
Hampton, VA 23665
Phone: (804) 865-3907

James F. Meyers
NASA Langley Research Center
Mail Stop 235A
Hampton, VA 23665
Phone: (804) 865-2791

William V. Feller (Retired)
28 School Lane
Yorktown, VA 23692

Dan Newhart
NASA Langley Research Center
Mail Stop 347
Hampton, VA 23665
Phone: (804) 865-2543

Robert D. Brown
NASA Langley Research Center
Mail Stop 281
Hampton, VA 23665
Phone: (804) 865-2246

W. D. Beasley
NASA Langley Research Center
Mail Stop 339
Hampton, VA 23665
Phone: (804) 865-4514

L. R. Gartrell
NASA Langley Research Center
Mail Stop 235A
Hampton, VA 23665
Phone: (804) 865-2791

M. T. Fletcher
NASA Langley Research Center
Mail Stop 235A
Hampton, VA 23665
Phone: (804) 865-2791

Jerry C. South, Jr.
NASA Langley Research Center
Mail Stop 103
Hampton, VA 23665
Phone: (804) 865-2664

Dale Satran
NASA Langley Research Center
Mail Stop 347
Hampton, VA 23665
Phone: (804) 865-2543

John M. Seiner
NASA Langley Research Center
Mail Stop 166
Hampton, VA 23665
Phone: (804) 865-3094

John R. Carlson
NASA Langley Research Center
Mail Stop 280
Hampton, VA 23665
Phone: (804) 865-2673

Wayne D. Erickson
NASA Langley Research Center
Mail Stop 246A
Hampton, VA 23665
Phone: (804) 865-2037

Amir Bar-Sever
NASA Langley Research Center
Mail Stop 359
Hampton, VA 23665
Phone: (804) 865-2631

Laguduva Kubendran
NASA Langley Research Center
Mail Stop 359
Hampton, VA 23665
Phone: (804) 865-2631

James Manning
NASA Langley Research Center
Mail Stop 461
Hampton, VA 23665
Phone: (804) 865-2645

William W. Hunter, Jr.
NASA Langley Research Center
Mail Stop 235A
Hampton, VA 23665
Phone: (804) 865-2791

Cecil E. Nichols, Jr.
NASA Langley Research Center
Mail Stop 441
Hampton, VA 23665
Phone: (804) 865-4641

Ralph Marinaro
NASA Langley Research Center
Mail Stop 471
Hampton, VA 23665
Phone: (804) 865-3761

CALCULATION OF PARTICLE DYNAMICS EFFECTS ON LASER VELOCIMETER DATA

R. H. Nichols
Arnold Engineering and Development Center
Arnold Air Force Station, Tennessee

PARTICLE EQUATION OF MOTION

In order to analytically assess the effects of particle dynamics on laser velocimeter measurements, the particle response to the fluid in which it is entrained must be modeled. At AEDC, the equation of particle motion derived by Maxey and Riley (Ref 1) is used to model the motion of the particle. The equation is derived from the Navier-Stokes equation under the assumption of unsteady Stokes flow. It should be noted that the Stokes flow eliminates the need for a far field boundary condition, and hence eliminates any normal (lift) forces.

$$m_p \frac{dV_i}{dt} = (m_p - m_f) g_i + m_f \left. \frac{DU_i}{Dt} \right|_{\hat{Y}(t)}$$

$$- \frac{1}{2} m_f \frac{d}{dt} \left\{ V_i(t) - U_i [\hat{Y}(t), t] - \frac{d^2}{40} \nabla^2 U_i \Big|_{Y(t)} \right\}$$

$$- \frac{3m_f}{4d} C_D \omega_i |\omega| - \frac{3\pi}{2} d^2 \mu \int_0^t \frac{\left\{ \frac{d}{d\tau} \omega_i [\hat{Y}_i(\tau), \tau] \right\}}{\sqrt{\pi \nu (t-\tau)}} d\tau$$

where

$$\omega_i = V_i(t) - U_i [\hat{Y}(t), t] - \frac{d^2}{24} \nabla^2 U_i \Big|_{\hat{Y}(t)}$$

$$|\omega| = \sqrt{\sum_i \omega_i^2}$$

$$\left. \frac{DU_i}{Dt} \right|_{\hat{Y}(t)} = \left(\frac{\partial U_i}{\partial x_i} + U_i \frac{\partial U_i}{\partial x_i} \right) \Big|_{\hat{Y}(t)}$$

$$\frac{d}{dt} \left\{ U_i [\hat{Y}(t), t] \right\} = \left(\frac{\partial U_i}{\partial t} = V_i \frac{\partial U_i}{\partial x_i} \right) \Big|_{\hat{Y}(t)}$$

To extend this equation to higher particle slip velocities, the Stokes drag is replaced with the particle drag law developed by Barnett and modified to include heat transfer effects by Nichols. The drag coefficient accounts for inertial, rarefaction, compressibility, shape, and heat transfer effects.

$$C_D = 24/Re \; F_1 \; F_2 \; F_3 \; F_4$$

WHERE $\quad F_1 = $ INERTIAL (RE) CORRECTION

$\qquad\qquad F_2 = $ COMPRESSIBILITY (M) CORRECTION

$\qquad\qquad F_3 = $ RAREFACTION (KN) CORRECTION

$\qquad\qquad F_4 = $ SHAPE CORRECTION

AND $\quad Re = \dfrac{\varrho_f \; d \; \sqrt{\sum\limits_i (U_i - V_i)^2}}{\mu_{app}}$

3

BASE FLOW EXPERIMENT

A test conducted in 1983 in the one foot transonic tunnel at AEDC emphasized the problems in the current seeding methodology. A missile base flow field was obtained at $M_\infty = 1.4$ and $M_j = 2.7$ at NPR of 50 and 150. Freestream, jet, and base flows were seeded separately with aluminum oxide particles.
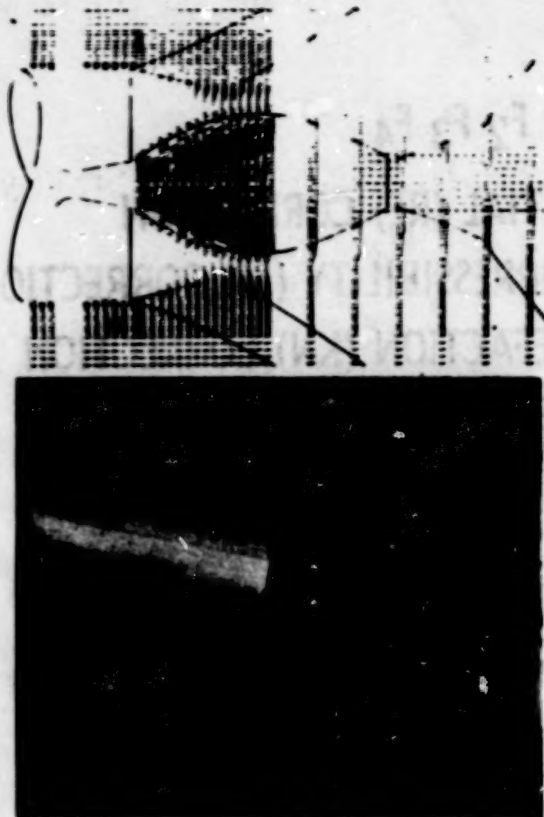
- **FLOWFIELD**
  $M_\infty = 1.4$
  $M_j = 2.7$
  NPR = 50,150
- **SEEDING**
  FREESTREAM - $.3\mu Al_2O_3$
  JET - $.3\mu Al_2O_3$
  BASE - $.3\mu Al_2O_3$, FLUORESCENT
- **MEASUREMENTS**
  BACKSCATTER
  SIMULTANEOUS
  2 COMP COUNTER
  2 COMP DFT

The velocity at the jet exit was much lower than expected from theory. In order to investigate this, particle lag calculations were made at the nozzle exit. These calculations indicated that the actual mean particle size on the centerline was 1.7 micron. Since the particle size limiting streamlines move closer to the nozzle wall as particle diameter decreases, it is expected that the centerline particle distribution will be weighted toward the larger particles. The apparent mean diameter is a function of the particle size distribution present in the flow and the transfer function of the laser velocimeter system.

PARTICLE VELOCITY AT THE NOZZLE EXIT CENTERLINE
FOR ALUMINUM OXIDE PARTICLES

5
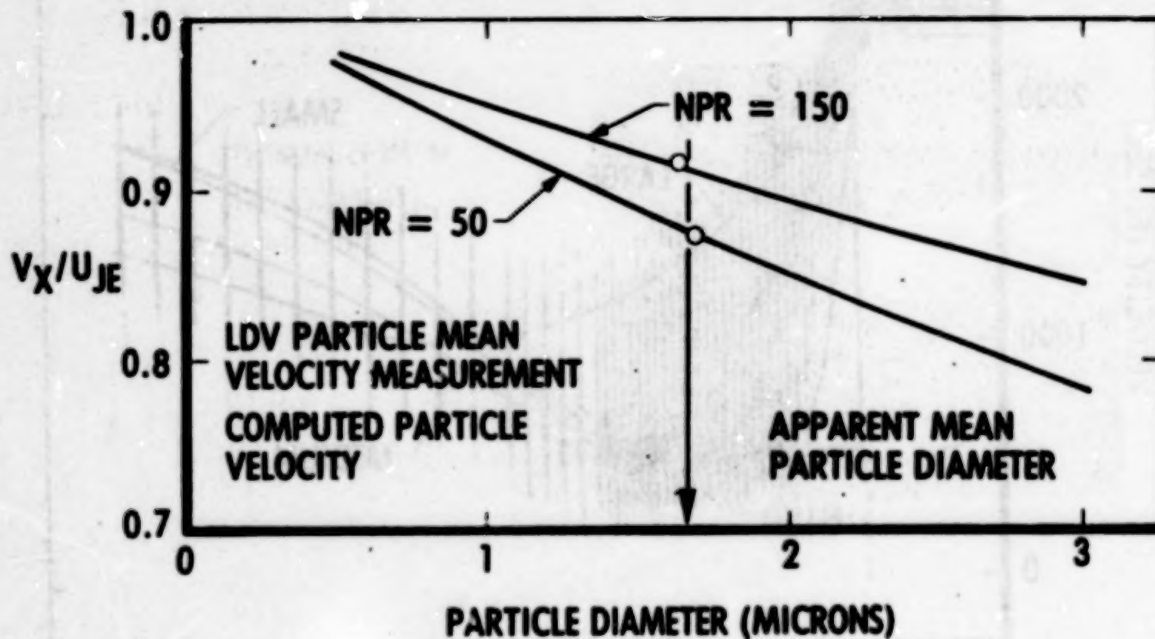
Particle dynamics effects can also be seen when the jet centerline measurements are examined. As the flow continues to expand, the different size particles accelerate at different rates, producing a broad velocity distribution which is often misinterpreted as fluid turbulence. This particle size induced broadening of the velocity distribution is especially noticeable behind the normal shock. It is also interesting to note that in the reacceleration region behind the shock the particle velocity lines cross, again obscuring the real turbulence and the mean velocity.

PARTICLE RESPONSE IN THE REACCELERATION REGION BEHIND A NORMAL SHOCK
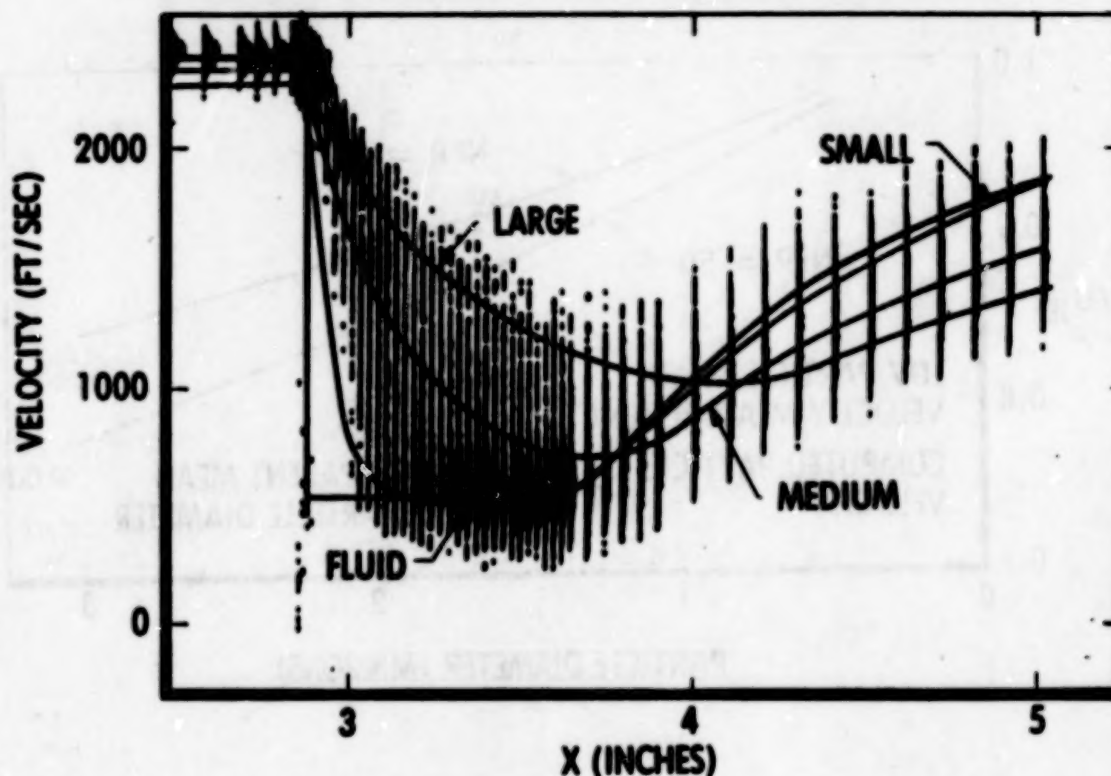
LDV measurements were also obtained in AEDC Tunnel A at M = 4.0, Re = 0.6 x 10⁶/Ft, and 0° angle of attack across the bow shock from a circular cylinder placed normal to the flow. Seeding was done using olive oil in a TSI Model 9306 seeder and in an AEDC developed laskin nozzle seeder. Calculations of particle lag were made to attempt to quantify particle size. The measurements indicate a broad particle distribution with an apparent mean about 1.5 micron. The calculations also indicate that a particle diameter of 0.5 micron would yield adequate mean flow velocity data for the boundary layer, but that a much smaller particle diameter is required for the bow shock measurements. It is interesting to note that the maximum particle lag in the boundary layer occurs in the middle rather that at the bottom of the boundary layer. The calculations did not include particles which had hit the surface and reflected back into the flowfield.

PARTICLE RESPONSE TO SHOCK

VKF TUNNEL A $M_\infty = 4.0$
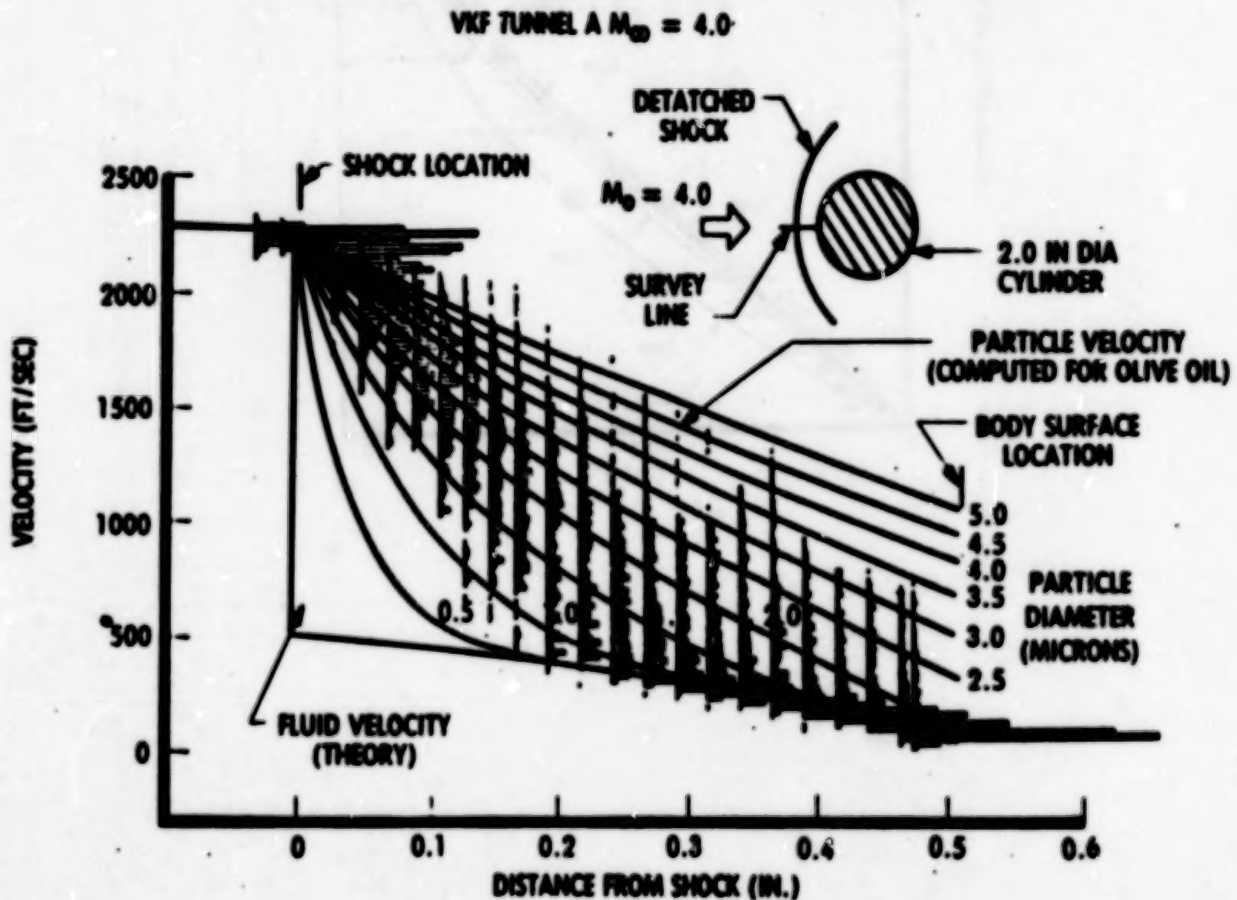
PARTICLE CALCULATIONS AND LDV VELOCITY DISTRIBUTIONS

LAMINAR BOUNDARY LAYER
VKF TUNNEL A 7 DEG CONE
M = 4.0 X = 35.0 IN.
OLIVE OIL SEED

FLUID

.5 μm

1 μm

2 μm

3 μm

HEIGHT ABOVE SURFACE (IN.)

U/U_e

As noted earlier, a broad particle size distribution creates a high apparent turbulence in the presence of a velocity gradient if particle lag occurs. Although a monodisperse particle distribution would alleviate this problem, the diameter must still be chosen so as to assure the particle responds properly to the turbulence. Calculations in low speed grid generated turbulence modeled from Snyder's experiment (Ref 2) indicate that particles may not properly reproduce the turbulent velocity fluctuations even when the mean flow particle lag is zero. For a water particle in air these calculations indicate that while the mean flow velocity can be measured to within less that one percent accuracy with a 46.5 micron particle, the measurement of turbulence quantities to the same level of accuracy would require a 4 micron particle.

PARTICLE SIZE REQUIREMENTS FOR MEAN AND TURBULENT FLOW MEASUREMENTS

CALCULATIONS FOR SNYDER'S EXPERIMENT IN GRID GENERATED TURBULENCE

9
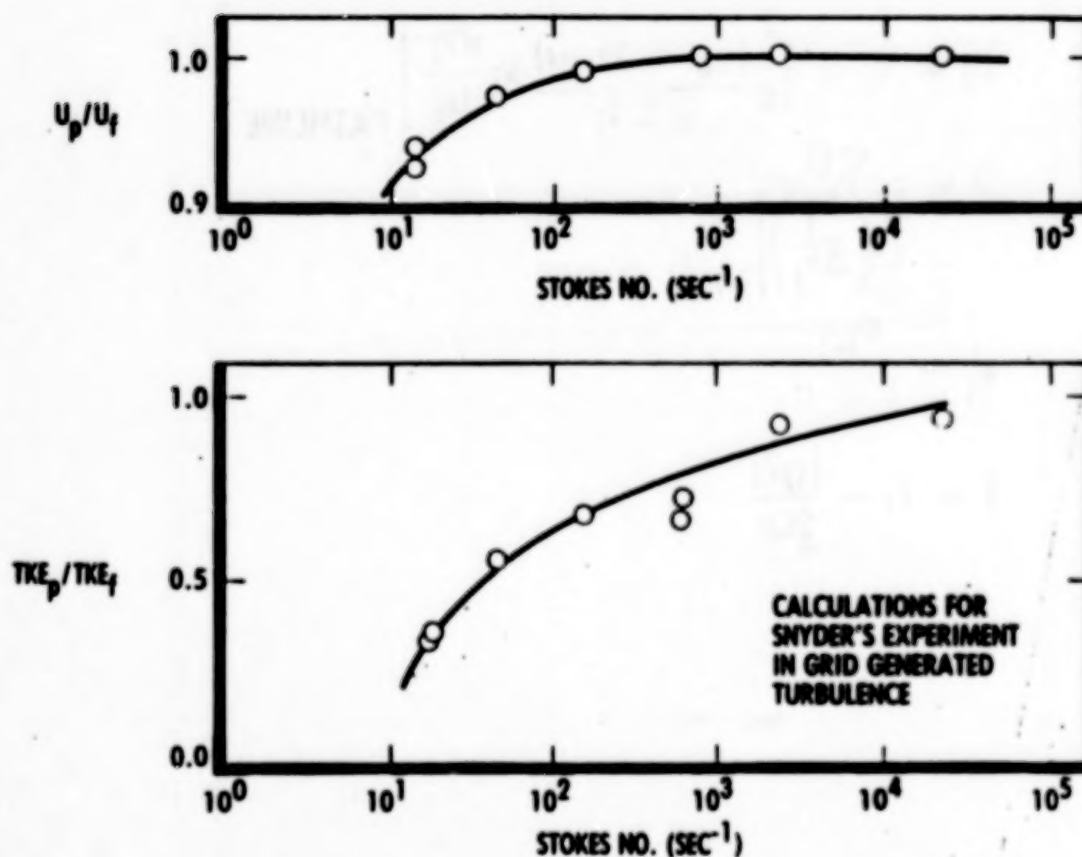
PARTICLE LAG CORRECTION SCHEME

Under the assumption that only the drag term of the particle equation of motion is relevant, it is theoretically possible to correct LV measurements for particle lag. The correction should be applied along particle path lines calculated from LV measurements. This also requires some method of determining fluid properties. The correction technique is only valid for a known monodisperse particle size, making its application impractical at this time. The technique can be useful in identifying regions of particle lag in a measured flowfield.

1. **ASSUMPTIONS:**

   A. **ALL TERMS BUT DRAG TERM NEGLIGIBLE**

   B. **KNOWN MONODISPERSE PARTICLE SIZE**

2. **CALCULATE PARTICLE PATHS FROM LDV DATA**

3. **ITERATIVELY SOLVE FOR FLUID VELOCITY, DENSITY, TEMPERATURE FROM:**

$$U_i = V_i + \frac{d^2}{18} \frac{(\varrho_p + \frac{1}{2}\varrho_f)}{\mu \Sigma F_i} V_i \frac{dV_i}{dx_i}\Bigg|_{\text{PATHLINE}}$$

$$G = \frac{\nabla \vec{U}}{\Sigma\limits_i \left(\frac{U_i}{\Delta x_i}\right)\Bigg|_{i-1}}$$

$$\varrho_i = \frac{\varrho_{i-1}}{1 + G}$$

$$T = T_T - \frac{|U^2|}{2C_p}$$

CONCLUSIONS

- **INTERPRETATION OF LDV MEASUREMENTS REQUIRES THE CAPABILITY OF ANALYTICALLY EXAMINING PARTICLE DYNAMICS EFFECTS**

- **BROAD PARTICLE SIZE DISTRIBUTIONS PRODUCE "ARTIFICIAL TURBULENCE" AND SHOULD BE AVOIDED**

- **MINIMUM ACCEPTABLE PARTICLE SIZE FOR TYPICAL AEDC LDV MEAN VELOCITY MEASUREMENTS IS LESS THAN 0.5 MICRONS**

- **ABSOLUTE MINIMUM ACCEPTABLE PARTICLE SIZE IS PROBABLY DRIVEN BY TURBULENCE, NOT MEAN FLOW, REQUIREMENTS**

- **CORRECTION FOR MEAN FLOW PARTICLE LAG MAY BE FEASIBLE FOR MONODISPERSE SEED PARTICLES**

REFERENCES

1. MAXEY, MARTIN R. AND JAMES J. RILEY, EQUATION OF MOTION FOR A SMALL RIGID SPHERE IN A NONUNIFORM FLOW, PHYS OF FLUIDS, VOL 26, NO. 4, PP. 883-889, APRIL 1983.

2. SNYDER, W. H. AND J. L. LUMLEY, SOME MEASUREMENTS OF PARTICLE VELOCITY AUTOCORRELATION FUNCTIONS IN A TURBULENT FLOW, J. FLUID MECHANICS, VOL 48, PART 1, PP. 41-71, JULY 1971.

CORRECTING FOR PARTICLE COUNTING BIAS ERROR IN TURBULENT FLOW

Robert V. Edwards and William Baratuci
Chemical Engineering Department
Case Center for Complex Flow Measurements
Cleveland, Ohio 44106

RATIONALE

Even if the result of this meeting is an ideal seeding device that generates particles that exactly follow the flow and are of sufficient major source of error, I refer to particle counting bias wherein the probability of measuring velocity _if it occurs_ is a function of velocity. The error in the measured mean can be as much as 25% (ref. 1).

Many schemes have been put forward to correct for this error, but there is not universal agreement as to the acceptability of anyone method. In particular it is sometimes difficult to know if the assumptions required in the analysis are fulfilled by any particular flow measurement system.

In an effort to check various correction mechanisms in an ideal way and to gain some insight into how to correct with the fewest initial assumptions, a computer simulation was constructed to simulate laser anemometer measurements in a turbulent flow. That simulator and the results of its use are the topic of this paper.

INTRODUCTION

All measurements of mean quantities in a sparsely seeded turbulent flow using a laser anemometer generate a _measured velocity probability function_ $P_m(v)$ that differs from the true Eulerian probability of interest $P(v)$. The relation between the two is given by

$$P_m(v) = \frac{r_m(v)}{<r_m>} P(v) ,$$

where $r_m(v)$ is the measurement rate _if_

the velocity is v. $<\ >$ denotes

average value.

Any correction scheme's function is to eliminate the effect of $r_m(v)$.

First a pseudo-continuous signal, the "hot wire" signal, is generated by passing a digital white noise signal through a digital filter. Shown here is a typical segment of the "hot wire" signal.

Sample Hot Wire Velocity Signal

Vbar = 1.0, TI = 0.30

15
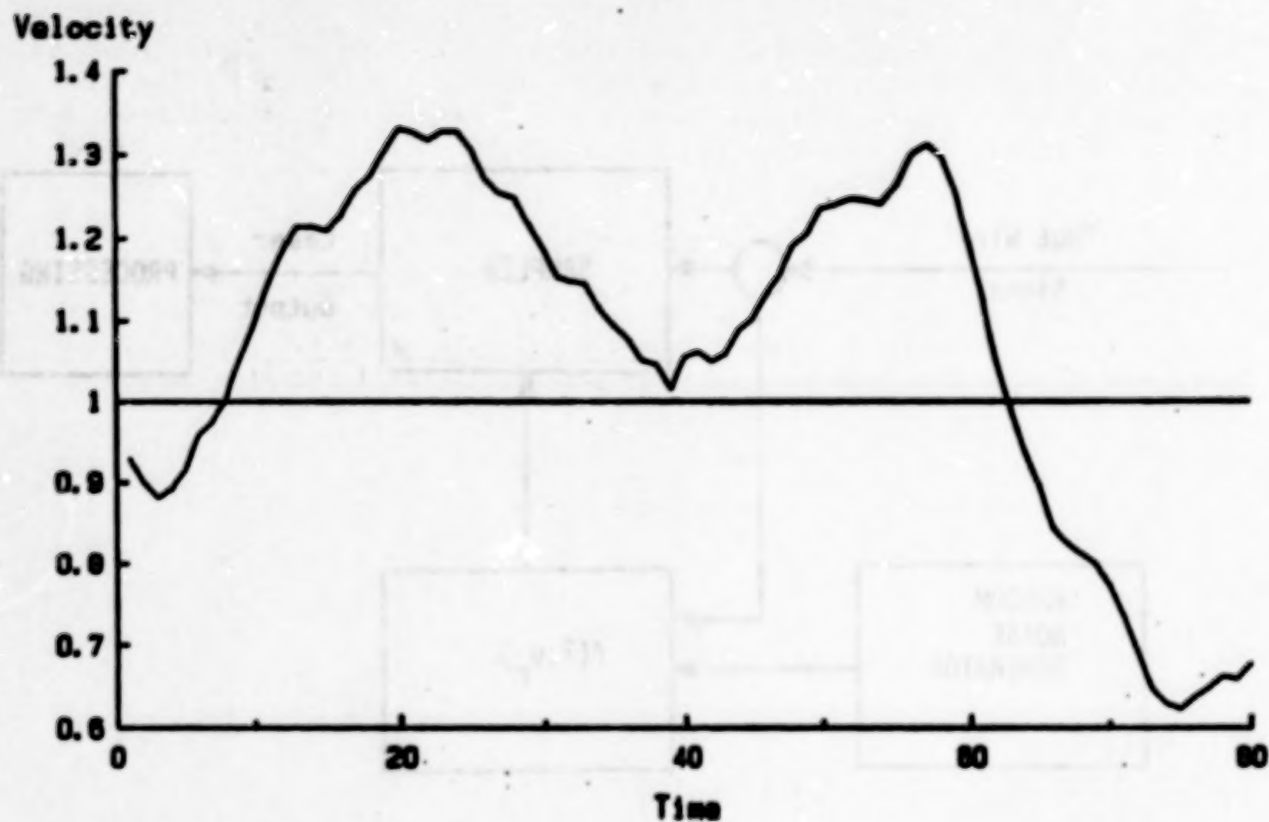
The "laser anemometer" signal is generated by a random sampling of the hot wire signal. The simulator is constructed so that the average measurement rate as a function of velocity can be set to be any desired function of the velocity. In this study the measurement probability, $r_a(v)$, was set to be either a linear or quadratic function of the velocity magnitude. Shown here is a block diagram of the particle sampling section.

Flow Diagram of Particle Arrival Simulation
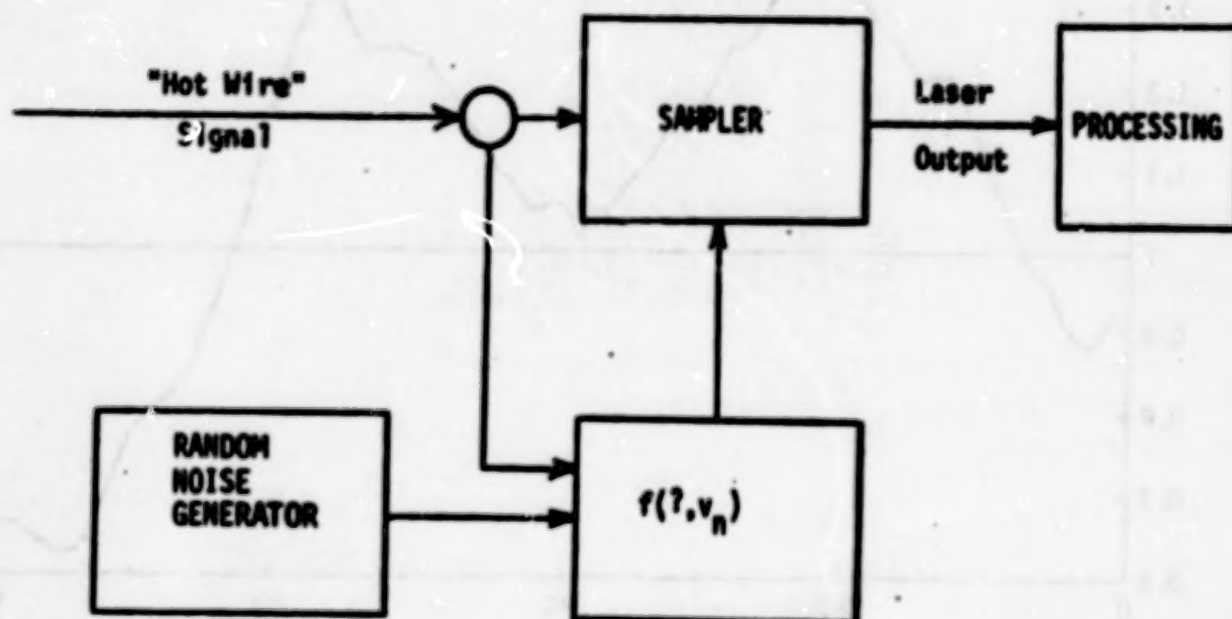
Shown here is a histogram of the hot wire signal and laser anemometer signal for a typical simulation. They are close in shape, but there are differences.

Hot Wire and Laser Velocity Histograms
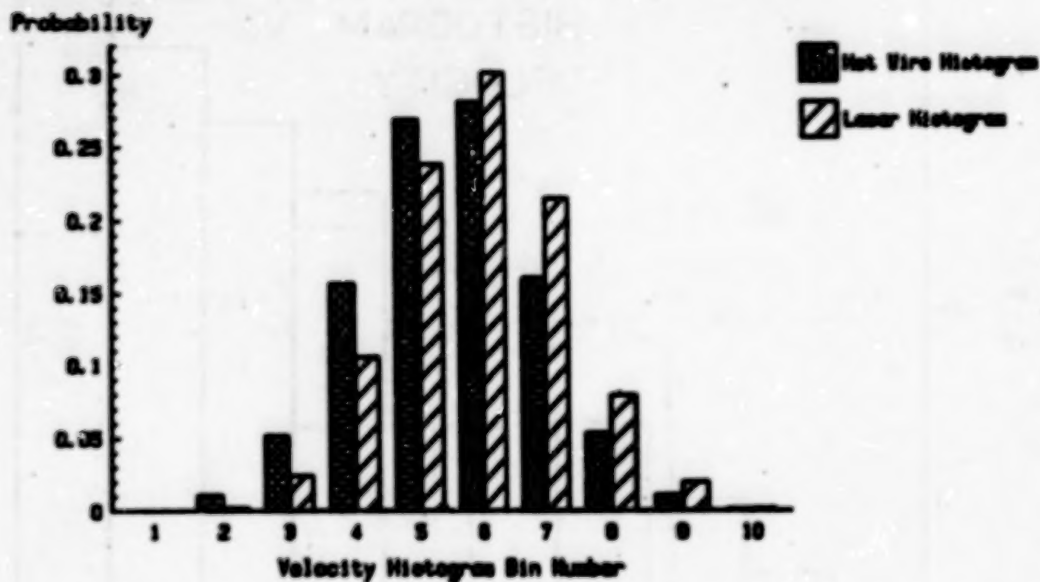
If one takes the ratio of the laser anemometer histogram to the hot wire histogram, the result should be the normalized rate corresponding to the velocity (see the first figure). That ratio is shown here. Note the linear dependence of the rate on velocity.

RATE BY
HISTOGRAM VS.
VELOCITY
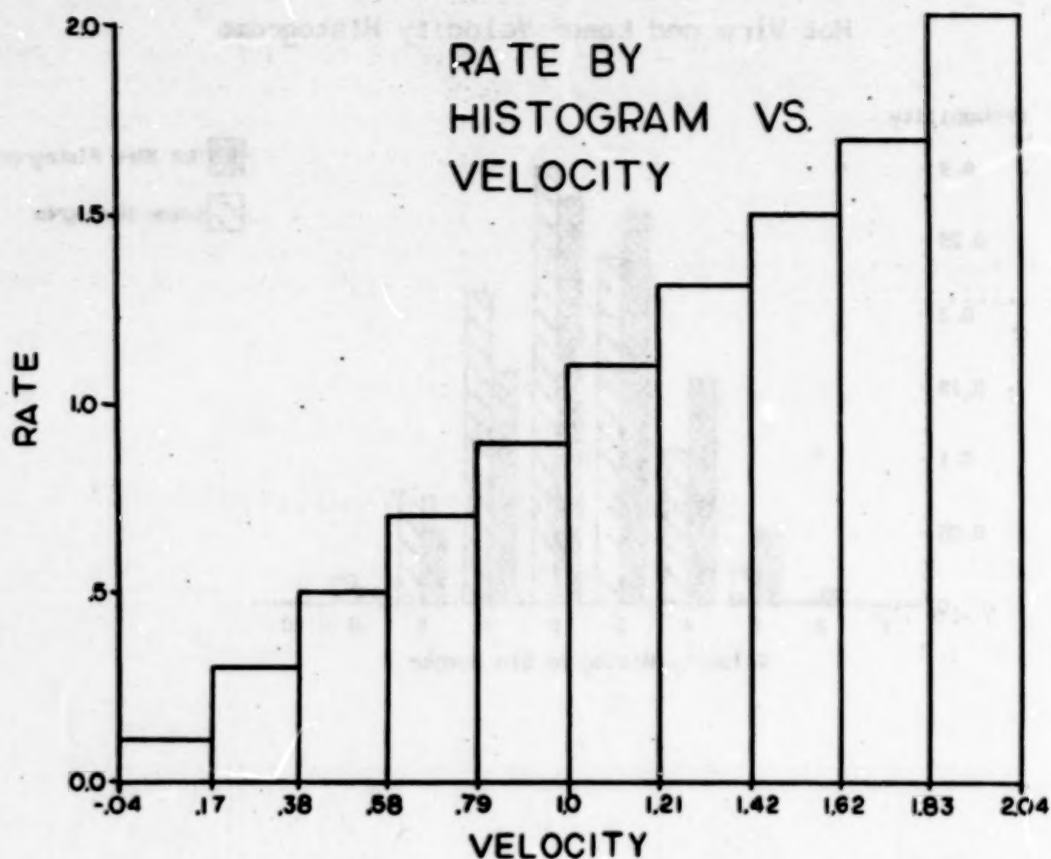
RATE

VELOCITY

Three correction schemes from the literature were checked using the simulator.

1) Sample and Hold. A continuous signal is generated by holding the last measured velocity until a new measurement arrives. That new one is the held... It has been predicted that in the limit of many measurements per flow correlation time, the continuous signal generates unbiased statistics.

2) Periodic Measurement. Time is divided into intervals of constant length. If only the first measure in each interval is recorded, a periodically sampled signal is generated. It has been predicted that all bias vanishes when it is highly probable that there is a measurement in each interval.

3) Dead Time. Any data recording device has a reset time during which no new measurement is recorded. If the dead time is small compared to the flow correlation time and if the particle rate is high enough, the bias should vanish.

This figure shows each scheme graphically.

Sample Hot Wire Velocity Signal
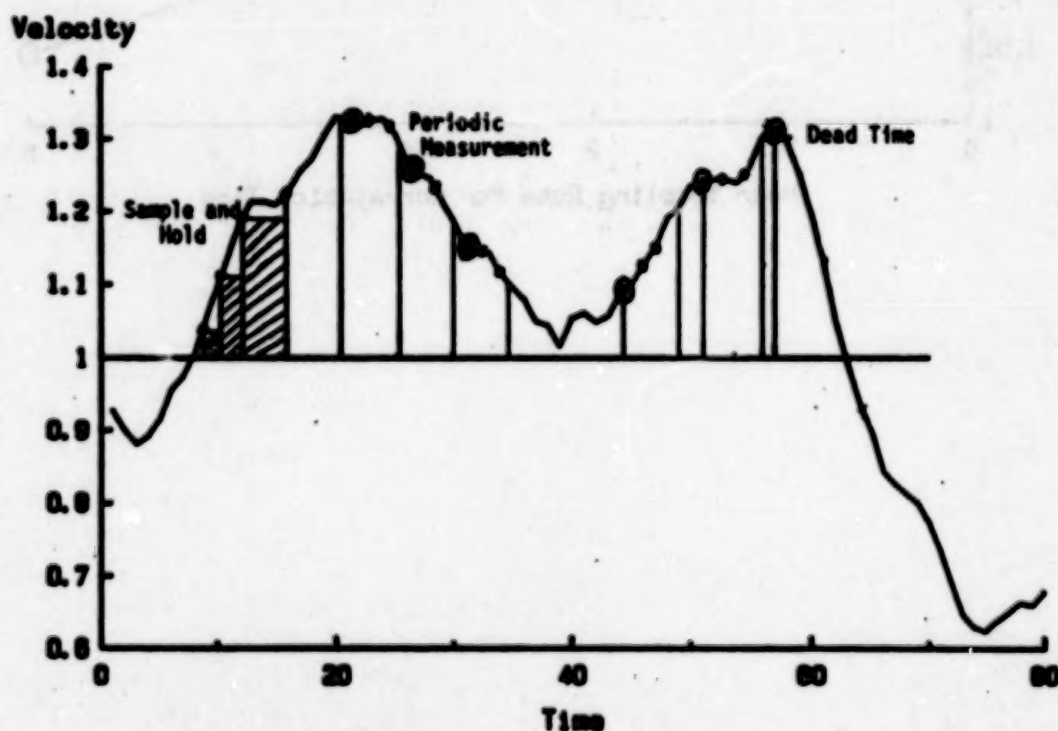
The bias in the mean definitely does decrease as the mean rate per flow correlation time increases. This is shown in the next figure.

Mean Measured Velocity vs. Sampling Rate
V = 1.0, TI = 0.30
Sample and Hold Analysis
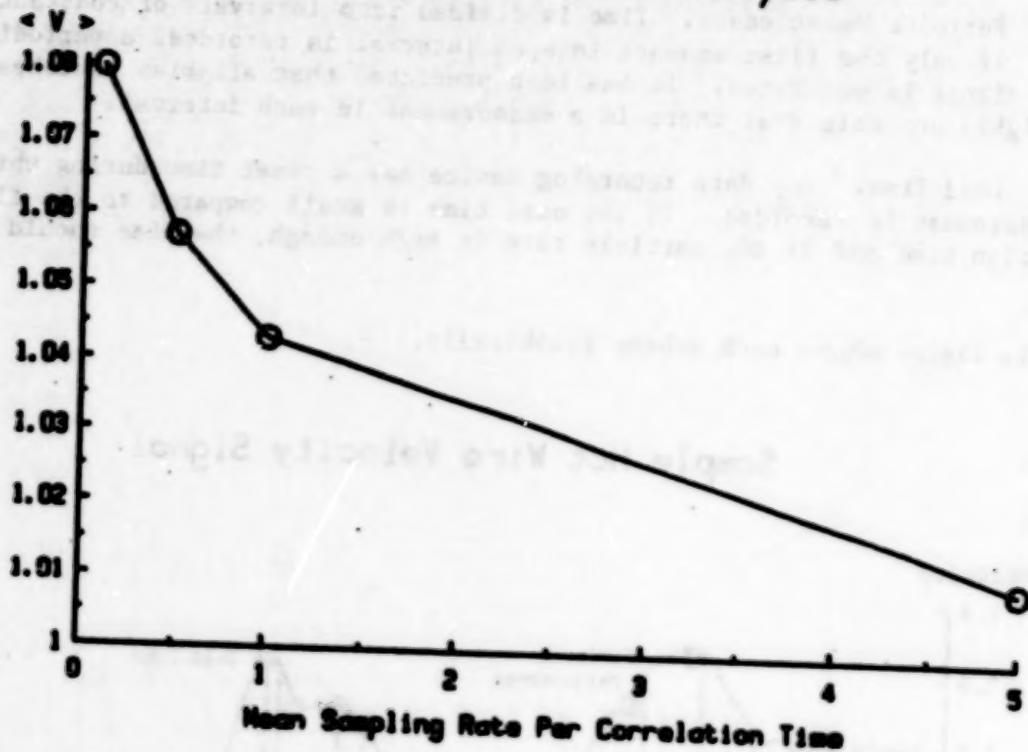
If the mean particle arrival rate is held constant and if the periodic sampling rate is varied, the bias in the measured mean does decrease but not to zero. See below.

Measured Mean Velocity vs. Q
V=.997+/-.008, TI=.300+/-.003, sampling rate=1.0
Periodic Sampling Analysis

Q = ratio of sampling period to correlation time
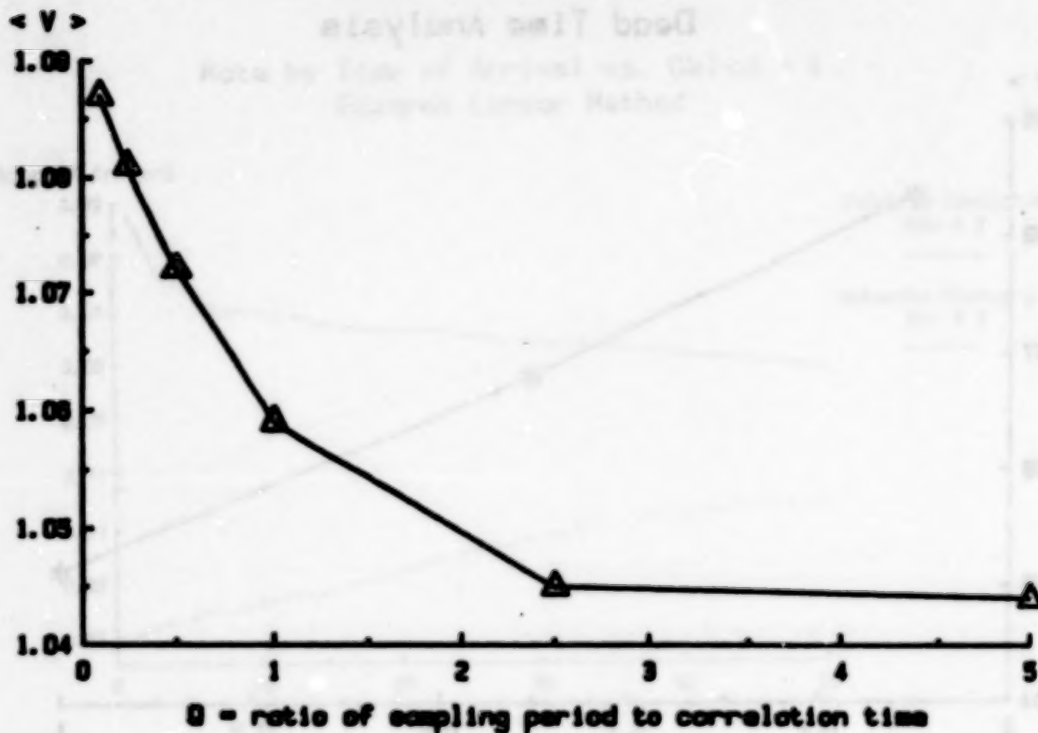
If the dead time is kept smaller than the flow correlation time, the bias is supposed to decrease to zero as the particle arrival rate increases. This is borne out by the following figure. Although the figure doesn't show the bias going to zero, the measurements closely fit the theory that does go to zero. We haven't had enough computer time to check the high particle rate limit.

Measured Mean Velocity vs. RT
V = 1.0, TI = 0.30
Dead Time Analysis
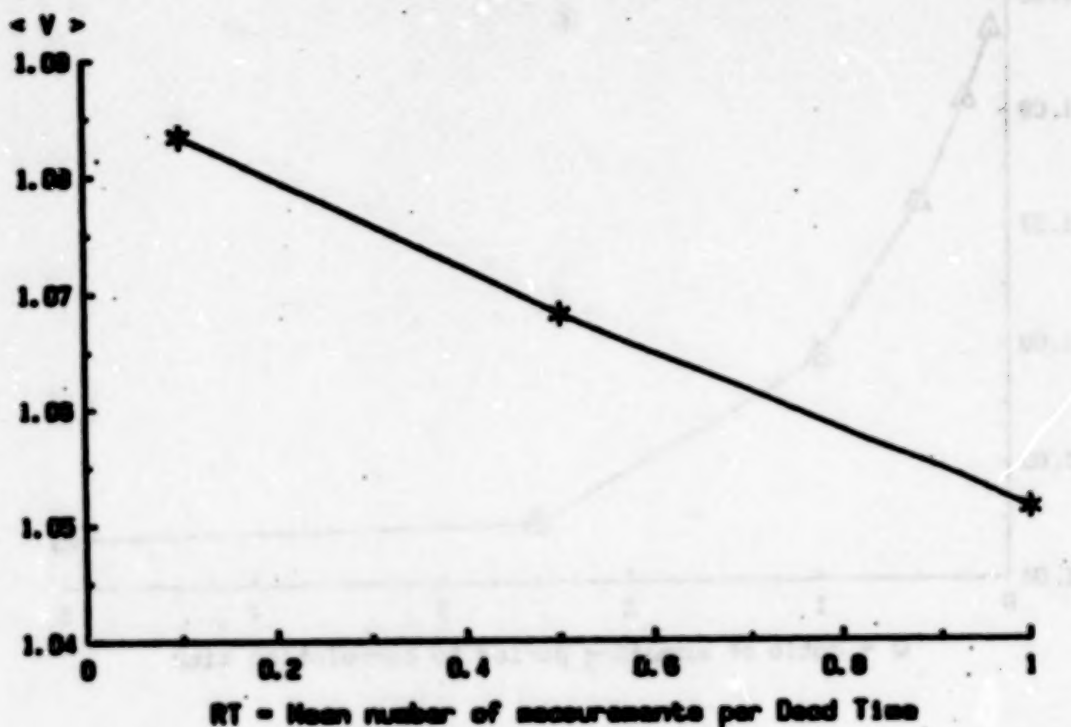
Recently Edwards and Meyers put forth a correction scheme that involved direct measurement of $r_m(v)$ (ref. 2). Simply, one measured that rate for each interval in the velocity histogram by counting the average number of measurements occurring in a small interval Δt after the appearance of a velocity in a given interval. It can be shown that the procedure's averaging result is exact in the limit of Δt going to zero. Unfortunately, it can also be shown that the relative measurement error goes to infinity as Δt goes to zero. The figure below shows the measured rate as a function of Δt. Note that as Δt increases, the measured rate tends toward the mean value, independent of which interval one starts in.

Rate by Time of Arrival vs. Delta - t
Edwards Linear Method
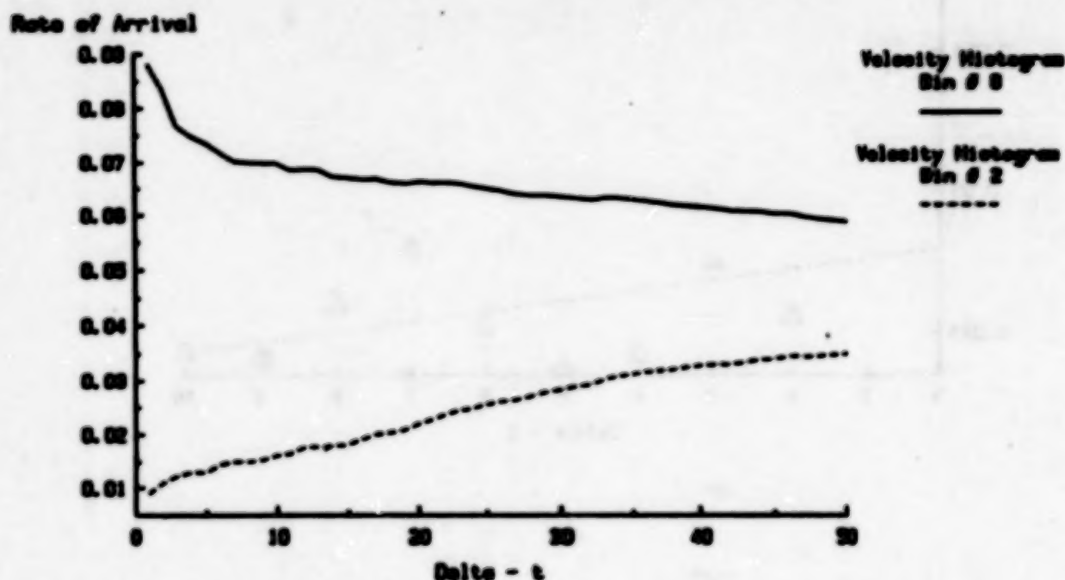
Edwards and Baratuci have invented a scheme that computes the limit as Δt goes to zero starting with relatively large values of Δt (ref. 3). A line is fit to the results for various Δt and the intercept is taken as the "correct" value.

Rate of Particle Arrival vs. Delta - t
Velocity Histogram Bin # 5
Edwards Method (Linear)
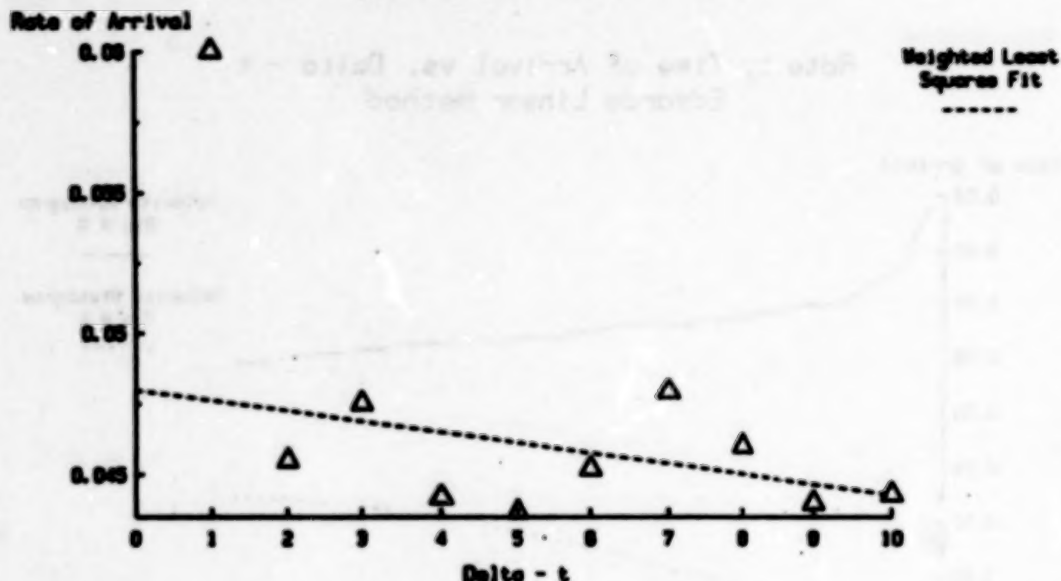
The following figure shows the measured rate versus velocity for a typical simulation with a quadratic dependence on velocity magnitude. The measured rates are very close to the values set by the simulation.

Rate by Histogram vs. Velocity
Edwards - Baratuci Method
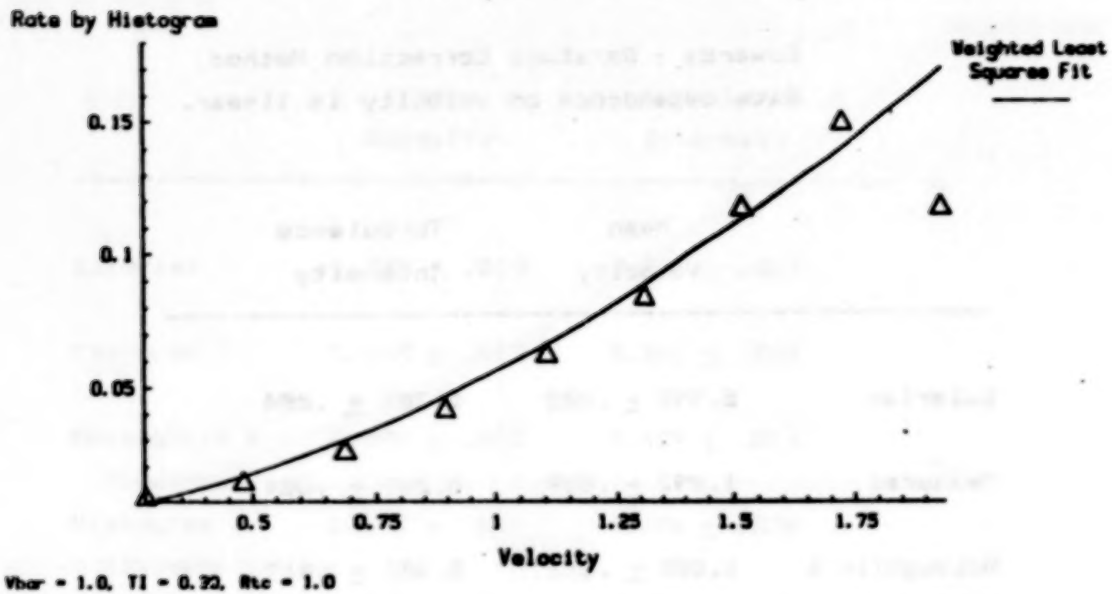
The following figure from reference 3 gives a summary of the results of our correction schemes for a set of simulations. McLaughlin and Tiederman (ref. 1) and the histogram corrections are included only as a self consistency check of the simulator. The two Edwards correction schemes are here because in general one does not know the functional form of $r_m(v)$. Edwards (quadratic) is a general quadratic fit to $r_m(v)$.

Edwards - Baratuci Correction Method.
Rate dependence on velocity is linear.

	Mean Velocity	Turbulence Intensity
Eulerian	0.998 ± .008	0.302 ± .004
Measured	1.092 ± .009	0.209 ± .004
McLaughlin & Tiederman	1.008 ± .012	0.302 ± .017
Histogram (linear)	1.002 ± .010	0.302 ± .006
Histogram (quadratic)	1.003 ± .012	0.300 ± .009
Edwards (linear)	1.008 ± .027	0.304 ± .014
Edwards (quadratic)	1.010 ± .023	0.298 ± .010

Note : Vbar = 1.0, TI = 0.30, Rt_c = 1.0.

Note : Edwards (linear) means a linear fit was
        done on $r_m(\Delta t, v_k)$ and Edwards (quadratic)
        means a fit was done to a second order
        polynomial. The same explanation applies
        to the Histogram Methods.

Note : Error bars are the standard deviation
        of the mean of the mean velocity obtained
        from twenty data sets of 2700 points each.

This table (from ref. 3) is the same as the previous except that $r_m(v)$ is generated as a quadratic function of v.

Edwards - Baratuci Correction Method.
Rate dependence on velocity is quadratic.

	Mean Velocity	Turbulence Intensity
Eulerian	1.000 ± .010	0.301 ± .004
Measured	1.169 ± .013	0.201 ± .004
McLaughlin & Tiederman	1.093 ± .013	0.429 ± .019
Histogram (linear)	1.047 ± .029	0.296 ± .030
Histogram (quadratic)	1.010 ± .019	0.297 ± .011
Edwards (linear)	0.968 ± .097	0.289 ± .053
Edwards (quadratic)	1.016 ± .045	0.274 ± .028

Note :   Vbar = 1.0, TI = 0.30, RT_c = 1.0, N = 2700.

Note :   Edwards (linear) means a linear fit was
         done on $r_m(\Delta t, v_k)$ and Edwards (quadratic)
         means a fit was done to a second order
         polynomial. The same explanation applies
         to the Histogram Methods.

Note :   Error bars are the standard deviation
         of the mean of the mean velocity obtained
         from twenty data sets of 2700 points each.

CONCLUSIONS

Sample and Hold eliminates bias for high particle densities.

Dead Time reduces bias for sampling rates tested [Prediction not checked due to large run time]

Periodic Sampling with long periods reduces but does not eliminate velocity bias

New correction is excellent when the form of rate as a function of velocity is known

Further work using "unknown" functional forms is in process

REFERENCES

1. McLaughlin, D.K. and Tiederman, W.G.: Biasing Corrections for Individual Realization of Laser Anemometer Measurements in Turbulent Flow. Phys. Fluids 16, 2082, 1973.

2. Edwards, R.V. and Meyers, J.: An Overview of Particle Sampling Bias. Presented at the Second International Symposium on Applications of Laser Anemometry to Fluid Mechanics, July 2-4, 1984, Lisbon, Portugal.

3. Baratuci W.: Particle Arrival Statistics in Laser Anemometry. M.S. Thesis, Case Western Reserve University, 1985.

ESTIMATION OF PARTICLE SIZE BASED ON LDV MEASUREMENTS IN A DE-ACCELERATING FLOW FIELD

James F. Meyers
NASA Langley Research Center
Hampton, Virginia

PARTICLE SIZE CONSIDERATIONS

The accuracy of velocity measurements made with a laser velocimeter is strongly dependent upon the response of the seeding particles to the dynamics of the flow field. The smaller the particle the better the response to flow fluctuations and gradients and therefore the more accurate velocity measurement. In direct conflict is the requirement of light scattering efficiency to obtain signals with the laser velocimeter which, in general, is better as the particle size is increased. In low speed flow fields these two requirements on particle size overlap and accurate measurements may be obtained. However in high speed flows, where the velocity gradients may be severe, very small particles are required to maintain sufficient dynamic response characteristics to follow the flow. Therefore if velocity measurements are to be made in these flows, the laser velocimeter must be designed with sufficient sensitivity to obtain signals from these small particles. The present paper describes an insitu determination of the size distribution of kaolin particles ($Al_2O_3 \cdot 2 \pm SiO_2 \cdot 2 H_2O$) in the 16-foot Transonic Tunnel and the sensitivity characteristics of the laser velocimeter system.

SMALL ENOUGH TO FOLLOW THE FLOW FIELD

- SIZE

- SHAPE

- DENSITY

LARGE ENOUGH FOR THE LV TO "SEE" IT

- SIZE

- SHAPE

- INDEX OF REFRACTION

APPLICATION CONSIDERATIONS

The choice of seeding material for laser velocimetry applications is limited to using particles naturally present in the flow, or injecting either liquid droplets or solid particles in the flow. Natural particulates have the advantage of not requiring a seeding generation system and no additional facility contamination; however, they are of unknown size and are very few in number. This leads to unknown measurement accuracies and long test times. Liquid seeding, especially liquids with relatively high vapor pressures, has the advantage of yielding large numbers of particles while maintaining little facility contamination because they will evaporate. Liquids, however, usually have fairly wide size distributions which are typically skewed toward the larger sizes. These distributions may also be modified by the test conditions within the facility. Solid particles have the advantage of yielding large numbers of particles while maintaining their size distributions. Solid particles may present a contamination problem, may have higher densities than liquid particles (which affects particle dynamics), and may erode the model/tunnel surfaces.

NATURAL PARTICULATES

- SIZE UNKNOWN

- LOW DATA RATE

LIQUID SEEDING

- SIZE DISTRIBUTION SKEWED

- MODIFICATION BY TEST CONDITIONS

## SOLID PARTICULATES

- SIZE DISTRIBUTION

- DENSITY

- MODEL EROSION

ARRANGEMENT OF THE LANGLEY 16-FOOT TRANSONIC TUNNEL

The figure illustrates the layout of the 16-foot transonic tunnel along with the location of the particle generation system. It is noted that only three generators are illustrated while the actual system contained ten. The laser velocimeter system is located within the plenum chamber surrounding the test section. The wind tunnel has a Mach number range up to 1.3 and an average Reynolds number of 13×10^6 per meter at Mach numbers above 0.6. The test section is octagonal with movable walls used to minimize the axial Mach number gradient and is slotted for removal of the boundary layer by evacuation of the surrounding 9.75 meter diameter plenum at Mach numbers above 1.03. The ambient conditions within the plenum chamber at Mach 1.0 are approximately 0.5 atm pressure, 50° C and 150 dBm of acoustic power. The structural members within the plenum chamber are subjected to vibration levels of up to 5 g. Optical access to the test section from the plenum is provided by an optical quality (BK-7 glass) window installed in the test section wall with a clear viewing area of 1.27 m by 0.91 m.

DIMENSIONS ARE IN meters (feet).

SECTION THROUGH STA. 33.53 (110.0)
(LOOKING DOWNSTREAM)
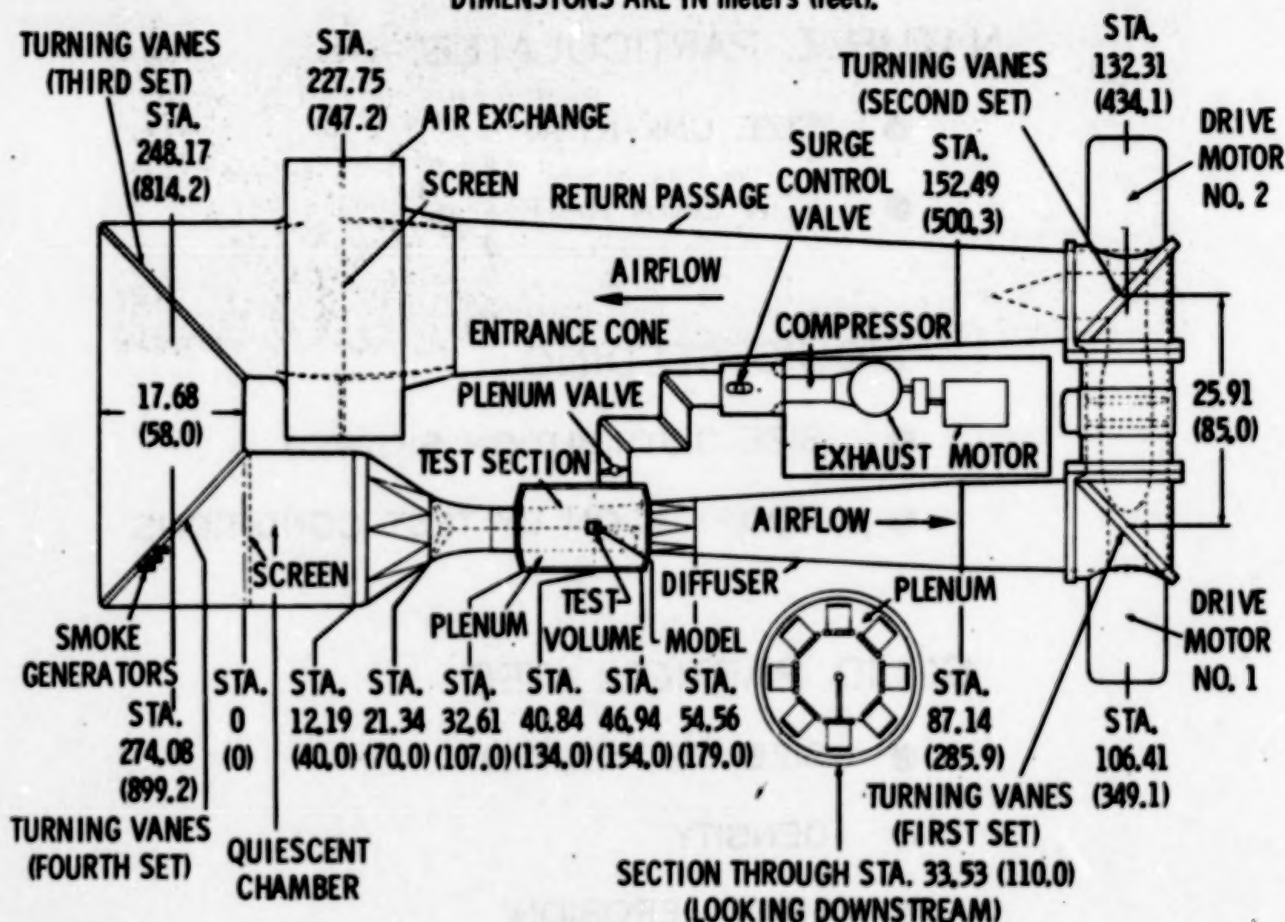
HEMISPHERE-CYLINDER MODEL INSTALLED IN THE TEST SECTION

The sting mounted hemisphere-cylinder model is shown in the figure located along the centerline of the 16-foot transonic tunnel test section. The laser beams from the laser velocimeter located in the plenum chamber are shown passing in front of the model.
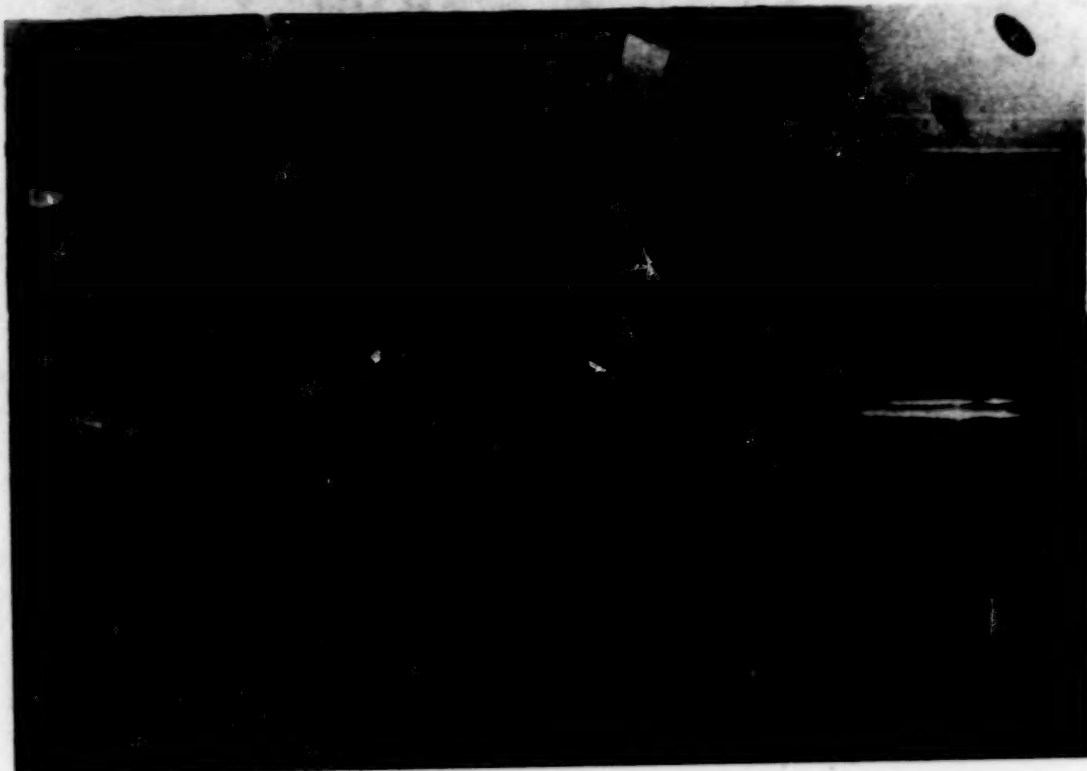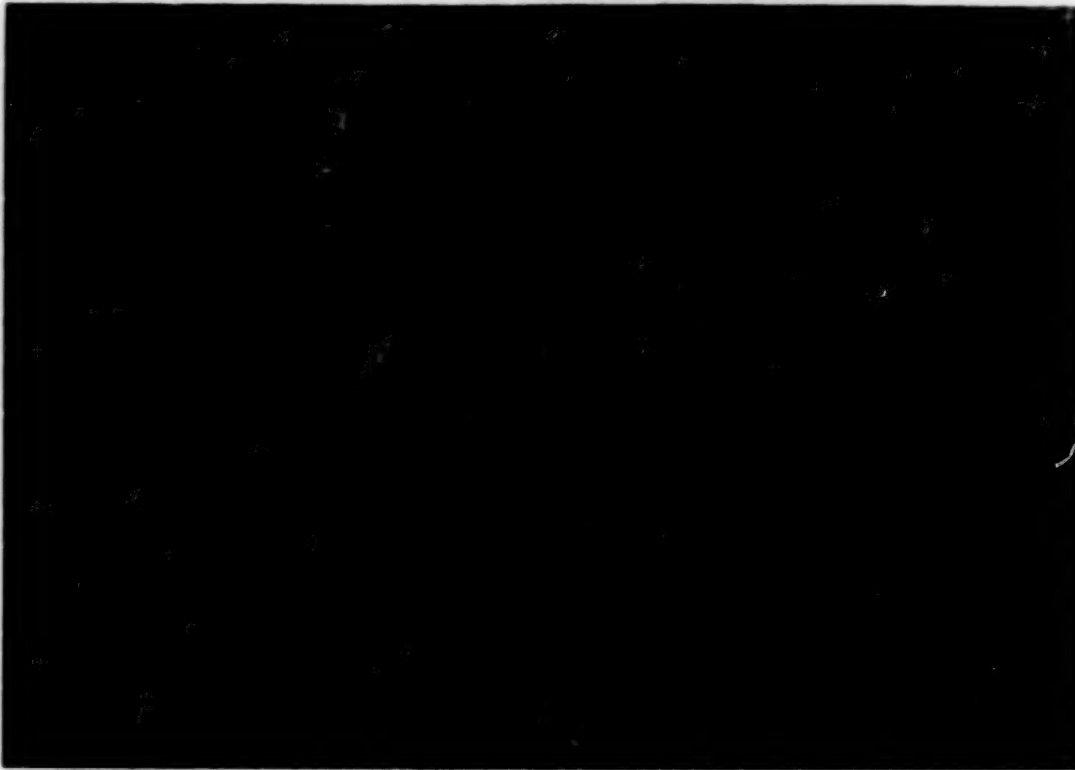
HEMISPHERE-CYLINDER MODEL

The hemisphere-cylinder model along with the laser beams is shown in the figure. The hemisphere is 19.05 cm in diameter followed by a 10.16 cm long cylinder.

OPTICAL PARTICLE SIZE ANALYSIS - KEROSENE

The first test of the laser velocimeter in the 16-foot transonic tunnel used kerosene as the seeding material. The particle size distribution of kerosene, the theoretical sensitivity function for the proof-of-concept laser velocimeter calculated using the simulation code described in reference 1, and the resulting detectable particle size distribution are illustrated in the figure. The measured particle size distribution was obtained in the laboratory using an optical particle size analyzer with the particle generator located a distance from the analyzer to yield a corresponding time-of-flight as in the tunnel to simulate the effects of evaporation.

The calculation of the theoretical sensitivity function begins with the determination of the electro-magnetic field resulting from the scatter of light from a particle of a given size (described by Mie in reference 2) as it passes through each pair of the laser beams comprising the sample volume. The interaction between the two scattered fields is calculated over the collecting solid angle of the laser velocimeter using the method described in reference 3 to yield the optical transfer function which is used along with the Gaussian intensity profile of the laser beams to obtain the theoretical signal burst. This burst is integrated and used to drive a Poisson random number generator yielding a Monte Carlo simulation of photon arrivals at the photocathode surface of the photomultiplier. The photons are convolved with the photomultiplier transfer function to obtain the electronic signal burst which is then input to a model of a high-speed burst counter with double threshold detection circuits and a 5:8 count comparison to determine if the signal has sufficient amplitude to yield a velocity measurement. If the signal does not have sufficient amplitude, following band pass filtering, for ten consecutive cycles to cross the thresholds with sufficient signal-to-noise ratio to satisfy the 5:8 count comparison test, a measurement can not be made and the sensitivity factor is zero for that particle size. If the signal is accepted by the counter, the amplitude of the signal is reduced in an exponential manner until the signal fails to be accepted by the counter. The amount of reduction in amplitude corresponds to a distance from the center of the sample volume in accordance with the Gaussian intensity profile of the laser beams. A sensitivity factor of unity is assigned where the distance from the center of the sample volume corresponds to the sample volume radius as defined by the intensity being $1/e^2$ of the intensity at the center. The resulting sensitivity function is then multiplied by the measured particle size distribution to yield the distribution of detectable particles.
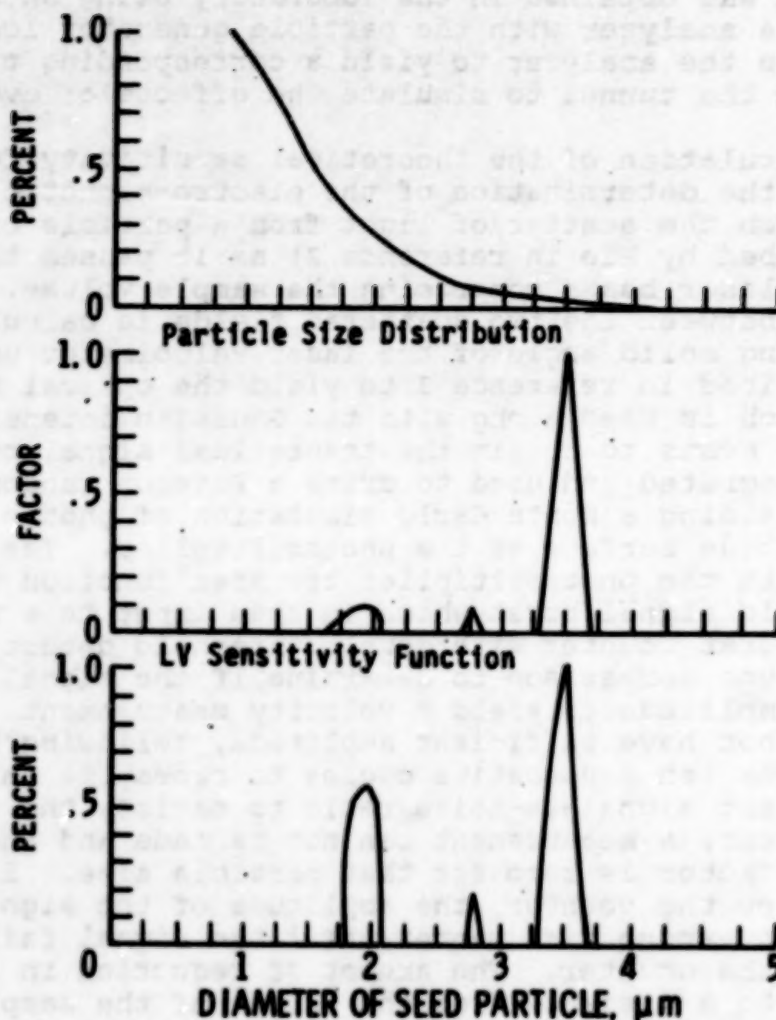
PERCENT

1.0

.5

0

Particle Size Distribution

FACTOR

1.0

.5

0

LV Sensitivity Function

PERCENT

1.0

.5

0

1 2 3 4 5

DIAMETER OF SEED PARTICLE, μm

Measurement Probability Distribution

LV MEASUREMENTS ALONG THE STAGNATING STREAMLINE

Velocity measurements were made along the stagnating streamline from one model diameter upstream to within an estimated distance of 1.9 mm from the model surface for several Mach numbers. These measurements along with the predicted gas velocity profiles using the potential flow method outlined in reference 4 are illustrated in the figure. The size of the kerosene particles which would yield the velocities measured by the laser velocimeter was determined using the particle dynamic prediction procedures outlined in reference 5. The resulting particle size was found to be in excess of 17 micrometers which indicates that the particle size distribution was modified by the conditions within the tunnel. Therefore kerosene has been shown to be a very poor choice as the seeding material for the 16-foot transonic tunnel.
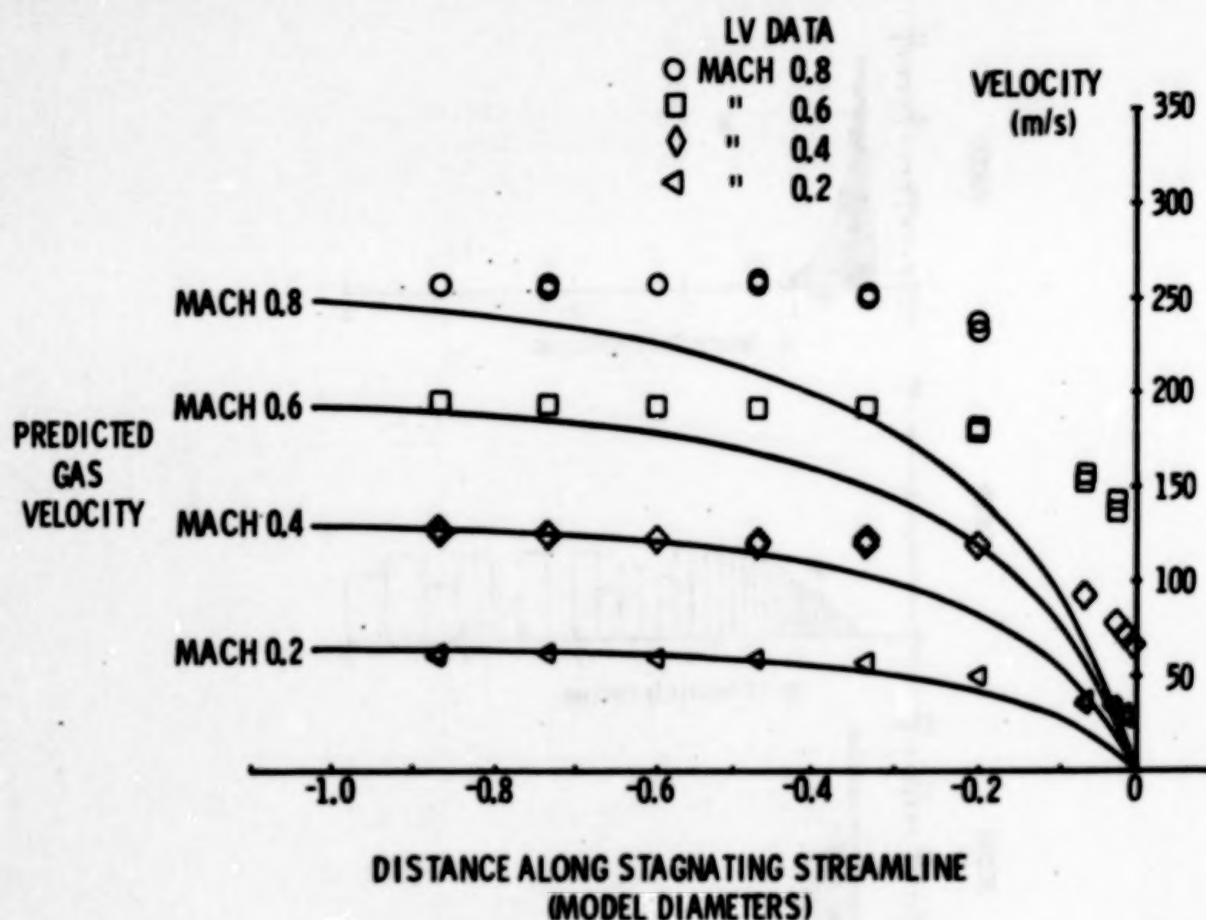
AERODYNAMIC PARTICLE SIZE ANALYSIS - KAOLIN

Kaolin was chosen as the next particle material. Kaolin particles are irregular in shape with a specific gravity of 2.58 and an index of refraction of 1.56. The particles were suspended in ethanol and injected into the tunnel using the same particle generators. Within a short distance from the generators, the ethanol evaporated leaving the kaolin particles embedded in the flow field. The measurement of the particle size distribution in the laboratory was performed using an aerodynamic particle size analyzer which yielded an equivalent spherical size distribution of the irregularly shaped kaolin. This size distribution was then used to determine the sensitivity function and the resulting detectable particle size distribution. These results, illustrated in the figure, indicate that the average detectable particle was 0.78 micrometers in diameter.

a) Particle Size Distribution

b) LV Sensitivity Function

c) Measurement Probability Distribution

PARTICLE SIZE (microns)
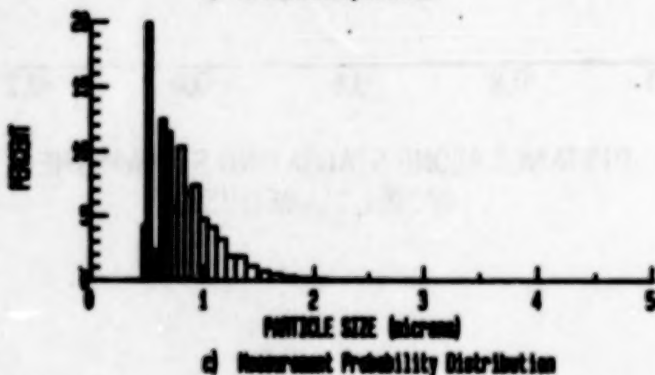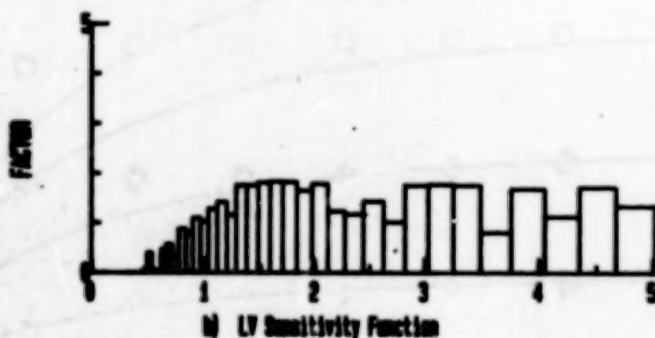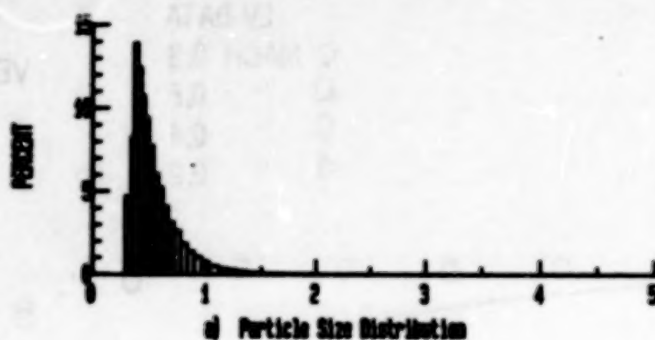
ELECTRON MICROSCOPE PHOTOGRAPH OF KAOLIN PARTICLES

The irregular shapes and various sizes of the kaolin particles are shown in the electron microscope photograph.
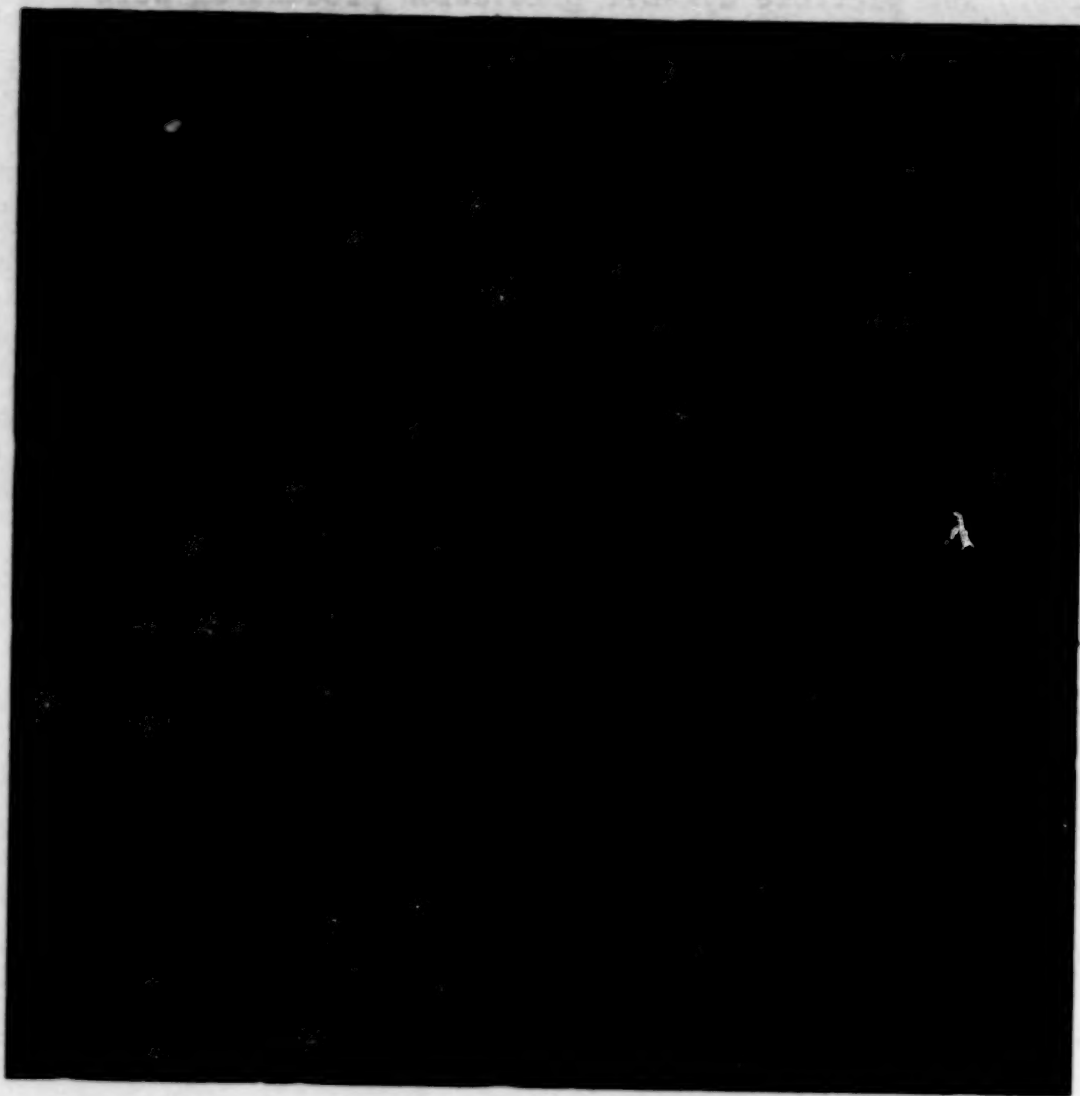
MEASUREMENTS ALONG THE STAGNATING STREAMLINE - MACH 0.8

The velocity measurements using kaolin along the stagnating streamline of the hemisphere-cylinder model at a tunnel setting of Mach 0.8 are presented in the figure along with the predicted gas velocity. The particle dynamic prediction procedures were used to determine that particles of 2.1 micrometers in diameter were the average kaolin particle size detected by the laser velocimeter.

DIFFERENCES BETWEEN PARTICLE DYNAMIC THEORY AND MEASUREMENTS

The differences between the measured velocities and the predicted velocities for a 2.1 micrometer diameter kaolin are illustrated in the figure as a function of distance along the stagnating streamline of the hemisphere-cylinder model at Mach 0.8.

O DIFFERENCE BETWEEN THEORETICAL PARTICLE VELOCITY (2.1 μ) AND MEASUREMENTS
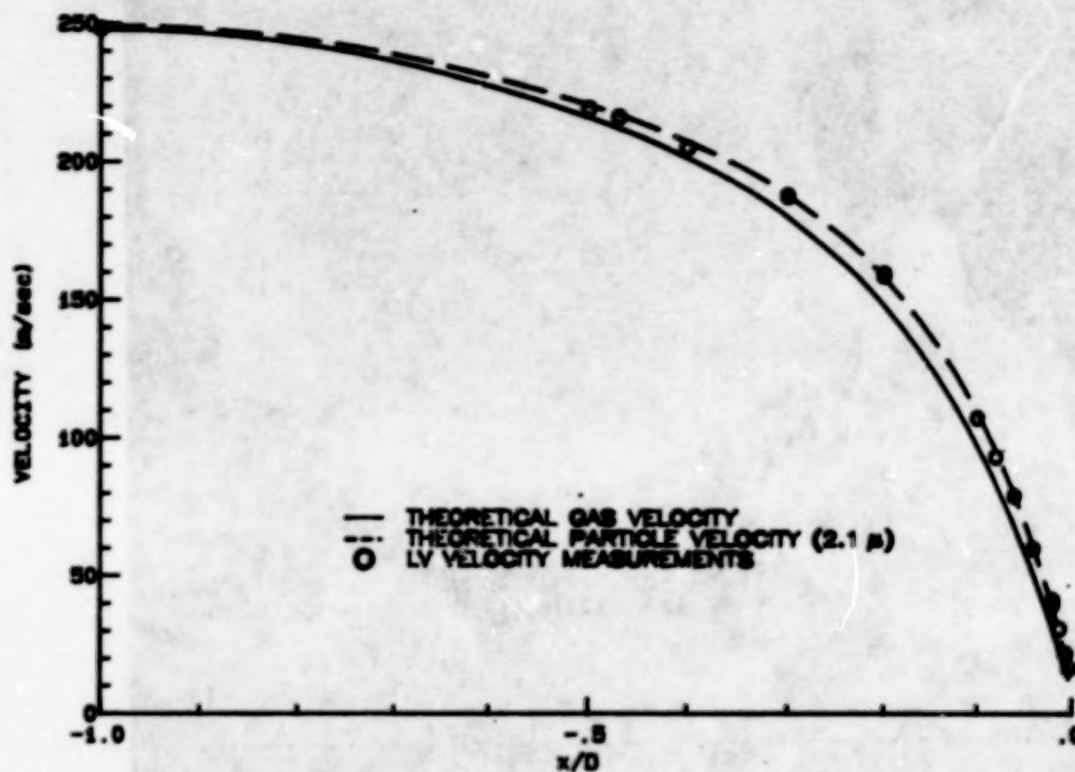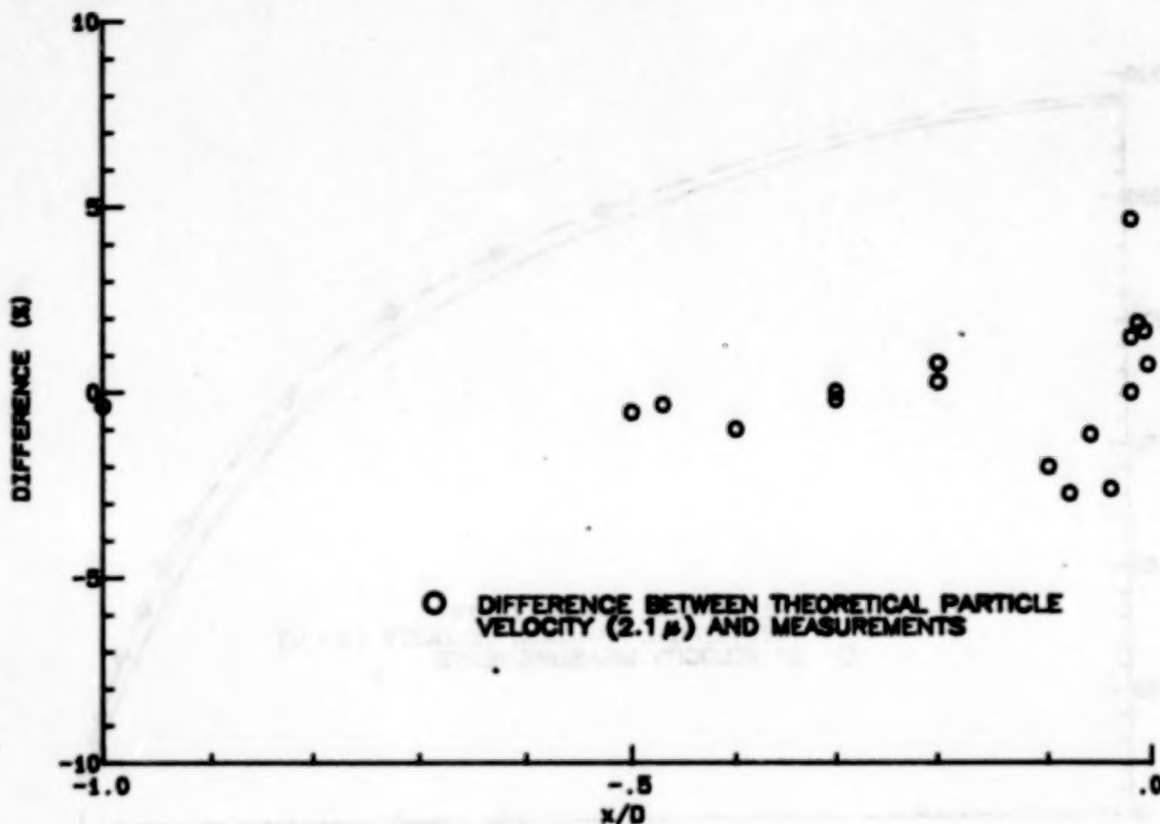
MEASUREMENTS ALONG THE STAGNATING STREAMLINE - MACH 1.0

The velocity measurements using kaolin along the stagnating streamline of the hemisphere-cylinder model at a tunnel setting of Mach 1.0 are presented in the figure along with the predicted gas velocity. The particle dynamic prediction procedures were used to determine that particles of 2.1 micrometers in diameter were the average kaolin particle size detected by the laser velocimeter.

DIFFERENCES BETWEEN PARTICLE DYNAMIC THEORY AND MEASUREMENTS

The differences between the measured velocities and the predicted velocities for a 2.1 micrometer diameter kaolin are illustrated in the figure as a function of distance along the stagnating streamline of the hemisphere-cylinder model at Mach 1.0.

MEASUREMENTS ALONG y/D = -0.533 AT MACH 1.0

The velocity measurements using kaolin along a line 0.533 model diameters below the stagnating streamline of the hemisphere-cylinder model at a tunnel setting of Mach 1.0 are presented in the figure along with the predicted gas velocity. The particle dynamic prediction procedures were used to determine that particles of 2.1 micrometers in diameter were the average kaolin particle size detected by the laser velocimeter.

O DIFFERENCE BETWEEN THEORETICAL PARTICLE
VELOCITY (2.1 μ) AND MEASUREMENTS
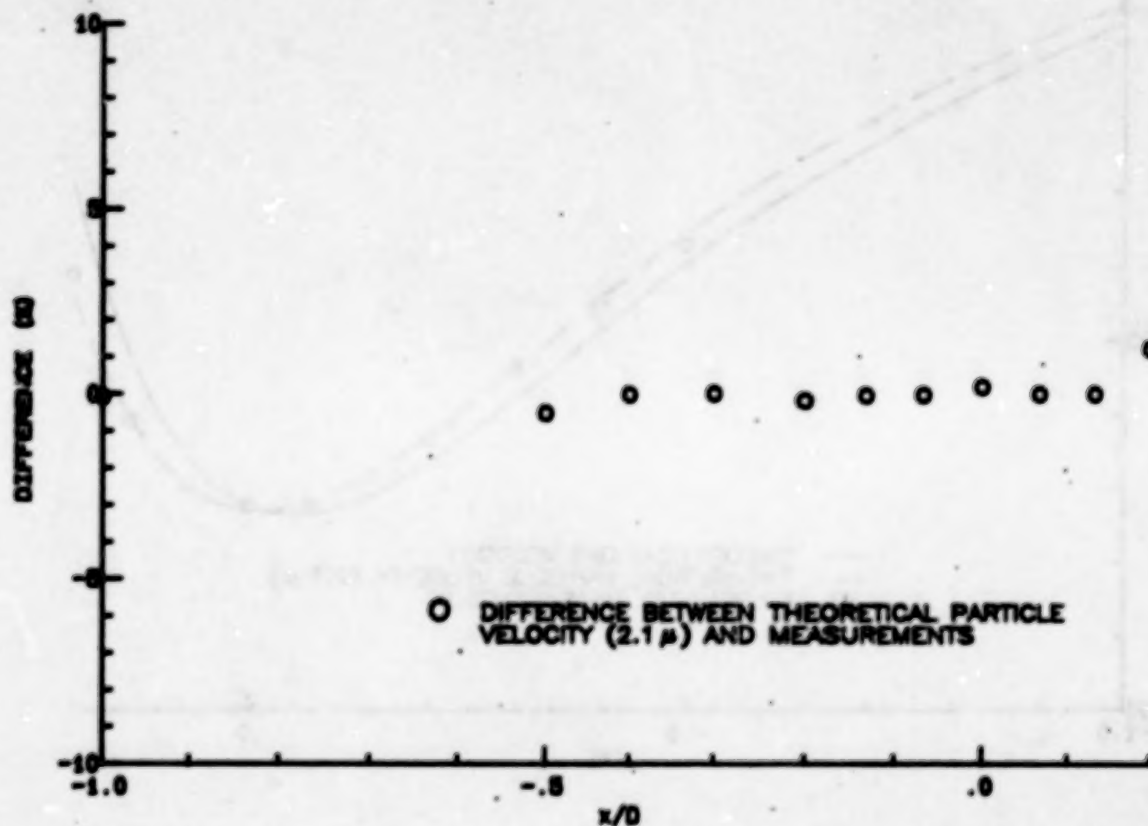
DIFFERENCES BETWEEN PARTICLE DYNAMIC THEORY AND MEASUREMENTS

The differences between the measured velocities and the predicted velocities for a 2.1 micrometer diameter kaolin are illustrated in the figure as a function of distance along the line 0.533 model diameters below the stagnating streamline of the hemisphere-cylinder model at Mach 1.0.

O DIFFERENCE BETWEEN THEORETICAL PARTICLE
VELOCITY (2.1 µ) AND MEASUREMENTS

x/D
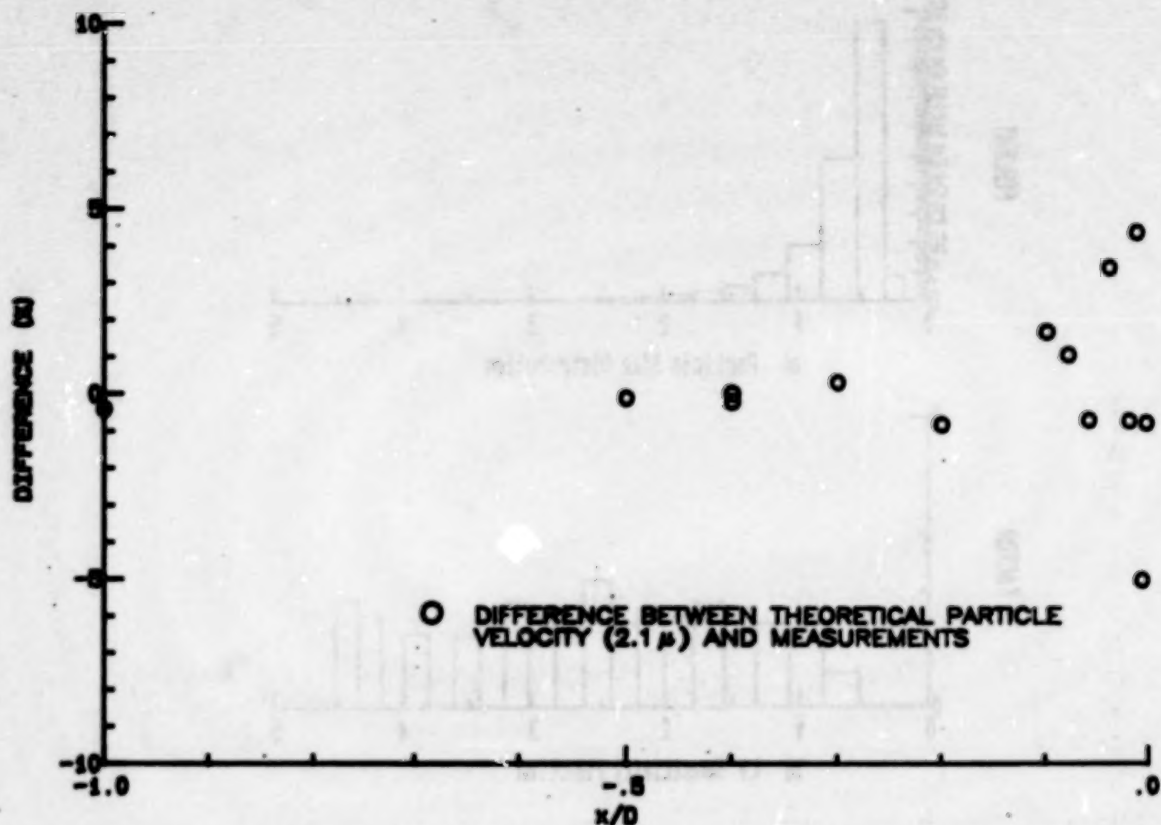
AERODYNAMIC PARTICLE SIZE ANALYSIS - KAOLIN

The particle size distribution measured with the aerodynamic particle size analyzer, laser velocimeter sensitivity function, and resulting particle size distribution of detectable particles for kaolin shown previously have been recalculated using the histogram widths for the optical particle size analyzer and are presented in the figure.
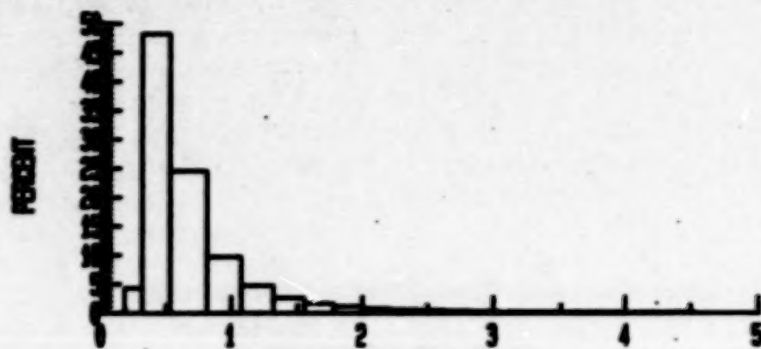
a) Particle Size Distribution
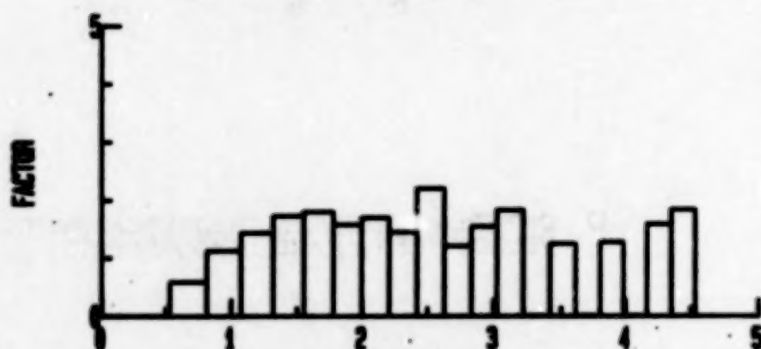
b) LV Sensitivity Function
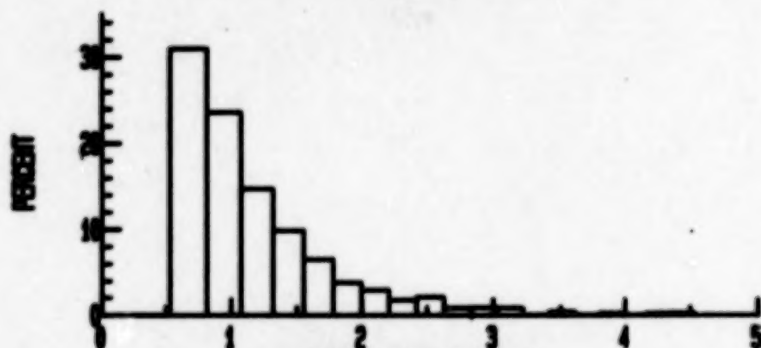
c) Measurement Probability Distribution

OPTICAL PARTICLE SIZE ANALYSIS - KAOLIN

Since the analysis of the predicted particle size distribution detectable by the laser velocimeter yielded an average particle of 0.78 micrometers in diameter and the velocity measurements obtained in the wind tunnel yielded an average particle of 2.1 micrometers in diameter, an optical particle size analyzer was used to remeasure the particle size distribution in the laboratory to determine the effect of the irregularly shaped particles on scattered light. The resulting measured distribution and the appropriate sensitivity function were combined to yield the detectable particle size distribution which had an average detectable particle size of 2.33 micrometers in diameter. Therefore the same particles have a different equivalent optical size from their equivalent aerodynamic size. This is most likely due to the greater optical effect from the random orientation of the irregularly shaped particles. Since the calculation of the laser velocimeter sensitivity function assumes a spherical particle, the effect of the irregularly shaped particles on the sensitivity of laser velocimeter cannot be predicted.

a) Particle Size Distribution

b) LV Sensitivity Function

PARTICLE SIZE (microns)

c) Measured Probability Distribution
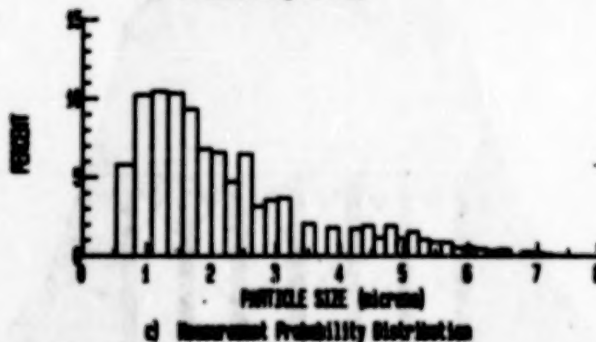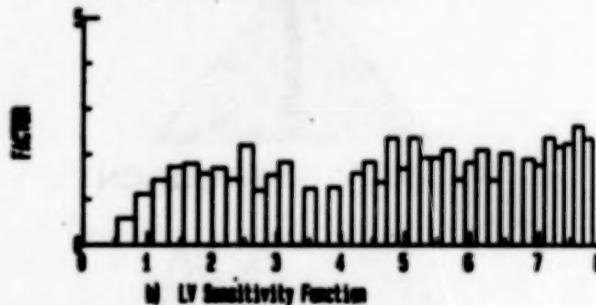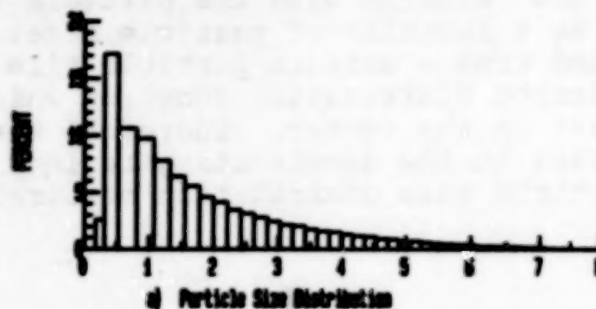
EFFECT OF PARTICLE DISTRIBUTION ON VELOCITY

As an aid in understanding the aerodynamic process involved
in the present situation, consider the effect on the laser
velocimeter measurements of the polydisperse particle
distribution within the decelerating flow field as a combination
of effects from each particle size. If the probability density
function of the gas velocity at a location in the decelerating
region is represented by the top figure, a uniformly
polydisperse particle size distribution (e.g., seven particle
sizes) within the flow would result in the probability density
function given in the lower figure. By considering the
polydisperse particle size distribution as being made up of
individual particles, one finds that a zero diameter particle
(i.e., the gas) would be found on the left or lowest velocity
side of the distribution in the lower figure. As the particle
size is increased, the resulting lag would shift its velocity
distribution to the right of the lower figure. Therefore the
resulting probability density function of particle velocity would
be determined by a convolution of the probability density
function of the gas velocity with the particle velocity lag
characteristics as a function of particle size. From the lower
figure it is found that a uniform particle size distribution
results in a velocity distribution function which is
approximately flat in the center. Therefore the measured
velocity histograms in the decelerating regions may be used to
estimate the particle size distribution measured by the laser
velocimeter.
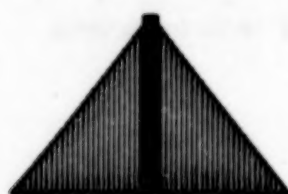
VELOCITY DISTRIBUTION
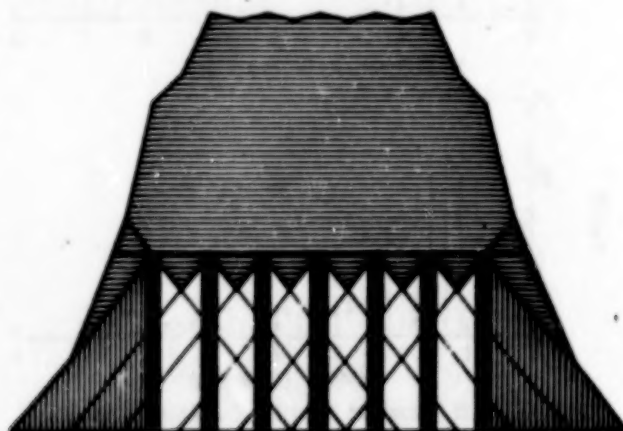
MEASURED HISTOGRAM

LV MEASUREMENT DERIVED PARTICLE SIZE - KAOLIN

At x/D distances of -0.4 and -0.5 the particle dynamic
predictions indicate that the spread in velocity due to particle
lag would be sufficient to segregate particle size provided the
turbulence intensity of the flow was low. The measurements at
these locations at Mach 1.0 indicated a "turbulence intensity" of
2 percent (including the spread due to particle lag). Assuming
the velocities within the measured histograms below the predicted
gas velocity were due to turbulence, the center portion of the
histogram may be isolated by removing these velocities along with
the corresponding high velocities (assuming symmetry). Each
velocity within the clipped histogram was equated to a particle
size based on the particle dynamic predictions to yield the
detected particle size distribution. By dividing this
distribution by the distribution obtained by the aerodynamic
particle size analyzer, the laser velocimeter sensitivity
function may be determined. It may be seen from the figure that
the resulting sensitivity function approximates the previous
sensitivity functions with the differences at the edges due to
statistical uncertainty. The average detectable particle for
this distribution was found to be 2.1 micrometers in diameter.

a) Particle Size Distribution

b) LV Sensitivity Function

PARTICLE SIZE (microns)

c) Measurement Probability Distribution

49
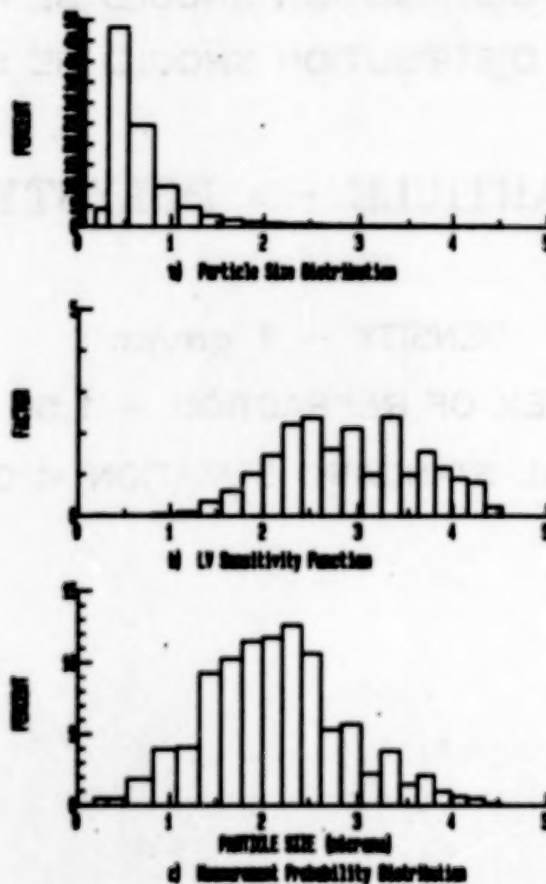
SEEDING RECOMMENDATIONS

The conclusion to be drawn from this investigation is that
solid particles with a symmetric and narrow distribution should
be used in laser velocimeter applications in high speed flows.
Solid particles maintain their size distributions within the flow
while liquids may be modified. A symmetric narrow distribution
is needed to minimize the spread in velocity within regions
containing velocity gradients thus increasing the accuracy of
turbulence intensity measurements. The specific gravity of the
material should be low but it should have a high index of refrac-
tion. The material which best fits these requirements is
polystyrene.

● SOLID PARTICLES

● DENSITY SHOULD BE LOW

● INDEX OF REFRACTION SHOULD BE HIGH

● DISTRIBUTION SHOULD BE NARROW

● DISTRIBUTION SHOULD BE SYMMETRIC

IDEAL PARTICLE -> POLYSTYRENE

DENSITY — 1 gm/cc

INDEX OF REFRACTION — 1.56

TYPICAL STANDARD DEVIATION < 0.1 μ

REFERENCES

1. Meyers, J.F., and Walsh, M.J.: "Computer Simulation of a Fringe Type Laser Velocimeter," Proceedings of Project Squid Workshop on the Use of the Laser Velocimeter for Flow Measurements, Purdue University, March 27-29, 1974.

2. Mie, G.: "Optics of Turbid Media," Ann. Phys., vol. 25, no. 3, 1908, pp. 377-445.

3. Adrian, R.J., and Earley, W.L.: "Evaluation of LDV Performance Using Mie Scattering Theory," Presented at the Symposium on Laser Anemometry, University of Minnesota, October 22-24, 1975.

4. Reyhner, T.A.: "Computation of Transonic Potential Flow About Three Dimensional Inlets, Ducts, and Bodies," NASA CR-3514, 1982.

5. Walsh, M.J.: "Influence of Particle Drag Coefficient on Particle Motion in High-Speed Flow with Typical Laser Velocimeter Applications," NASA TN D-8120, 1976.

PARTICLE SIZE DISTRIBUTIONS OF SEVERAL
COMMONLY USED SEEDING AEROSOLS

F. L. Crosswy
Calspan Corporation/AEDC Division
Arnold Air Force Station, Tennessee

INTRODUCTION

The classical dilemma in wind tunnel laser velocimetry is the necessity to provide flow entrained particles large enough for detection by the laser velocimeter (LV) system yet small enough to closely follow the gas velocity gradients. The number density of proper size intrinsic particles is oftentimes inadequate for productive LV operations, especially in closed-circuit wind tunnels, so that particle seeding of the flow is required. An ideal aerosol generator for wind tunnel seeding purposes can be defined as one which has the following characteristics:

a. monodispersed particle size distribution
b. selectable particle size
c. controllable particle production rate
d. particles with large scattering cross section
e. particles with low mass density
f. non-toxic, non-contaminating and inert aerosol
g. long particle lifetime in the test environment
h. seed material readily available and reasonably priced

Several different processes can be exploited for seed particle generation purposes. These include:

1. fluidization of solid particles
2. atomization of liquids
3. vaporization/condensation of liquids
4. atomization of solid particle suspensions
5. atomization of solid material solutions
6. chemical reaction
7. combustion

In practice, all of these processes fall short of the ideal, with monodispersity being one of the more important but one of the more elusive requirements.

The particle size characteristics of several commonly used seeding aerosols were recently studied at AEDC. In general, undesirable polydispersed particle size characteristics were observed. However, reasonably narrow size distributions were produced by the atomization of polystyrene spheres and by the vaporization/condensation of dioctyl phthalate (DOP).

The purpose of this paper is to provide brief descriptions of the aerosol generation devices and aerosol particle sizing system used in this study and to provide a catalog of particle size distributions for the aerosols studied to date.

FLUIDIZED BED SEEDER

The apparatus used at AEDC to produce solid particle aerosols at low pressure (<100 psi) is shown in Figure 1. This device is referred to as a mechanically agitated, fluidized bed seeder. Solid particles in powder form are continuously stirred by a rotating hollow tube assembly. Carrier gas, usually air or nitrogen, flows through the tube assembly and jets into the powder through small holes to create the solid particle aerosol. Studies to date include aerosols derived from various powders of aluminum oxide, magnesium oxide and titanium dioxide.
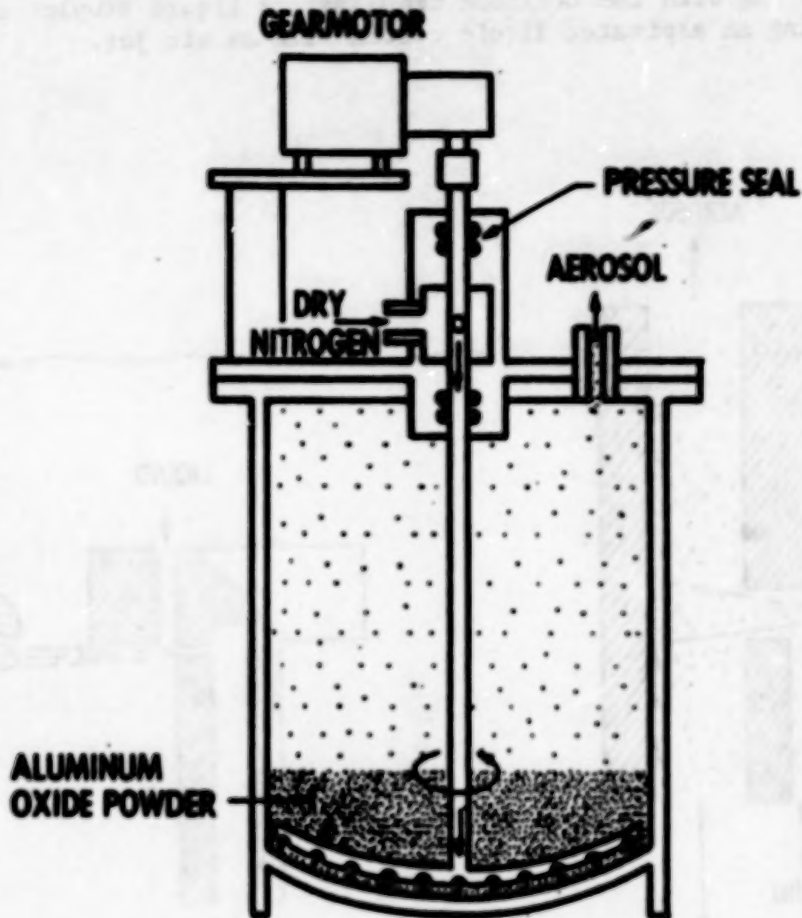
Figure 1. Fluidized Bed Seeder

LIQUID ATOMIZERS

Two types of liquid atomizers are often used to create liquid droplet aerosols for laser velocimetry. One of these, the Collison nebulizer (Ref. 1), is shown in Figure 2. A jet of air or other gas is used to shear a column of flowing liquid to create a large number of small liquid droplets. The larger droplets are usually eliminated by impact upon a solid surface just downstream of the air jet. The liquid column can be either pumped or aspirated into the air jet.

The second type of atomizer is the Laskin nozzle, a form of which is shown in Figure 3 (Ref. 2). As with the Collison nebulizer, a liquid droplet aerosol is produced by shearing an aspirated liquid column with an air jet.
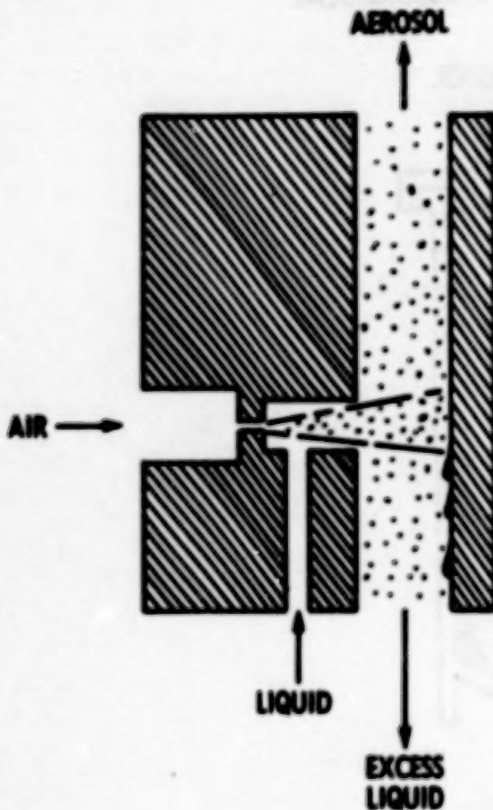
Figure 2.   Collison Nebulizer   Figure 3.   Laskin Nozzle
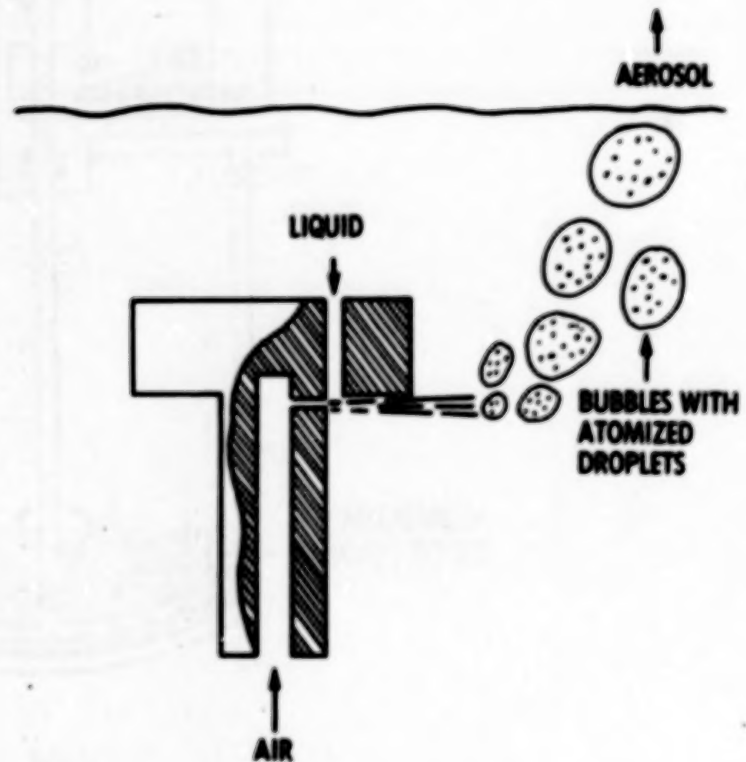
VAPORIZATION/CONDENSATION SEEDER

Condensation of a vapor homogeneously dispersed in a carrier gas can yield a narrow size distribution of condensate particles. In addition, control of the mass fraction of vapor with respect to the carrier gas affords some control over the size of the condensate particles. These two principles are exploited in the vaporization/condensation seeder shown in Figure 4.

The atomizer in Figure 4 can be either the Laskin nozzle type or the Collison nebulizer type. The atomizer assembly includes a provision for introducing dilution carrier gas as a means for varying the vapor mass fraction. The polydispersed aerosol from the atomizer is passed through a 5-ft long, 2-in. diameter stainless steel tube. The top part of the tube is heated by an electrical heater tape capable of temperatures up to 900°F. The atomizer aerosol droplets are vaporized in this section of the tube. In the lower part of the stainless tube the vapor condenses to form an aerosol with a more uniform particle size distribution than that originally produced by the atomizer.

The AEDC vap/con seeder is based upon fundamental information provided in the scientific (Ref. 3) and commercial (Ref. 4) literature. However, the high operating pressure (1000 psi) and high particle production rate capabilities are based upon design condensations provided by Yanta (Ref. 2).
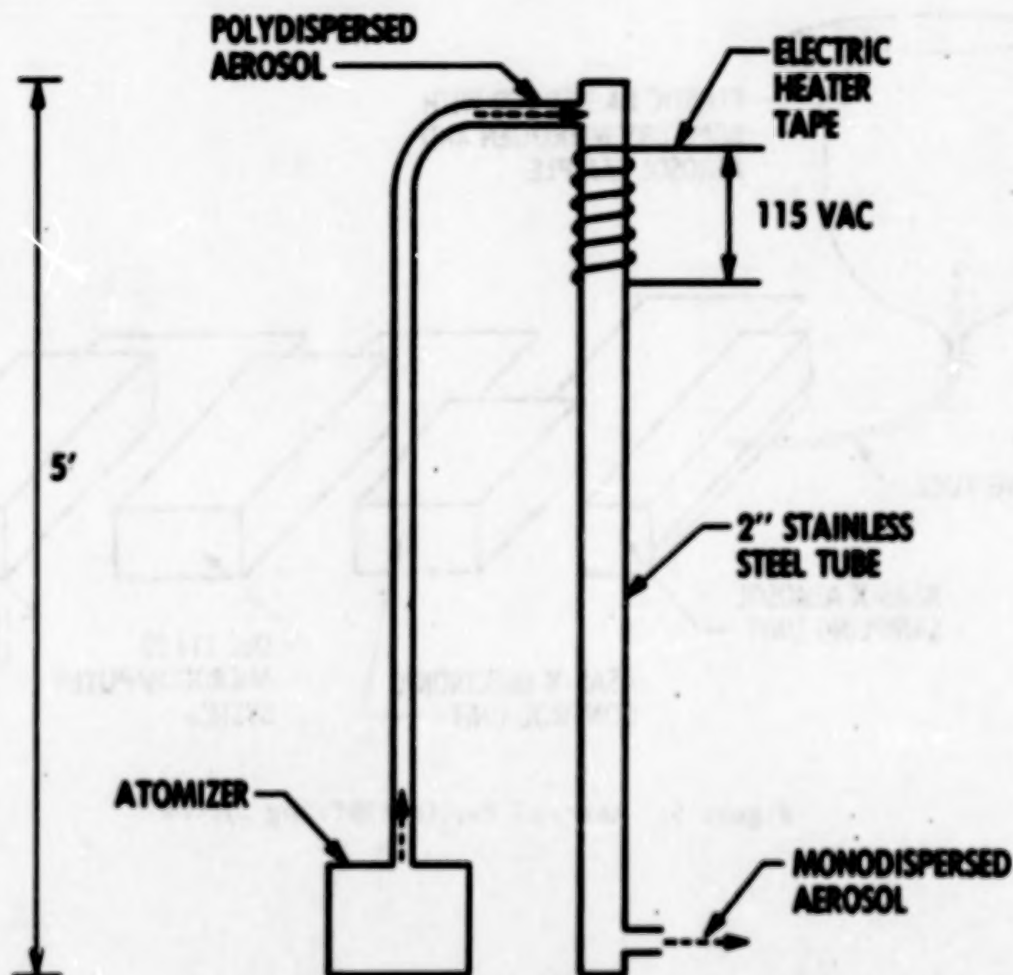
Figure 4. Vaporization/Condensation Seeder

AEROSOL PARTICLE SIZING SYSTEM

The system shown in Figure 5 was used to determine the particle size characteristics of the various seeding aerosols. This system consists of an ASAS-X particle sizer interfaced to a DEC 11/23 microcomputer system and Tektronix 4631 Hard Copy Unit. The ASAS-X is a laser light scattering device produced by Particle Measuring Systems, Inc. The particle diameter range from 0.09-3.0 microns is covered by four fifteen-bin instrument ranges of 0.09-0.195 microns, 0.15-0.3 microns, 0.24-0.84 microns and 0.6-3.0 microns. The ASAS-X is calibrated with precisely sized latex spheres so that particle size measurements, even for irregularly shaped particles or particles with a complex index of refraction, are in terms of equivalent latex spheres. The DEC 11/23 was programmed to display and tabulate the high resolution data from each of these four instrument ranges or to provide the wide-range, quick-look histogram data used in this paper.

The test aerosol was introduced into a large plastic bag (6 ft^3) which had previously been purged and filled with bone-dry nitrogen. Background particle counts using this scheme were typically less than 50, while aerosol particle counts were typically in the range from 50,000 to 800,000 counts. Although rarely necessary, the DEC 11/23 was programmed to subtract the background count from a test aerosol count.

PLASTIC BAG FILLED WITH BONE-DRY NITROGEN AND AEROSOL SAMPLE

AEROSOL SAMPLING TUBE

ASAS-X AEROSOL SAMPLING UNIT

ASAS-X ELECTRONIC CONTROL UNIT

DEC 11/23 MICROCOMPUTER SYSTEM

HARD COPY UNIT

Figure 5. Aerosol Particle Sizing System

METAL OXIDE POWDER AEROSOLS

Because of their high melting points, various metal oxide powders are oftentimes used for seeding high temperature flows. Table 1 compares the properties of several commonly used metal oxides. The MgO is attractive for its high melting temperature, the T_1O_2 for its large index of refraction and the Al_2O_2 polishing powder because it is specified as being nominally sized.

Table 1. Physical Properties of Metal Oxide Powders

Material	Index of Refraction	Density, (gm/cc)	Melting Temperature, ^oF
M_gO	1.74	3.58	5072
Al_2O_3	1.76	3.96	3660
T_1O_2	2.6-2.9	3.7-4.1	3326

Alumina Powder Aerosols

The alumina (Al_2O_3) polishing powders are of interest for possible use in LV seeding applications since the manufacturer's specifications include a nominal particle size. Figure 6 shows the particle size characteristics of an aerosol derived from 1.0 micron alumina polishing powder. Note that no peak occurs at 1.0 micron while many agglomerates larger than 1.0 micron are evident as well as a large number of particles smaller than 1.0 micron. A polydispersed aerosol like this is undesirable for LV seeding purposes since the large agglomerates will not closely follow the flow velocity gradients while the very small particles, below the LV system detection limit, can only contribute spurious scattered light.

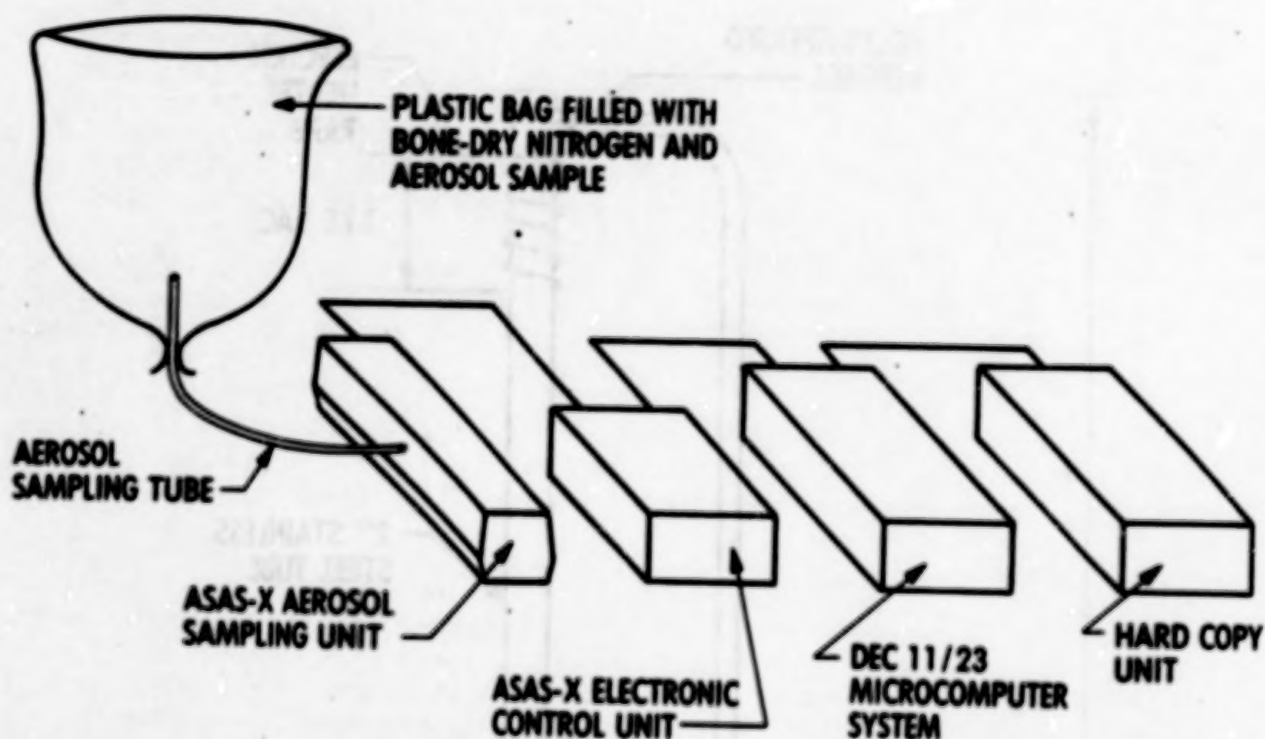The particle size spectrum for 0.3 micron alumina polishing powder is shown in Figure 7. The agglomerate problem is not as bad as for the 1.0 micron alumina powder but the small particle problem is worse. Note, once again, that the size spectrum does not peak at the specified particle size.

The spectrum for 0.05 micron alumina polishing powder is shown in Figure 8. If individual particles are no larger than the 0.05 micron manufacturer's specification, then the entire spectrum within the range of the ASAS-X must be made up of agglomerates.

The "Super-Finish" alumina polishing powder is a relatively new product. The 0.3 micron version of this powder was recently evaluated for LV seeding purposes since the manufacturer's specifications indicate that this product exhibits a lessened tendency to form agglomerates compared to the standard polishing powder. However, a comparison of Figure 9 with Figure 7 shows that, for aerosol generation purposes at least, the Super-Finish powder actually has a greater tendency to form agglomerates. On the other hand, the Super-Finish powder exhibits a lower percentage of particles at the small particle end of the size spectrum and it also has a histogram peak in the vicinity of the specified 0.3 micron particle size.

The search for means to reduce the percentage of agglomerates in powder aerosols includes the use of additive flow agent materials. One flow agent that has been reported (Refs. 5-6) to be effective in reducing agglomerates in metal oxide powder aerosols is a hydrophilic material described as a flame phase silica. This

material is widely used to enhance the bulk flow properties of powdered foods, industrial chemicals and pharmaceuticals (Ref. 7). A commercially available but proprietary mixture of 1.0 micron alumina polishing powder and silica flow agent was obtained for evaluation. The aerosol particle size characteristic is shown in Figure 10. Comparison of this particle size characteristic with that of the 1.0 micron alumina without flow agent (Fig. 6) shows that this particular flow agent preparation is, at best, only marginally effective in reducing aerosol agglomerates. A mixture of 0.7 micron alumina and silica powders was obtained from the same commercial source and evaluated. The size spectrum is shown in Figure 11. Again, the agglomerate content is objectionable.

A mixture of 1.0 micron alumina polishing powder and 0.5 percent by weight of silica flow agent with a nominal particle size of 0.007 microns was prepared at AEDC and tested. The aerosol particles size characteristic was found to be virtually identical to that of Figure 10. A 5-percent mixture of the silica flow agent and 0.3 micron alumina powder was also prepared and tested. This mixture ratio was entirely unsatisfactory since an increase in agglomerates was observed rather than a decrease.

TOTAL PARTICLE COUNT = 63223
SAMPLE TIME - 40 SECONDS
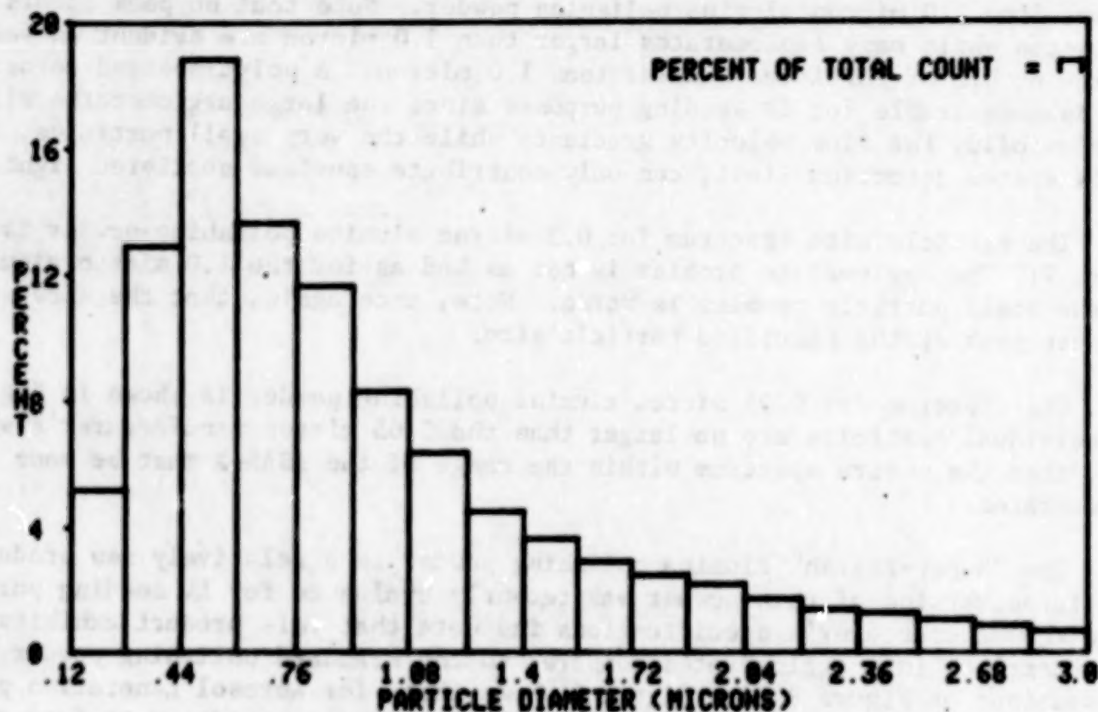
Figure 6. Alumina Polishing Powder, Nominal Size - 1.0 Micron

60

Figure 7.   Alumina Polishing Powder, Nominal Size - 0.3 Micron

TOTAL PARTICLE COUNT = 310903
SAMPLE TIME - 40 SECONDS
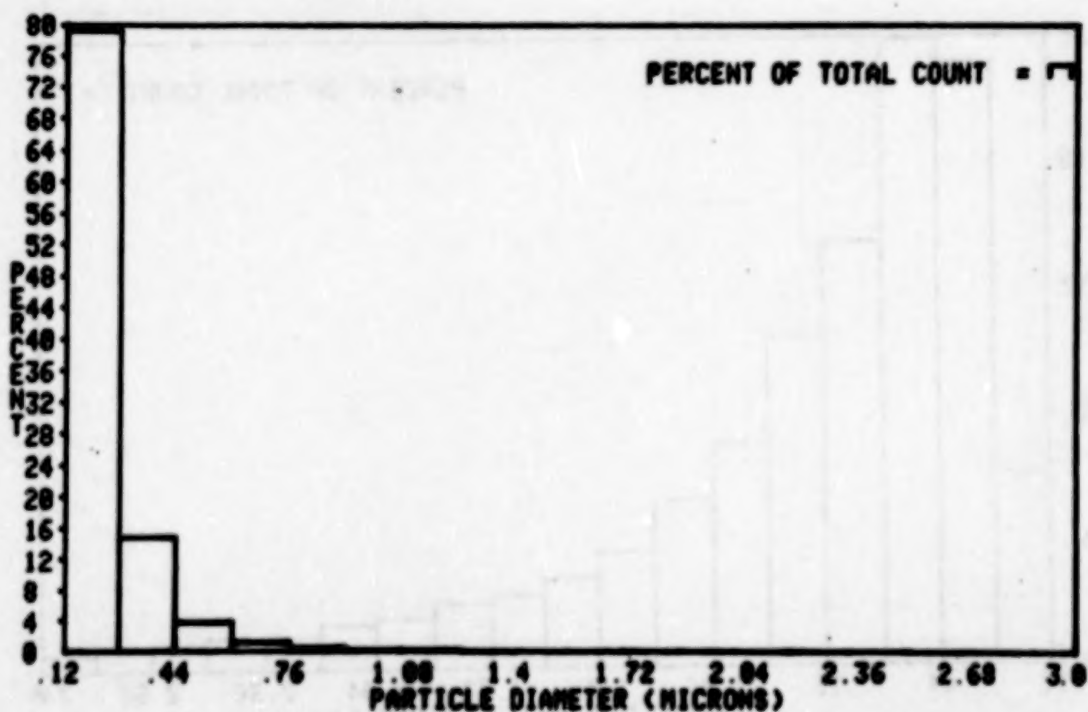
Figure 8.   Alumina Polishing Powder, Nominal Size - 0.05 Micron

61
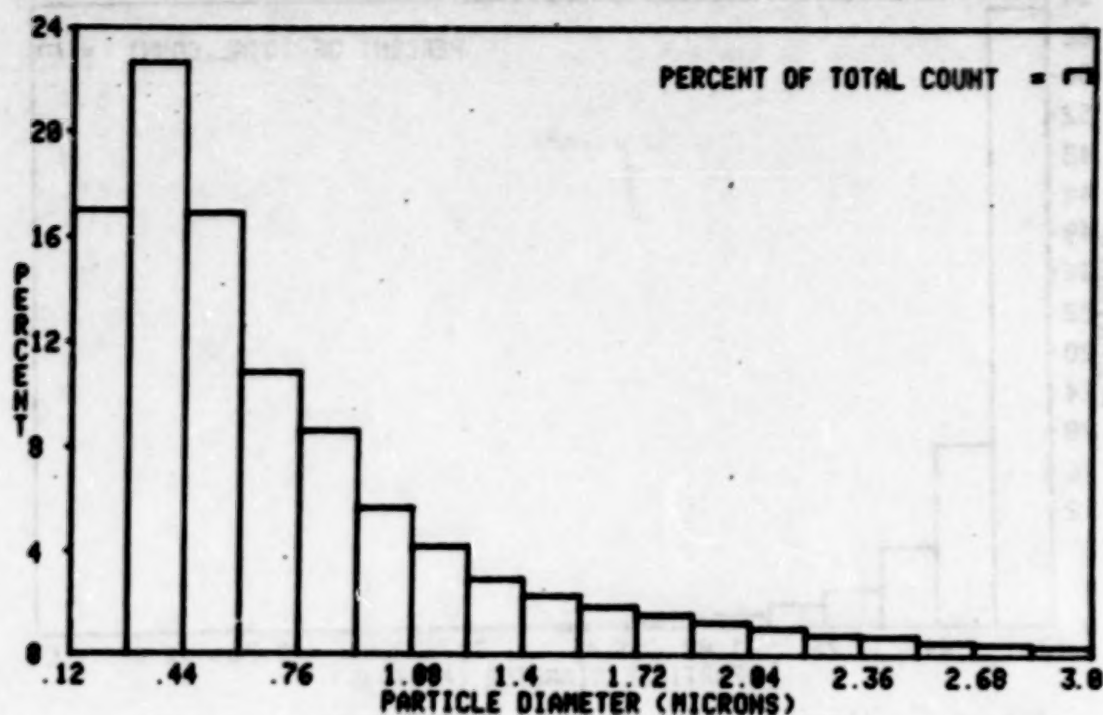
Figure 9.   Super-Finish Alumina Polishing Powder,
Nominal Size - 0.3 Micron
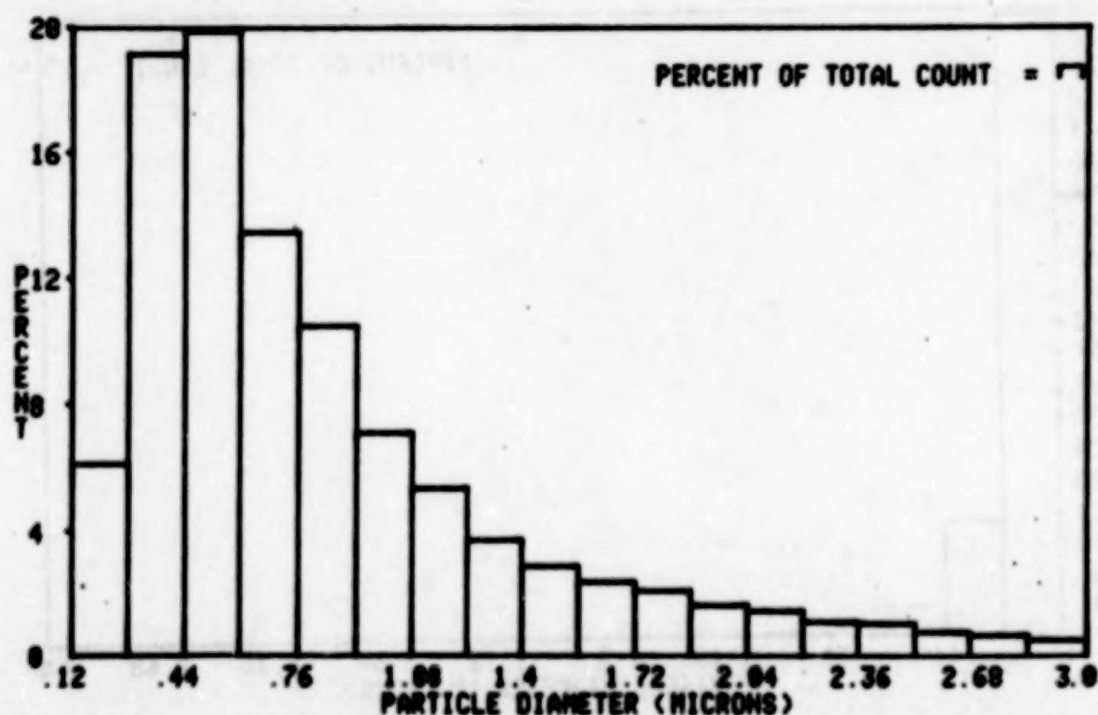
Figure 10.   Alumina Polishing Powder With Silica Flow Agent,
Nominal Alumina Particle Size - 1.0 Micron
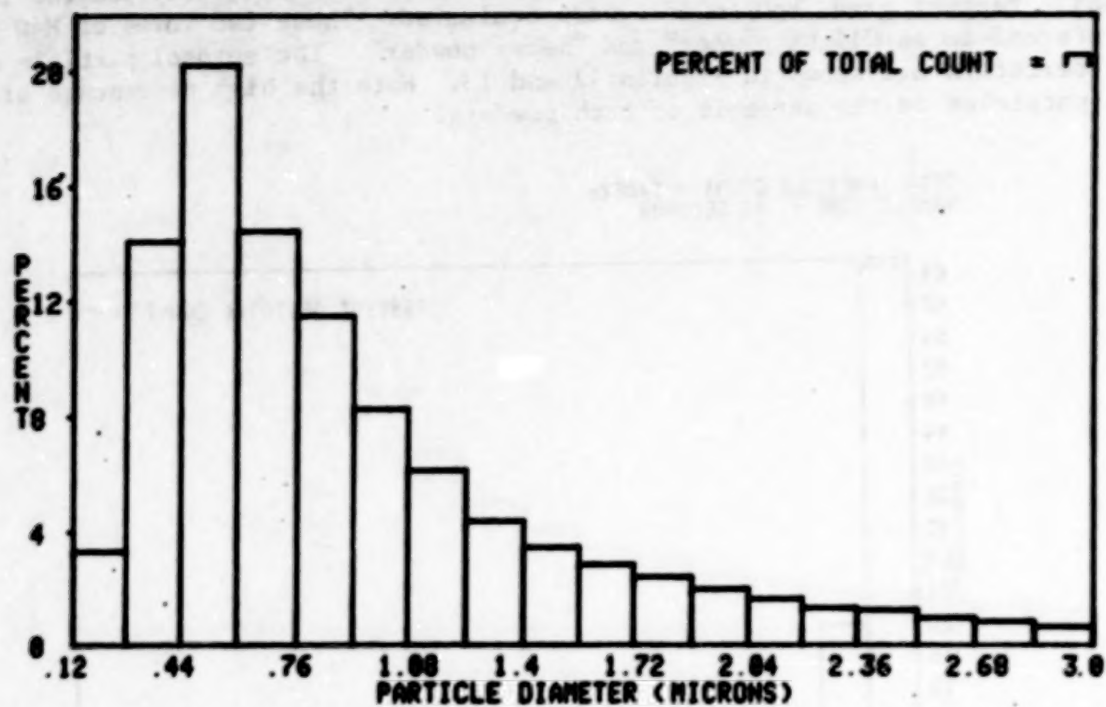
Fig. 11. Alumina Polishing Powder With Silica Flow Agent,
Nominal Alumina Particle Size – 0.7 Micron

Magnesium Oxide Powder Aerosols

For this study, no magnesium oxide (MgO) powder could be found for which the manufacturer could quote a nominal particle size. Therefore, only the two readily available reagent grade MgO powders were evaluated. These two forms of MgO powder are referred to as "light powder" and "heavy powder". The aerosol particle size characteristics are shown in Figures 12 and 13. Note the high percentage of very small particles in the aerosols of both powders.

TOTAL PARTICLE COUNT = 140624
SAMPLE TIME - 40 SECONDS
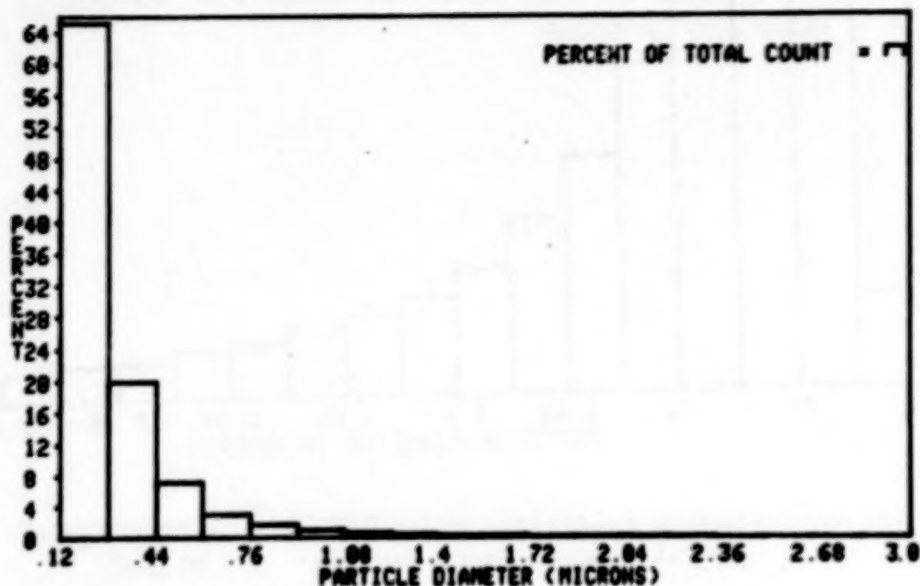
Fig. 12. MgO Reagent Grade Light Powder

TOTAL PARTICLE COUNT = 107621
SAMPLE TIME - 39 SECONDS
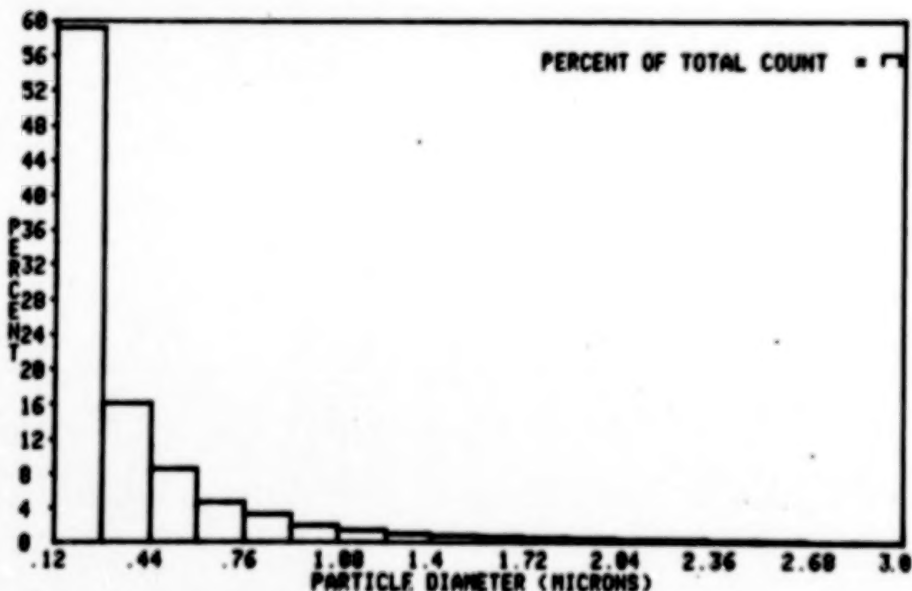
Fig. 13. MgO Reagent Grade Heavy Powder

Titanium Dioxide Powder Aerosols

Several different titanium dioxide (TiO_2) powders were acquired for which the manufacturer furnished particle size specifications. These powders are produced for use as pigment additives for paint, paper, and plastics. The particle size range is quoted as 0.1-5.0 microns with most particles being in the range of 0.25 micron. The aerosol particle size spectrums for two of these powders are shown in Figures 14 and 15. The particle size spectrum for the plastic pigment powder (Fig. 14) was found to exhibit a peak in the size range 0.44-0.6 microns whereas the paint pigment powder produced an aerosol with a size spectrum peak in the same size range plus a large percentage of agglomerates and/or large particles. The specified particle size of 0.25 microns is not dominant in the aerosol particle size spectrum of either powder.

TOTAL PARTICLE COUNT = 341687
SAMPLE TIME - 40 SECONDS

PERCENT OF TOTAL COUNT = ☐
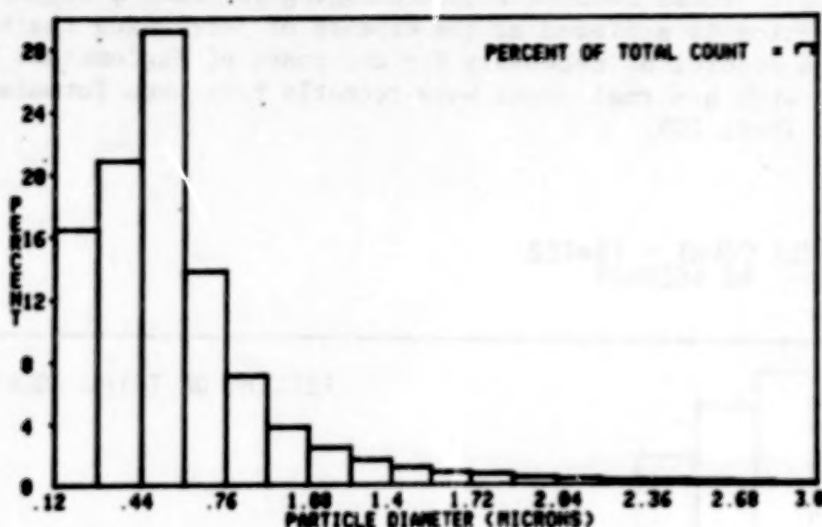
Fig. 14. TiO_2 Plastic Pigment Powder

TOTAL PARTICLE COUNT = 77636
SAMPLE TIME - 40 SECONDS

PERCENT OF TOTAL COUNT = ☐
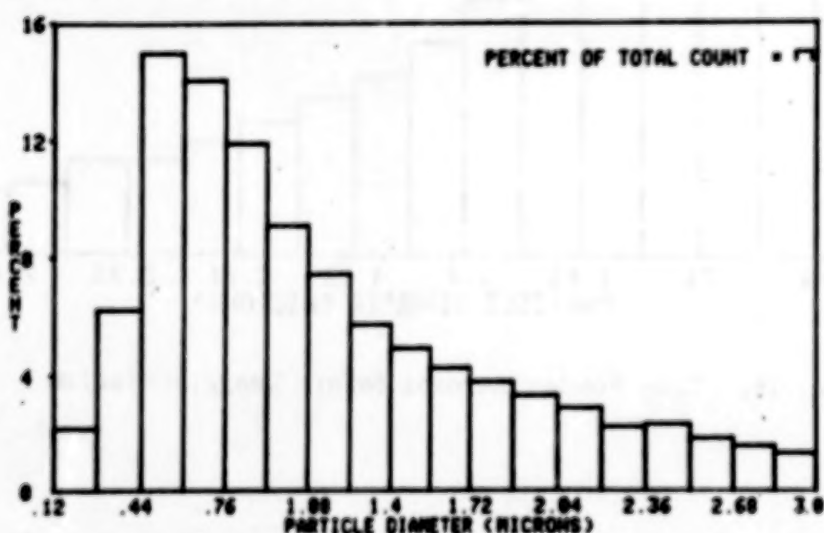
Fig. 15. TiO_2 Paint Pigment Powder

Aerosol Flow Conditioning

The ever-present tendency of submicron particles to form agglomerates and the undesirable presence of very small particles have led to the use of various aerosol flow conditioning schemes in pursuit of the ideal mondispersed size distribution. Cyclone type separators have been reported (Refs. 6 and 8) as being useful for size fractionation of LV seeding aerosols. Marteney (Ref. 9) has described a dispensing nozzle with near-sonic conditions in the nozzle passage which was shown to be useful for breaking up agglomerates. The use of sonic flow in an array of 25 x 300 micron slits in the wall of a tube has been reported for breaking up agglomerates. A simple, circular sonic orifice was recently evaluated at AEDC for breaking up the metal oxide powder agglomerates. A TiO_2 powder size spectrum is shown in Figure 16 just before attachment of the sonic orifice assembly to the aerosol generator (Fig. 1). The particle size spectrum after deagglomeration by the sonic orifice is shown in Figure 17. These results are encouraging for such a simple procedure. However, deagglomeration is achieved at the expense of increasing the small particle number density. The conditions necessary for the onset of agglomerate breakup by aerosol interaction with a normal shock wave recently have been formulated by Forney and McGregor (Ref. 10).
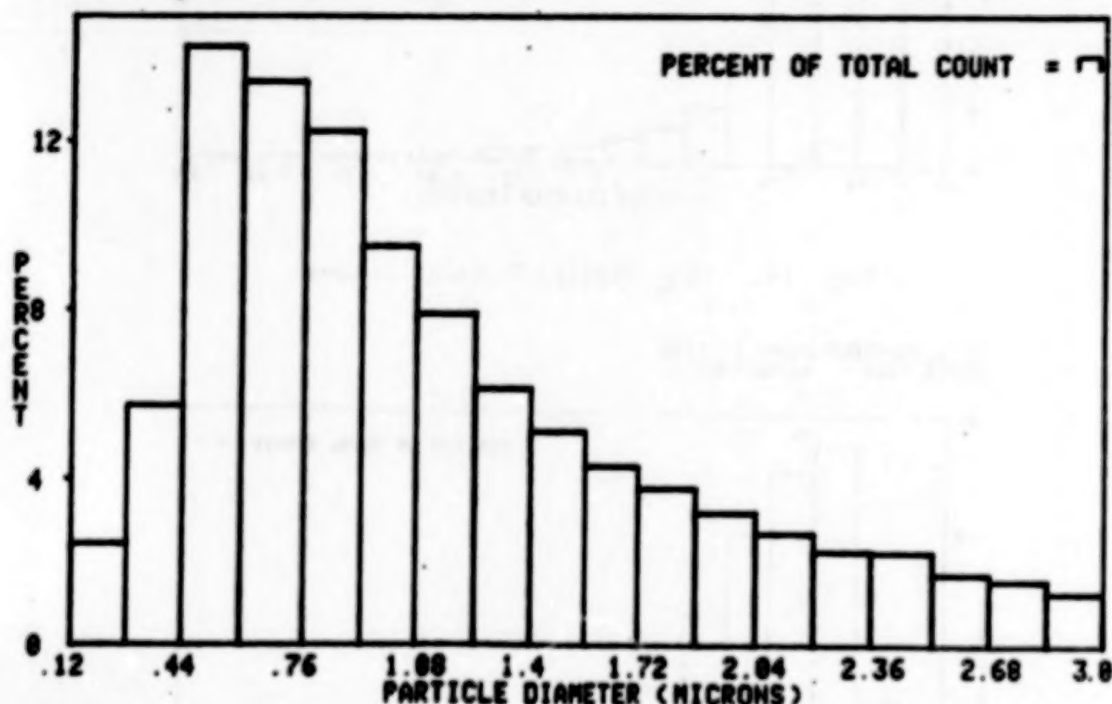
Fig. 16. TiO_2 Powder Aerosol Before Deagglomeration
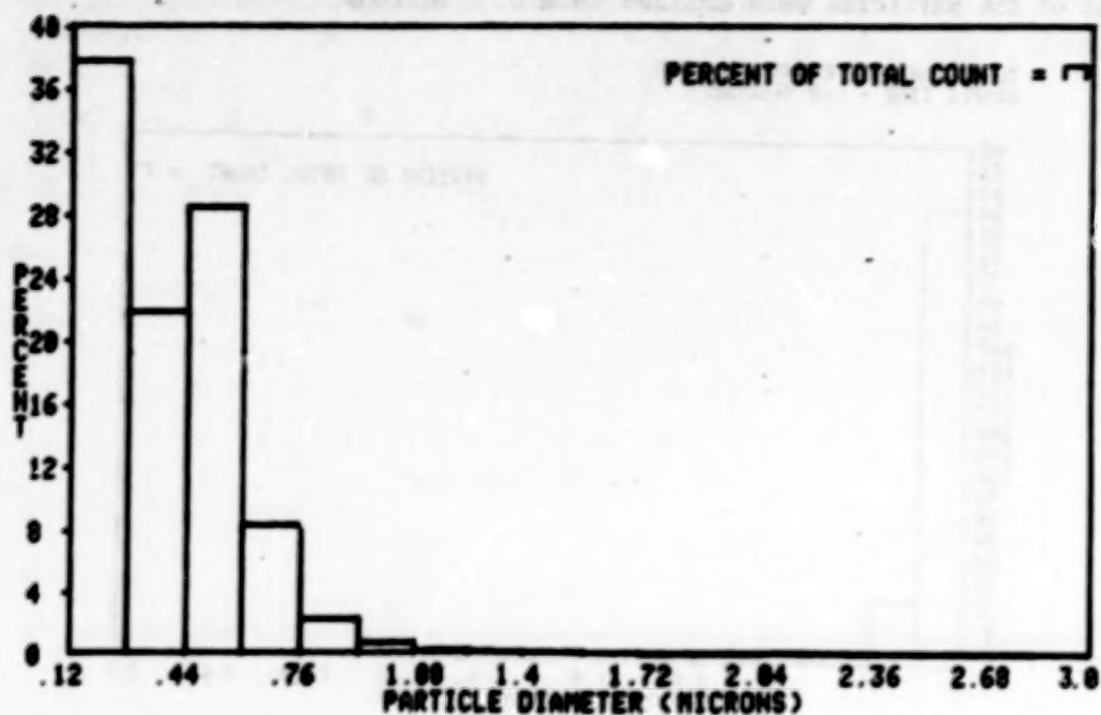
Fig. 17. TiO$_2$ Powder Aerosol After Deagglomeration by a Sonic Orifice

The particle size characteristics of aerosols produced by burning cigarette tobacco and incense are shown in Figures 18 and 19. For the cigarette smoke, 94 percent of the particles were smaller than 0.32 microns. For the incense smoke, 97 percent of the particles were smaller than 0.32 microns.
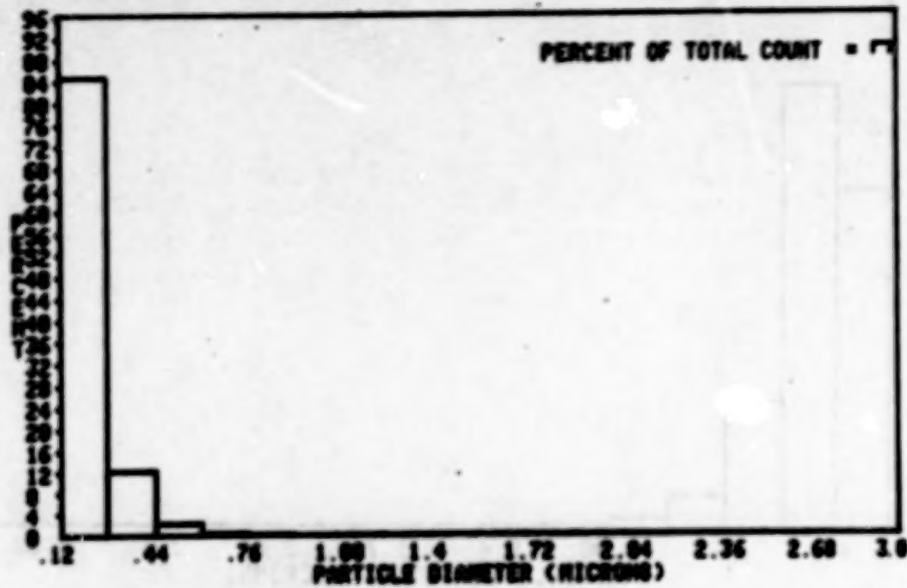
Fig. 18. Cigarette Smoke
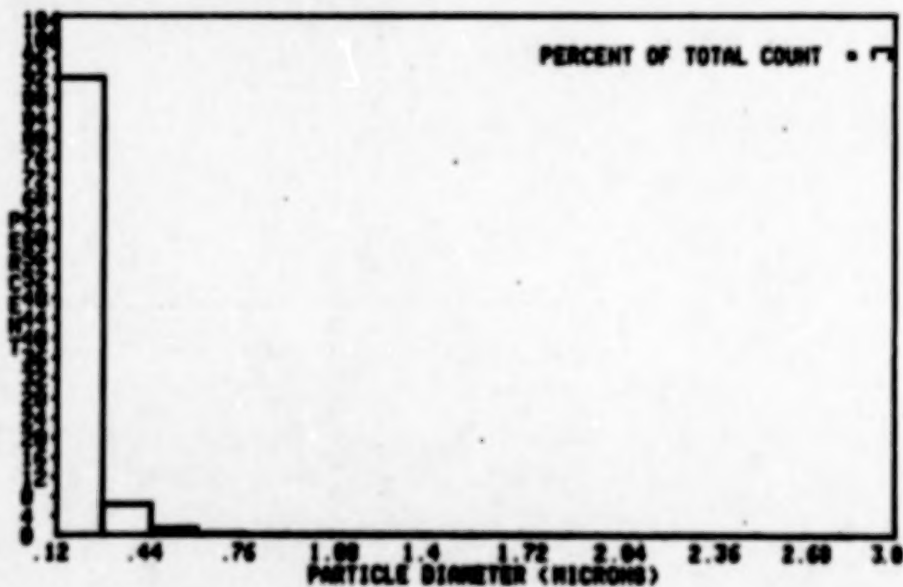
Fig. 19. Incense Smoke

AEROSOLS BY LIQUID ATOMIZATION

Liquid atomizers are simple to operate and produce stable particle number densities. Unfortunately, however, those tested to date at AEDC produce high percentages of very small particles.

The Laskin Nozzle

The particle size distribution for dioctyl phthalate (DOP) aerosol as generated by the Laskin nozzle is shown in Figure 20. The DOP droplets are seen to be polydispersed with a preponderance of small particles.

The Collison Nebulizer

The size spectrum for DOP in the Collison nebulizer is shown in Figure 21. The percentage of small particles is seen to be larger than the Laskin nozzle and interestingly, this spectrum is similar to that of the 0.3 micron alumina powder (Fig. 7). The size spectra for olive oil and soybean oil were also found to be similar to that of Figure 21.

TOTAL PARTICLE COUNT = 856984
SAMPLE TIME - 39 SECONDS
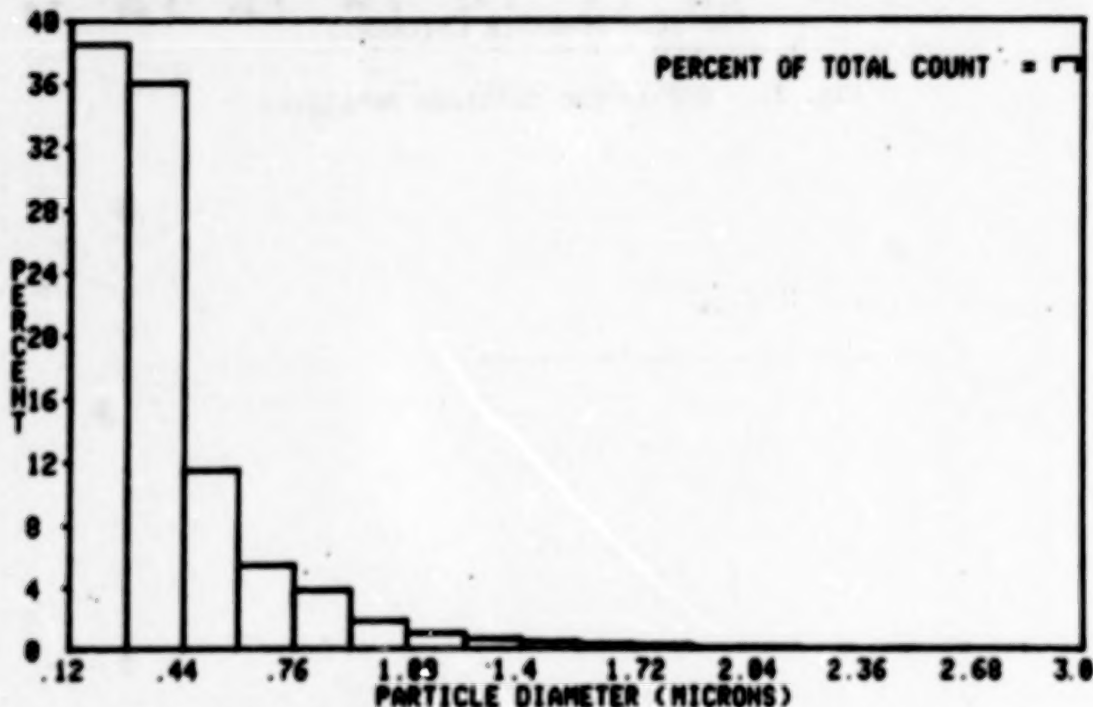
Fig. 20.   DOP in the Laskin Nozzle
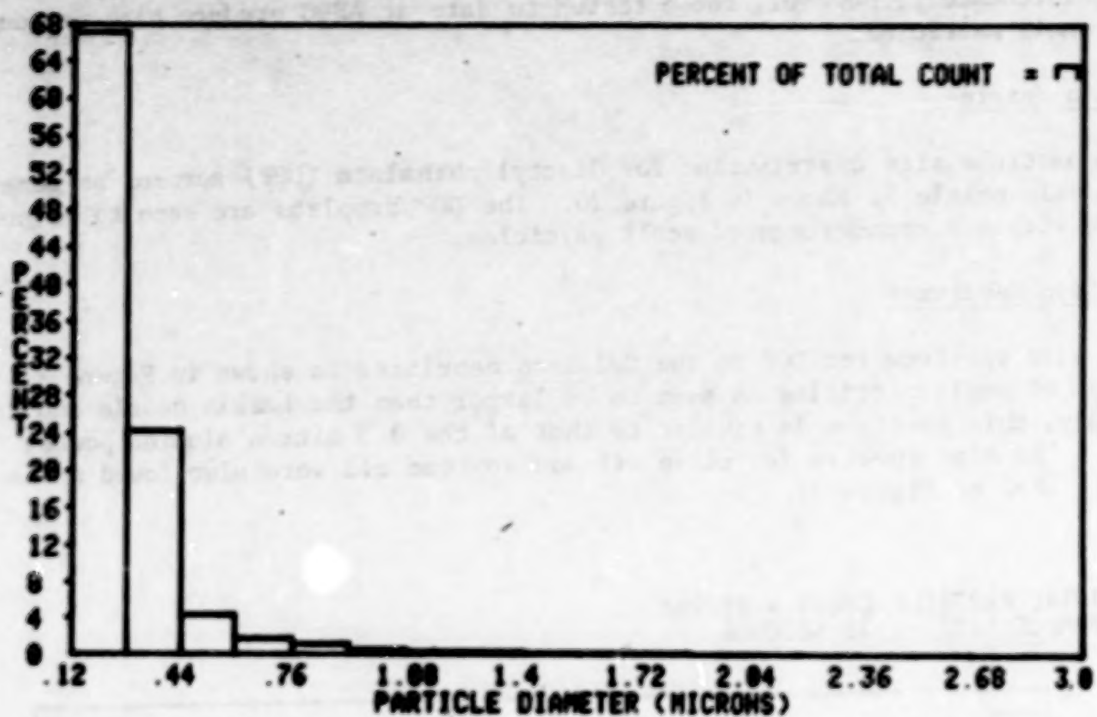
Fig. 21. DOP in the Collison Nebulizer

ATOMIZATION OF SOLID PARTICLE SUSPENSIONS

A notable example of this technique for generating a seeding aerosol is the atomization of a water or methanol suspension of latex spheres. With a sufficiently dilute suspension, most of the atomizer droplets will evaporate to leave a single latex sphere. The analytical, reference grade, latex spheres are attractive because of their extremely narrow size distribution. However, this product is prohibitively expensive for LV seeding purposes. A reasonably priced product is the base material used in latex paint. The manufacturer's specified particle size range is 0.35 - 0.55 microns. A sample of this material was prepared by mixing 5 parts by volume of the latex sphere suspension with 95 parts water. The Collison nebulizer was then used to atomize this suspension. The resultant aerosol produced the particle size distribution shown in Figure 22. An identical distribution was obtained with a 5/95 mixture of latex suspension and methanol. The peak in the distribution is coincident with the manufacturer's specification. However, the overall distribution is disappointingly polydispersed.

TOTAL PARTICLE COUNT = 20405
SAMPLE TIME - 40 SECONDS
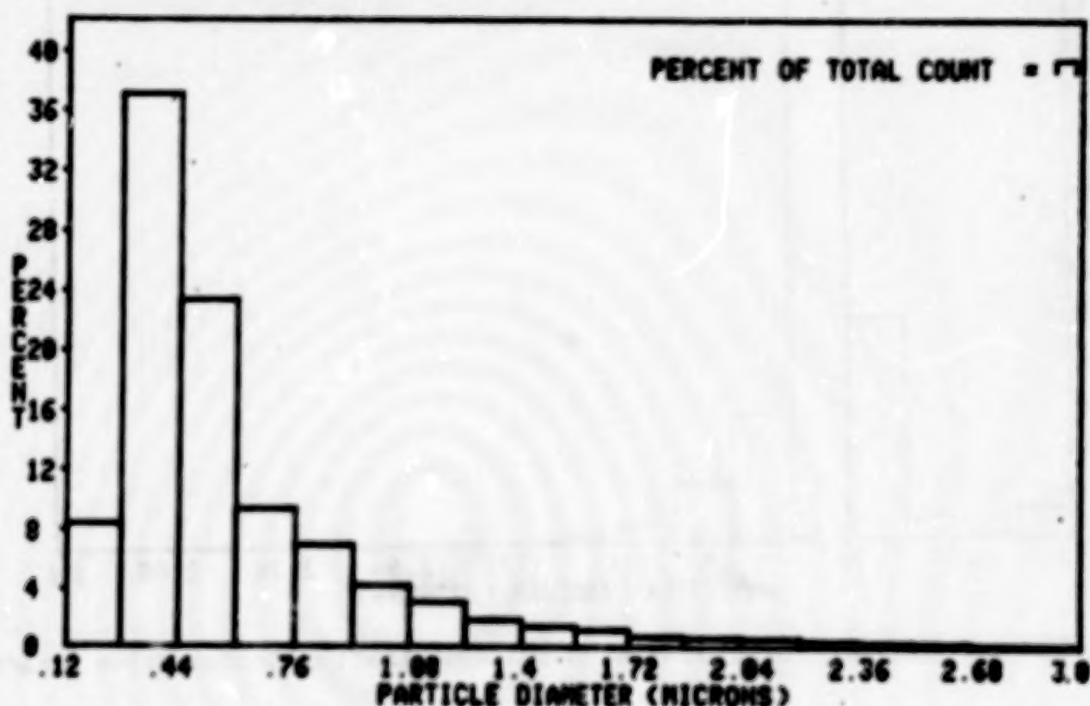
Fig. 22.   Latex Sphere Suspension in the Collison Nebulizer

AEROSOLS BY LIQUID VAPORIZATION/CONDENSATION

The first laboratory tests of the AEDC vap/con seeder involved comparisons of spontaneous and nucleate condensation processes. Consistent with the findings of Liu and Lee (Ref. 3) the intentional introduction of condensation nuclei resulted in more repeatable particle size distributions. Figure 23 shows the size spectrum for a 10,000/1 solution of DOP and anthracene with no dilution flow. The anthracene, with a higher vaporization temperature than DOP, became condensation nuclei for the vaporized DOP. By adding a dilution flow of nitrogen, the size spectrum of Figure 24 was obtained which illustrates the shift of the size spectrum toward smaller particles. Finally, the 10,000/1 DOP/anthracene solution was diluted in the volume ratio of 1 part DOP/anthracene to 99 parts ethanol and used in the vap/con seeder without dilution flow. The resultant particle size spectrum shown in Figure 25 is seen to be close to the ideal monodispersed size distribution.
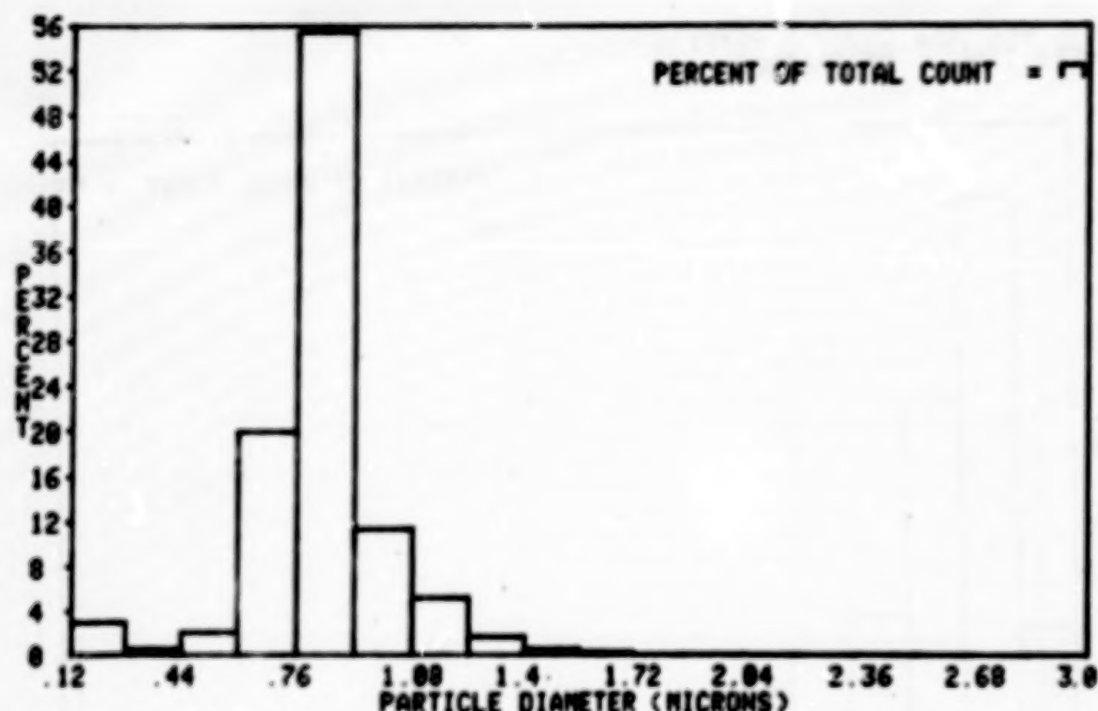
Fig. 23. DOP Without Dilution Flow in the Vaporization/Condensation Seeder

TOTAL PARTICLE COUNT = 203709
SAMPLE TIME - 39 SECONDS
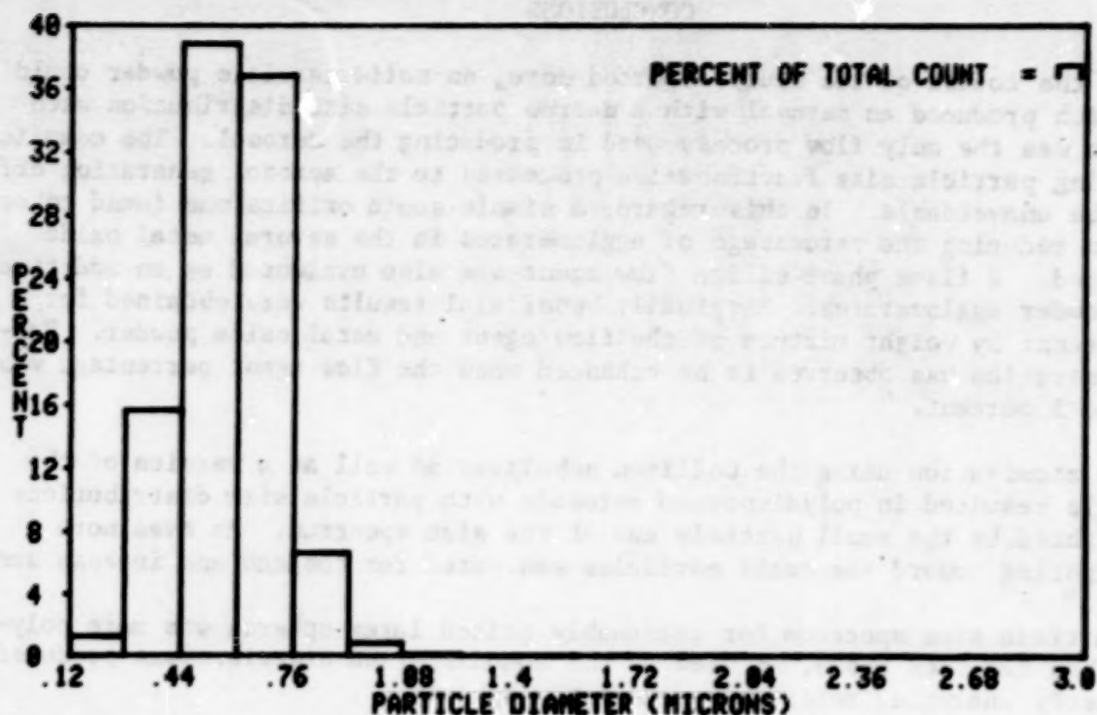
Fig. 24. DOP with Dilution Nitrogen Flow in the
Vaporization/Condensation Seeder

TOTAL PARTICLE COUNT = 122731
SAMPLE TIME - 20 SECONDS
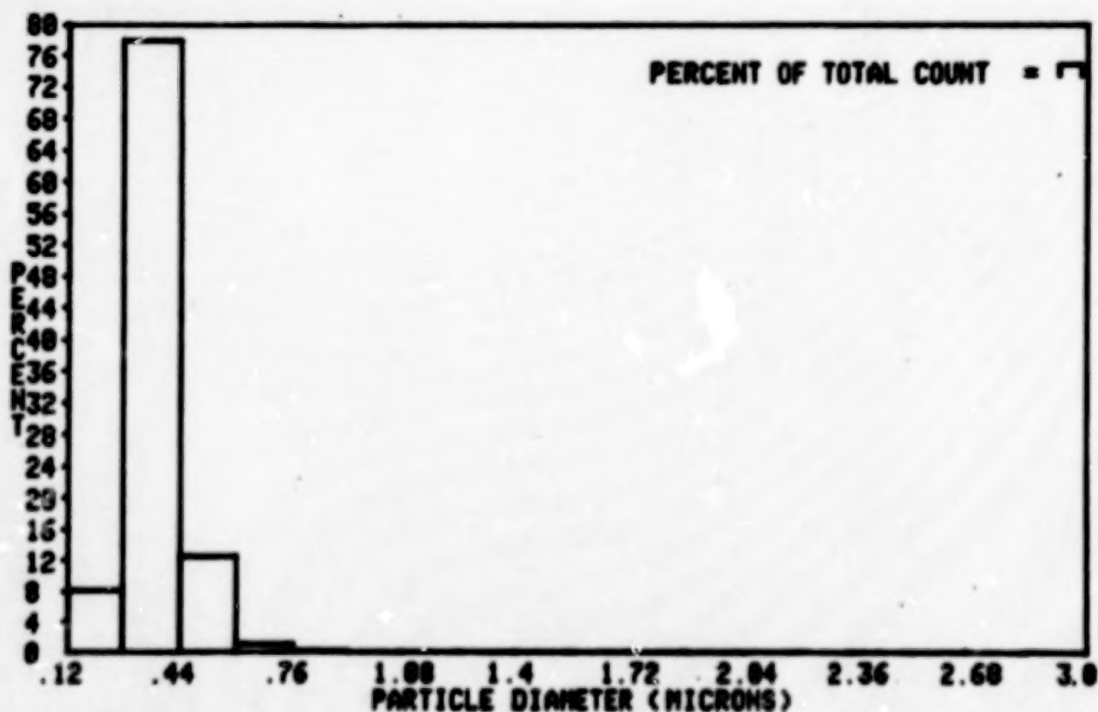
Fig. 25. Ethanol and DOP in the Ratio 99/1 in the
Vaporization/Condensation Seeder

CONCLUSIONS

During the course of the study reported here, no solid particle powder could be found which produced an aerosol with a narrow particle size distribution when fluidization was the only flow process used in producing the aerosol. The complication of adding particle size fractionation processes to the aerosol generation effort appears to be unavoidable. In this regard, a simple sonic orifice was found to be effective in reducing the percentage of agglomerates in the several metal oxide powders tested. A flame phase silica flow agent was also evaluated as an additive to reduce powder agglomerates. Marginally beneficial results were obtained for a 0.5/99.5 percent by weight mixture of the flow agent and metal oxide powder. However, agglomeration was observed to be enhanced when the flow agent percentage was increased to 5 percent.

Liquid atomization using the Collison nebulizer as well as a version of the Laskin nozzle resulted in polydispersed aerosols with particle size distributions heavily weighted by the small particle end of the size spectrum. An even more extreme weighting toward the small particles was noted for tobacco and incense smoke.

The particle size spectrum for reasonably priced latex spheres was more polydispersed than had been hoped, in view of the monodispersed distributions produced by the more costly analytic, reference grade latex spheres.

The aerosol particle size distributions produced by the vaporization/condensation seeder were closer to the ideal monodispersed aerosol than any of the other aerosols tested. In addition, this seeding approach affords a measure of control over particle size and particle production rate.

REFERENCES

1. May, K. R.: The Collison Nebulizer: Description, Performance and Application. Aerosol Science, Vol. 4, 1973, pp. 235-243.

2. Yanta, W. J.: A Three-Dimensional Laser Doppler Velocimeter (LDV) For Use In Wind Tunnels. ICIASF Record 1979, Monterey, California, September 24-26, 1979.

3. Liu, B. Y. H. and Lee, K. W.: An Aerosol Generator of High Stability. American Industrial Hygiene Association Journal, 36, December, 1975, pp. 861-865.

4. Agarwal, J. K. and Johnson, E. M.: Generating Aerosol For Laser Velocimeter Seeding. TSI Quarterly, Vol. VII, Issue 3, July-September 1981, pp. 5-12.

5. Meadows, D. M., Whiffen, M. C., and Mayo, W. T.: Laser Velocimeter For Supersonic Jet Turbulence and Turbulence Spectra Research. Appendix IV to The Generation and Radiation of Supersonic Jet Exhaust Noise. ADAPL-TR-24, June 1974, pp. 163-189.

6. Pfiefer, H. J.: Measurements In Gas Flows And Flames. Von-Kharman Institute Lecture Series 1981-3-Laser Velocimetry, Rhode-Saint Genese, Belgium, February 23-26, 1981.

7. Cabot Corporation: Cab-O-Sil Properties and Functions. Tuscola, Illinois 61953.

8. Patrick, W. P. and Paterson, R. W.: Seeding Technique for Laser Doppler Velocimetry Measurements In Strongly Accelerated Nozzle Flow Fields. AIAA-81-1198, Palo Alto, California, June 23-25, 1981.

9. Marteney, P. J.: Experimental Investigation of the Opacity of Small Particles. NASA CR-211, April 1965.

10. Forney, L. J. and McGregor, W. K.: Scaling Laws For Particle Breakup in Nozzle Generated Shocks. Particulate Science and Technology, Hemisphere Publishing Corp., 1983, pp. 419-431.

EXPERIMENTS WITH SOLID PARTICLE SEEDING

Cecil E. Nichols, Jr.
NASA Langley Research Center
Hampton, Virginia

INTRODUCTION

This paper will discuss some of the laboratory experiments that are presently being conducted at Langley pertaining to solid particle seeding.

GRAVITY SEDIMENTATION OF KAOLIN FINEPARTICLES IN ETHANOL

Kaolin, a hydrated aluminum silicate clay, is being investigated by LaRC as a seeding material for laser velocimetry. It is inexpensive but is polydisperse with some of the fineparticles being too large to follow wind tunnel flow and is in the form of non-spherical platelets having an aspect ratio of approximately 4/1. Gravity sedimentation experiments as a means of narrowing the fineparticle size distribution are being conducted. Figures 1(a), 1(b), and 1(c) show the fineparticle size distribution of Engelhard ASP 200 kaolin suspended in ethanol (0.00792 grams kaolin/ml ethanol) "as received," after 24 hours gravity sedimentation and after 48 hours sedimenation, respectively. A shearing atomizer (fig. 2) was used to inject the fineparticles. Gravity sedimentation was carried out in an 800 ml pyrex beaker (fig. 3). Following gravity sedimentation, the top 3.5 inches were siphoned from the liquid, which had a column height of 4.5 inches. In a like manner, longer settling times will serve to further narrow the fineparticle distribution range. As successive sedimentations are effected, the number of fineparticles per unit volume of ethanol decreases markedly. I have been able by means of a simple distillation to remove 90 volume percent of the ethanol which is then recycled for sedimentation of the next batch.

This work is still in progress; however, all indications are that gravity sedimentation can be successfully used to classify kaolin fineparticles for accurate laser velocimeter measurements.
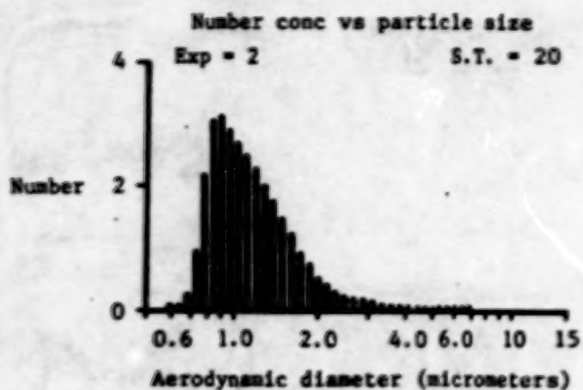
(a)

As received, 0.00792 grams ASP 200 Kaolin/ML Ethanol,
99% of particles ≤ 3.78μ, peak = 0.897μ
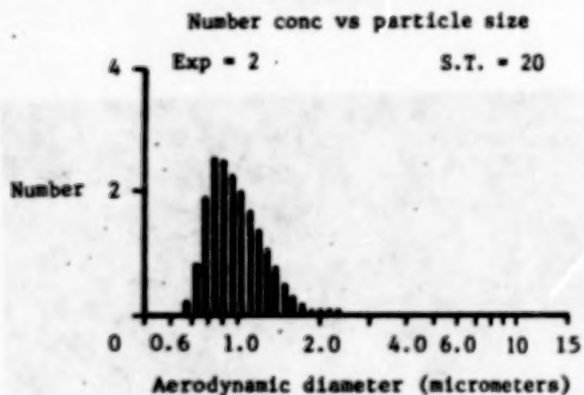
(b)

24 hour settling time, 99% of particles ≤ 1.98μ, peak = 0.835μ
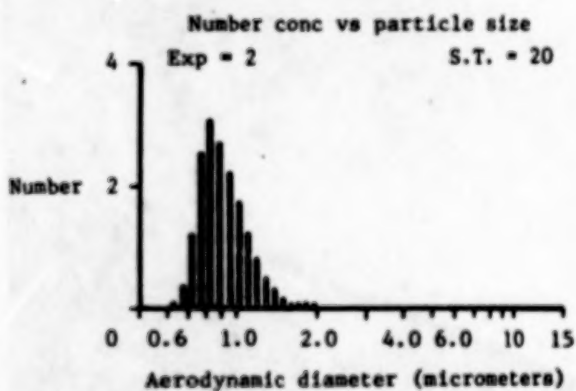
(c)

48 hour settling time, 99% of particles ≤ 1.71μ, peak = 0.835μ

Figure 1

Figure 2

Figure 3

80
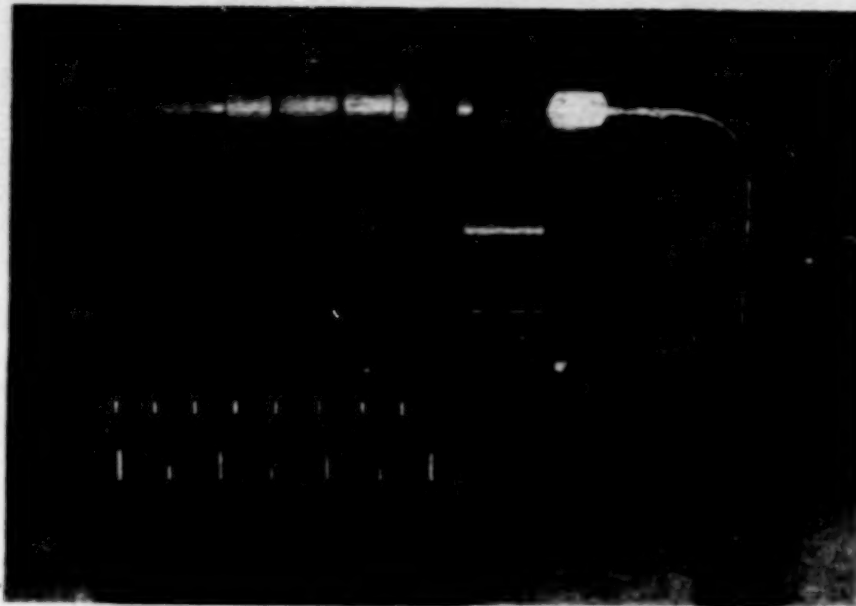
SEPARATION OF OVERSIZE FINEPARTICLES BY USE OF
A CYCLONE SEPARATOR

Figure 4 shows the seeder used to inject the kaolin fineparticles, "as received". This seeder consists of a variable speed, rotating slotted wheel onto which the fineparticles are delivered from an air vibrated hopper. The fineparticles are aspirated from the wheel's surface into the airstream. Figure 5(a) shows the fine particle size distribution. Figure 5(b) shows the result of adding a small, "in-house fabricated" cyclone separator to the discharge of the above-mentioned seeder (fig. 6). Note however that 99 weight percent of the fineparticles still includes particles that are too large, being 3.05 micrometers in diameter. Since this is approaching the limit for size separation with a cyclone separator other means will be examined and this effort will be placed "on the back burner".

Figure 4

Number conc vs particle size

Exp = 2   S.T. = 20

10 ⊤

Number 5 ⊣

0   0.6 1.0   2.0   4.0 6.0   10   15

Aerodynamic diameter (micrometers)
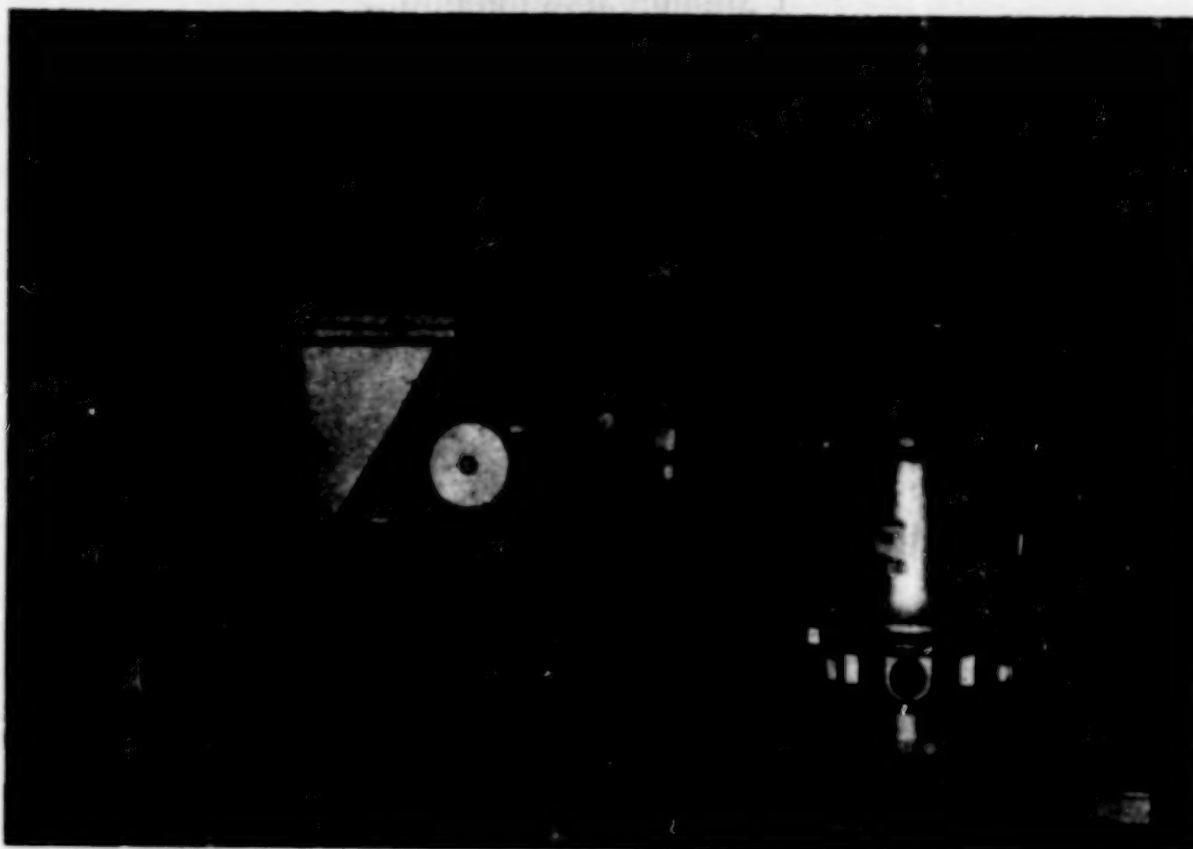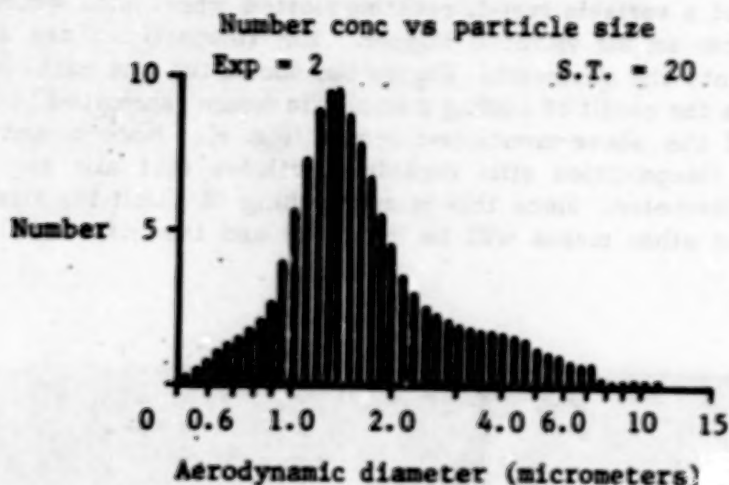
(a)

As received, injected with NBS seeder
99% of particles ≤ 6.73µ, peak, 138µ

Number conc vs particle size

Exp = 1   S.T. = 20

4 ⊤

Number 2 ⊣

0   0.6 1.0   2.0   4.0 6.0   10   15

Aerodynamic diameter (micrometers)
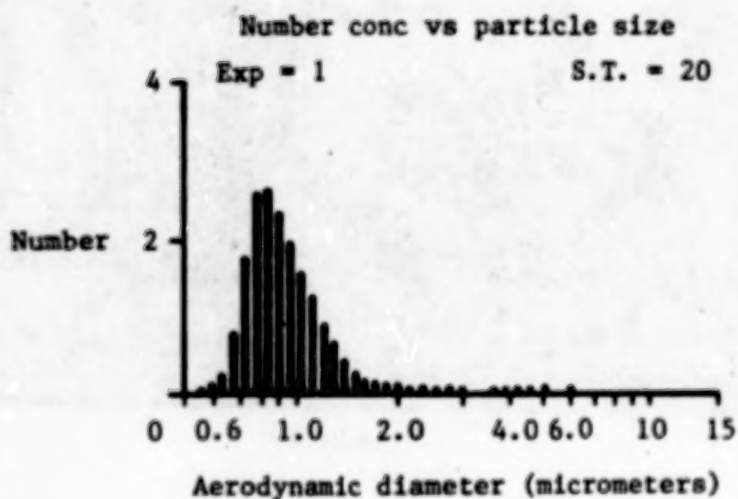
Through cyclone separator, 99% of particles ≤ 3.05µ,
peak = 0.897µ
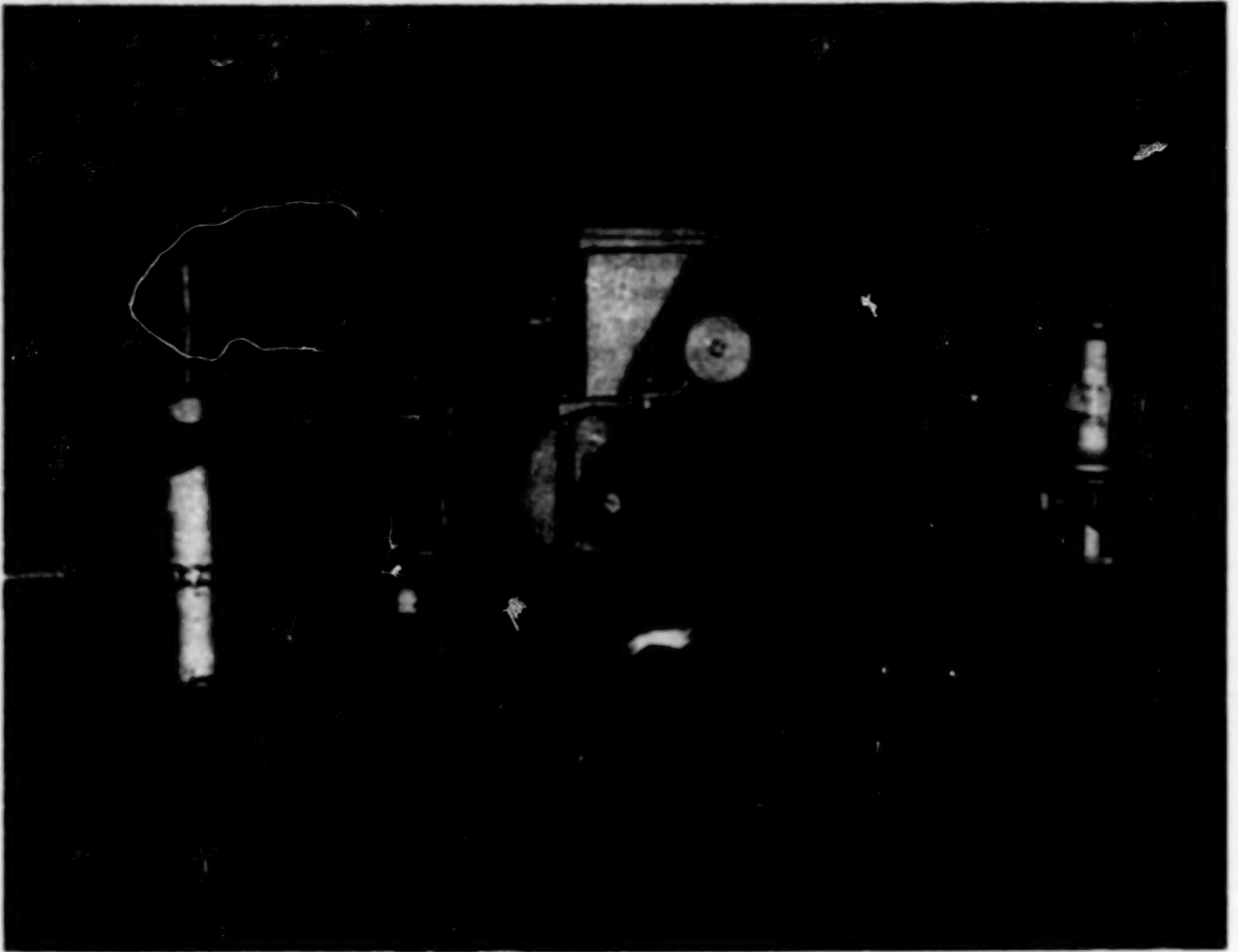
Figure 5

Figure 6

CONCLUDING REMARKS

You will notice that the data presented above is characterized in terms of "99 percent of the fineparticle size equal to or less than "a certain size. Actually this is not deemed to be good enough separation - the goal is size distribution such that "100 percent of the fineparticles are equal to or less than" the desired size. Work is ongoing in an effort to get cleaner, more precise cut-off points of fineparticle size with kaolin. Prime consideration is being given to the elimination of liquid convection currents during gravity sedimentation as a means to this end.

We are also investigating in-house manufacture of monodisperse Polystyrene latex (PSL) fineparticles in 1 micrometer diameter. PSL is commercially available (suspended in water) in an assortment of micrometer and submicrometer diameters but with the exception of 0.55 micrometer size is very expensive which can make its use prohitive in large wind tunnels unless the higher cost can be offset by a higher data rate resulting in shorter run times. Several laboratory batches of PSL have been made and although not perfect each batch is a little better than the last. If successful, PSL will result in a viable low cost option to kaolin as a liquid-suspended solid seeding material.

SEEDING TECHNIQUES USED IN THE VORTEX RESEARCH FACILITY

Dale R. Satran
NASA Langley Research Center
Low-Speed Aerodynamics Division
Analytical Methods Branch
Hampton, Virginia

The Vortex Research Facility, shown schematically in figure 1 and described in reference 1, is a converted model towing basin about 1800 feet in length. An instrumented automobile-type research vehicle is used to accelerate the test model to a constant test speed of approximately 100 feet per second at the test section entrance. The test section is covered to prevent the vehicle wake from interfering with the aircraft model wake. A slot in the ceiling accomodates passage of the model support strut. This slot is lined with brush-like material to further block the vehicle wake downwash. The brushes are pushed aside by the passing strut and close together behind it. The model is instrumented to provide aerodynamic loads while flow visualization and a laser velocimeter (LV) provide details of the wake vortex flow field. During the last 10 years, the Vortex Research Facility has been active in the vortex wake research program. The research objective for the facility is to provide basic understanding of the physics of vortex flows. To achieve this objective, the facility has been upgraded and experimental data are being acquired for developing methods which reduce vortex wake intensity and for verification of computational methods which predict vortex flow behavior.

Figure 1

C-2
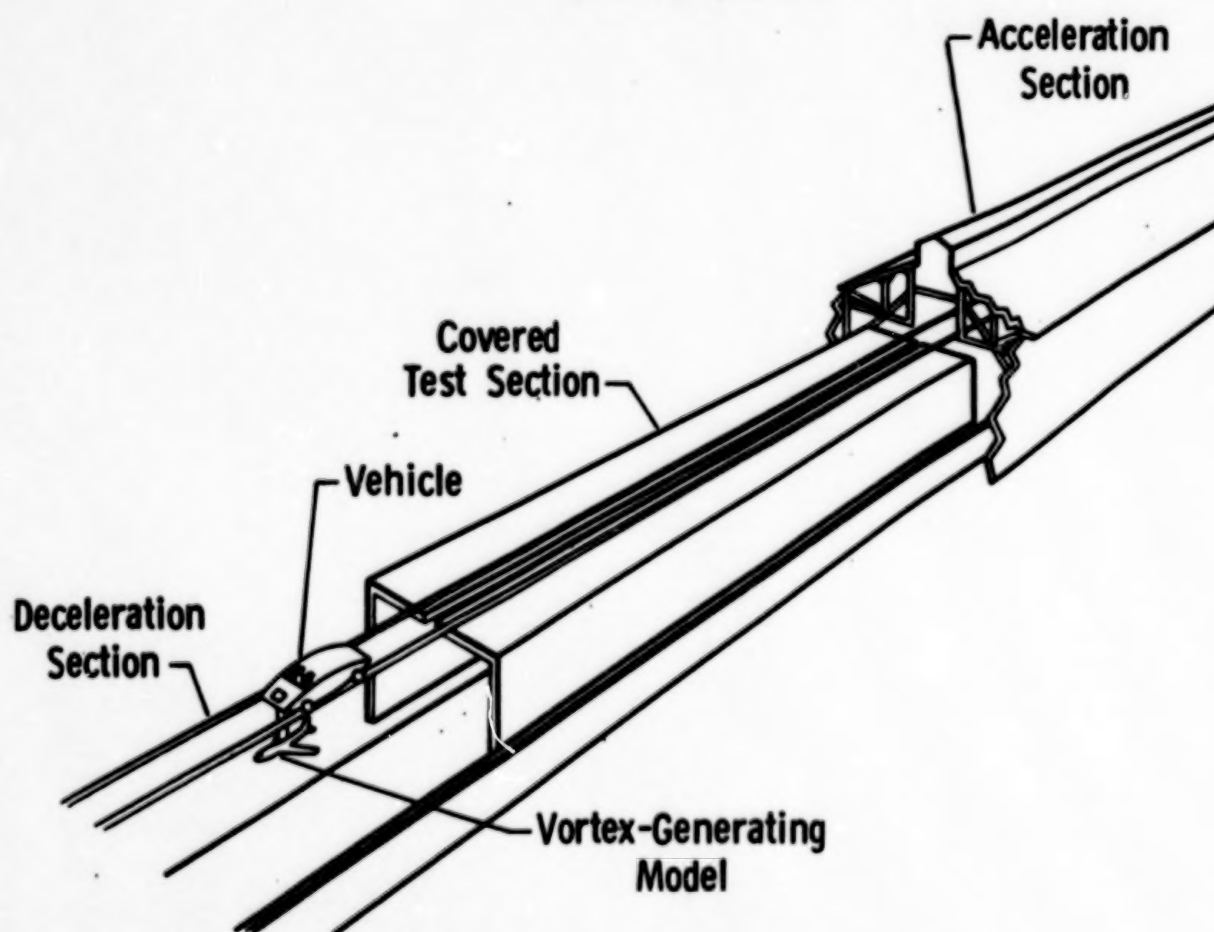
Detailed flow field measurements are made with a laser velocimeter (LV)
system. The laser velocimeter optics system, described in reference 2, has been
modified from a back-scatter mode to a forward-scatter mode. This modification has
increased the signal-to-noise level of the LV system by 30 dB and yielded better
resolution of the velocities in the flow field. The LV system is currently being
modified to provide dual optical paths in the test section (see Figure 2). For a
single run, this will allow two sets of wake measurements. The LV system still
incorporates the high speed scanning system which provides scan rates (longitudinal
displacement of the focus along the optical axis) up to 30 times per sec, with 16
discrete individual measurement positions for each scan. The region scanned can be
located over any region of the optical axis with the use of a zoom lens. With the
original LV system, the laser velocimeter measurements were input into a separate,
small minicomputer with 30 kilobytes of memory for data processing. This computer
has been replaced with an LV data acquisition buffer which acquires the data and then
transmits the data to a large minicomputer for processing.
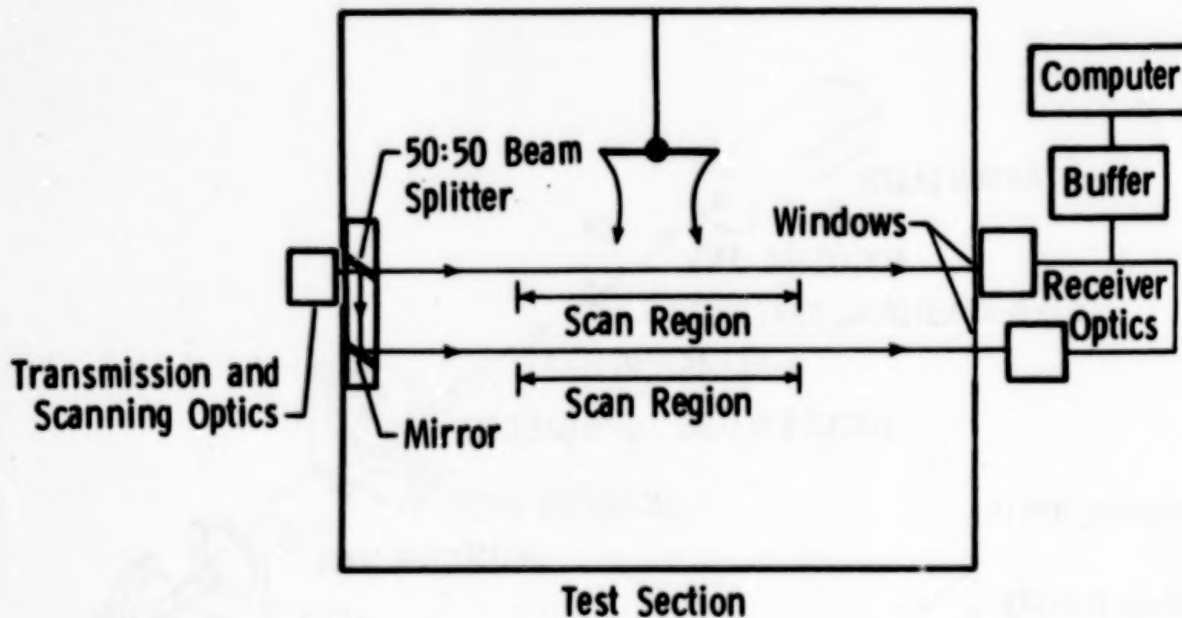
Figure 2

The optical system is configured to operate in the forward-scatter mode (figure 3). The laser velocimeter uses an argon-ion laser that operates in the TEM_{00} mode and at .6 W of continuous power at the 514.5-nm wavelength. The laser output beam is focused by a 2-diopter lens into the center of a two-dimensional ultrasonic Bragg cell. The Bragg cell allows two orthogonal velocity components (axial and vertical) to be measured. The four orders from the Bragg cell are then collimated by a 1.5-diopter lens and imaged into the dead air space of an optical cell by a 20-diopter F1:1.5 lens. The optical cell is used to eliminate extraneous Doppler signals from particles passing through this primary focus. The beams emerging from the optical cell then pass through the scan wheel. This wheel is a 40.5-cm-diameter disk containing 16 windows. The windows vary in thickness from 0 to 30 mm, in 2-mm increments. The scan wheel operates on the refraction principle, whereby the insertion of plane parallel windows (of various thicknesses) between the primary focus in the optical cell and a projection lens arrangement produces an apparent incremental longitudinal displacement of the primary focus. This displacement is magnified (by a factor of approximately 50) by the 2-lens projection system. The receiving optics are adjusted to focus the scattered light from the sample volume onto the photomultiplier tube. Beam masks are used to block the primary beams.
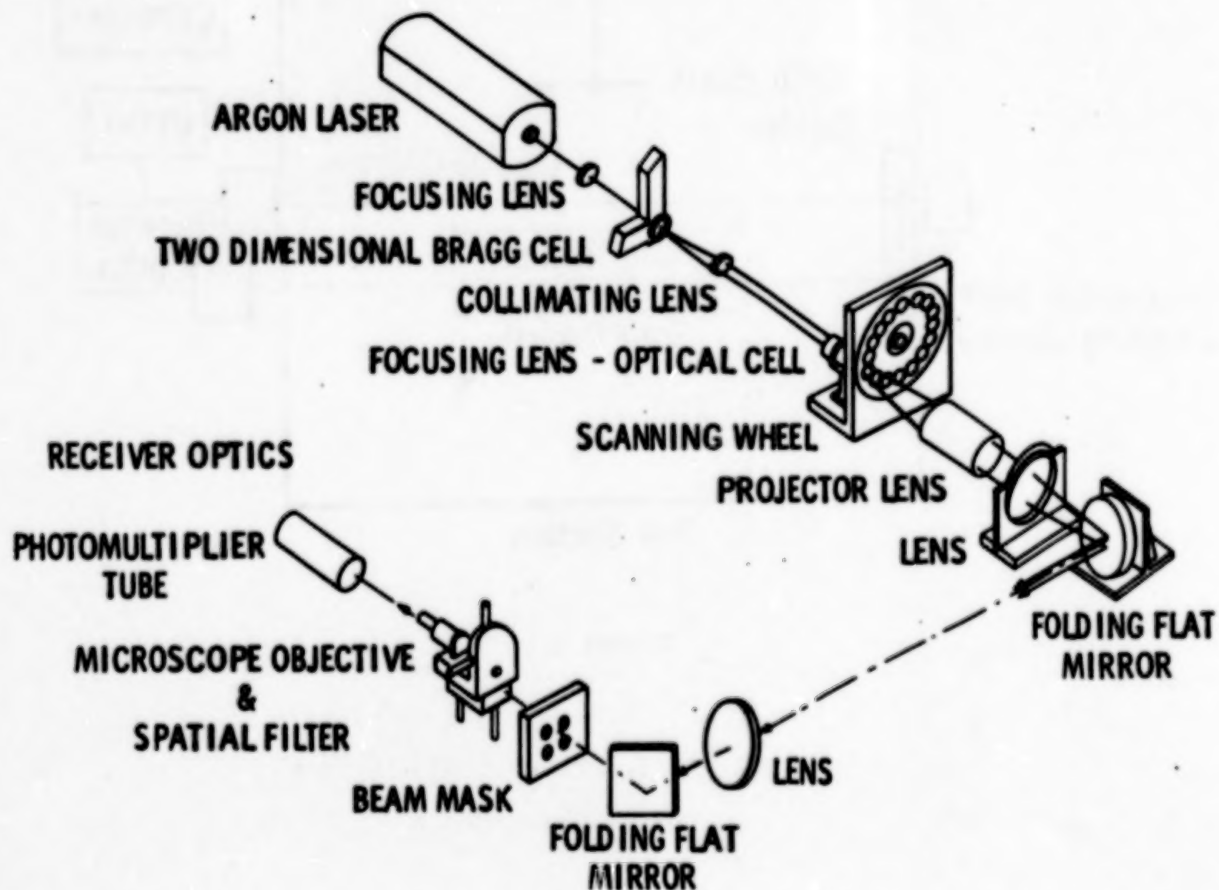
Figure 3

For many years, the Vortex Research Facility has used kerosene vapor as seeding particles. The kerosene vapor formed (~ 1µm) particles initially. After injection into the test section, the vaper would begin to condense and form larger particles. By switching to solid particles, this has been eliminated. The solid particle size distribution is shown in figure 4. The uniform-sized (~1µm) solid particle seeding is used both to seed the LV system and for flow visualization. After injection, the solid particles reach a uniform suspension before the vehicle is launched. It was found that the kerosene vapor posed a problem because it is a heated gas which modified the test section temperature distribution. It also produced high turbulence and secondary air currents because it was continually injected from the time of vehicle launch until model passage. In cases where the effects of either turbulence or the vertical temperature distribution were of interest, this hot gas injection method was unsuitable. Both types of seeding particles provided adequate flow visualization but are sensitive to vertical temperature distributions.

SOLID PARTICLE SIZE
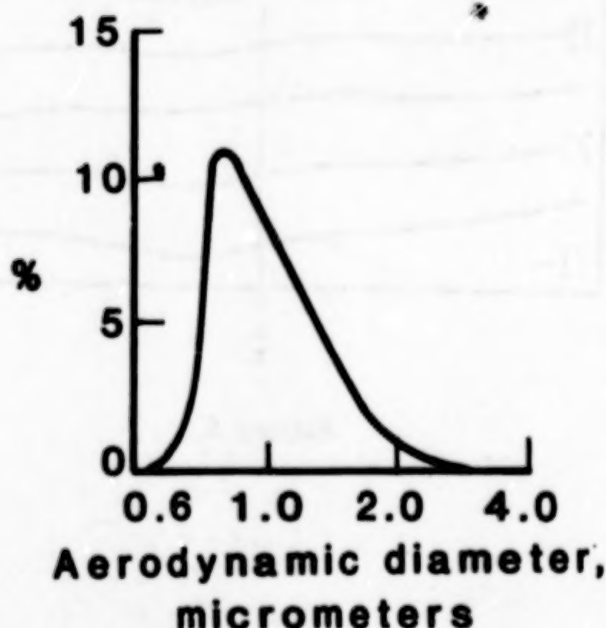
DISTRIBUTION

Figure 4

Although the test section is enclosed within the facility, the environment within the test section is still influenced by the outdoor meteorological conditions. In particular the temperature near the ceiling tends to track the daily variation in outdoor temperature while the temperature near the floor, which is thick concrete and below ground level, is relatively constant. This results in a vertical temperature gradient which varies with the time of day and season. Thirteen thermocouples were mounted off the test section floor and side walls to measure the test section temperature distribution during test runs. To verify that the wall measurements were providing an accurate indication of the temperature gradient at the tunnel centerline, detailed measurements were made with 24 uniformly distributed thermocouples. A contour plot of a typical test section temperature distribution is shown in figure 5. All but the wall mounted thermocouples were removed from the test section during runs. Testing on a typical summer day covered the range from near zero gradient conditions in the early morning to a maximum gradient between 0.5 and 1.0 degree F per foot in the afternoon.
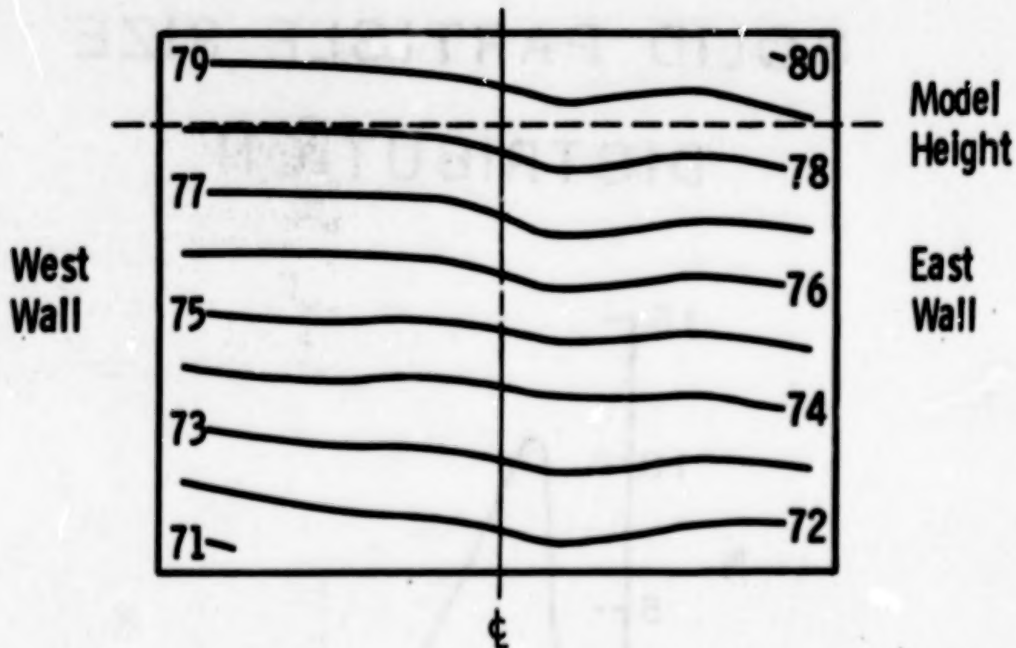
Figure 5

TEMPERATURE DISTRIBUTION EFFECTS ON SEEDING

In the Vortex Research Facility, the test section temperature distribution can be a primary factor in achieving a satisfactory seeding distribution. If the seeding particles are at a different temperature than the air being seeded, the particles will drift from the desired height. When the height of the particles differs significantly with the model's height, a poor seeding distribution occurs. The mild stratification case has a 0.2° F per foot temperature distribution. For the heavy stratification case, the temperature distribution was 1.4°F per foot. The large temperature distribution caused the seeding particles to sink below the model which resulted in a poorer seeding distribution. The seeding levels shown are for flow visualization although similar results occur for the lower LV seeding levels. (See figure 6.)
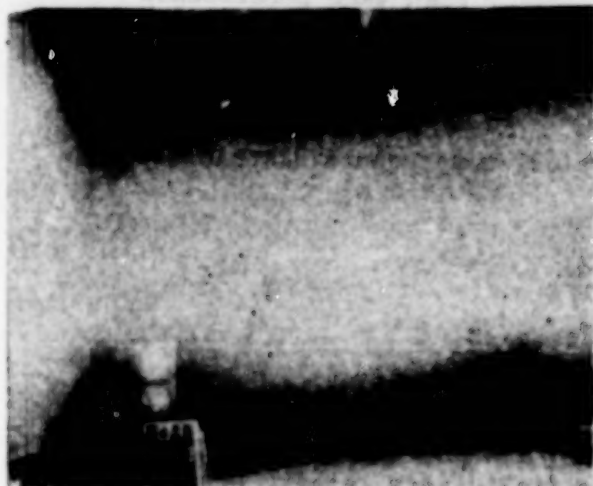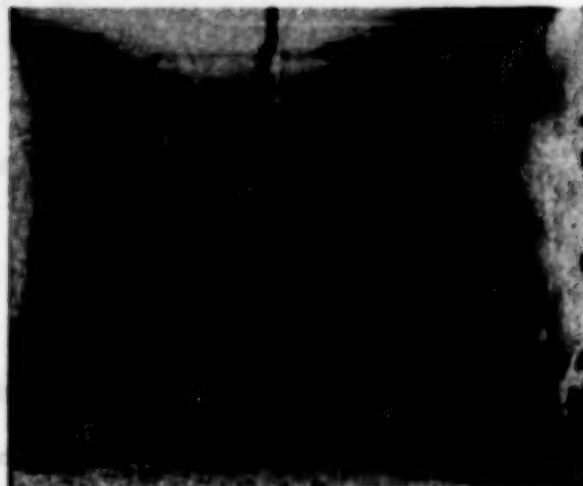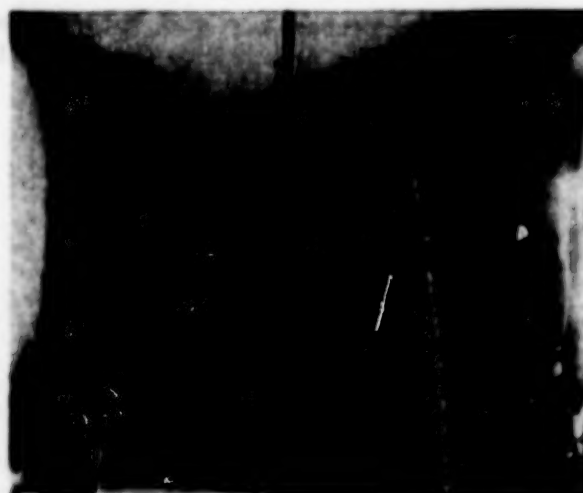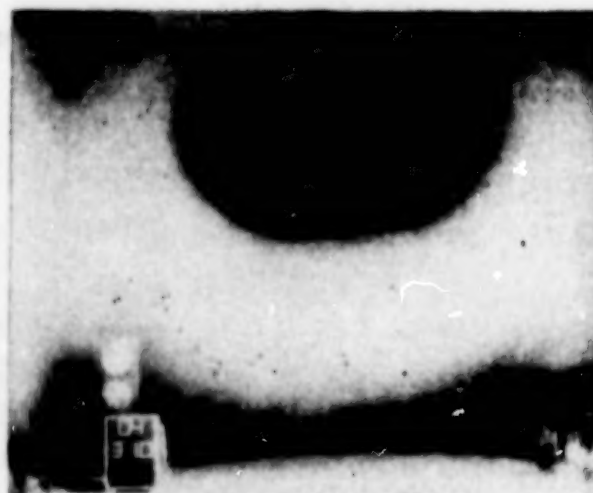
Figure 6

CONCLUSIONS

Two types of seeding particles have been used in the Vortex Research Facility. Hot kerosene vapor does not maintain uniform particle size when it cools and has been shown to influence vortex wake persistence. Solid particle seeding seems to provide a better indication of vortex wake behavior. Seeding distributions for both types of seeding particles are affected by vertical temperature distributions.

o   VRF has used two types of particles

o   Kerosene vapor becomes non uniform in size when vapor cools

o   Kerosene vapor has been shown to influence vortex wake persistence

o   Solid particle seeding seems to provide a better indication of vortex wake behavior

o   Seeding distributions affected by vertical temperature distributions

REFERENCES

1.   Satran, Dale R.; Neuhart, Dan; Holbrook, G. Thomas; and Greene, George C.: Vortex Research Facility Improvements and Preliminary Density Stratification Effects on Vortex Wakes.   AIAA Paper No. 85-0050, January 1985.

2.   Gartrell, Luther R.; and Rhodes, David B.: A Scanning Laser-Velocimeter Technique for Measuring Two-Dimensional Wake-Vortex Velocity Distributions.   NASA TP 1661, May 1980.

SEEDING SYSTEMS FOR USE WITH A LASER VELOCIMETER

IN LARGE SCALE WIND TUNNELS

Joe W. Elliott
Rotorcraft Aerodynamics Office
Army Structures Lab, USARTL
NASA Langley Research Center
Hampton, Virginia

Cecil E. Nichols
NASA Langley Research Center
Hampton, Virginia

4- BY 7- METER TUNNEL

The Langley 4- by 7- Meter Tunnel which is shown in figures 1 and 2 is a closed circuit, atmospheric wind tunnel which may be operated with a closed or open test section. The test section ceiling and walls can be raised to provide the open configuration that is closed on the bottom. The test section, or the jet entrance in the open configuration, is 14.5 ft high, by 21.75 ft wide. In each case the test section is 50 ft long and is configured into two test bays each equipped with interchangeable model support mechanisms.

Figure 1
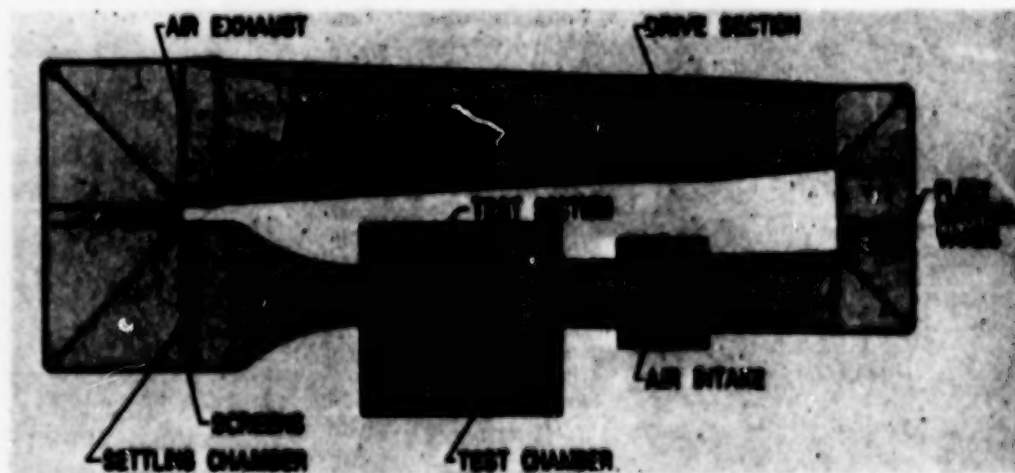
Figure 2

The laser velocimeter (LV) is configured to measure the instantaneous component of velocity in the horizontal (U component) and vertical (V component) directions (ref. 1). The system is comprised of three subsystems: optics, traverse, and data acquisition and control.

Optics

The optics subsystem which is shown schematically in figure 3 is operated in the backscatter mode and at high laser power (4 watts in all lines) in order to accommodate the long focal lengths required by the wide test section. The commercially available transmitting and receiving optics packages are augmented by a zoom lens system consisting of a 3 in. clear aperture negative lens and a 12 in. clear aperture positive lens. Bragg cells in each of the optical paths provide a directional measurement capability.

Traverse

The traverse subsystem uses a combination of mechanical and optical schemes to provide five degrees of freedom. Translation of the sample volume along the horizontal and vertical axes is accomplished by displacing the entire optics platform. Translation along the lateral axes is accomplished by translating the negative lens located in the zoom lens assembly thus refocusing the sample volume along the axis of optical transmission. The other two degrees of freedom, pan and tilt, are implemented by rotating the final mirror about its vertical and horizontal axis in order to change the direction of optical transmission. The total inclusive range of the traversing system is: Vertical: 7 ft; Streamwise: 6 ft; Lateral: 16.5 ft; Pan: 30°; Tilt: 30°
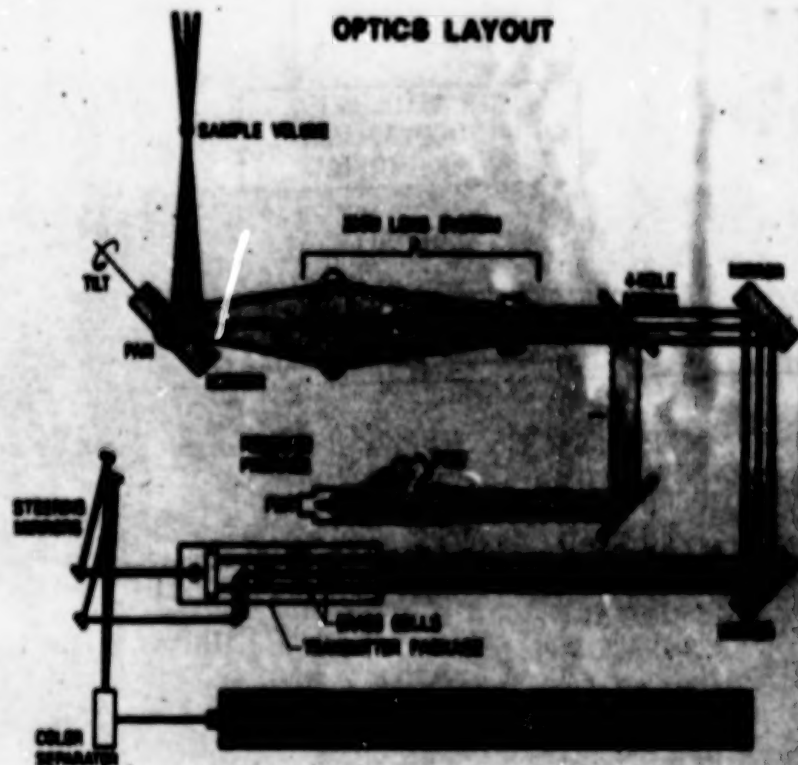
Figure 3

DATA ACQUISITION AND CONTROL

The data acquisition and control subsystem is shown schematically in figure 4 and performs the following functions:

1. Interfaces with the optical signal processing equipment to receive two channels of raw LV data and one channel of auxiliary data.

2. Converts that raw data to engineering units.

3. Statistically analyses the data and reports the results so that the test results can be evaluated on line.

4. Stores the test results on magnetic tape for subsequent analysis.

5. Interfaces with and controls the five degree of freedom scan system.
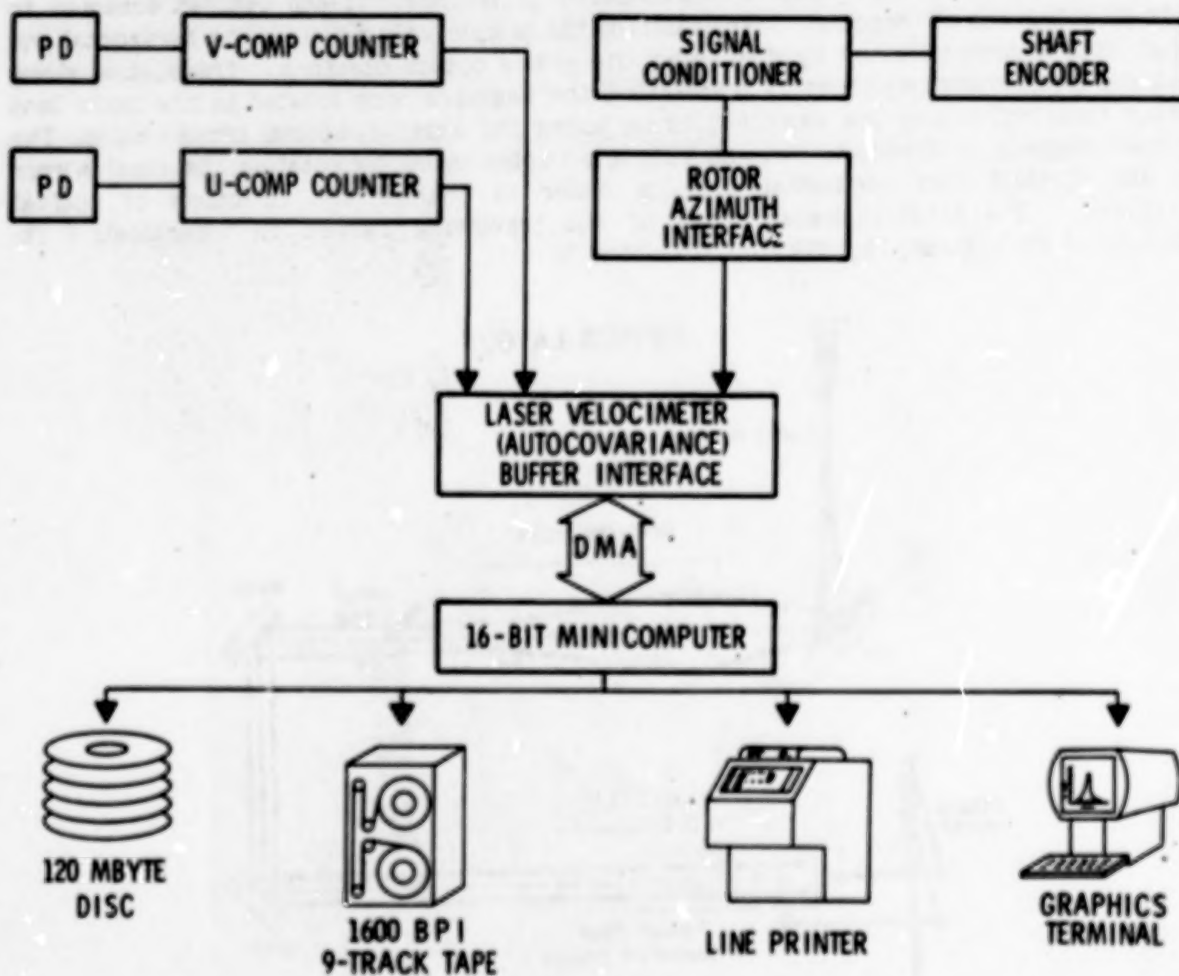
Figure 4

SEEDING REQUIREMENTS

The models shown in figure 5 are representative of those tested in the 4- by 7-Meter Tunnel. The areas that are to be seeded in support of such tests are on the order of 7 to 20 square feet. Each square foot of area requires 5.0×10^7 particles per minute to achieve a uniform data rate of 4000 samples per minute. The shapes of the seeded areas which are required to support such tests are vertical or horizontal rectangles, squares or circles.
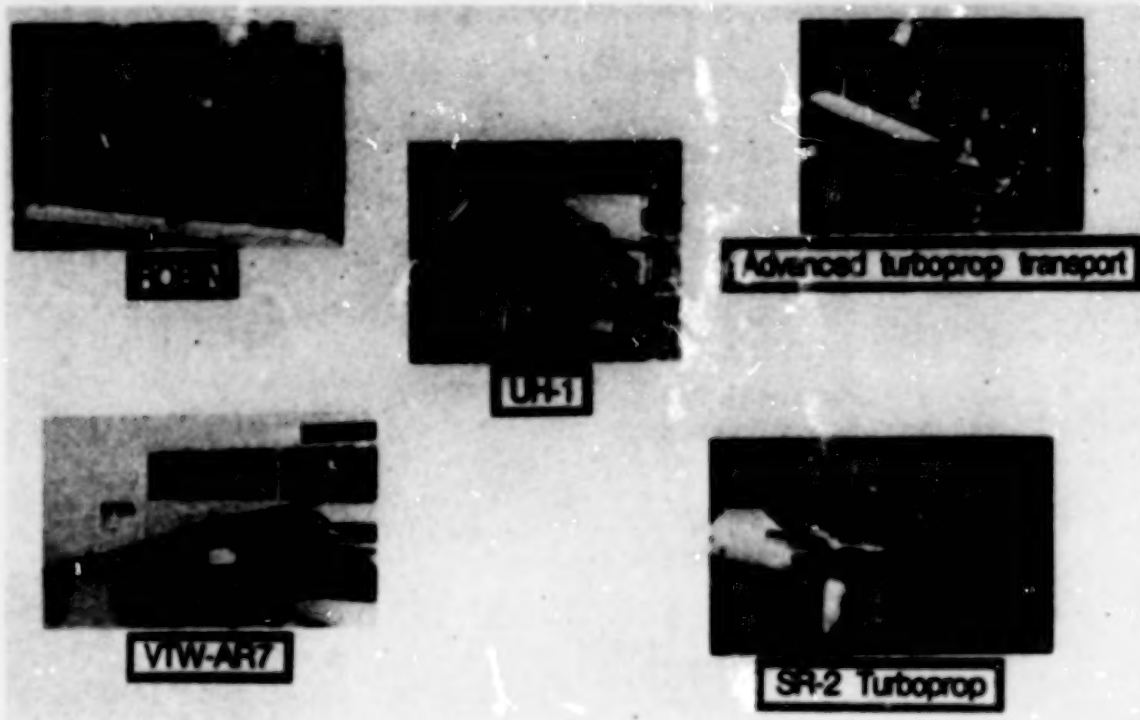
Figure 5

SEEDING TECHNIQUES

Three seeding techniques have been utilized thus far in the 4- by 7-Meter Tunnel: (1) kerosene smoke, (2) dry dispensing of solid particles and (3) liquid dispensing of solid particles. In all three cases seeding material was injected into the air stream in the settling chamber (fig. 1) because of the relatively low velocity, easy access, up-stream proximity to the test section and relatively safe environment that exists at that location during tunnel operations.

KEROSENE SMOKE SYSTEM

A schematic of the kerosene smoke seeding system is shown in figure 6. Pressure, applied to the storage tank, causes the kerosene to flow to the wand where it is heated and expelled through a nozzle that is sized to maximize the number of 2 micron particles. The output of this system is a single plume on the order of 18 in. in diameter which can be increased to 36 in. with the addition of a diffuser plate located downstream of the nozzle. The pressure that is applied to the storage tank and the voltage across the d.c. electric heater in the wand are the only control variables on this system. The position of the wand in the settling chamber and thus the location of the particle plume in the test section is changed by raising or lowering it on a system of cables that stretched from the floor to the ceiling. The size of the particles that are generated is dependent on the rate at which kerosene flows through the system and the temperature of the kerosene. Since temperature is critical, anything that causes a change in that temperature will cause the size of the particles to change. For example:

1. A local tunnel temperature increase during tunnel operation will increase the kerosene temperature and decrease the size of the particles.

2. A tunnel velocity increase will decrease the temperature of the kerosene and increase the size of the particles.

3. A kerosene tank pressure increase, in order to increase the number of particles, will decrease the temperature of the kerosene and increase the size of particles.

Thermocouples located in the wand provide the necessary inputs to control the temperature, and therefore the particle output, but the system still requires a great deal of operator skill and intervention.

Nitrogen bottle   Fuel tank   Power supply   Smoke wand
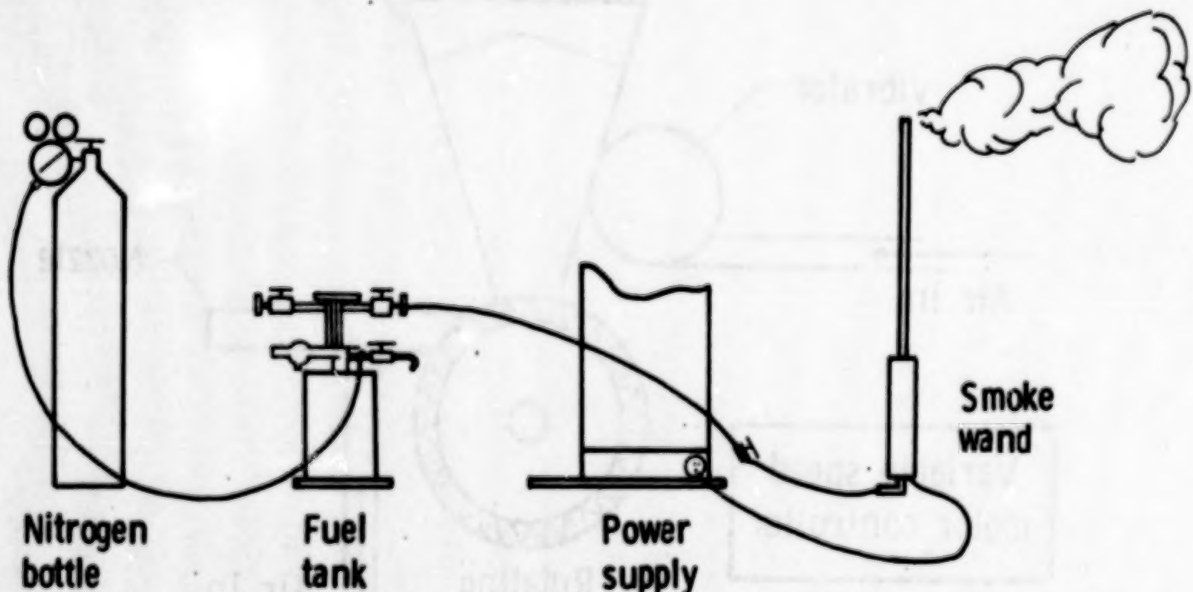
Figure 6

SOLID PARTICLE DRY DISPENSING SYSTEM

A schematic of the solid particle dry dispensing system is shown in figure 7. The dry particles which are contained in the hopper are deposited on the rotating toothed wheel, removed at the low pressure entrance to the nozzle and subsequently injected into the tunnel in a single plume which is on the order of 12 in. in diameter. The seeder is installed on the cable system in the settling chamber for dispersal of particles. Pressure applied to the hopper vibrator, pressure applied to the nozzle and voltage applied to the motor which drives the toothed wheel are the three control inputs to the system. The two major characteristics of the particles, size and quantity, are controlled by the selection of raw particles to be put in the hopper and the control of the speed of the toothed wheel. Two controls are provided to optimize the performance of the seeder:

1. The air supply to the hopper vibrator is used to vary the frequency of the vibrator. This insures that a continuous supply of particles will be available to the toothed wheel.

2. The air supply to the nozzle controls the effectiveness of the removal process and at higher settings acts to break up agglomerated masses of particles.

The system is fairly easy to set up and adjust, but does experience particle agglomeration. This condition occurs when clumps of the seeding material fail to break-up as they are removed from the toothed wheel. These clumps of seeding material, some estimated to be as large as 0.050 in., may not follow the flow and may change the model characterstics when they impact and adhere to the surface. Coating of the seeding material with particles of a sub-micron size reduces this problem and also improves the flow of the seeding material in the hopper (ref. 2).
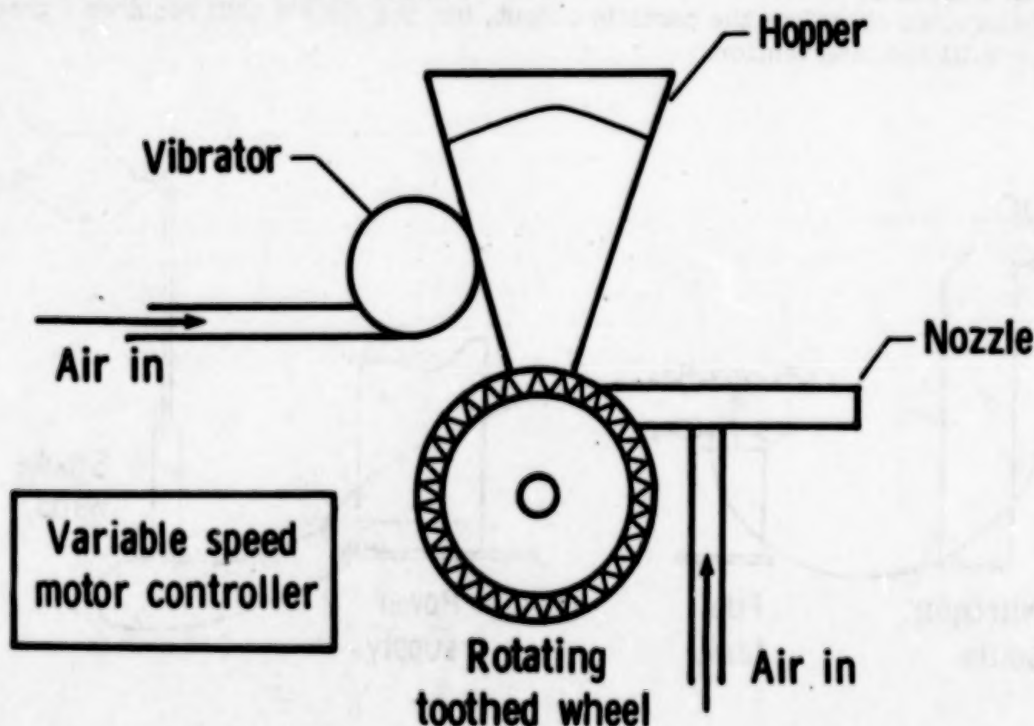
Figure 7

SOLID PARTICLE LIQUID DISPENSING SYSTEM

A schematic of the solid particle liquid seeding system is shown in figure 8. The storage tank is filled with up to 20 gallons of ethyl alcohol in which the particles to be dispensed have been mixed. The pump delivers the mixture under pressure to a series of nozzles where a source of compressed air acts to atomize the mixture. Up to 40 nozzles can be conveniently mounted on the frame that is 6 ft high and 8 ft wide and is then positioned with the same cable arrangement as the other systems. The pumping apparatus will support up to two arrays of nozzles which can be configured to meet the area and density requirements of the test in progress. Because of its low vapor pressure, alcohol evaporates as it travels from the settling chamber to the test section, a distance of approximately 85 ft. The particles that were contained in the droplets remain in the flow to be used in the velocity measurement. The array of nozzles which are connected in series on the liquid supply line is not capable of dispensing the amount of liquid which is supplied by the pump so the excess is returned to the storage tank where it circulates with the remaining fluid and acts to prevent the particles from settling out of the mixture. The active controls in the system are three pressure regulators:

1. Number 1 establishes the pressure of the air which will be supplied to the array of nozzles. This pressure is monitored at the array so that it can be accurately set.

2. Number 2 establishes the maximum pressure of the circulating alcohol particle mixture. The regulator also prevents damage to the pump which could be caused by excessive head pressure resulting from blocked or disconnected supply lines.

3. Number 3 establishes the pressure of the alcohol particle mixture that will be delivered to the array of nozzles. A pressure transducer is also used to monitor this pressure and is likewise mounted on the array housing to facilitate accurate settings.

Once the controls on this system have been set its output remains constant and requires no attention. The nozzles are commercially available units which dispense the atomized mixture in a wide angle round spray pattern approximately 12 in. in diameter. The volumetric flow rate of the liquid mixture is controlled by changing the ratio of air to liquid pressures, and the droplet size is controlled by changing both pressures. When the pressure of the alcohol mixture and the air are increased, the atomized droplets are smaller, vaporize faster and contain fewer particles. The droplets should be small so that they will completely evaporate by the time that they arrive at the test section and should contain only one particle.
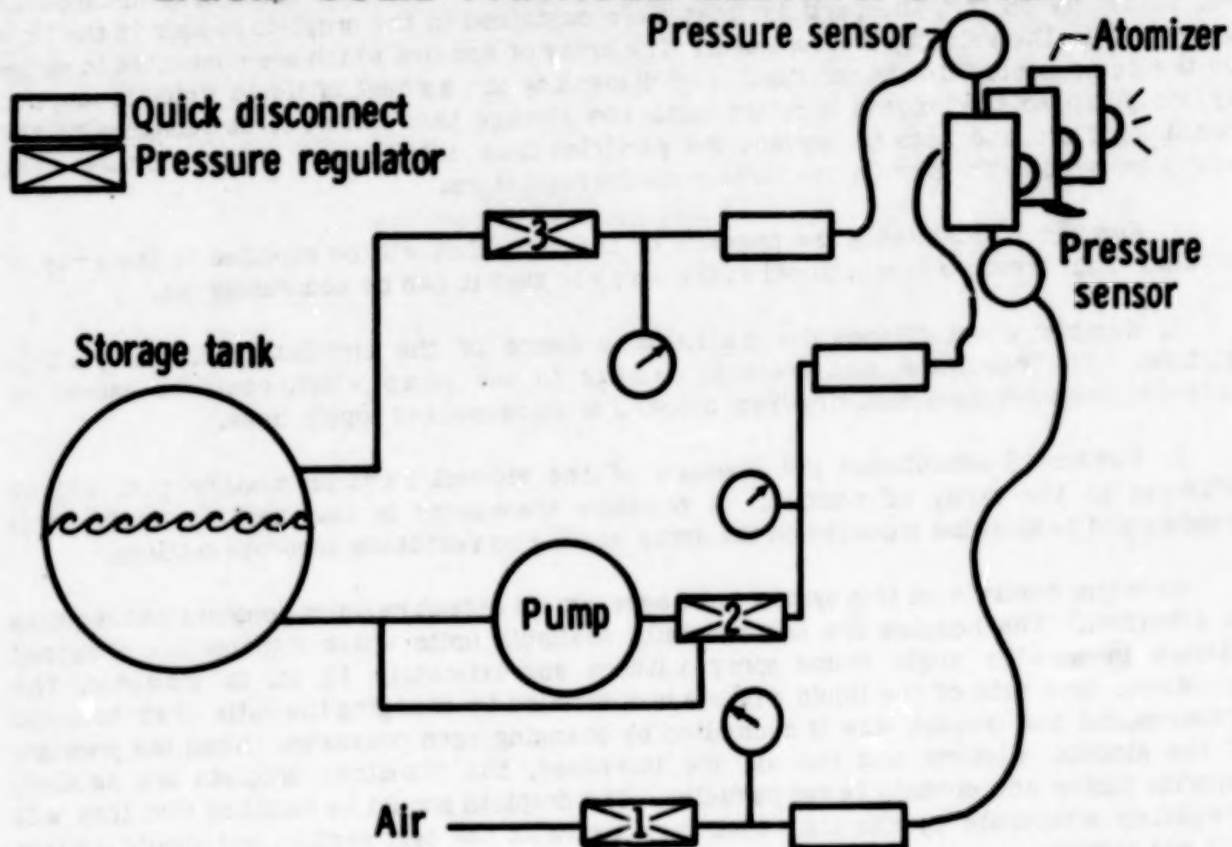
Figure 8

CONCLUSIONS

Three seeding systems have been used in the 4- by 7- Meter Tunnel: kerosene smoke, solid particle dry dispensing and solid particle liquid dispensing. It is anticipated that the liquid dispensing system will be used in all of the applications at this facility because:

1. It has a steady output.
2. It is easy to operate and reconfigure.
3. It delivers particles of near uniform size.

REFERENCES

1. Sellers, William L.; and Elliott, Joe W.: Applications of a Laser Velocimeter in the Langley 4- by 7-Meter Tunnel. NASA CP 2243, "Flow Visualization, and Laser Velocimetry for Wind Tunnels," pp. 283-294, 1982.

2. Nichols, Cecil E.: Experiments With Solid Particle Seeding: Wind Tunnel Seeding Systems for Laser Velocimeters. NASA CP-2393, 1985, pp 77-84.

OVERVIEW OF SOLID PARTICLE LV SEEDING
TECHNIQUES USED AT UTRC

W. P. Patrick
United Technologies Research Center
East Hartford, Connecticut

PERFORMANCE OF ORIGINAL FLUIDIZED BED SEEDER

The original solid particle seeder (fig. 1) consisted of a thick-walled steel cylinder (18 cm dia x 15 cm long) which was closed by a welded hemispherical cap at one end and a bolted cover plate at the other. Copper tubes (.48 cm ID) aligned tangentially along the cylinder walls near its base were used to inject dry nitrogen into the seed powder to agitate the seed and to induce a swirling flow above the seed bed. Large seed particles (or agglomerates) entrained in the swirling flow were transported toward the outer wall by centrifugal force where they were bled off by two ports in the cover plate. The remaining seeded nitrogen was ducted to the rig.

The seeder was charged with $0.3 \mu m$ dia alumina particles (CR-type agglomerate free). Although the powder is free of large agglomerates, it consists of naturally occurring $3 \mu m$ aggregates (ref. 1) which must be broken down by vigorous action within the seeder. The measured particle size distributions produced by the original seeder are also shown in figure 1. At low pressure operation (30 psig.) 77 percent of the measured particles were in the submicron range ($0.3 - 1.0 \mu m$). At 50 psig. and 100 psig. the percentage of submicron particles deteriorated to 36 percent and 15 percent, respectively.

	SEEDER PRESSURE (PSIG)	$d^*_{50\%}$ (μm)	σ^*_g
O	30	0.70	2.26
□	50	1.42	1.80
△	100	3.08	2.32
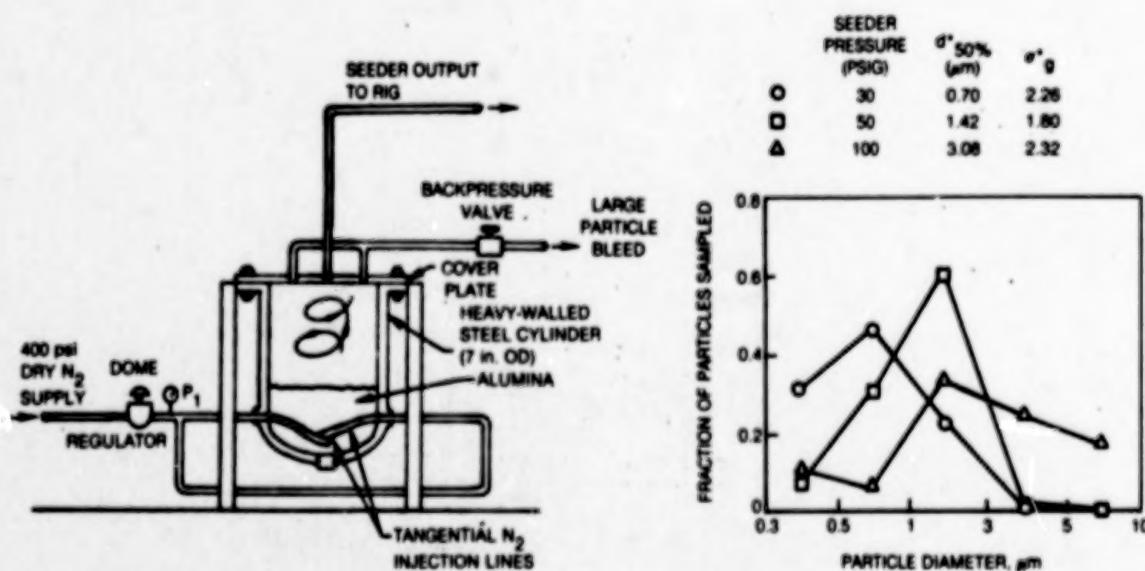
Figure I

DESCRIPTION OF FLUIDIZED BED SEEDER WITH VORTEX SEPARATOR

Due to the failure of existing seeders to meet the stringent specifications required for benchmark experiments in high pressure, high temperature, rapidly accelerating flowfields, an effort was made to improve the existing solid particle seeder (ref. 2). The goal was to produce a more monodisperse seed from the 0.3 μm alumina powder with more than 99 percent of the particles in the submicron range while maintaining a high seeding rate. The modified seeder is shown in figure 2.

Coiled-wire inserts were installed within the ends of the nitrogen injection lines in the primary seeder to produce swirling conical jets to vigorously agitate the seed bed. A secondary swirler, constructed from a 25 cm length of 3.8 cm ID steel pipe having threaded end caps, was connected to the output line of the primary seeder. The seeded nitrogen from the primary seeder was injected tangentially at near sonic velocity into the secondary swirler 9.4 cm above its base. Independently controlled auxiliary nitrogen used to increase the swirl in the secondary chamber was also injected tangentially 2.5 cm below the seeded nitrogen lines. Large seed particles were collected by bleeds in the swirler cap and directed overboard. The remaining seeded nitrogen was collected on the centerline of the secondary swirler and ducted to the rig.
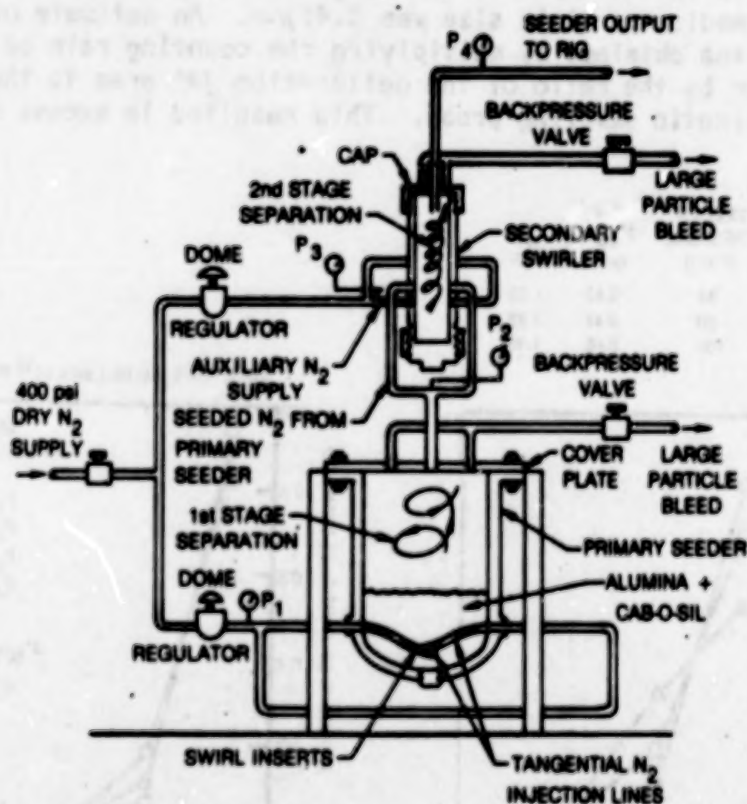
Figure 2

PERFORMANCE OF FLUIDIZED BED SEEDER WITH VORTEX SEPARATOR

Isokinetic particle sampling in a calibration jet seeded with $0.3\mu m$ alumina powder was performed to determine the effectiveness of the seeder modifications shown in figure 2. In the first series of tests the modified seeder was operated with a passive secondary swirler. The auxiliary nitrogen supply was not activated for these tests. The results for low pressure operation are shown in figure 3.

At 30 psig operating pressure, the seeder exceeded the required specifications. More than 88 percent of the measured seed particles were in the $0.3\mu m$ range, 11 percent were in the $0.5\mu m - 1\mu m$ range, the mean particle diameter was $0.413\mu m$ and the standard deviation, δ_g, was 1.19, indicating a monodisperse seed distribution. At 50 psig, the distribution remained satisfactory with only 1.5 percent of the particles being larger than $1\mu m$. At 100 psig the distribution deteriorated badly; the median diameter increasing to $0.742\mu m$ and 25 percent of the particles were larger than $1\mu m$.

A second series of tests demonstrated the effectiveness of the auxiliary nitrogen supply in optimizing the seed distribution at higher pressure operation. Figure 3 shows the optimized particle distributions obtained from three tests at 140 psig. As indicated in the figure, the seed particle distribution was monodisperse with almost 90 percent of the measured particles in the $0.3 - 0.5\mu m$ range and only 0.7 percent greater than $1\mu m$. The median particle size was $0.41\mu m$. An estimate of seed generation rate was obtained by multiplying the counting rate of the particle analyzer by the ratio of the calibration jet area to the capture area of the isokinetic sampling probe. This resulted in excess of 10^{10} particles/min.

	SEEDER PRESSURE (PSIG)	$d^*_{50\%}$ (μm)	σ^*_g
O	30	0.42	1.20
□	50	0.44	1.82
△	100	0.48	1.95

SEED RATE = $0.92\text{-}1.68 \times 10^{10}$ PARTICLES/MIN
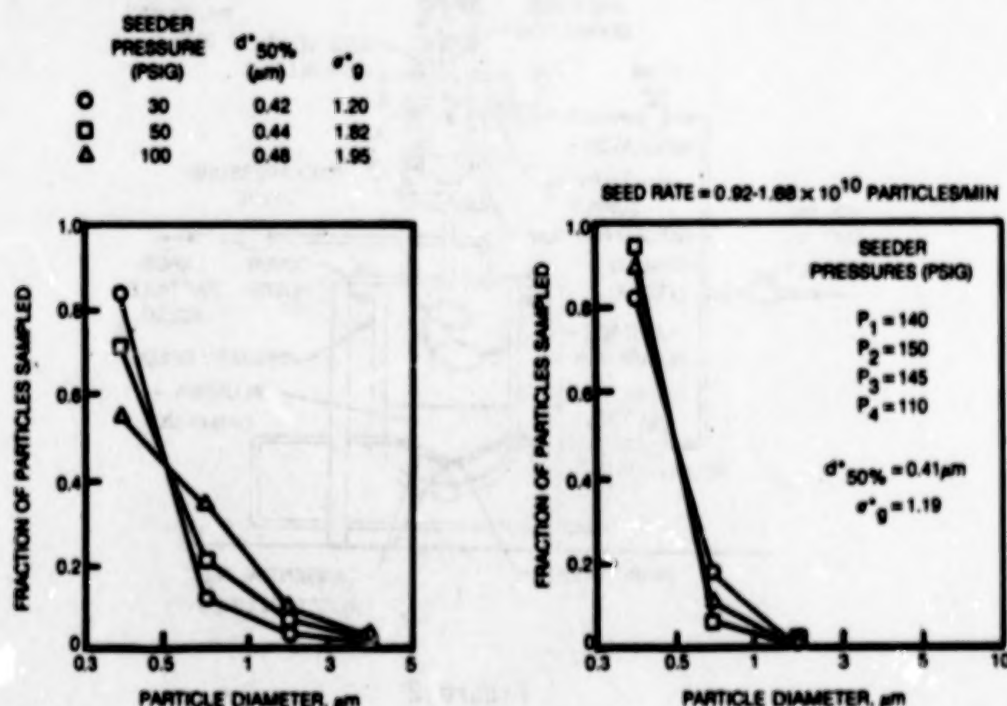
Figure 3

LV MEASUREMENTS IN HIGHLY ACCELERATED TRANSONIC MODEL FAN DUCT EXHAUST

LV measurements were made in the exit plane of a model turbofan engine
fan duct shown in figure 4. Operating at a pressure ratio of 2.5, flow
within the fan duct was subsonic up to the throat (located just upstream of
the exit plane) and mixed supersonic-subsonic in the exit plane. Strong
acceleration fields existed just upstream of the exit and in the downstream
exhaust flowfield which was bounded on the inner side by the simulated
engine afterbody. LV measurements in the fan duct exit plane are shown
in figure 4. The original seeder produced a distribution with a maximum
Mach number of 1.0 even though the nozzle was operated at a pressure ratio
of 2.5 and the exit plane was located downstream of the choked throat.
When the modified seeder was used with an active vortex separator, the
measured flow showed the desired supersonic-subsonic velocity profile.
Accelerations on the order of 7600 m/sec/m were measured at one radial
position in the immediate vicinity of the fan duct exit.

Figure 4

109
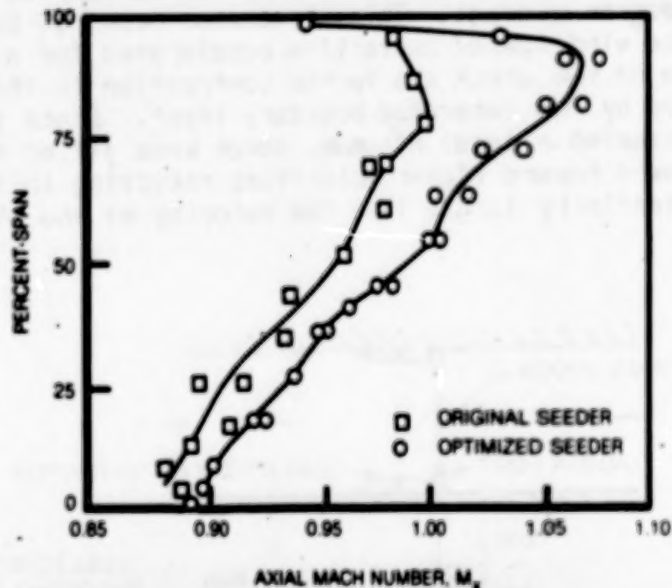
Direct measurements of the velocity lag characteristics of seed particles encountering a normal shock have been made at UTRC. The measurements were made in a supersonic wind tunnel test section designed for the study of shock-boundary layer interactions (fig. 5). The seeded air was accelerated to M = 1.4 before encountering the normal shock. LV measurements taken on the wind tunnel centerline are shown in figure 5 for two seed materials, 30 μm dia glass microballoons and 0.3 μm dia alumina.

The 30 μm dia hollow glass microballoons were reputed to have been capable of following extreme flowfield gradients. The velocities measured in the vicinity of the shock wave, however, showed that the microballoons not only barely responded to the step change in flow speed across the shock but they also lagged the flow by 15 percent upstream of the shock. The 0.3 μm dia alumina particles generated in the fluidized bed seeder with the vortex swirler activated followed the flow through the shock with minimal error. The alumina particles decelerated at the rate of 20,000 m/sec/m through the shock. Just downstream of the shock (x = .25 cm) the velocity determined from the peak in the histogram of measured samples was 20 m/sec lower than the histogram average. This phenomenon occurred because the subsonic flow on the wind tunnel centerline accelerated for a short distance downstream of the shock due to the contraction in the aerodynamic cross-section caused by the separated boundary layer. Since the velocity at x = .25 cm represented a local minimum, shock wave jitter caused the histogram to be skewed toward higher velocities resulting in the histogram average being substantially larger than the velocity at the histogram peak.
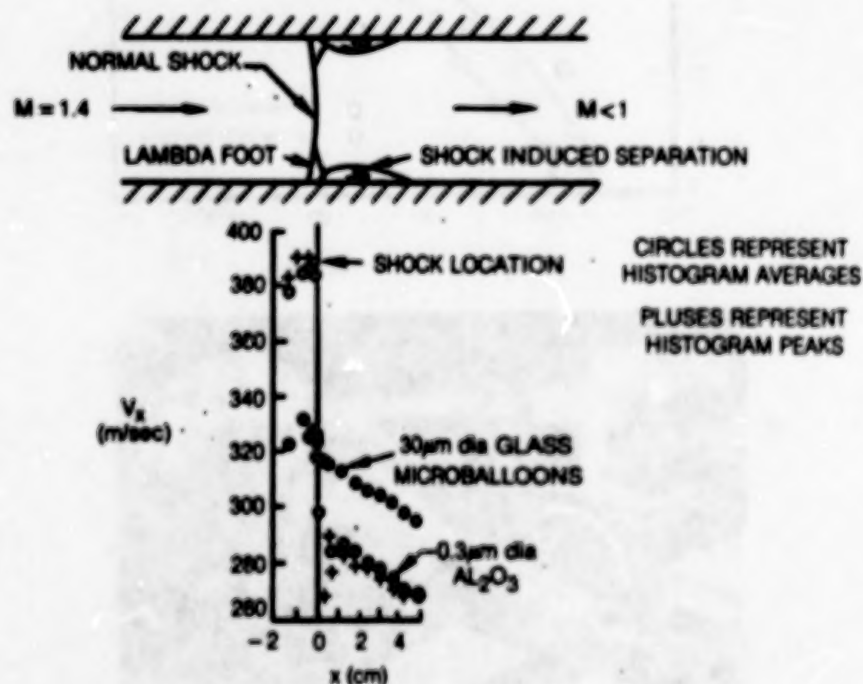
Figure 5

ZERO-WAKE SEEDING PROBE

A cylindrical seeder probe, shown in figure 6, has been designed at UTRC to effectively seed the flow while minimizing the disturbances to the wind tunnel airstream. A similarly configured probe designated the "zero-wake seeder" has been developed independently by Simpson (ref. 3). In principle, the flowrate through the seeding probe is adjusted until the momentum of the seeded air injected into the base region of the cylinder equals the cylinder drag and eliminates the wake deficit.

The zero-wake seeding probe has been used successfully to seed the flow field in a recently completed subsonic separated turbulent boundary layer separation bubble experiment at UTRC (ref. 4). The seed was injected into the wind tunnel plenum upstream of a 4 to 1 tunnel contraction. The seeding probe produced a seed cloud having an approximately circular cross-section with a 15 cm dia at the test section inlet 500 probe diameters downstream. Total pressure probing revealed no discernible wake deficit at the test section inlet during seeder operation. Similarly, hot-film measurements showed no difference in freestream turbulence level at the test section inlet during seeder operation compared to the clean tunnel operation with the seeder probe out of the tunnel. As expected, the turbulence level was increased when the probe was in the flow but not operating.

Figure 6

111
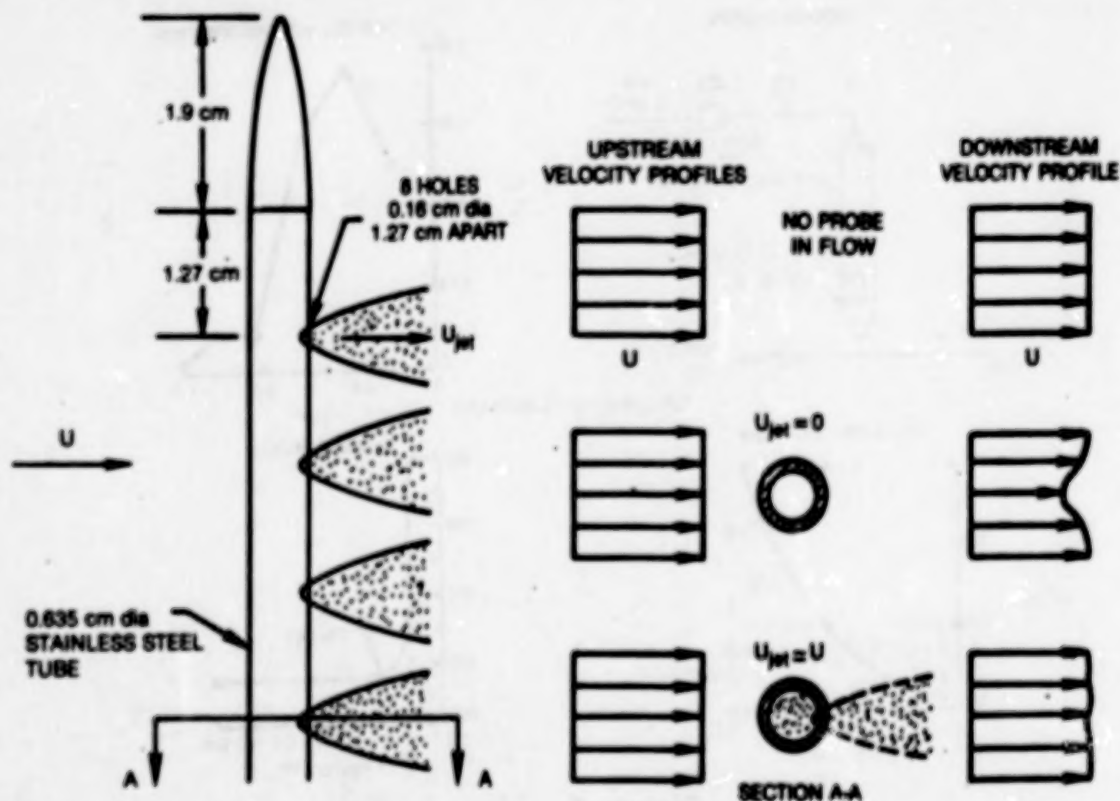
SUBMICRON SEED PARTICLE GENERATION WITH INCENSE SEEDER

D. C. McCormick of UTRC has developed the incense seeder, shown schematically in figure 7, to generate submicron seed particles. The measured size distribution of seed generated by the seeder from No. 2 Gonesh Incense cones* is also shown. All the measured particles were submicron with 90 percent of the particles being in the 0.10-0.45 μm dia. range. The incense seeder was used to seed the flow in a model turbofan engine fanduct exhaust which was half the scale of the model shown in figure 4. The acceleration field within the model fanduct was estimated from wall static pressure measurements. Maximum velocity lag in the accelerating flowfield for incense seed having the particle size distribution measured above was estimated to be 1.25 percent, and occurred just downstream of the model throat where the acceleration approximated 30,000 m/sec/m. Additional calculations showed that the incense seed would achieve 99 percent of the step change in velocity across an idealized M=1.4 normal shock within 1 mm of the shock front. The accuracy of LV mean velocity measurements subsequently made in the afterbody flowfield was verified by comparing the measured velocities to the velocities determined from pitot measurements and Rankine-Hugoniot shock relationships at selected locations. The advantages of the incense seeder are its submicron size distribution which produces minimal rig contamination and its simple operation. Disadvantages are that the seed particles cannot be seen in backscatter and the incense cones burn out in 10 minutes.
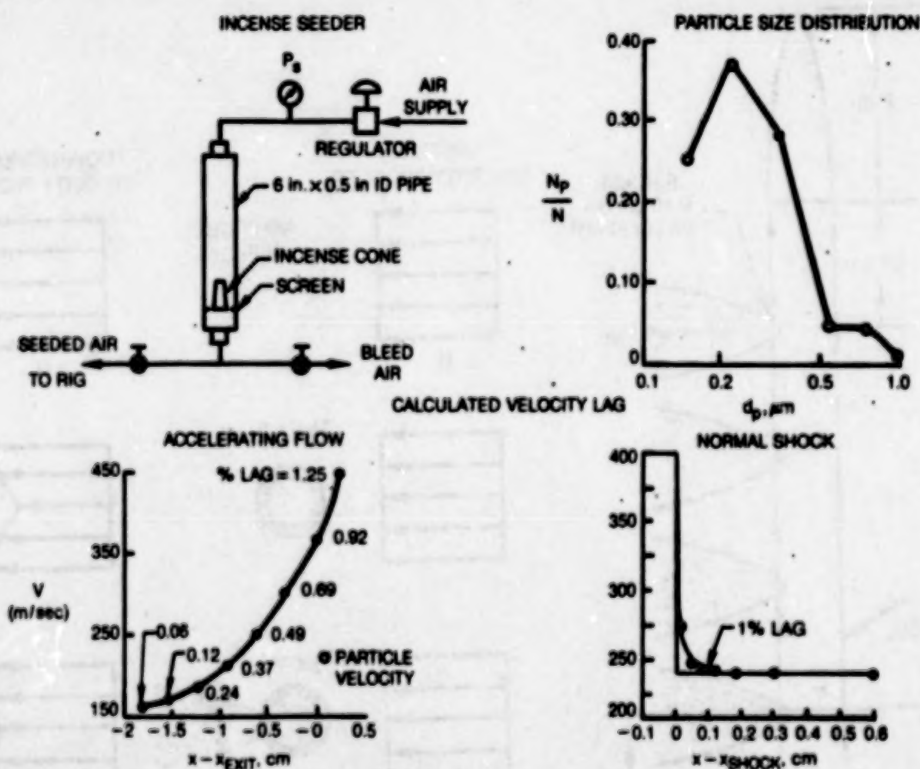
Figure 7

*Gonesh Incense, 200 North Laflin St., Chicago, IL 60607

REFERENCES

1. Electronic, Optical, Laser Materials and Components Catalog, Adolf Meller Co., Providence, R.I., 1980.

2. Patrick, W.P., and R.W. Paterson: Seeding Technique for Laser Doppler Velocimetry Measurements In Strongly Accelerated Nozzle Flowfields, AIAA Paper No. 81-1198, 16 pp., 1981.

3. Simpson, R.L., B. Chehroudi, and B.G. Shivaprasad: Pointwise and Scanning Laser Anemometer Measurements In Steady and Unsteady Separated Turbulent Boundary Layers, <u>Proceedings of the International Symposium on Applications of Laser - Doppler Anemometry to Fluid Mechanics</u>, Paper 11.3, Lisbon, Portugal, July 5-7, 1982.

4. Patrick, W. P.: Mean Flowfield Measurements In a Separated and Reattached Flat Plate Turbulent Boundary Layer. AIAA 85-1568, 1985.

SEEDING REQUIREMENTS FOR SCANNING LASER VELOCIMETRY *

C. E. Hackett
Sandia National Laboratories
Livermore, California

ABSTRACT

To measure the velocity distributions within time depenedent turbulent flow fields, a continuously scanning laser velocimeter system is being developed at SNLL. A prototype of this system has produced results which show that spatial and temporal variations in particle seed distribution seriously compromise the overall performance and operation of this device. To alleviate some of these problems, alternate flow seeding concepts have been explored. The most promising appear to be those that actively induce laser "sparks" within the gas flow, the velocity of which may be measured by a Fourier transformed velocimetry system.

OUTLINE:

1. Scanning Laser Velocimeter Configurations

Conventional Dual-Beam, three component
Multibeam - Fourier Transformed

2. Seeding Concepts Investigated

Passive: Conventional Pre-Mixed Systems
Active: In Situ Particle Seeding
         In Situ Laser Induced Seeding

3. Data Processing Implications

1. Scanning Laser Velocimeter Configurations

a) Conventional Dual-Beam Systems

Longitudinal Scanning
Transverse - Focal Plane Scanning

b) Multibeam - Fourier Transformed Systems

Real Fringe
Virtual Fringe

c) Data Processing Systems

Single processor
Multi-processor with virtual addressing

a) Conventional Dual-Beam Velocimeter Systems

Longitudinal Scanning
Zoom lenses, moving stages
Transverse Scanning - Focal Plane
Rotating Planar Mirrors

Advantages:

Commercial equipment is available
Large experience base for optics & processing

Disadvantages:

Requires separate laser line for each component
Small depth of modulation within the fringe pattern
Unsatisfactory three component performance so far!

b) Multibeam - Fourier Transformed Velocimeters

Longitudinal Scanning - Optical Axis
Zoom lenses, stages
Transverse Scanning - Focal Plane
Rotating Planar Mirrors

Advantages:

Deep Fraunhofer Modulation - high Signal/Noise ratio
Only ONE laser beam need be used for 3 components

Disadvantages:

Integrated commercial equipment is NOT available
Low absolute signal strength with current systems
Requires ELABORATE computer systems development

117

2. LV Seeding Concepts Investigated

Passive: Conventional Pre-mixed Seeding

Particle/Aerosol Production Techniques
Spatial & Temporal Dispersion

Active: In Situ Particle Seeding

Condensed & Solid Phase Particles
Chemically Formed Particles - TiO2

Active: Laser Induced Phenomena

Multiphoton Absorption
Breakdown - Laser Sparks

❦

Passive: Conventional Pre-mixed LV Seeding

Atomizers - liquid droplets - polydispersed: 0.5-2 microns
Berglund-Liu Aerosol Generator - monodispersed: 1-40 microns
Pre-formed Particle Dispersers - monodispersed: 1-10 microns

Advantages:

Good results obtained in homogeneously seeded flows
Integrated commercial equipment is available
Large experience base exists

Disadvantages:

Difficult to achieve uniform concentrations in space & time
Low absolute data rates due to the stochastic nature
Performance of scanning LV systems is seriously compromised

Active: In Situ Particle LV Seeding

Condensed liquid droplets formed from vapor/gas mixtures
Supercooled solid crystals formed from vapor/aerosol/gas mixes
Solid products from in situ vapor phase chemical reactions

Advantages:

High local particle concentrations within interaction zones
Seed high speed accelerating flows without acoustic dispersion
Seed fine scale flows, e.g. porous membranes and surfaces

Disadvantages:

Integrated commercial equipment is NOT available
Polydispersed, inhomogeneous in space & time - poor LV data
Difficult to characterize size & concentration of particles

Active: Laser Induced Seeding Phenomena

Multiphoton Absorption:
Pre-ionization condition, avalanche absorption
No emission, but scattering crossection enhanced

Breakdown - Laser Sparks:
For air   High E field > 6E+7 V/cm
at 1 atm.: High power density > 1E+5 MW/cm2
Laser: 900 mJ at 694.3 nm focused on spot 200 um dia.
Peak Power = 30MW, pulse duration = 30 ns, spark = 50us
Copper Vapor Lasers at 5kHz repetition rate

Advantages: Definitive scattering at high rates, with potential for
          molecular spectroscopy to determine density & temperture

Disadvantages: Additional excitation laser needed, with high power
          density optics required and conetained velocity range

SUMMARY:

Passive Seeding Techniques
Conventional particle/aerosol seeding may be of limited
value in any high rate scanning 3 component application

Active Seeding Technqiues
Laser induced phenomena may be used to provide definitive
scattering zones for LV and molecular spectroscopy

Conclusion:

For high rate 3 dimensional scanning LV active
seeding techniques should be used to produce uniform
scattering zones in space and time.

RECENT EXPERIENCE IN SEEDING
TRANSONIC/SUPERSONIC FLOWS AT AEDC

Fred L. Heltsley
Calspan Corporation, AEDC Division
Arnold Air Force Station, Tennessee

INTRODUCTION

The laser velocimeter has been utilized for several years at AEDC as a flow diagnostics tool. Most applications, following the initial proof-of-concept experiments, have involved relatively complex "unknown" flow fields in which the more conventional, intrusive techniques had either not been attempted or had yielded unsatisfactory results. The blunt-base nozzle-afterbody base flow study listed in Figure 1 will be discussed as a representative example of such applications. A wide variety of problems have been encountered during these tests, many of which have proven to be closely related to the size and/or size distribution of the seeding material within the fluid. Resulting measurement uncertainties could often not be conclusively resolved because of the "unknown" nature of the flow field. The other experiments listed in Figure 1 were conducted to provide "known" aerodynamic conditions for comparison with the velocimeter results.

TESTS

CONFIGURATION	FACILITY
BLUNT-BASE NOZZLE-AFTERBODY	AEDC/PWT TUNNEL 1T
7-DEG HALF-ANGLE CIRCULAR CONE	AEDC/VKF TUNNEL A
2-DIMENSIONAL CIRCULAR CYLINDER	AEDC/VKF TUNNEL A

Figure 1

BLUNT-BASE NOZZLE-AFTERBODY TEST

Figure 2 presents some details of the blunt-base nozzle-afterbody test.

- **MODEL CONFIGURATION**
  - **2.5 IN DIA CIRCULAR CYLINDER**
  - **0.5 IN EXIT DIA, MACH 2.7 NOZZLE AT CENTER**

- **TEST CONDITIONS**
  - **EXTERNAL STREAM**
    - MI = 1.4, RE = 4.75 x 10^6/FT
  - **JET (COLD NITROGEN)**
    - MJE = 2.7, NP   70 AND 150 (UNDEREXPANDED)

- **CONFIGURATION CHARACTERISTICS:**
  - **LARGE BASE FLOW SEPARATION REGION**

- **LDV SYSTEM:**
  - **2-COMPONENT BACKSCATTER/COUNTER PROCESSORS**
  - **2-COMPONENT BACKSCATTER/FOURIER PROCESSORS**

Figure 2

BLUNT-BASE NOZZLE-AFTERBODY INSTALLED IN AEDC/PWT TUNNEL 1T

Figure 3 is a photograph of the blunt-base nozzle-afterbody installed in the AEDC/PWT Tunnel 1T.
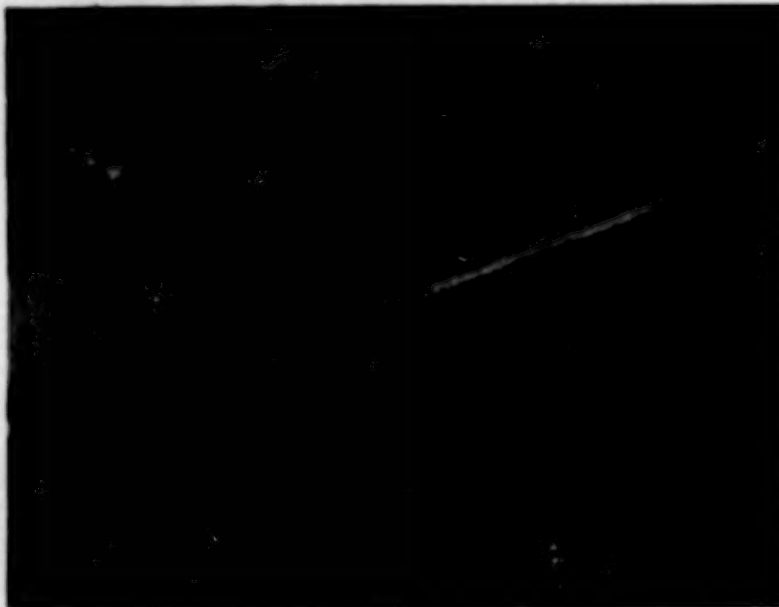
Figure 3

123

NOZZLE-AFTERBODY VELOCITY VECTORS

Mean velocity vectors obtained in the nozzle-afterbody flow field are presented in Figure 4. Flow features, i.e., shocks, expansion fans, Mach disc and shear layers obtained from shadowgraphs, are superimposed. The absence of vectors in the outer edge of the jet plume reflects the absence of seed particles in that region large enough to provide a signal processable by the LDV counter processors. The signals observed were strong enough, however, for processing by the discrete Fourier processor (DFT). These data are not included on the plot since the analysis is not complete at this time.

MI = 0.4   NPR = 150   RE = 4.75 x 10⁴/FT
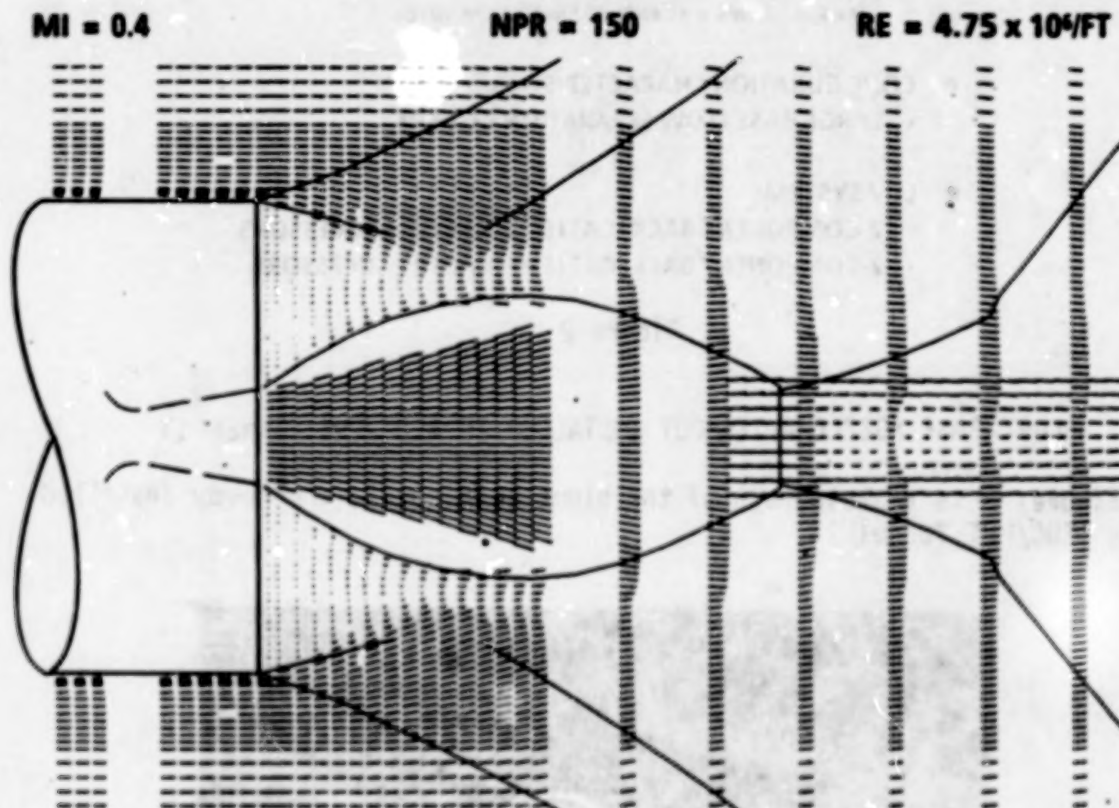
Figure 4

BLUNT-BASE TEST SEEDING

Seed material was added to the tunnel flow (external stream) in the stilling chamber approximately ten feet upstream of the test article. Seed were also injected into the tube which provided high pressure gas for the test article exhaust jet. The redistribution of seed particles within the flow field by the severe aerodynamic conditions resulted in an extremely low particle number density within the separation region near the model base. Seed were introduced into the region from a manifold within the model. Although no difference was observed in the base pressure with the base seeder on or off, other measurements, presented in Reference 1, cast some doubt upon the conclusion that the seeding induced flow disturbance was negligible. The types of aerosol generators and the seed materials used during the test are presented in Figure 5.

- **EXTERNAL FLOW (STREAM TUBE):**
  - **FLUIDIZED BED/0.3 MICRON ALUMINUM OXIDE PARTICLES**

- **JET PLUME:**
  - **FLUIDIZED BED/0.3 MICRON ALUMINUM OXIDE PARTICLES**

- **SEPARATED BASE FLOW (INTERNAL MANIFOLD):**
  - **FLUIDIZED BED/0.3 MICRON ALUMINUM OXIDE PARTICLES**
  - **COLLISON NEBULIZER/MINERAL OIL**
  - **COLLISON NEBULIZER/GLYCEROL AND RHODAMINE 590 FLUORESCENT DYE**

Figure 5

PARTICLE SIZE ESTIMATION

A comparison of particle velocity computed by Nichols (Ref. 2) with LDV measurements at the jet exit of the blunt-base model is presented in Figure 6. The apparent mean particle diameter of 1.7 microns is significantly larger than the nominal 0.3 microns advertised by the manufacturer. The same aluminum oxide powder was found by Crosswy (Ref. 3) to be quite polydisperse, with a significant number of particles or agglomerates larger than 2.0 microns.
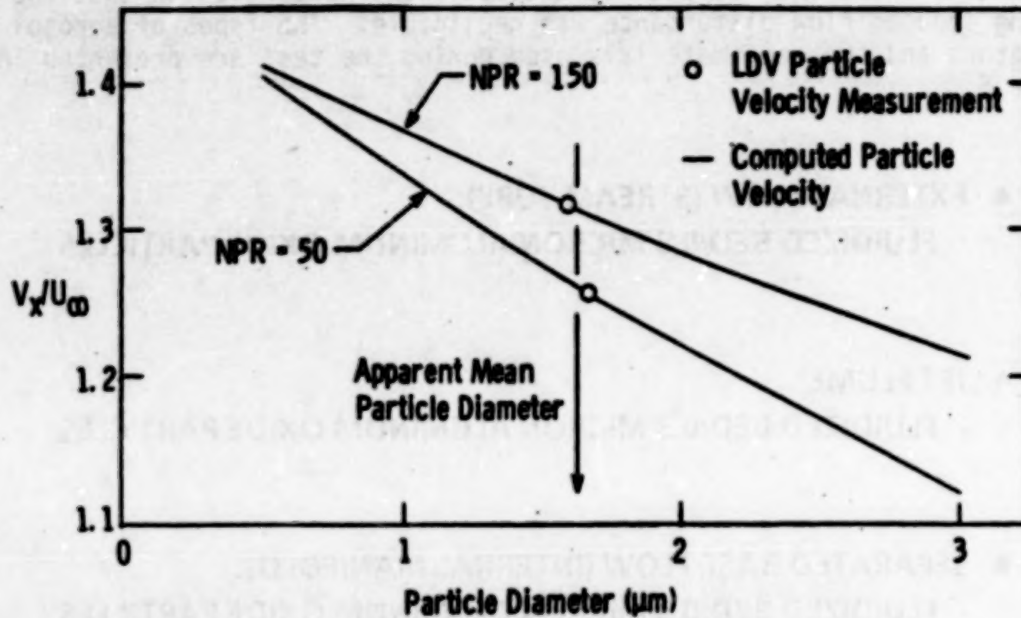
Figure 6

7.0 DEG HALF-ANGLE CONE TEST

Cone models have been studied extensively and provide a well-known reference for assessing the ability of the laser velocimeter to obtain boundary layer measurements in low density, supersonic flow. Pitot probe surveys were obtained during the test for three Reynolds numbers selected to produce laminar, transitional and turbulent boundary layers at the survey station (Fig. 7). In addition theoretical calculations were made for the same test conditions. The test was designed for comparison of forward and backscatter collection as well as counter and Fourier type processors.

A schematic of the cone model installed in the tunnel is presented in Figure 8. All surveys were obtained thirty five inches downstream of the cone nose.

- **MODEL CONFIGURATION**
    - **40.0 IN LONG, SHARP CIRCULAR CONE**

- **TEST CONDITIONS**
    - **MI = 4.0**
    - **RE = 0.6 x 10⁶/FT, 1.0 x 10⁶/FT, and 3.0 x 10⁶/FT**

- **CONFIGURATION CHARACTERISTICS:**
    - **FORWARD-FACING SURFACE, ATTACHED FLOW**

- **LDV SYSTEM:**
    - **2-COMPONENT BACKSCATTER/COUNTER PROCESSORS**
    - **1-COMPONENT FORWARD SCATTER/COUNTER PROCESSORS**
    - **1-COMPONENT FORWARD SCATTER/FOURIER PROCESSORS**

Figure 7

Figure 8 shows the 7.0-degree half-angle cone installed in the AEDC/VKF Tunnel A.
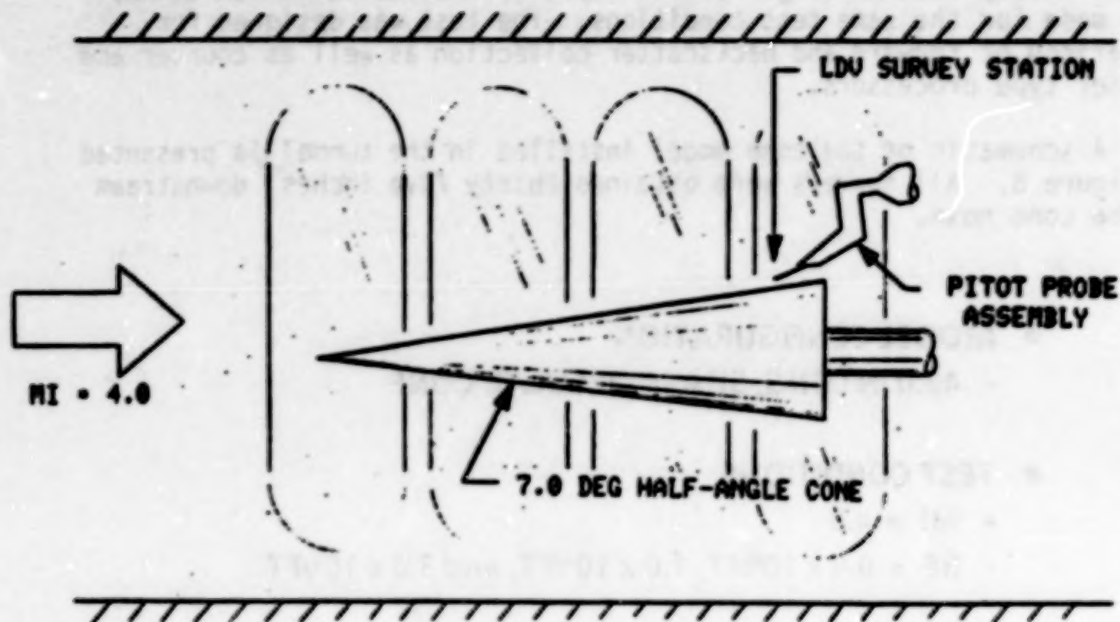
Figure 8

SEEDING

Figure 9 shows the types of seeding employed.

- **EXTERNAL FLOW (STREAM TUBE)**
  - **COLLISON NEBULIZER/OLIVE OIL**
  - **LASKIN NOZZLE/OLIVE OIL**

Figure 9

COMPARISON OF LDV MEASUREMENTS WITH THEORY AND PITOT PROBE RESULTS FOR THE CONE LAMINAR BOUNDARY LAYER

LDV measurements in the cone laminar boundary layer are compared with pitot probe data and theory in Figure 10. The polydisperse particle distribution and the high percentage of relatively large particles resulted in significant LDV measurement errors. The technique used for editing the LDV data is presented in Figures 11 and 12.
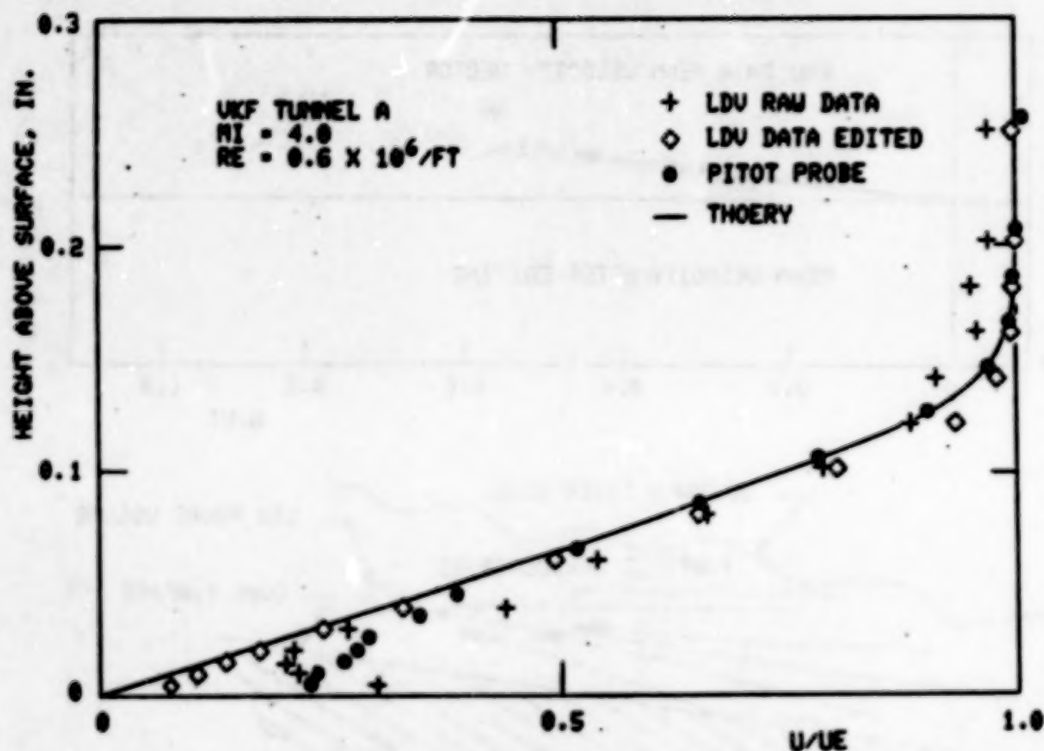
Figure 10

LDV SCATTER PLOT FOR LDV MEASUREMENT IN CONE BOUNDARY LAYER AND SUGGESTED TRAJECTORIES OF OBSERVED PARTICLES

A velocity scatter plot, typical of those observed in the lower portion of the cone laminar boundary layer, is presented in Figure 11 to provide additional insight. An observed high data rate near the model is evidence of the integrating effect of the forward facing surface. The number density of the large, fast particles appears to increase more rapidly than that of the smaller, slow, fluid following ones, causing a high bias.
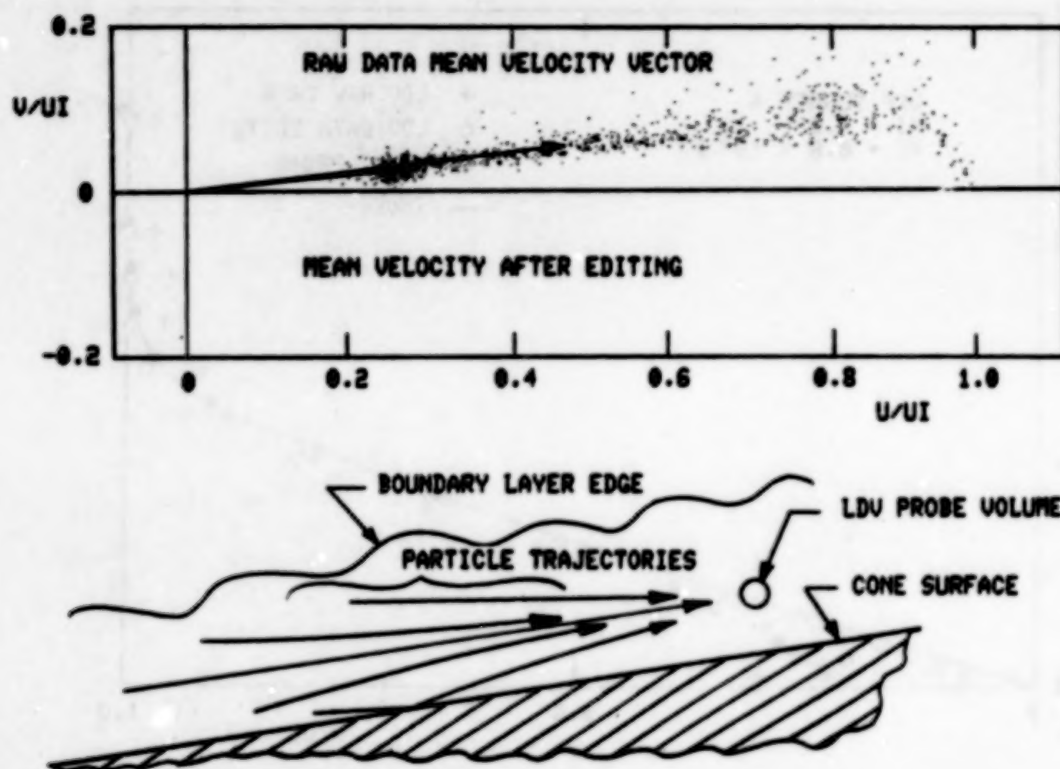
Figure 11

LDV VELOCITY PROBABILITY DISTRIBUTION IN THE CONE LAMINAR BOUNDARY LAYER

The typical axial velocity probability distribution is presented in Figure 12 to illustrate the results of rejecting the large particle bursts. Such editing required caution and cannot be done in situations where the large particles dominate the sample. A monodisperse sample not containing the larger particles could render such editing unnecessary.
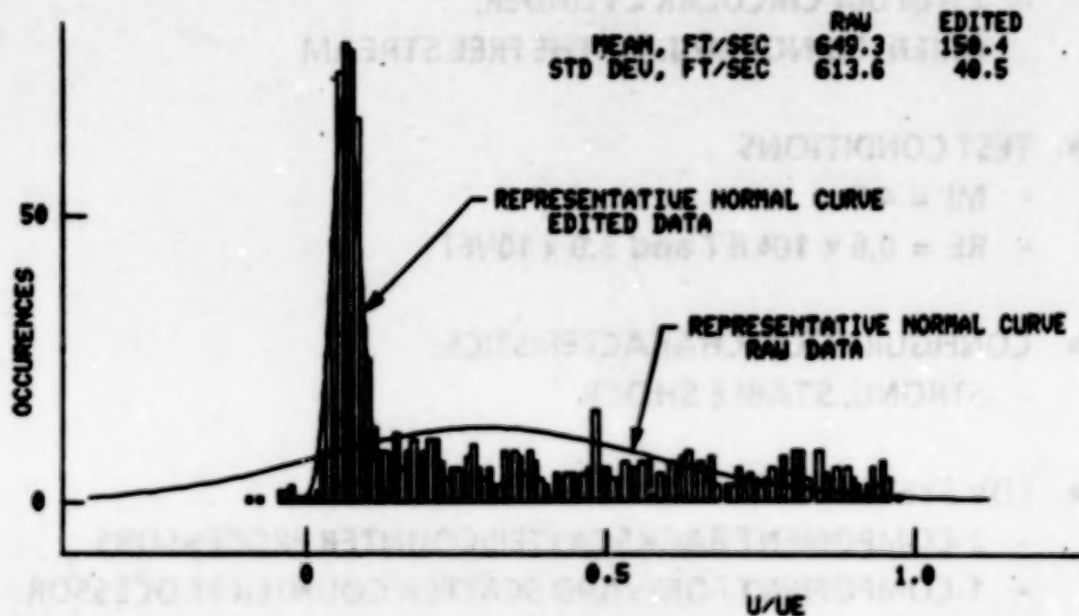
Figure 12

TWO-DIMENSIONAL CIRCULAR CYLINDER TEST

The 2-Dimensional cylinder configuration provided a strong, stable detached bow shock. Such an extreme velocity gradient is useful for the on-line "determination" of seed particle size. Horizontal LDV surveys were obtained through the shock on the model centerline for two Reynolds numbers (Figures 13 and 14). The aerosol generators and seed materials used are presented in Figure 15.

- **MODEL CONFIGURATION**
  - **2.0 IN DIA CIRCULAR CYLINDER, ORIENTED NORMAL TO THE FREE STREAM**

- **TEST CONDITIONS**
  - **MI = 4.0**
  - **RE = 0.6 x 10⁶ /FT and 3.0 x 10⁶/FT**

- **CONFIGURATION CHARACTERISTICS:**
  - **STRONG, STABLE SHOCK**

- **LDV SYSTEM:**
  - **2-COMPONENT BACKSCATTER/COUNTER PROCESSORS**
  - **1-COMPONENT FORWARD SCATTER/COUNTER PROCESSOR**
  - **1-COMPONENT FORWARD SCATTER/FOURIER PROCESSOR**

Figure 13

TWO-DIMENSIONAL CYLINDER MODEL IN MACH 4.0 STREAM

Figure 14 shows a sketch of the two-dimensional cylinder model in the Mach 4.0 stream.

MI = 4.0

DETACHED SHOCK

2.0 IN DIA
CIRCULAR CYLINDER

SURVEY LINE
LINE
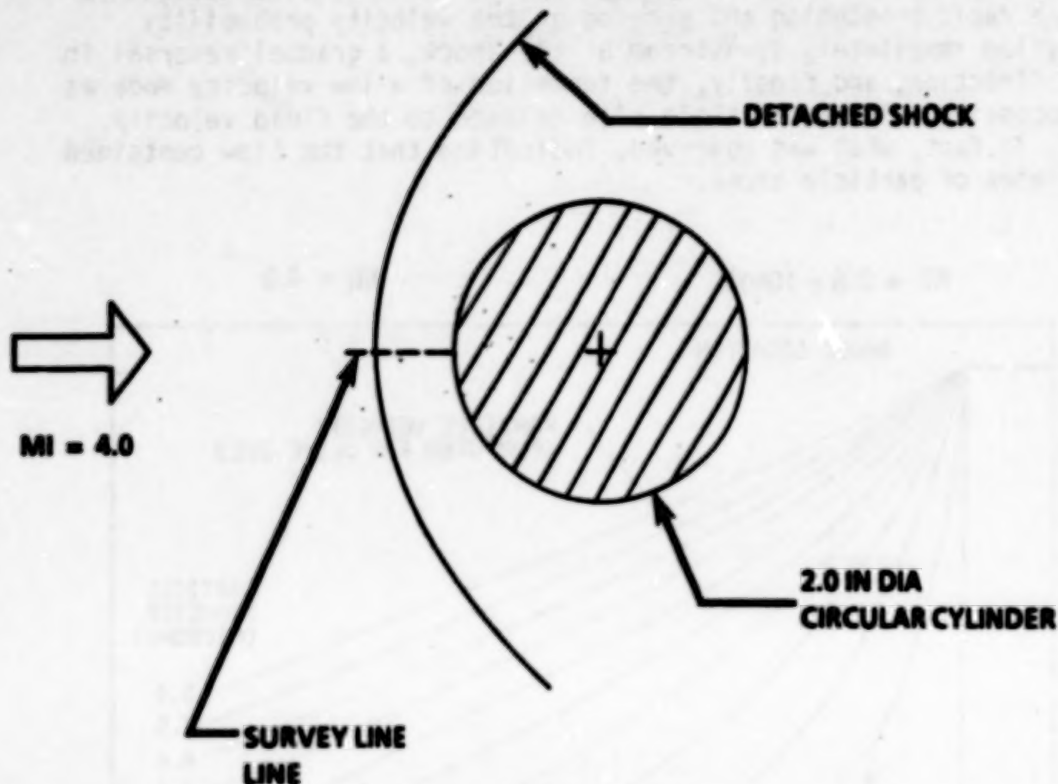
Figure 14

SEEDING

Figure 15 shows the types of seeding employed.

- **EXTERNAL FLOW (STREAM TUBE):**
  - **COLLISON NEBULIZER/OLIVE OIL**
  - **COLLISON NEBULIZER/OLIVE OIL AND FREON**
  - **LASKIN NOZZLE/OLIVE OIL**
  - **AMBIENT PARTICLES**

Figure 15

COMPUTED PARTICLE RESPONSE TO A NORMAL SHOCK

The computed responses of several sizes of oil droplets to the cylinder bow shock are presented in Figure 16. Based upon the computations, one would expect a polydisperse particle distribution to produce a rapid broadening and skewing of the velocity probability distribution immediately downstream of the shock, a gradual reversal in skewing direction, and finally, the formation of a low velocity mode as each successively larger particle size relaxed to the fluid velocity. This is, in fact, what was observed, indicating that the flow contained a wide range of particle sizes.

Figure 16

134
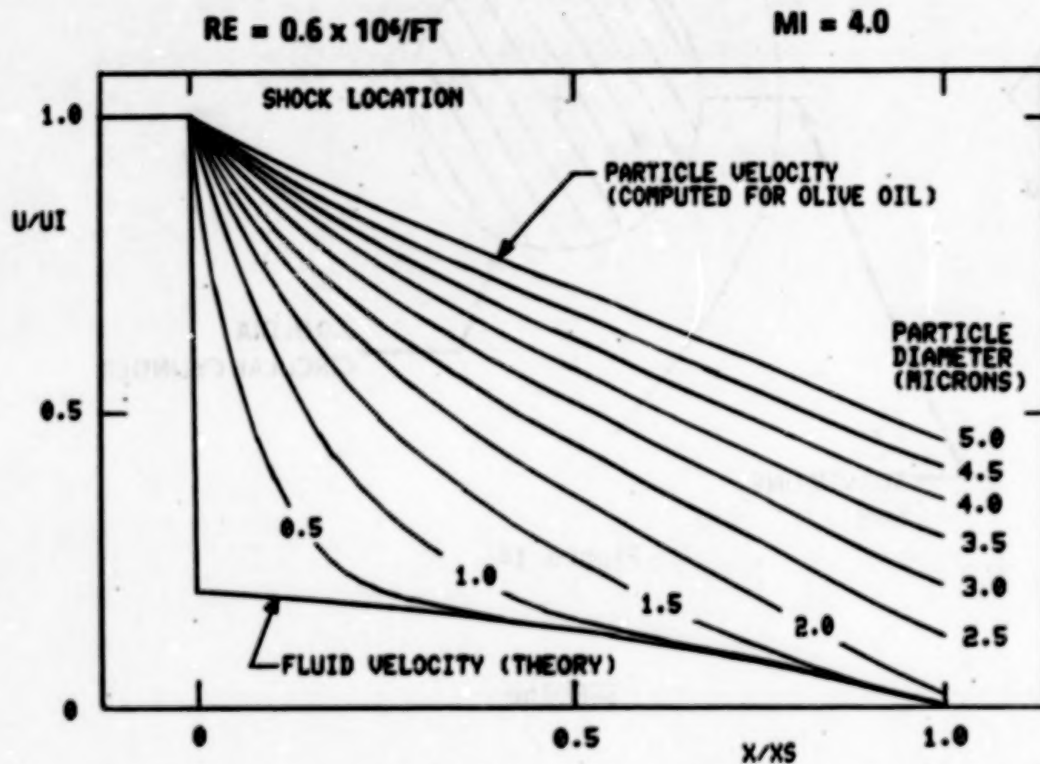
EFFECTS OF REYNOLDS NUMBER ON PARTICLE RESPONSE TO A SHOCK

Velocity probability distributions obtained upstream of the cylinder are presented in Figures 17 through 21 to illustrate the effects of several variables. Theoretical fluid velocity is represented by the solid line.

The particle response is strongly dependent upon Reynolds number as shown in the results presented in Figure 17. The particle relaxation distance was reduced significantly in the high Reynolds number case.

COUNTER PROCESSOR
FORWARD SCATTER

COLLISON NEBULIZER
OLIVE OIL

Figure 17

135
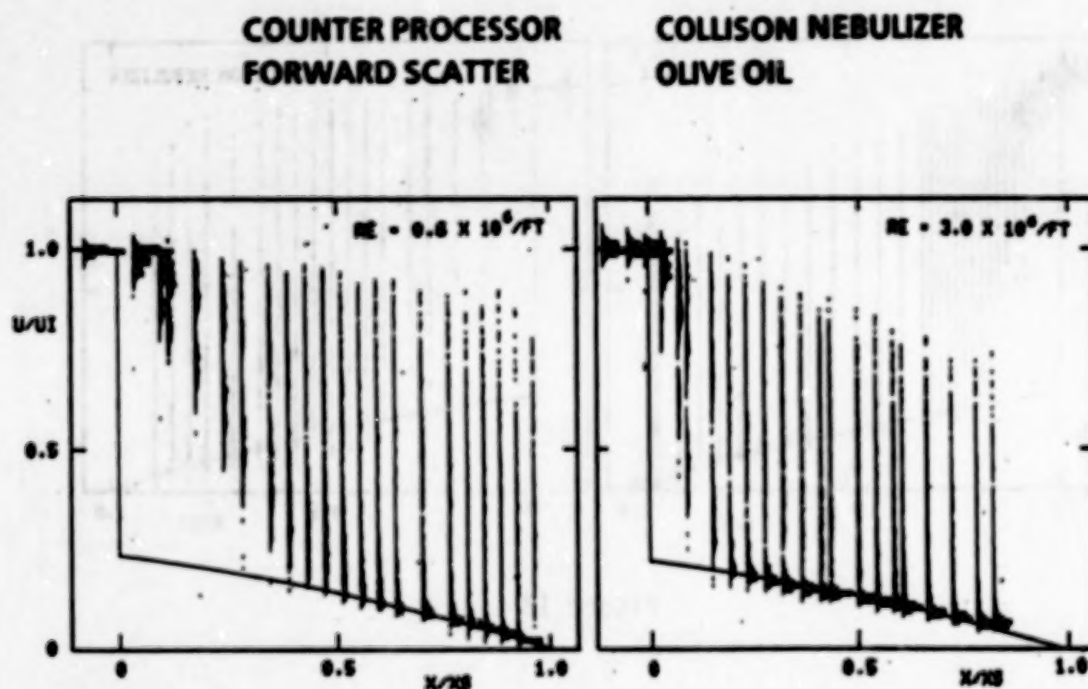
EFFECTS OF SEED GENERATOR ON LDV MEASUREMENTS

The 2-D cylinder flow was utilized to assess the performance of two types of liquid atomizers. The particle size distributions produced by the two devices were very similar, with the Laskin nozzle providing slightly smaller particles as well as fewer large ones. Both distributions were highly polydisperse as shown in Figure 18.

COUNTER PROCESSOR   **BACKSCATTER**

RE = 0.6 x 10⁴/FT   **OLIVE OIL**
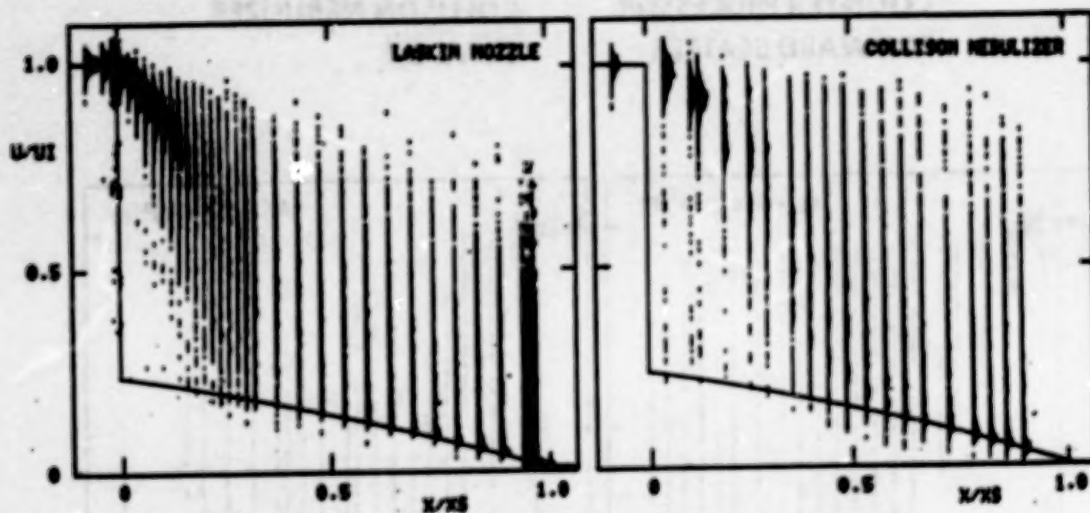
Figure 18

COMPARISON OF LDV MEASUREMENTS IN SEEDED AND UNSEEDED FLOW

Figure 19 indicates that the most accurate mean velocity measurements and shortest relaxation distances were obtained using only the ambient aerosols in the Tunnel A flow. The data rate, however, was extremely slow. Backscatter signals from the particle were too weak for processing by the counter processor in the high velocity flow upstream of the shock.

COUNTER PROCESSOR
RE = 3.0 x 10⁶/FT   **FORWARD SCATTER**
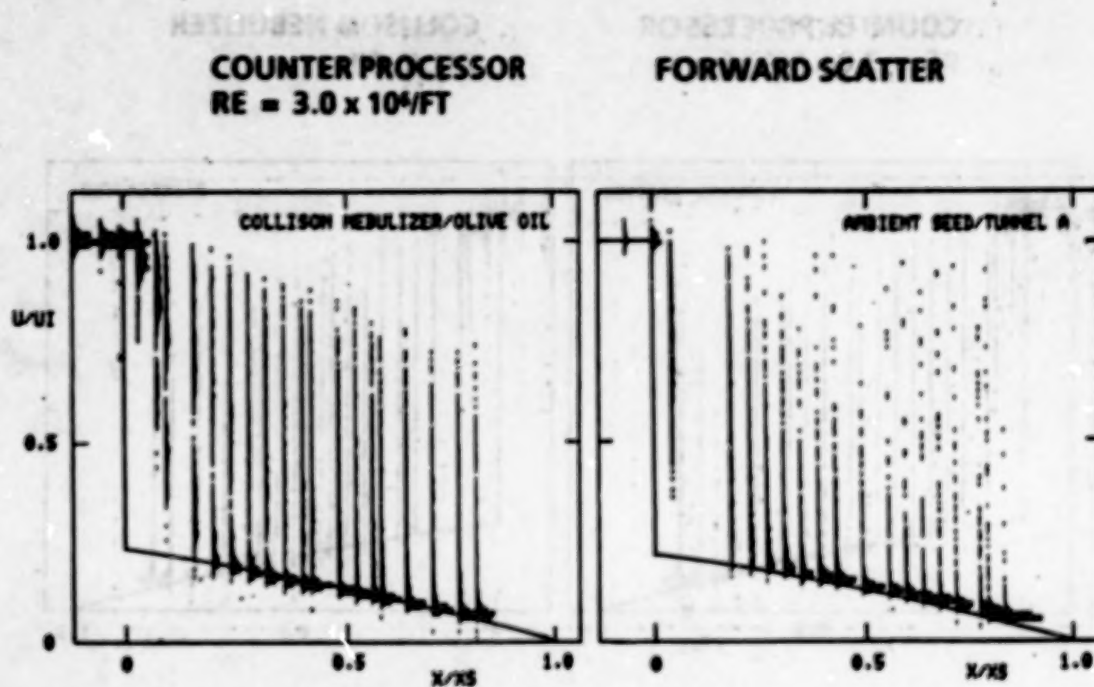
Figure 19

COMPARISON OF FORWARD SCATTER AND BACK SCATTER RESULTS

As would be expected, the forward scatter signal was significantly stronger than that available in backscatter. Thus, the signal from smaller particles could be processed by the forward scatter system as indicated by the earlier probability mode buildup at the fluid velocity shown in Figure 20.

COUNTER PROCESSOR
RE = 3.0 x 10⁴/FT

COLLISON NEBULIZER
OLIVE OIL
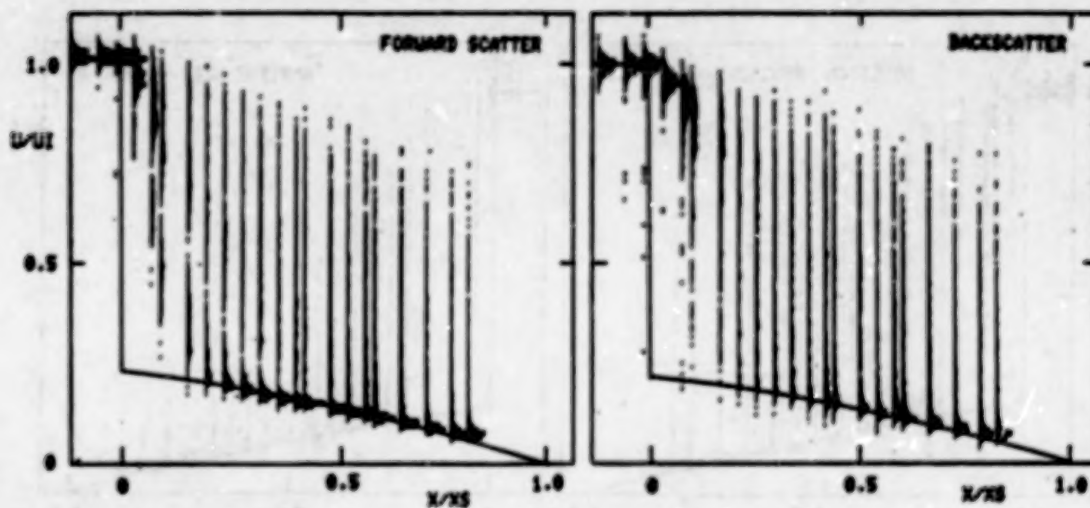
Figure 20

COMPARISON OF RESULTS FROM TWO LDV PROCESSORS

Figure 21 results from the cylinder shock also indicate that the Fourier processor can "see" smaller particles than the counter type. The primary differences appear to be the strength of the mode at the fluid velocity and the relative number of larger particles observed by the two instruments.

BACKSCATTER
RE = 0.6 x 10⁶/FT

LASKIN NOZZLE
OLIVE OIL
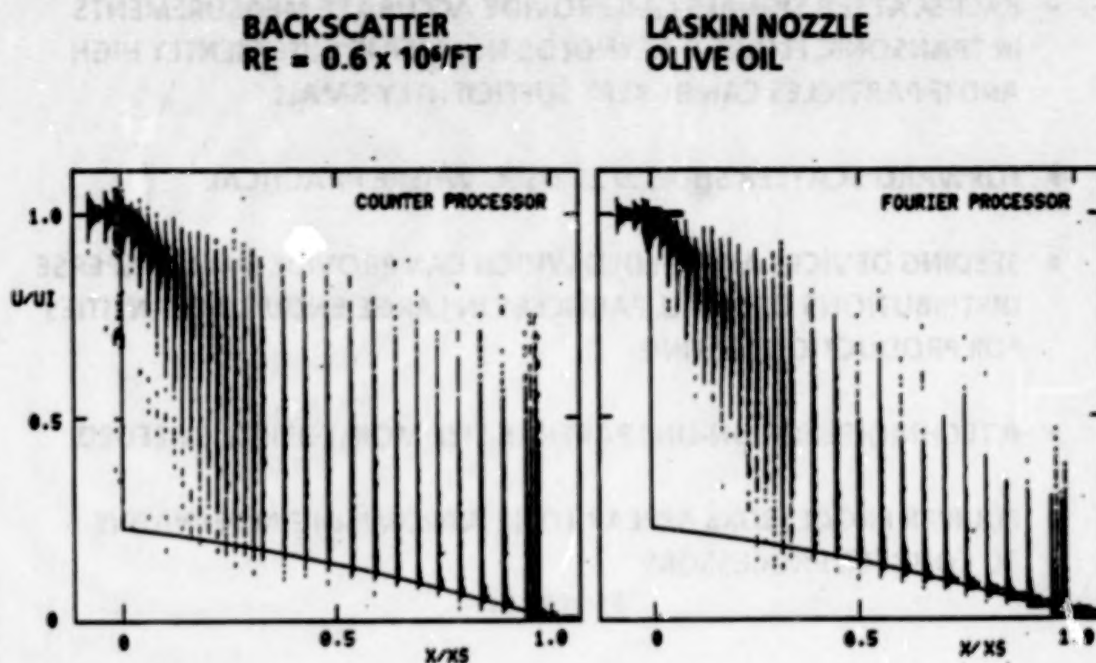
Figure 21

CONCLUSIONS

Conclusions are presented in Figure 22.

- **POLYDISPERSE PARTICLE DISTRIBUTIONS CAN YIELD MISLEADING LDV RESULTS WHICH ARE DIFFICULT, IF NOT IMPOSSIBLE, TO DEAL WITH OFF-LINE**

- **BACKSCATTER SIGNALS CAN PROVIDE ACCURATE MEASUREMENTS IN TRANSONIC FLOWS IF REYNOLDS NUMBER IS SUFFICIENTLY HIGH AND IF PARTICLES CAN BE KEPT SUFFICIENTLY SMALL**

- **FORWARD SCATTER SHOULD BE USED WHERE PRACTICAL**

- **SEEDING DEVICES ARE NEEDED WHICH CAN PROVIDE MONODISPERSE DISTRIBUTIONS OF SMALL PARTICLES IN LARGE ENOUGH QUANTITIES FOR PRODUCTION TESTING**

- **A TECHNIQUE FOR ON-LINE PARTICLE SIZE MONITORING IS NEEDED**

- **FOURIER PROCESSORS APPEAR TO BE A PROMISING ALTERNATIVE TO COUNTER PROCESSORS**

Figure 22

REFERENCES

1. Heltsley, F. L.; Walker, B. J.; and Nichols, R. H.: Transonic Nozzle-Afterbody Flow Field Measurements Using a Laser Doppler Velocimeter. Presented at 53rd meeting of Fluid Dynamics Panel Symposium on Wind Tunnels and Testing Techniques, Cesme, Turkey, Sept. 26-29, 1983.

2. Nichols, R. H.: Calculation of Particle Dynamics Effects in Laser Velocimeter Data. Wind Tunnel Seeding Systems for Laser Velocimeters, NASA CP-2393, 1985. pp. 1-12.

3. Crosswy, F. L.: Particle Size Distributions of Several Commonly Used Seeding Aerosols. Wind Tunnel Seeding Systems for Laser Velocimeters, NASA CP-2393, 1985, pp. 53-76.

LASER VELOCIMETRY MEASUREMENT IN A TRANSONIC TUNNEL

T. Terry Ng

and

Thomas J. Mueller

University of Notre Dame
Notre Dame, Indiana 46556

INTRODUCTION

The design of efficient airfoils for transonic vehicles has been a goal of aerodynamicists over the past four decades. Although advances have been made, there are several problems which require careful investigation if additional improvements are to be realized. These problems are related to the management of the boundary layer and associated problems such as shock induced separation and shock-boundary layer interaction.

In the last decade, computational methods have been developed which, when combined with analytical and experimental studies, have added to our understanding of the flow over transonic airfoils. Computational methods, like analytical methods, required physical experiments in order to formulate and verify the modelling assumptions made and the numerical procedure used. The sensitivity of flows near a Mach number of one is well known. Wind tunnel wall interference like blockage and shock wave reflection and flow disturbances caused by physical measurement probes have made transonic experiment difficult, especially since even boundaries far away will influence an airfoil near Mach one. Many advances have been made in recent years to alleviate the wall interference problem by reducing model size, utilizing ventilated wall wind tunnels, and applying theoretical and empirical corrections (ref. 1). In addition, advances in non-intrusive measurements techniques have enabled the obtaining of quantitative flow data without introducing probes which invariably disturb the flow.

Optical methods of investigation which depend on density changes are especially suited to the visual study of transonic flows. The interferometer, the schlieren, and the shadowgraph are commonly used optical methods of this type. These methods provide an overall picture of the density field. The recent development of another optical technique--the laser velocimeter (LV)--provides the opportunity to make detailed and potentially more reliable quantitative velocity measurements. This report will describe a transonic airfoil study currently under way at the University of Notre Dame. The study is supported by the Naval Research Laboratory under contract No. N00014-84-K-2013.

TRANSONIC TUNNEL

The transonic tunnel used for the experiment has slotted walls, 6% open area on the top and bottom walls and solid and easily removable glass side walls with a square cross-section and area 16 sq. in. (104.0 cm^2). The flow in the tunnel is controlled using a second throat downstream of the test section. The second throat is composed of a series of cylindrical rods normal to the flow. Rods of various diameters can be used to provide different throat areas. The plenum pressure can be controlled by two valves connected into the diffuser downstream of the second throat. A schematic of the test section is shown in Figure 1. This is an indraft tunnel which draws air from inside the laboratory and exhausts outside.

As shown in Figure 2, the inlet of this tunnel consists of 11 screens (five aluminum and six nylon) followed by a 150:1 contraction in area to the test section. This inlet produces excellent smoke streakline quality in the test section. Preliminary data indicates the turbulence intensity in the test section is less than 0.5%. Three 3130 cubic ft (17.70 m^3)/minute vacuum pumps, each driven by a 125 hp AC motor, permit continuous operation of this tunnel with schlieren and shadowgraph systems. The maximum Mach number attainable is about 1.4, depending on the ambient pressure and temperature.

The bi-convex airfoil used in the study, shown in Figure 3, is pinned between the circular plexiglass test section windows. These windows can be rotated as one unit to change the angle of attack. The airfoil has a one inch cord and a 10% thickness.

LASER VELOCIMETRY SYSTEM

The relatively high velocity of the flow under study is one of the major considerations for choosing a suitable LV system. The LV system used for the study is a single-component system (manufactured by TSI) with provision for later expansion to two-component. Due to the high flow velocity, a 4-Watt argon ion laser is used to provide sufficient scatter light intensity. With the green (514.5 nm) line the maximum single line power output is about 1.2 Watt. To maximize the signal to noise ratio and to minimize light reflection from solid surfaces into the receiving optics, an off-axis, forward scattering configuration is used. Both the transmitting lens and the receiving lens have a focal length of 241.9 mm, with beam spacing of 50 mm. Windows on the sides of the test section facilitate optical access to flow for LV scanning. The LV system is placed on a 3-dimensional traversing table (modified from a milling table) with position resolution of one thousandth of an inch. The receiving optics are physically connected to the traversing table by an overhanging structure so that the receiving and the transmitting optics can be moved as a single unit. A counter is used for signal processing and data acquisition is carried out using a PDP-11/23 computer.

PARTICLE GENERATION FOR LV MEASUREMENT

Two major factors influence design of the particle generation system for the LV measurement: (1) the open-loop design of the wind tunnel; and (2) the high flow velocity. The open-loop design coupled with the high speed of the flow means that a large quantity of particles would have to be generated continuously. Furthermore, the high speed flow requires particles of very small size in order that velocity slip not be a problem.

The particle used in this experiment is kerosene smoke generated by an oil smoke generator. This four-tube oil smoke generator is shown schematically in Figure 4. A flat electric heater strip is located inside a 51 mm square thin wall conduit tube. The entire unit is set at a convenient angle (about 60°) and the sight-feed-oiler is mounted on the unit at the upper end of each tube so the oil drips on the upper end of the heater strip. The drip rate can be adjusted to give the desirable amount of smoke. A squirrel cage blower mounted at the low end of the unit is used to force the smoke through the system. The squirrel cage blower is more or less mandatory--in the event of backfiring the sudden increase in pressure is easily transmitted through the rotor.

After leaving the generator, the smoke is allowed to pass through a heat exchanger made of 42 millimeter diameter pipe, as shown in Figure 5. In passing through the heat exchanger the smoke is cooled down to near room temperature, and the larger size droplets will coalesce and settle at the bottom of the heat exchanger tube. The entire system has drain corks conveniently located; one at the bottom of each tube of the generator itself to remove excess oil not converted to smoke, and others at the bottom of the heat exchanger to remove whatever oil might have condensed. After passing through the heat exchanger condenser system, the smoke flows into a 117 millimeter manifold and is passed through an absorbent cloth filter.

143

This filter is made of thick cloth and removes most of the remaining lighter tars, allowing only very fine and even sized smoke particles to pass through. After the filtering, the smoke is passed into a circular tube of about 30 mm in diameter with several fine mesh screens inside to produce a uniform stream of smoke at the tube outlet. The entire smoke generating assembly can be traversed up and down, as desired, by using the attached remotely controlled motor.

A high quantity of very fine smoke particle suitable for LV application can be generated continuously using the smoke generator. The smoke has to be distributed into the test section. If the smoke is to be evenly distributed over the entire flow field, a very effective mixing system will be required at the inlet of the tunnel. The designing of such a system can be very difficult. Furthermore, the high air flow rate will require an enormous amount of smoke to be generated. Thus a more practical way, though less convenient, is to direct the smoke stream at the exit of the smoke generating system to the position of the LV probe in the flow. Since the smoke stream does not cover the entire flow field, measurements at different locations will require the repositioning of the smoke stream. This method of smoke distribution is being used in this study and is found to be satisfactory.

PRELIMINARY TESTING

Some preliminary velocity measurements had been carried out inside the transonic tunnel using the LV system in association with the smoke generator. Pressure measurments were also performed using a pressure tap located on the side wall of the test section slighly upstream of the windows. Though the pressure measurements and the LV measurements were not taken at exactly the same location, extrapolation of the pressure data into the location of the LV measurements indicated a very close agreement between the velocity values obtained using the two different methods. Thus it is believed that the smoke particle is following the air flow with little or no velocity slip. Velocity measurements with airfoil at various angles of attack are now being carried out in conjuction with schlieren flow visualization. In the near future pressure distribution around and on the airfoil will be obtained by putting pressure taps on the side windows and using a pressure tap model (currently under construction) of the airfoil.

REFERENCE

1. Blackwell, J.A. Jr., "Experimental Testing at Transonic Speeds," Progress in Astronautics and Aerodynamics, Vol. 81, pp. 189-238, 1981.
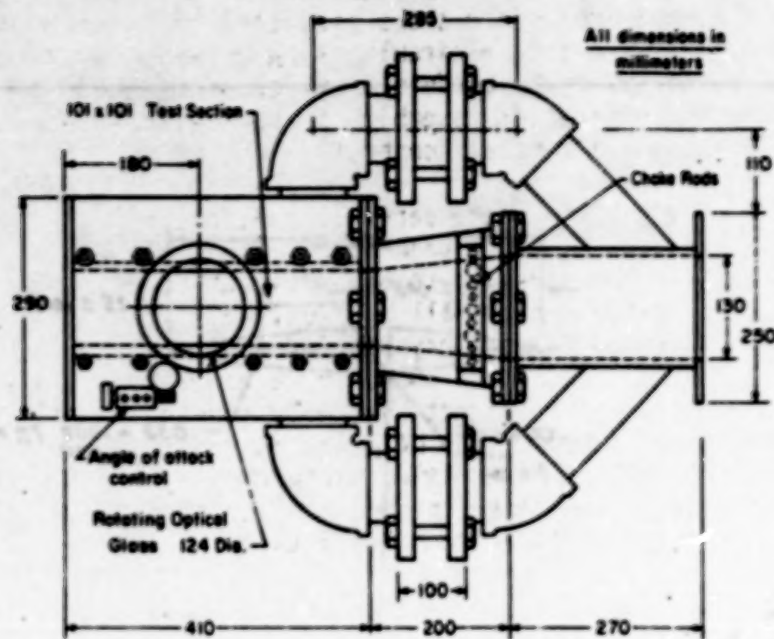
Figure 1. Schematic of the transonic tunnel test section.
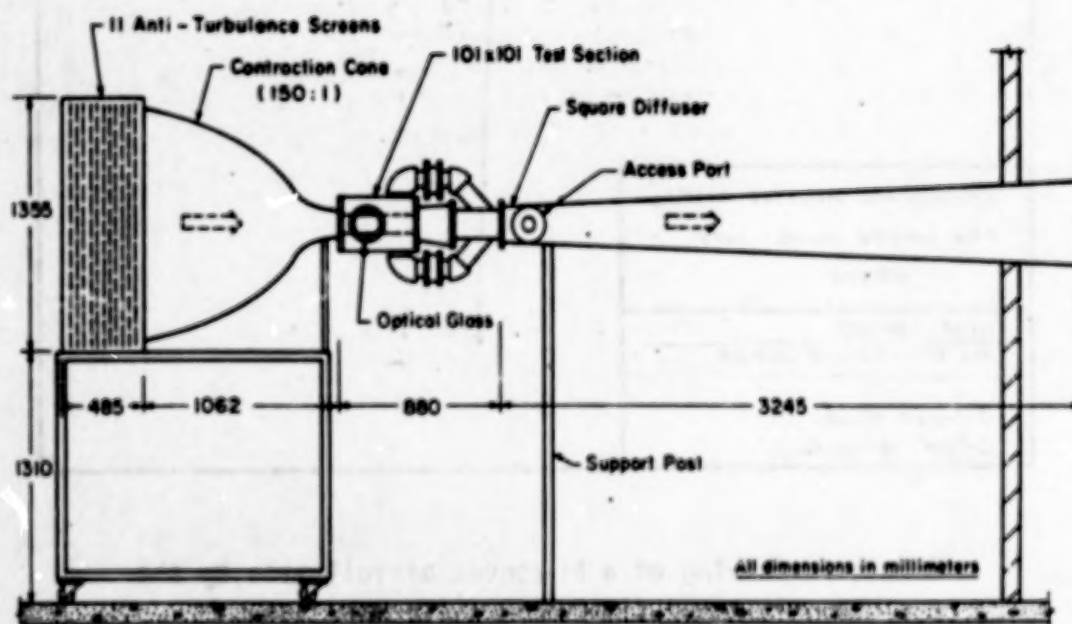
Figure 2. Schematic of the transonic tunnel.

145
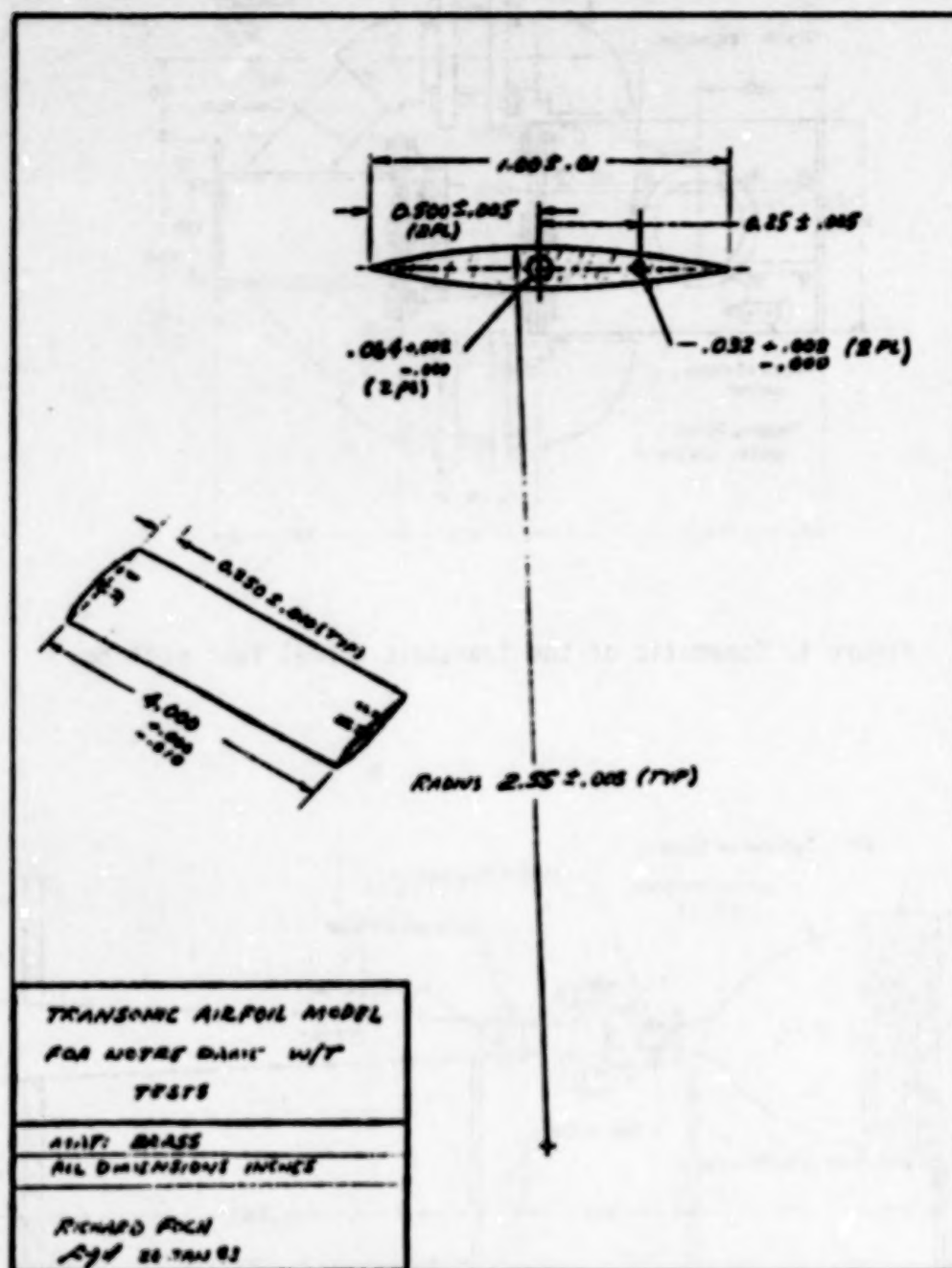
Figure 3. Drawing of a bi-convex airfoil made by the
Naval Research Laboratory.
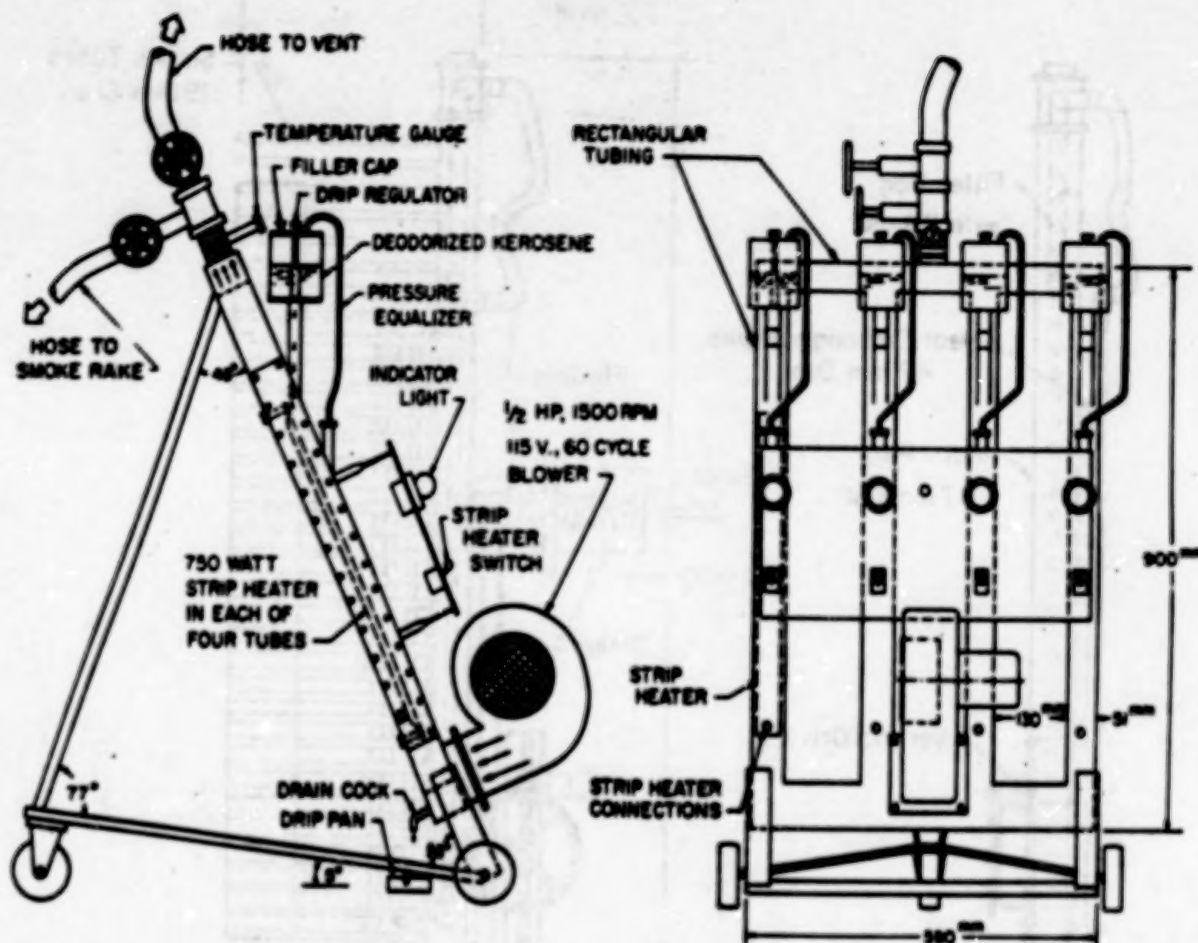
Figure 4. Kerosene smoke generator.
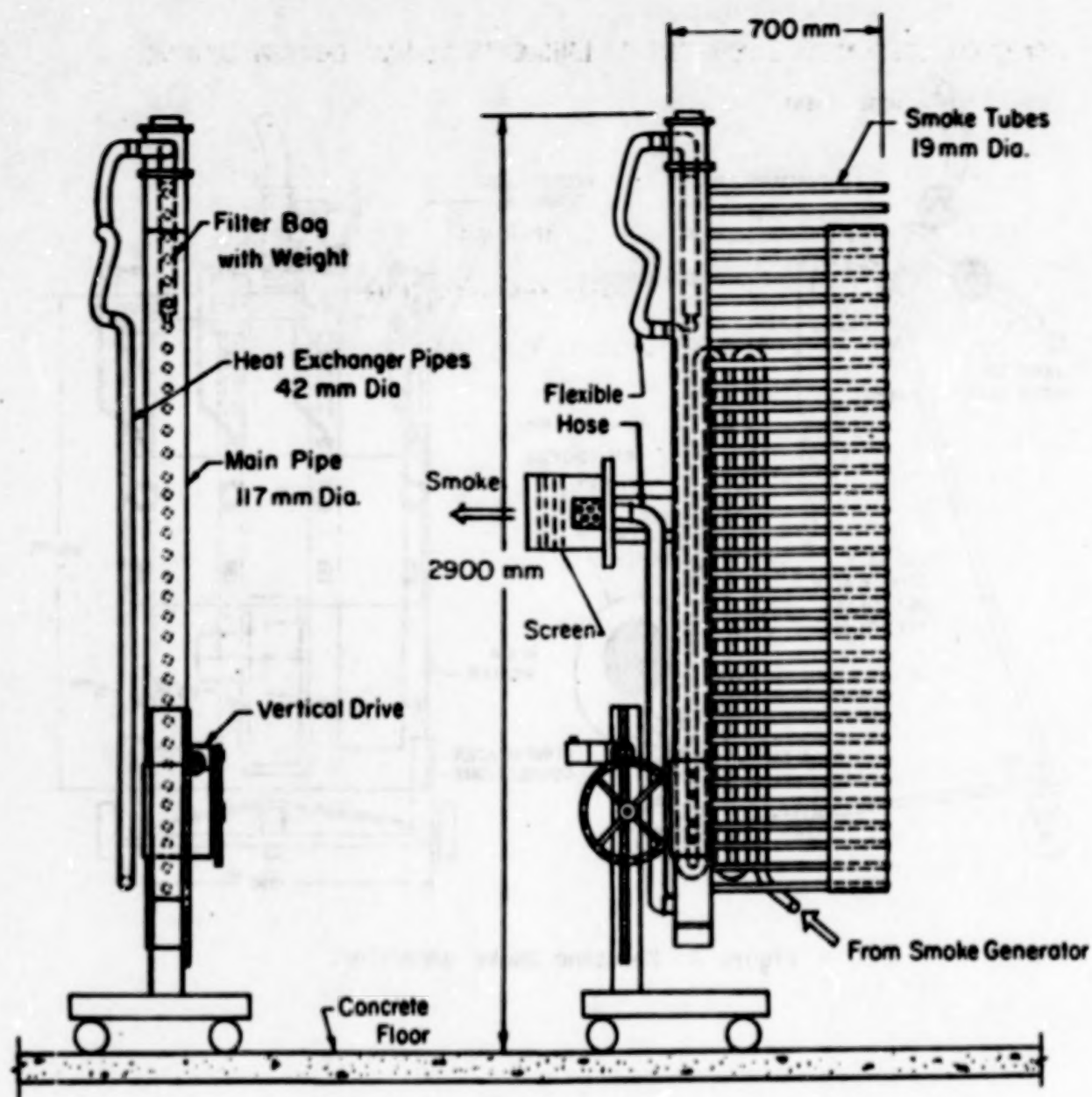
Figure 5. Smoke filter/condenser system.

Labels in figure:
- 700 mm
- Smoke Tubes 19 mm Dia.
- Filter Bag with Weight
- Heat Exchanger Pipes 42 mm Dia.
- Flexible Hose
- Main Pipe 117 mm Dia.
- Smoke
- 2900 mm
- Screen
- Vertical Drive
- From Smoke Generator
- Concrete Floor

PARTICLE GENERATION EXPERIENCE IN LANGLEY'S 16-FOOT TRANSONIC TUNNEL

D. E. Reubush

NASA   Langley Research Center

Hampton, Virginia
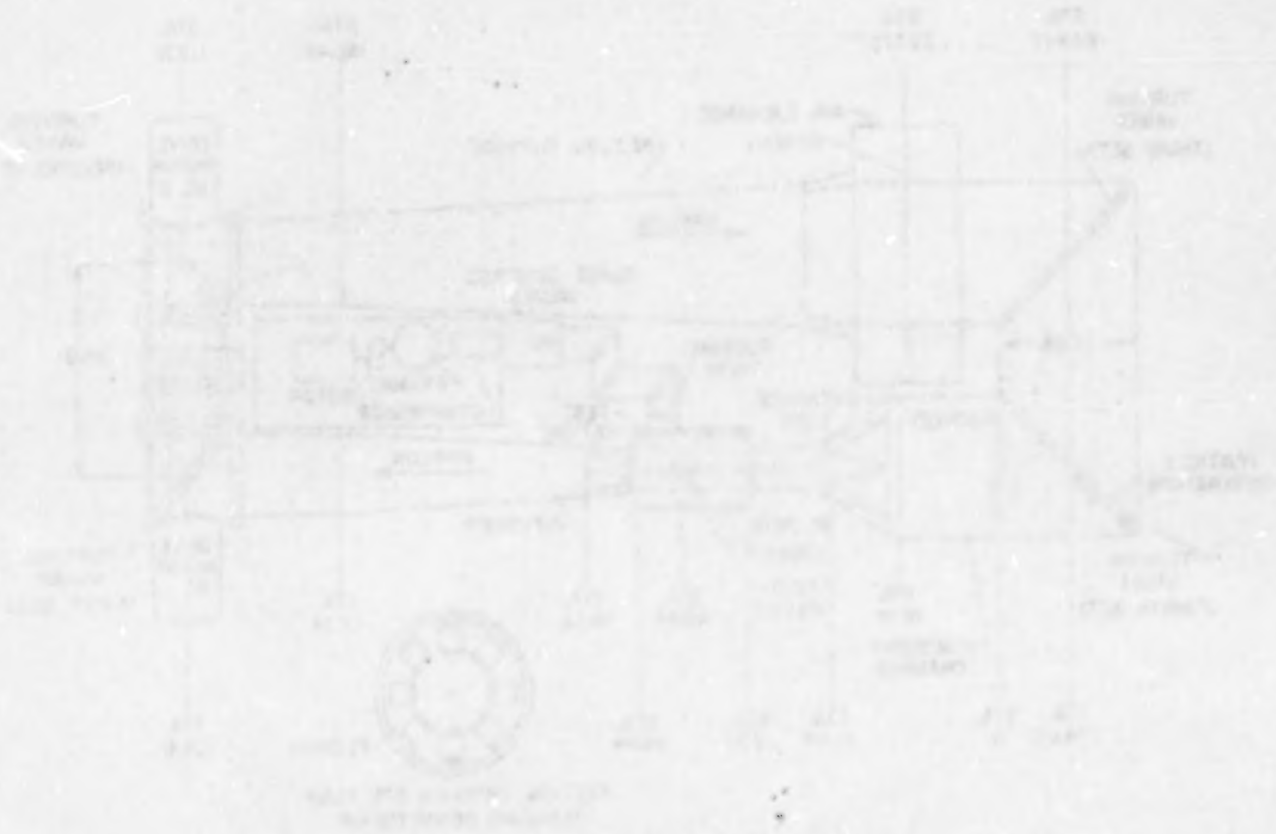
THE LANGLEY 16-FOOT TRANSONIC TUNNEL

The Langley 16-Foot Transonic Tunnel is a single-return, continuous-flow, atmospheric tunnel which uses air exchange for cooling. The tunnel speed is continuously variable from Mach 0 to 1.30. The test section is a regular octagon in cross-section with slots at the corners of the octagon. The laser velocimeter optics, laser, photomultipliers, etc. are mounted in the test section plenum chamber which surrounds the test section. The test volume is approximately a 1-meter cube about the tunnel center line centered on tunnel station 40.84 meters. The seeding system particle generators are mounted on the upstream side of the fourth set of turning vanes approximately 49 meters upstream of the test volume. At this point the tunnel has a diameter of 17.68 meters which meant that installation of the generators was a difficult procedure. It might be noted that particle generation had to be continuous as when the generators were turned off the data rate rapidly deteriorated to zero.

SECTION THROUGH STA. 33.53
(LOOKING DOWNSTREAM)
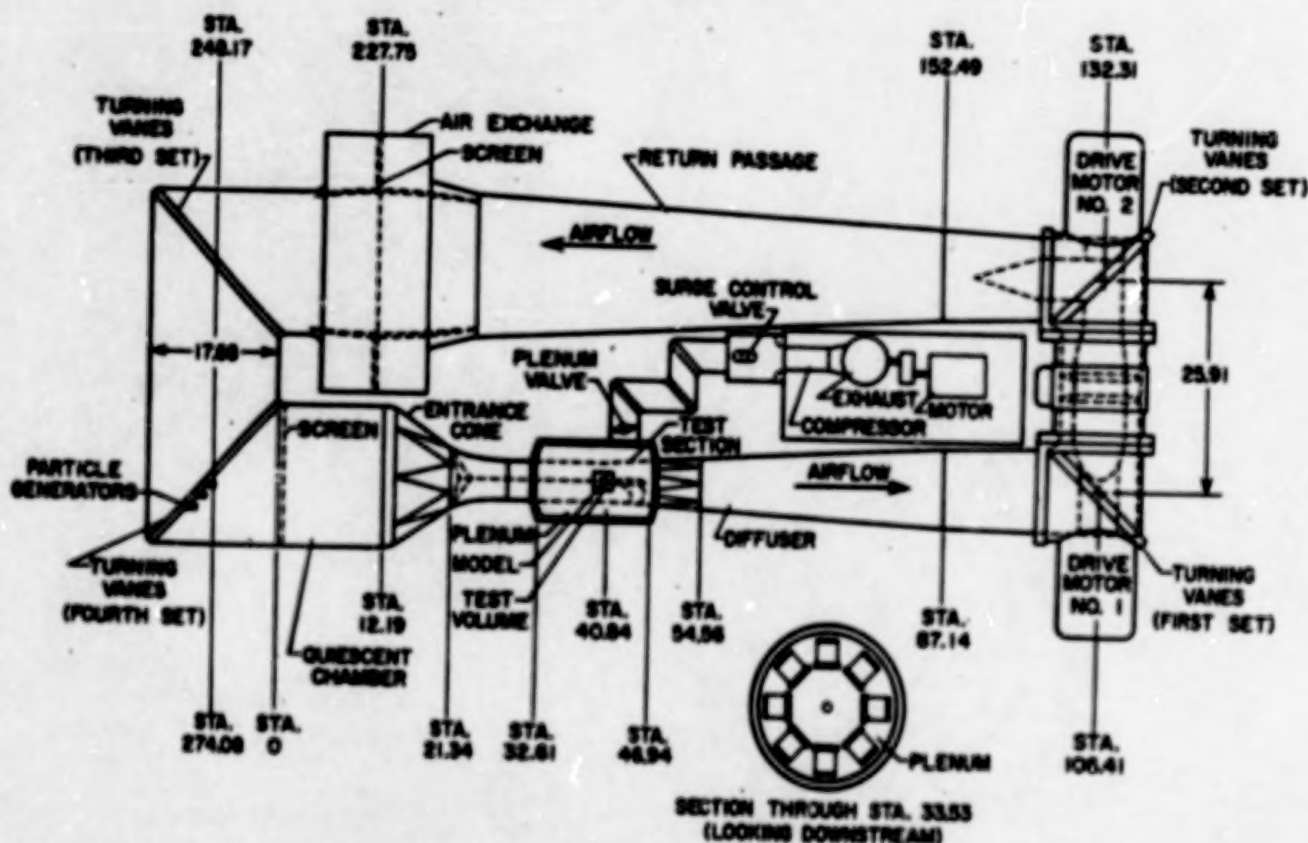
SCHEMATIC OF THE LANGLEY 16-FOOT TRANSONIC TUNNEL LASER VELOCIMETER

This is a schematic of the laser velocimeter system as it is installed in the test section plenum chamber. The plenum chamber is a 9.75 meter diameter cylinder which surrounds the test section. The laser and optics etc. ride on a scan platform which allows movement in two directions: vertically and horizontally. The capability of scanning the sample volume across the tunnel is provided by a zoom lens system. Unfortunately, the plenum chamber is not the most hospitable location for the installation of the delicate optics and electronics. The ambient noise level has been measured to be in excess of 150 .dB at some Mach numbers and the g level has exceeded 10. The scan platform is currently being rebuilt to compensate for the harsh environment.
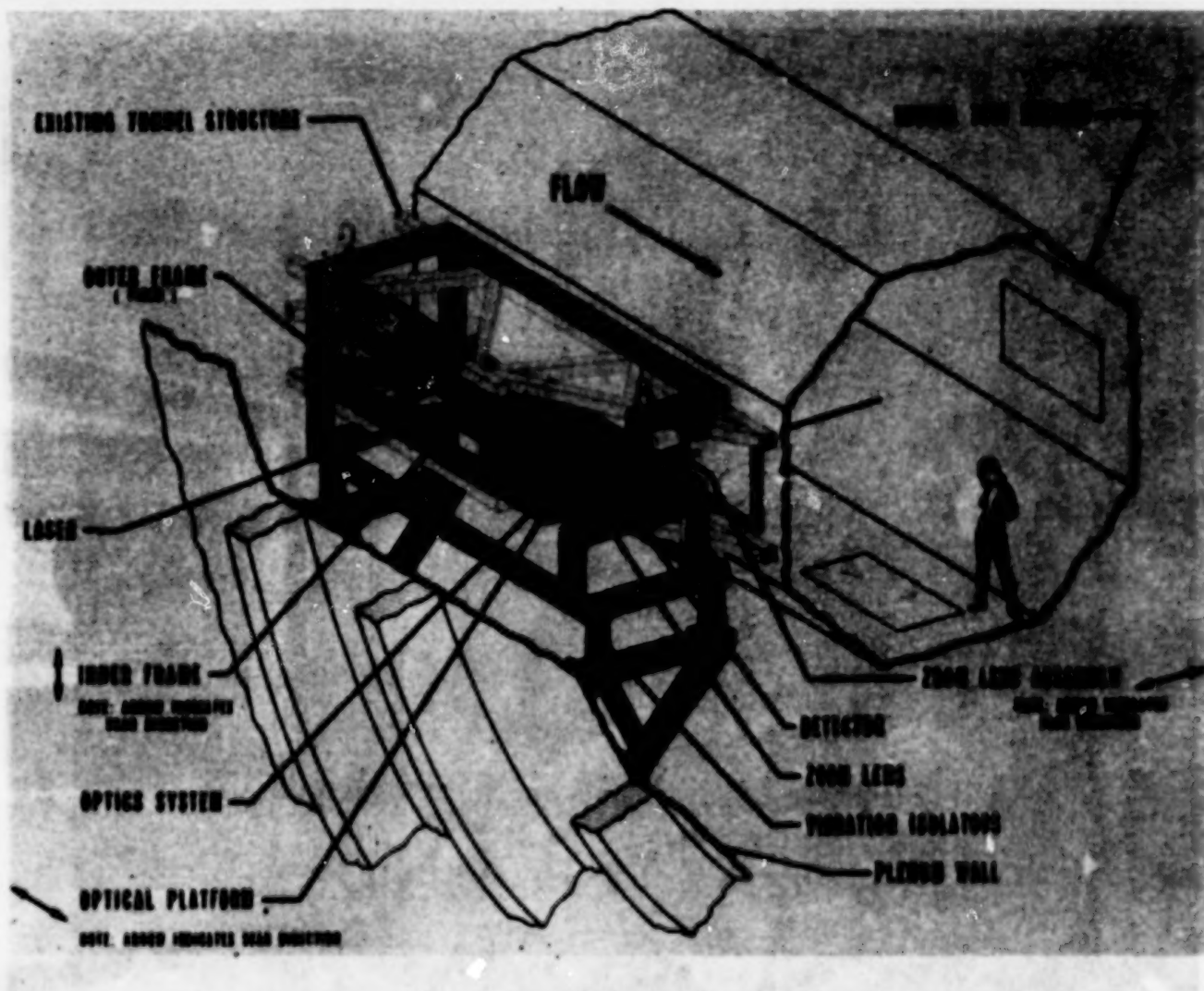
LASER VELOCIMETER CALIBRATION MODEL

In order to assess the performance of the laser velocimeter system
(including seeding) it is desirable to experimentally test a configuration
which can be readily computed (to provide a standard) and which presents a
stringent test of the laser velocimeter's capabilities. The configuration
which has been used since the proof of concept tests which were done in 1975
is a hemisphere-cylinder model. This model is simple enough that its flow can
be computed reliably, but the stagnating stream-line presents a severe test of
the laser velocimeter and the capability of the seeding system to deliver
small enough particles that the lag problem does not invalidate the data.
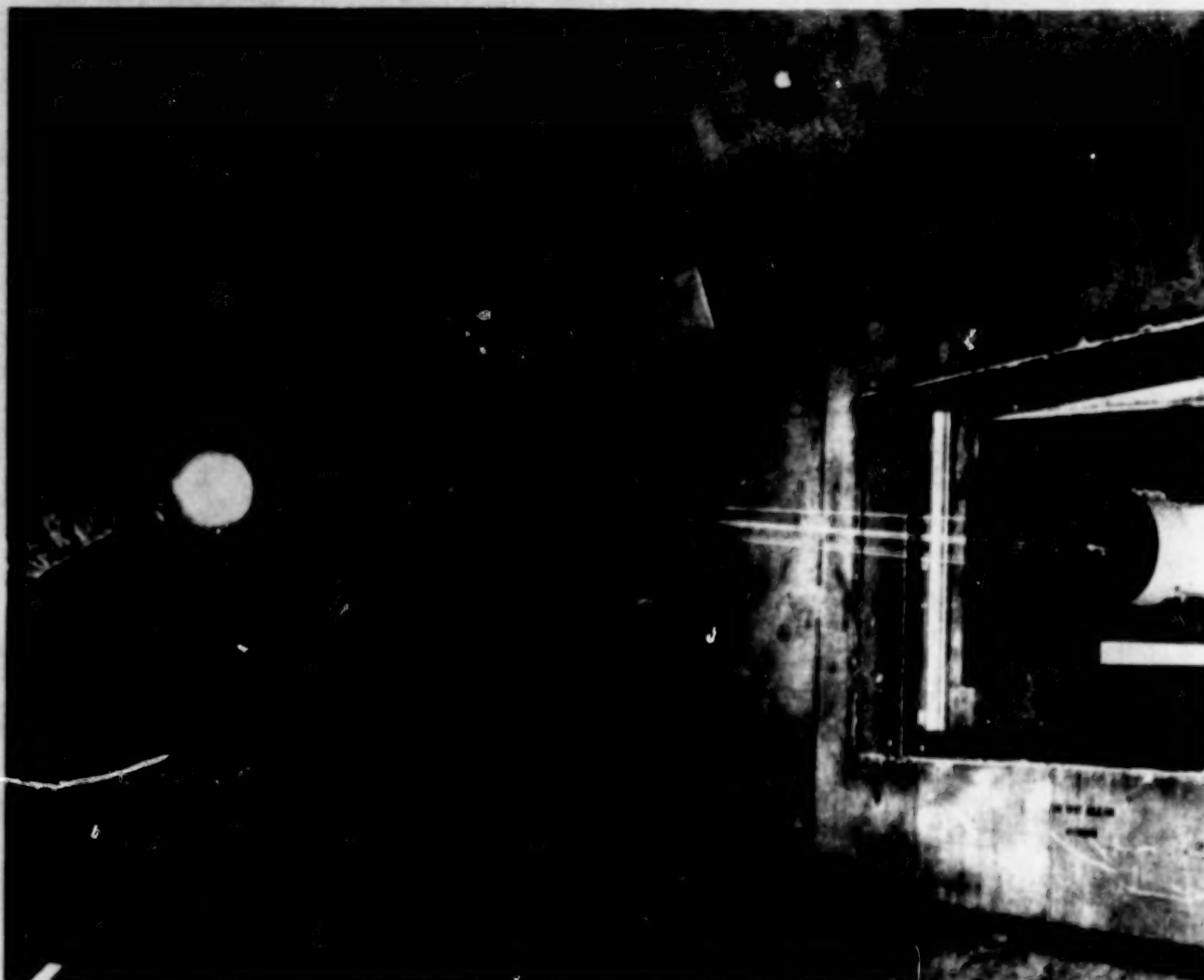
PROOF OF CONCEPT TEST PARTICLE GENERATOR

This is a sketch of the particle generator used in the proof of concept test in 1975. It is described in detail in reference 1. This generator was designed to utilize a liquid seed material. For the 1975 test a mineral base lubricating oil of viscosity index SAE 10 was used because of concerns about flammability and health aspects. Unfortunately, the particle size produced by these generators was extremely large. This problem will be addressed in the following figures. In addition, the tunnel became coated with the oil, a technician fell and broke his arm, and it required in excess of $25,000 to clean the tunnel.

TUNNEL AIR FLOW →

AIR

OIL

OUTER ORIFICE
0.032

AIR JET
0.028

OIL GAP
0.008

TUNNEL TURNING
VANE
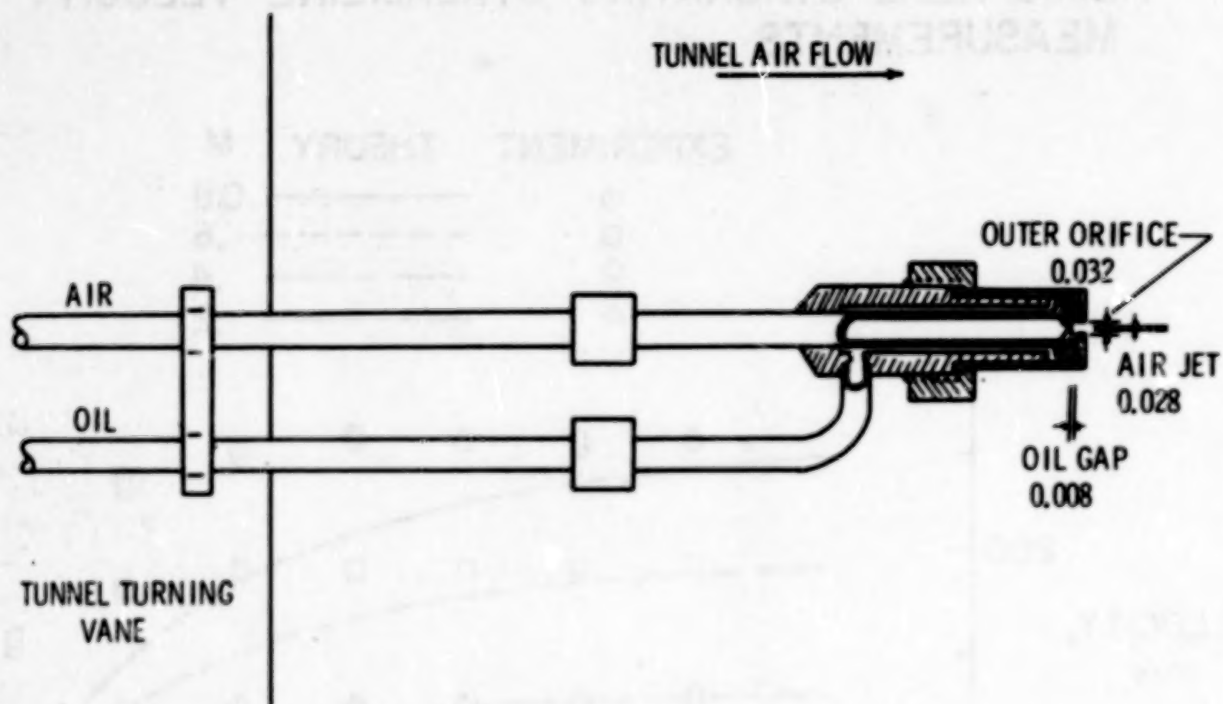
In the proof of concept test the hemisphere-cylinder stagnating streamline was surveyed at Mach numbers from 0.2 to 0.8. As can be seen from the figure, the laser velocimeter data does not agree very well with the predicted flow velocity, especially at the higher Mach numbers and near the stagnation point. This immediately points to a particle which is too large and whose inertia is such that the particle will not follow the strongly decelerating stagnation streamline. The proof of concept test is documented more fully in reference 2.

HEMISPHERE STAGNATING STREAMLINE VELOCITY MEASUREMENTS
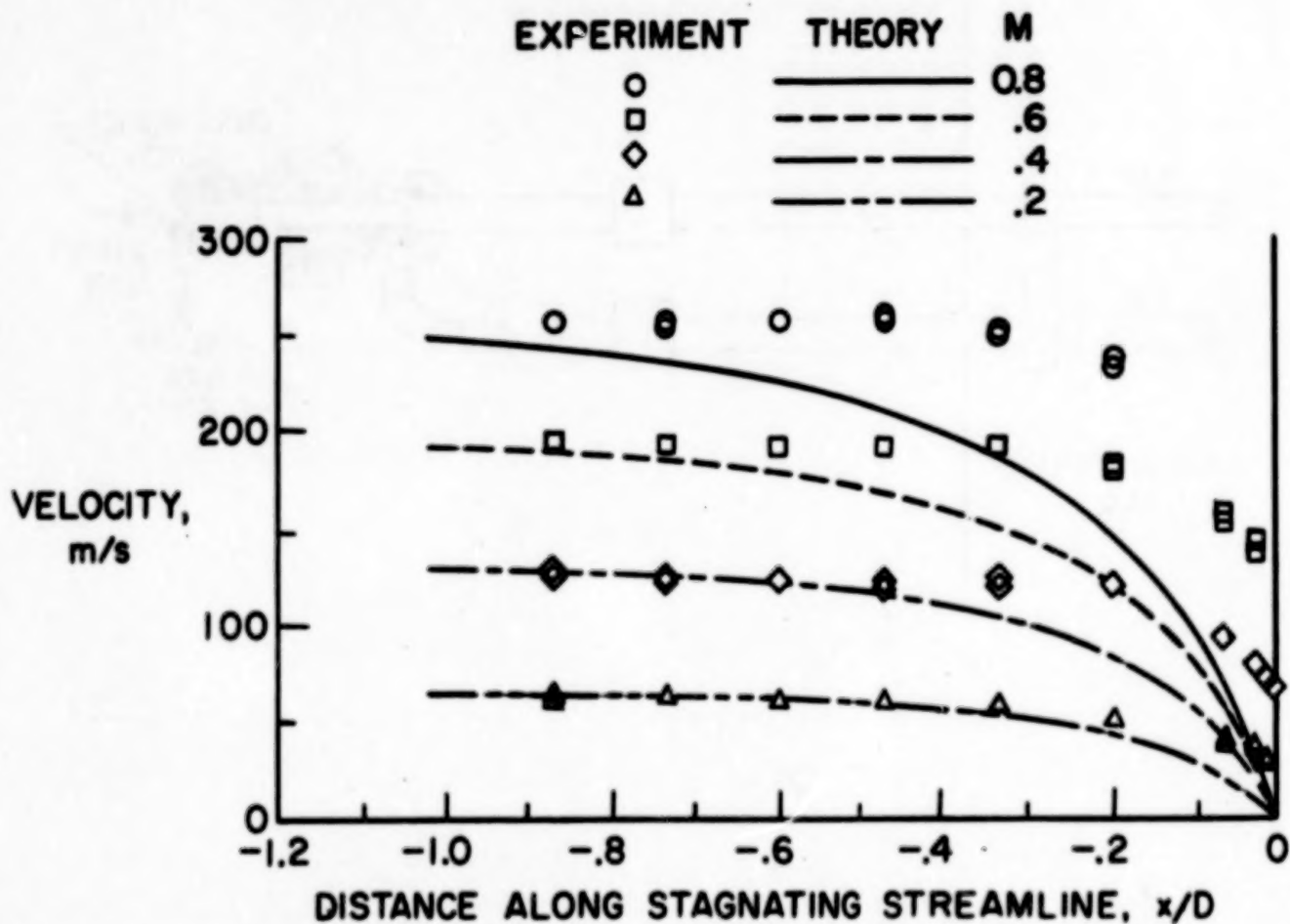
PROOF OF CONCEPT PARTICLE SIZE ANALYSIS

The size of the particles produced in the proof of concept test was analyzed using a procedure which predicts the lag of a given particle. The predicted stagnation streamline velocity data was adjusted for a variety of particle sizes and the results compared with the measured laser velocimeter data for a Mach number of 0.6. As can be seen, the particles produced by the particle generator were at least 25 microns or larger. Obviously, for a successful laser velocimeter system the particles would have to be much smaller than 10 microns.

VELOCITY
(m/s)

350

300

250

LV DATA

200

150

10 micron PARTICLE TRAJECTORY
15 micron PARTICLE TRAJECTORY
20 micron PARTICLE TRAJECTORY
25 micron PARTICLE TRAJECTORY

100

50

PREDICTED GAS VELOCITY

-1.0   -0.8   -0.6   -0.4   -0.2   0

In order to determine the necessary size for the production laser velocimeter system the particle analysis procedure was carried to particles of one micron in size. As can be seen, a one micron particle will follow the stagnation streamline flow quite well. This became the goal for further research in the generation of particles. In addition, it was determined that the seeding material had to be volatile enough not to accumulate on the walls of the tunnel but not volatile enough to present a significant explosion hazard.

COMPUTED LAG OF A ONE-MICRON PARTICLE IN HEMISPHERE FLOW FIELD
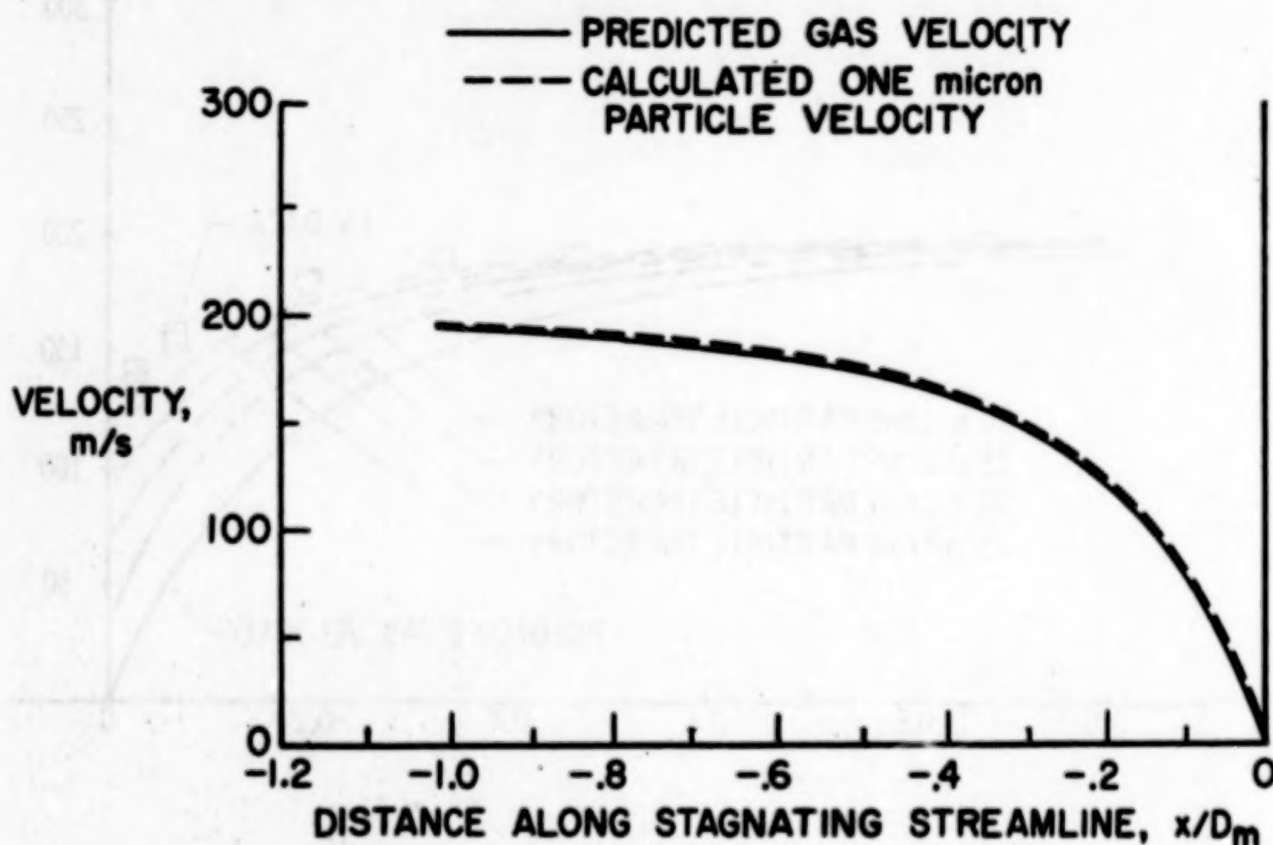
Shortly after the decision to develop a production laser velocimetry capability for the 16-Foot Transonic Tunnel and the necessary seeding system to produce significant quantities of one micron particles was made the only person at Langley who knew anything about particle generation, Mr. William V. Feller, retired. Fortunately, we were able to hire Mr. Feller under contract to continue his research on particle generation. This is a photograph of his research set-up in a corner of the 16-Foot Static Test Facility. Here one can see a prototype generator set-up blowing into a sampling tube which leads to a Royco particle size analyzer. The pedestal fan surrounded by the cardboard is a ducted fan to generate a wind tunnel effect. With this apparatus Mr. Feller was able to develop a prototype generator which did produce one micron particles.

157

This is a close-up photograph of the prototype seeding generator developed by Mr. Feller. The basic design consists of a two-dimensional air nozzle with the tube carrying the seed material centered in it. The tube carrying the seed material has been flattened at its end to another two-dimensional nozzle with a throat height of approximately 0.008 cm. In operation, air is exhausted through the air nozzle, the lowered static pressure at the air nozzle throat draws the liquid seed material through the supply tube, and the thin jet of seed material is then broken up into small droplets of the desired size. Kerosene was picked as the seed material for this generator as it has sufficient volatility to ensure that there would be no accumulation on the tunnel walls and for the amount that would be introduced into the tunnel there would be no fire or explosion hazard. The Royco particle size analyzer indicated that this generator design produced a distribution of particles over a range of sizes from below one micron to no larger than three microns.

PRODUCTION SEEDING GENERATOR DESIGN

This is a cross section of the final seeding generator design. It is a scaled up version of the prototype. It was constructed of brass instead of the plexiglass of the prototype. The seed material nozzle throat height was kept to approximately 0.008 cm. The number of particles generated can be regulated by the needle valve which controls the amount of seed material allowed to pass through the generator.
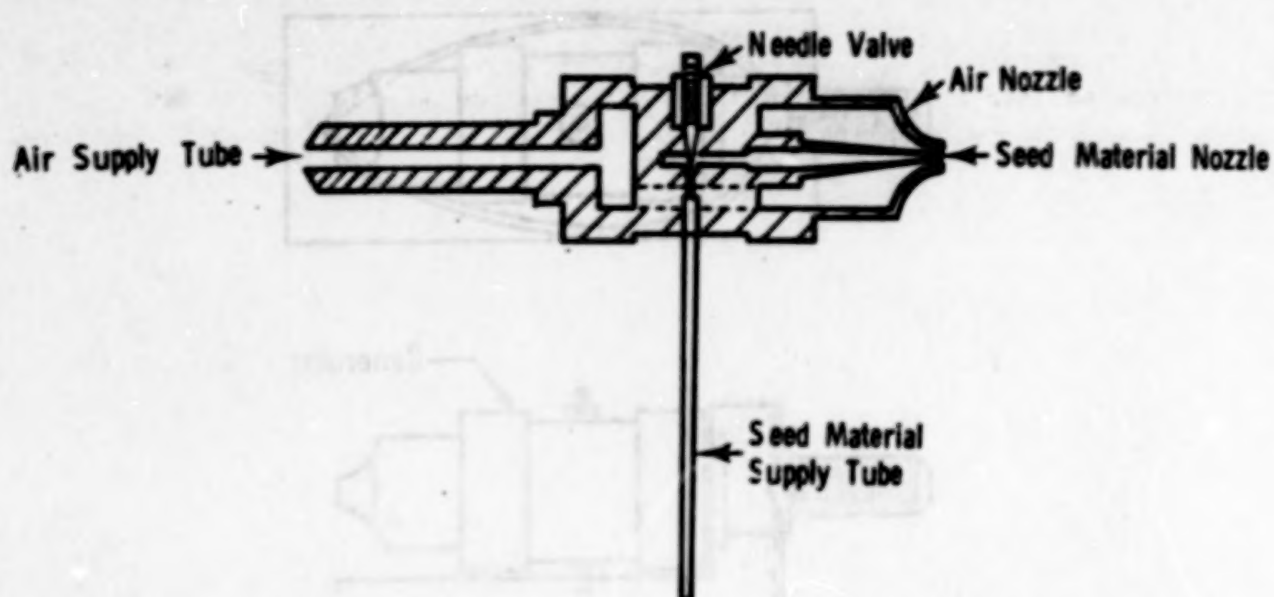
SEEDING GENERATOR ASSEMBLY

This is a sketch of an individual seeding generator assembly. It consists of a single generator and a local reservoir for the liquid seed material. When mounted in the tunnel the local reservoir is fed by gravity from a tank mounted on the tunnel turning vanes above the generator arrays.

Generator
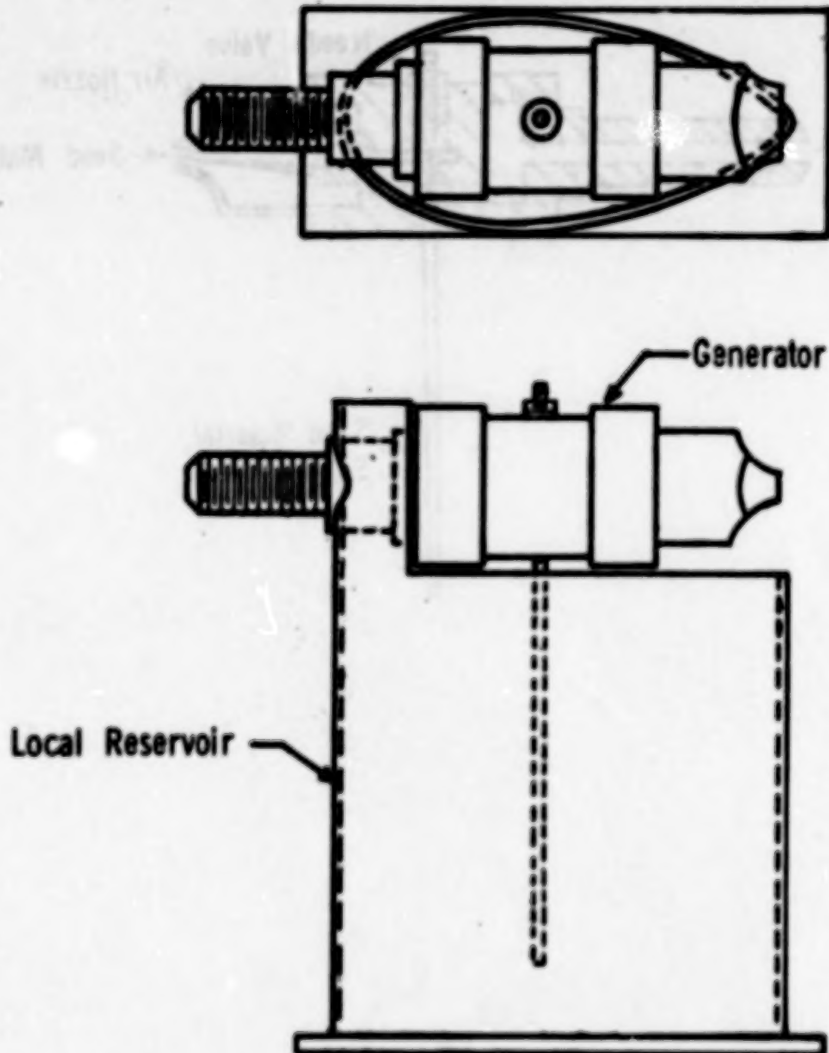
Local Reservoir

This is a photograph of an early version of one of the generator arrays which are mounted on the tunnel turning vanes. In this photograph only two generators are mounted on the local reservoirs. In the production seeding system there are two of these linear arrays of ten generators each mounted on the turning vanes. The arrays are spaced 2.03 meters apart with one plane 1.83 meters above the tunnel centerline and the second 0.2 meters below the tunnel centerline. The generators are spaced 0.46 meters apart on the streamline tubing support which also serves as a part of the overflow and drain system for the liquid seed material. The arrays were mounted on the turning vanes in such a manner that when facing upstream six generators were to the left of the tunnel centerline, three to the right of the centerline, and one on the centerline. Since the tunnel flow contains some swirl it is impossible to determine beforehand exactly which generator will be required to seed a given area of the test section. The generators are controlled in pairs from the control room by solenoid valves which regulate the air supplied to the generators. Choice of the generators in use was based on visual observation of the seed material passing through the laser beams and the data rate measurements.

161
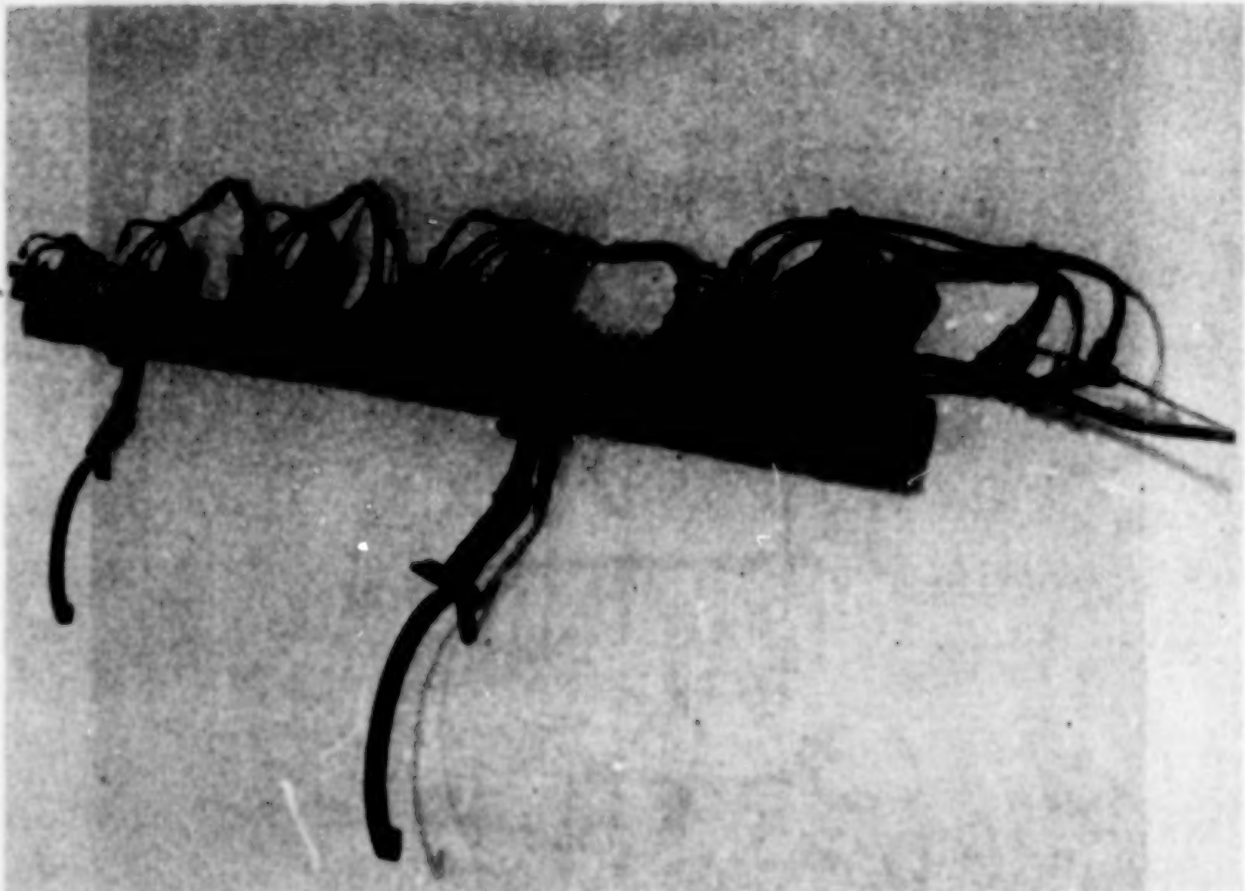
This is a photograph looking downstream at the turning vane location where the generator arrays are mounted (during the installation process). The tunnel at this location is 17.68 meters in diameter and the installation was a considerable task.
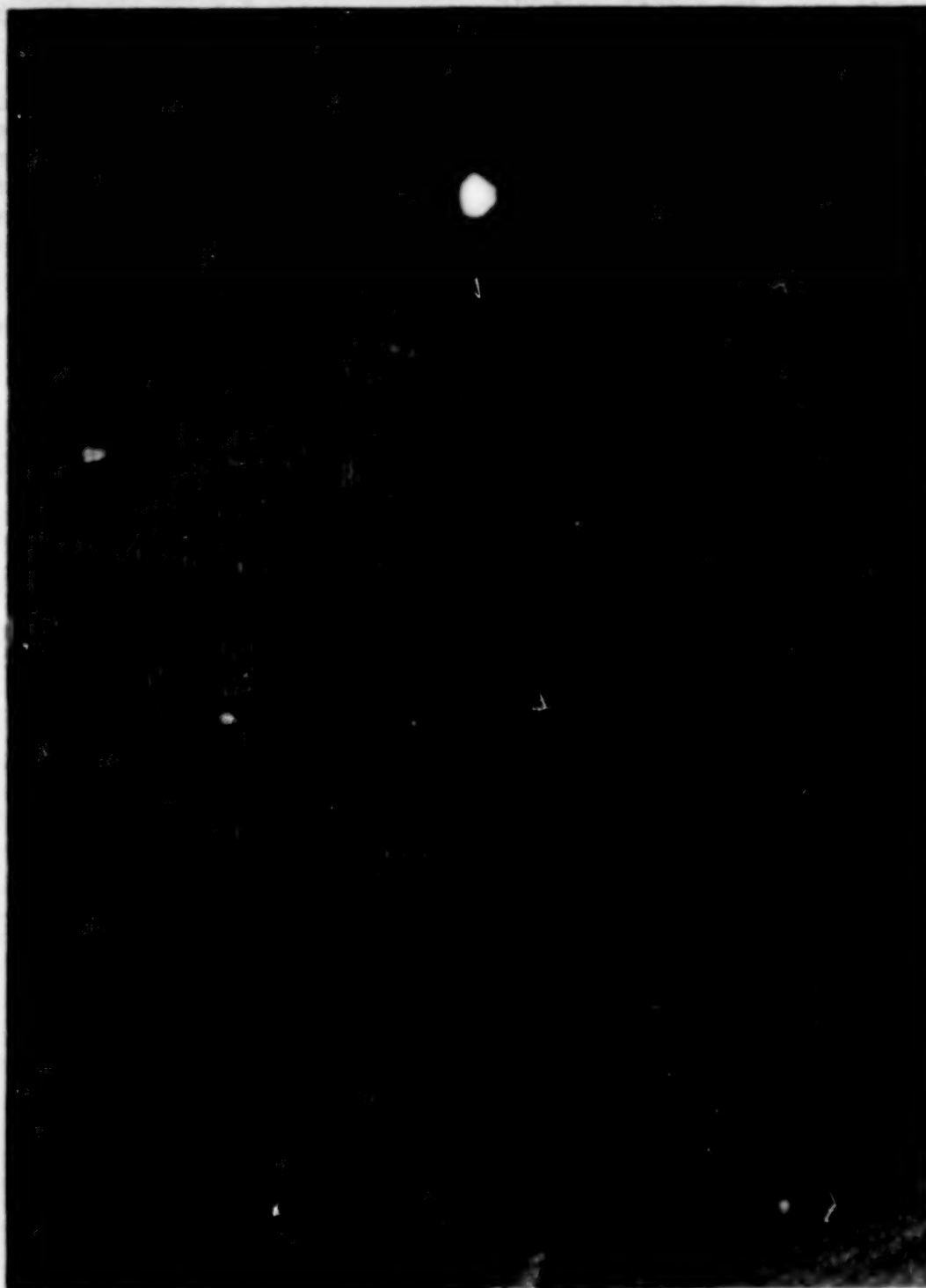
PARTICLE SIZE DISTRIBUTION

After the seeding generator system was installed the hemisphere-cylinder model was installed in the tunnel and laser velocimeter data were taken. Unfortunately, these data indicated that the particle size reaching the test section was considerably larger than the one micron desired size (which had been verified by the Royco particle size analyzer). A number of theories were advanced to try to explain this phenomenon but none was really satisfactory. At this point Mr. Cecil Nichols became involved. He investigated the particle generators with the TSI aerodynamic particle sizer. This figure shows the results of sizing kerosene particles from the generators. As can be seen, the size distribution goes as high as ten microns. This is unacceptable. Evidently, the optical particle size (which is what is measured by the Royco sizer) is not the same as the aerodynamic particle size (which is what is measured by the TSI sizer). The aerodynamic size is the size which is applicable to the particle flow following capability. As a result it was decided to investigate other seeding materials.

TSI AERODYNAMIC PARTICLE SIZER
SA KEROSENE

SAMPLE # 1   DATE: 2/28/84   SAMPLE TIME: 20 SEC
DIL. RATIO: 1:1   EFFIC. CORRECT.: NONE
                                             DENSITY: 1

163
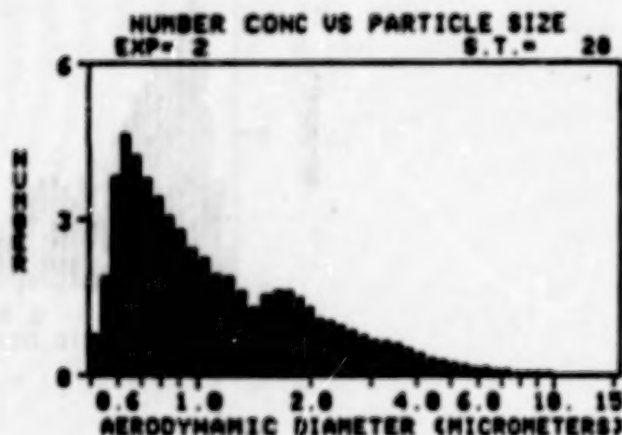
KEROSENE-ALCOHOL MIXTURES

At this point in time Mr. Nichols was investigating the use of Kaolin
particles suspended in ethyl alcohol as a seed material. It was decided to
investigate the use of this mixture in the existing generators in the
tunnel. However, since the local generator reservoirs, tanks, pumps etc. were
full of kerosene it was decided to do some additional investigation of other
seeding mixtures during the transition from kerosene to alcohol. Various
combinations of alcohol and kerosene were tried and the results are documented
in the next three figures. Use of a 50% kerosene - 50% alcohol mixture
resulted in a shift downward in the particle size but there were still too
many large particles. Similarly, 25% kerosene - 75% alcohol and 10% kerosene
- 90% alcohol resulted in further shifts in the particle size distribution
toward the smaller particles; however, there were still too many large
particles for acceptable performance.

TSI AERODYNAMIC PARTICLE SIZER
50%KEROSENE-50% ETOH

SAMPLE # 1   DATE: 2/28/84   SAMPLE TIME: 20 SEC
DIL. RATIO: 1:1   EFFIC. CORRECT.: NONE   DENSITY: 1

NUMBER CONC VS PARTICLE SIZE

164
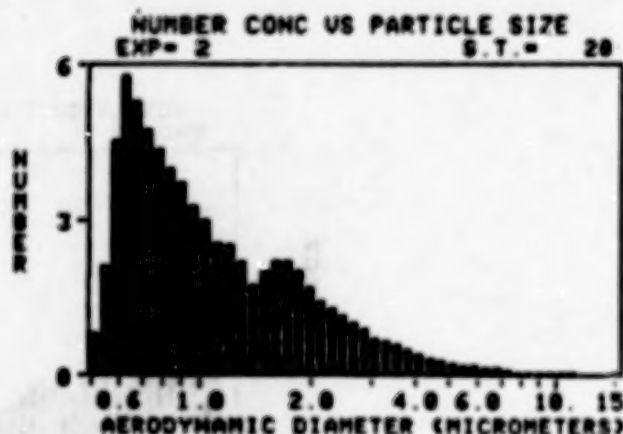
TSI AERODYNAMIC PARTICLE SIZER
25% KEROSENE-75% ETOH

SAMPLE # 1   DATE: 2/28/84   SAMPLE TIME: 20 SEC   DENSITY: 1
DIL. RATIO: 1:1   EFFIC. CORRECT.: NONE

NUMBER CONC VS PARTICLE SIZE
EXP= 2   S.T.= 20

AERODYNAMIC DIAMETER (MICROMETERS)
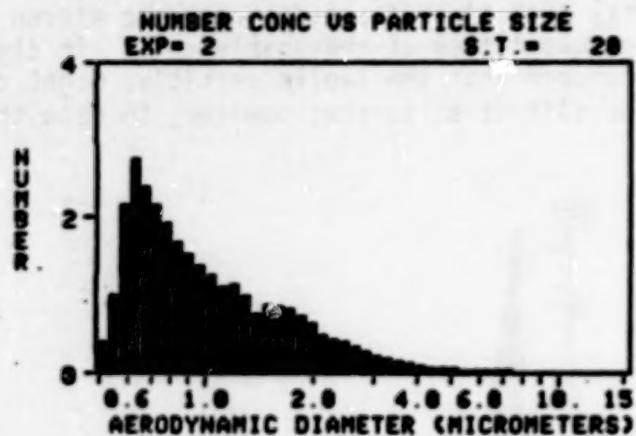
TSI AERODYNAMIC PARTICLE SIZER
10% KEROSENE-90% ETOH

SAMPLE # 1   DATE: 2/28/84   SAMPLE TIME: 20 SEC   DENSITY: 1
DIL. RATIO: 1:1   EFFIC. CORRECT : NONE

NUMBER CONC VS PARTICLE SIZE
EXP= 2   S.T.= 20

AERODYNAMIC DIAMETER (MICROMETERS)
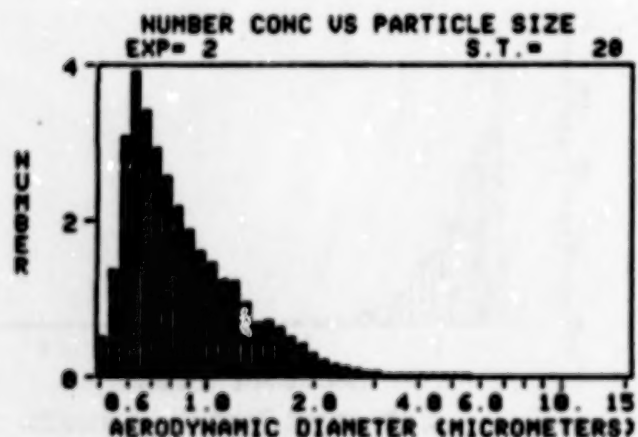
ALCOHOL - KAOLIN SEEDING MIXTURE

After transitioning to pure alcohol in the seeding system, Kaolin particles were mixed in the alcohol. This last figure is taken from the paper by J. F. Meyers (ref. 3) and shows the particle size distribution resulting from the generators using the Kaolin - alcohol mixture. This distribution, while not monodisperse at one micron, does give a satisfactory distribution until such time as monodisperse one micron particles can be obtained in large quantities at reasonable cost. It also might be noted that there was some concern that the Kaolin particles might clog up the seed nozzles since the slit is so narrow; however, to date this has not occurred.

a) Particle Size Distribution

b) LV Sensitivity Function

c) Measurement Probability Distribution
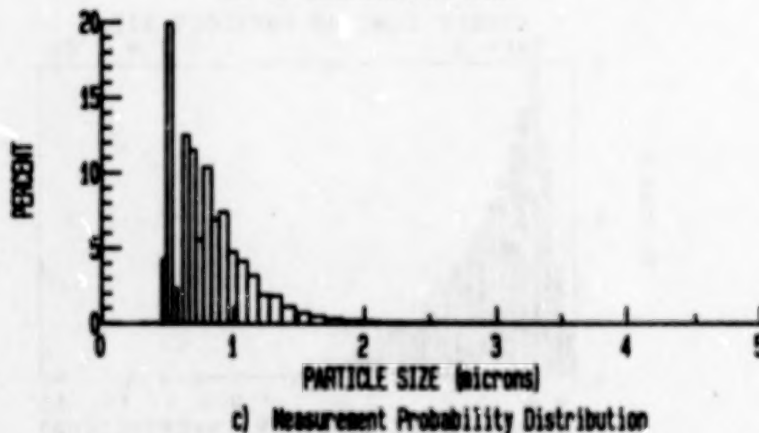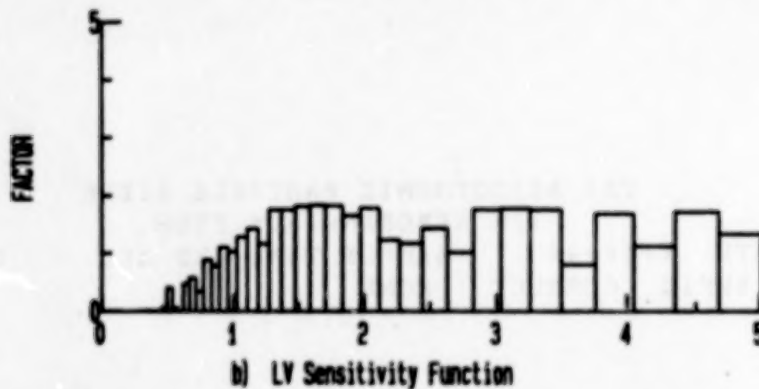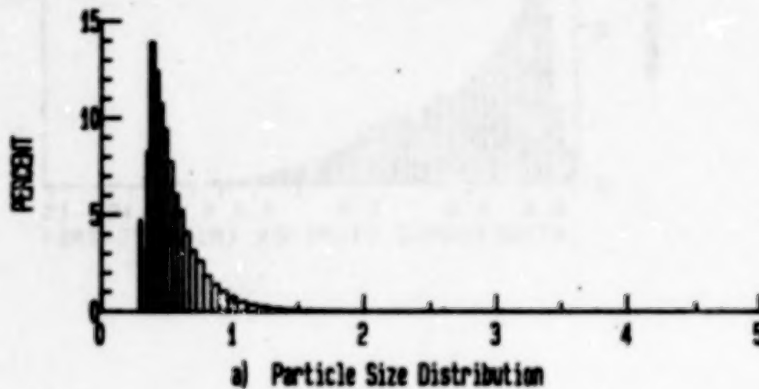
REFERENCES

1. Feller, W. V., and Meyers, James F.: Development of a Controllable Particle Generator for Laser Velocimeter Seeding in Hypersonic Wind Tunnels. Presented at the Symposium on Laser Anemometry, Bloomington, Minnesota, October 22-24, 1975.

2. Putnam, Lawrence E. and Meyers, James F.: Measurement of Flow Fields in a Large Transonic Wind Tunnel Using a Laser Velocimeter. Presented at the AIAA General Aviation Technologyfest, Wichita, Kansas, November 13-14, 1975.

3. Meyers, James F.: Estimation of Particle Size Based on LDV Measurements in a De-Accelerating Flow Field. Wind Tunnel Seeding Systems for Laser Velocimeters, NASA CP-2393, 1985, pp. 29-52.

LDA SEEDING SYSTEM
FOR
THE LANGLEY LOW TURBULENCE PRESSURE TUNNEL

J. Scheiman and L. R. Kubendran
NASA Langley Research Center
Hampton, VA 23665

Introduction

A Laser Velocimetry seeding system has been specifically developed for the Langley Low Turbulence Wind Tunnel (LTPT), and it has been successfully used for LV measurements in two major tests (Juncture Flow Experiment and Görtler Experiment). Detailed description of the LV system is found in Ref. 1. The LTPT (Fig. 1) is capable of operating at Mach numbers from 0.05 to 0.50 and unit Reynolds numbers from 100,000 to 15,000,000 per foot. The test section is 3 feet wide and 7.5 feet high. The turbulence level in the test section is relatively low because of the high contraction ratio and because of the nine turbulence reduction screens in the settling chamber. A primary requirement of the seeding system was that the seeding material not contaminate or damage in any way these screens. Both solid and liquid seeding systems were evaluated, and the results are presented herein. They can provide some guidelines for setting up seeding systems in other similar tunnels.
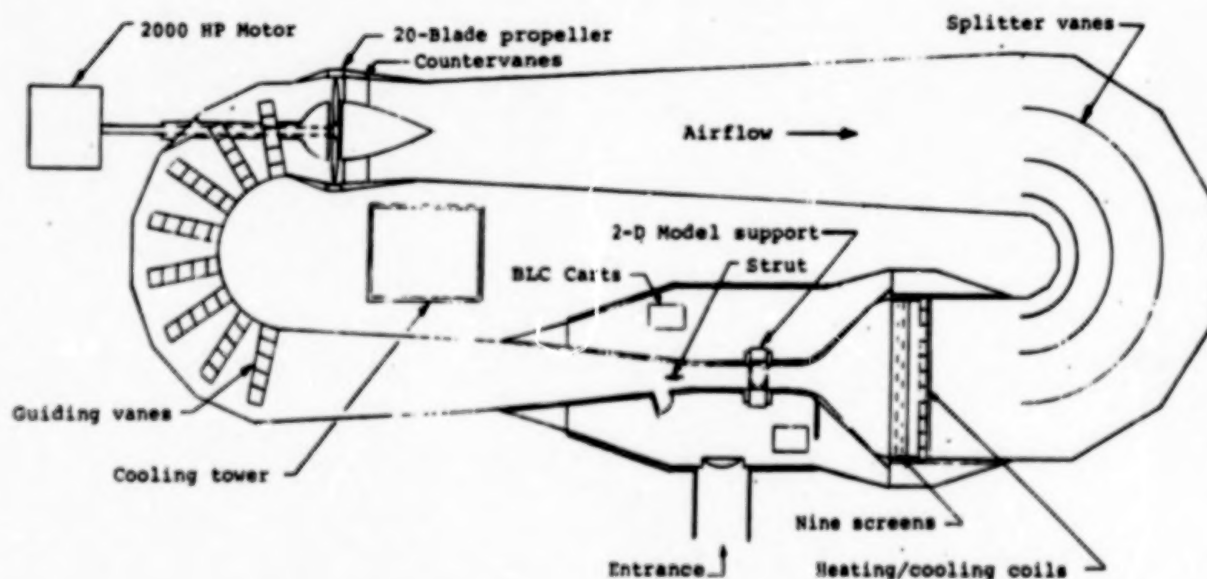
Figure 1

Desired Size of Seeding Particles

Since the LDV measures particle velocity and not fluid velocity, the particles must be small enough to follow the flow stream but large enough to be detected. The particles must have small diameter variation (mono-dispersed) in order to make reliable turbulence measurements.

The particle size is also governed by the requirement that there be no deposits on the screens. A potential flow analysis of kaolin particles of various sizes moving past a cylinder was conducted, and the results are shown in Fig. 2. These results indicate that the fraction of particles impacting on the cylinder increases with increasing particle size. It was concluded from these results that the desired size of the particles should be below one micron in diameter, in order to minimize particle build-up on the screens.

Figure 2

171
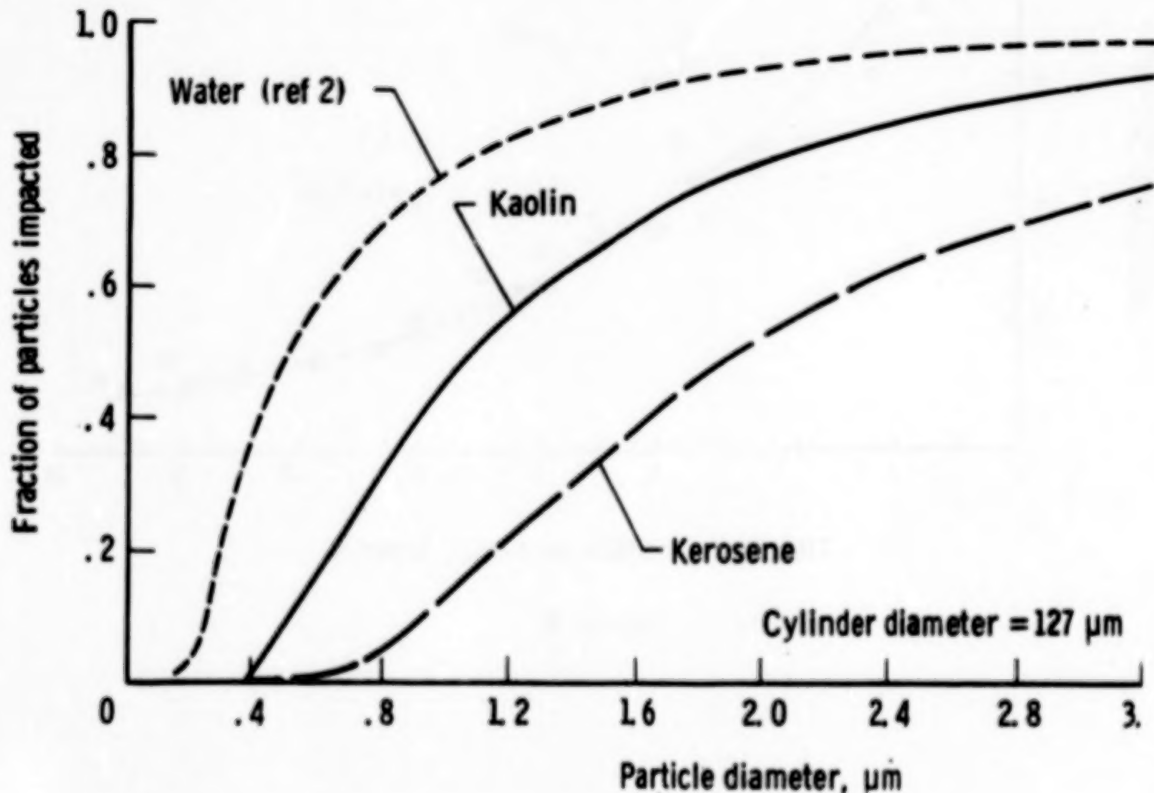
A special experiment was set up to evaluate and gain insight into solid-particle seeding problems. In an attempt to minimize electric forces exerted on electrically charged particles, kaolin, an inert material, was chosen first. The particles were injected into the flow stream in the diffuser between the test section and the drive fan, and the particle data rate was measured with a Laser Transit Anemometer. The particle data rate is shown in Fig. 3 as a function of time.

TIME FROM MAXIMUM DATA RATE, MINUTES
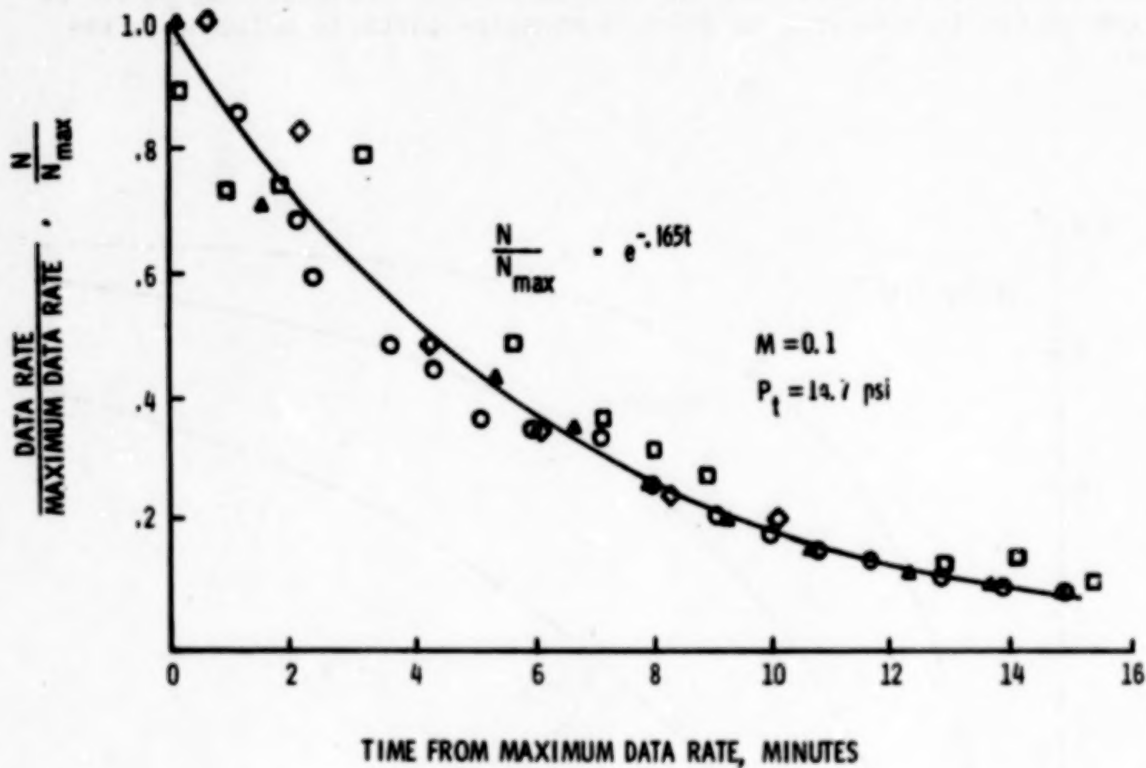
Figure 3

Solid Particle Seeding

In order to evaluate gravitational settling the wind tunnel was turned off for a 10-20 minute time period and then the tunnel was restarted. Fig. 4 shows that the particle decay rate is not a function of time when there is no flow, i.e., gravitational settling rate is insignificant. Figs. 3 and 4 indicate that the decay rate is proportional to tunnel speed, with a 15% loss of particles every minute at M=0.1. Globs of particles were found just downstream of the insertion point, usually on the tunnel turning vanes. Tests conducted with gold particles yielded similar results. This implies that continuous tunnel operation will require continuous seeding. But, accumulation of solid particles inside a closed-cicuit tunnel is not considered desirable since this will involve frequent, time-consuming tunnel cleanups.

$$\frac{N}{N_{max}} = e^{-.086t}$$

$$M = 0.05$$

$$P_t = 14.7 \text{ psi}$$

$$\frac{N}{N_{max}} = e^{-.07(t-13)}$$

TUNNEL STOP
NO AIRFLOW

TIME FROM MAXIMUM DATA RATE, MINUTES

Figure 4

173
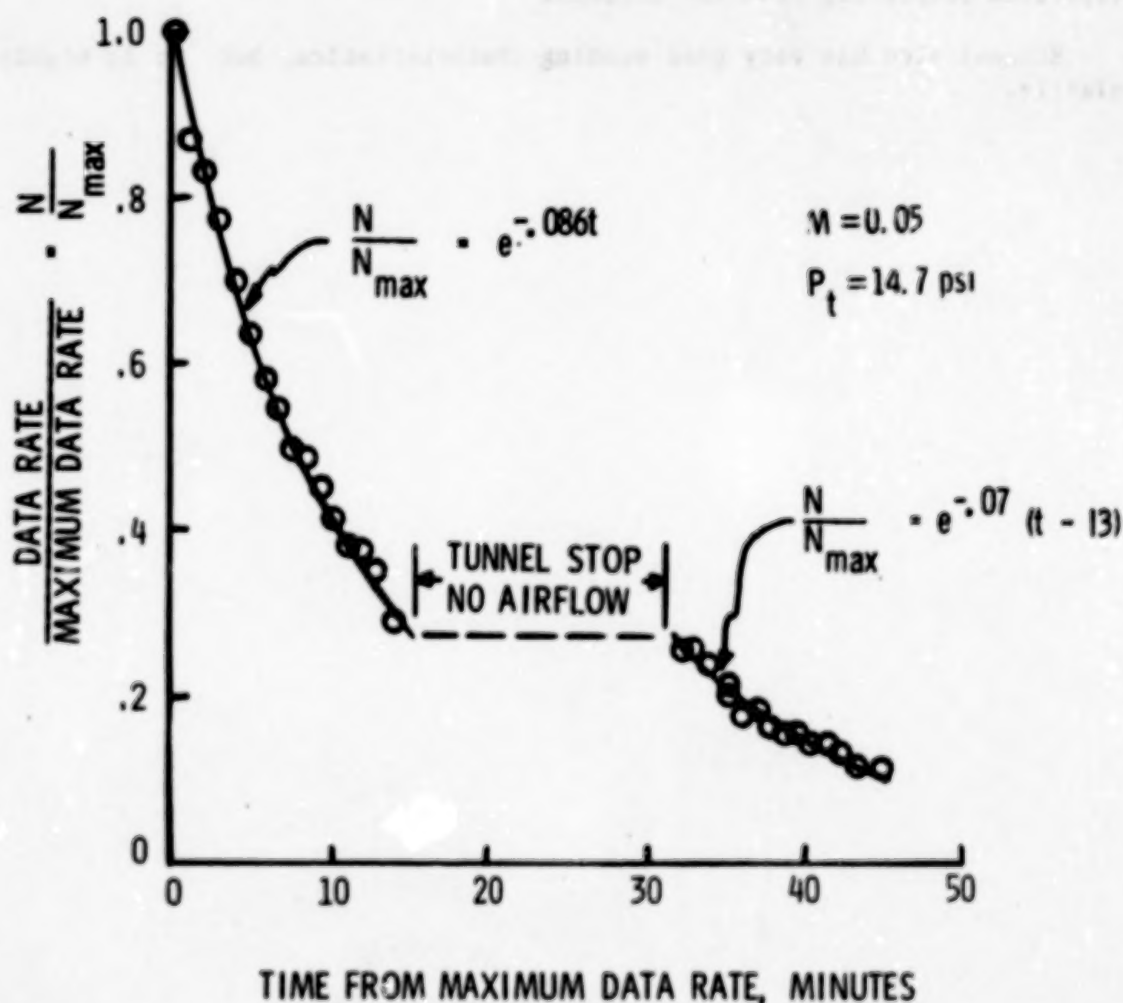
If the liquid particles are too large, then a larger percentage of them will impact on the screens (Fig. 2). If the screen wetting rate is faster than the drying rate due to liquid evaporation, the liquid could collect dirt in the tunnel. Therefore, it is desirable to generate small particles and to use a liquid which is volatile enough that it will evaporate. Further, a safe and readily available liquid is desirable.

Kerosene, which satisfied most of the requirements, left residues on a test screen, and therefore it was not acceptable.

However, kerosene is made up of a number of pure hydrocarbon components. Of these, dodecane, tridecane, and tetradecane have droplet forming characteristics very nearly equal to that of kerosene. These hydrocarbon fluids can be obtained in a highly refined state, and they evaporated completely from the screens.

Ethanol also has very good seeding characteristics, but it is highly volatile.

Before the particle size analyzer could be used for evaluating the seeding particles, it was important to check the calibration of the analyzer. Ref. 3 indicated that the percentage of ambient particles of radius greater than r varies as r^{-3} for particles between 0.05 micron and 1 micron in diameter. The particle size analyzer was used to sample ambient particles, and the sample data in Fig. 5 are shown with different symbols for each ambient particle size test. Also shown on the figure is the r^{-3} line, which is straight on the log-log plot. In general the measured ambient condition agrees fairly well over the particle diameters of interest. It was concluded from ambient measurements that the particle analyzer was working properly and would be adequate for measuring the particles generated by the generator.

Figure 5

Polystyrene particles of very small size (e.g., 0.5 micron) with a very
narrow variation in particle size can be commercially purchased. But in
order to have mono-dispersed particles in the flow stream the ability to
maintain these individual particles is important. This aspect was evaluated
by dispersing polystyrene particles with an atomizer and analyzing the
resulting size distribution. The results (Fig. 6) showed that a substantial
percentage of the particles is larger than the original particle size. This
illustrates the difficulty in maintaining the particle size.
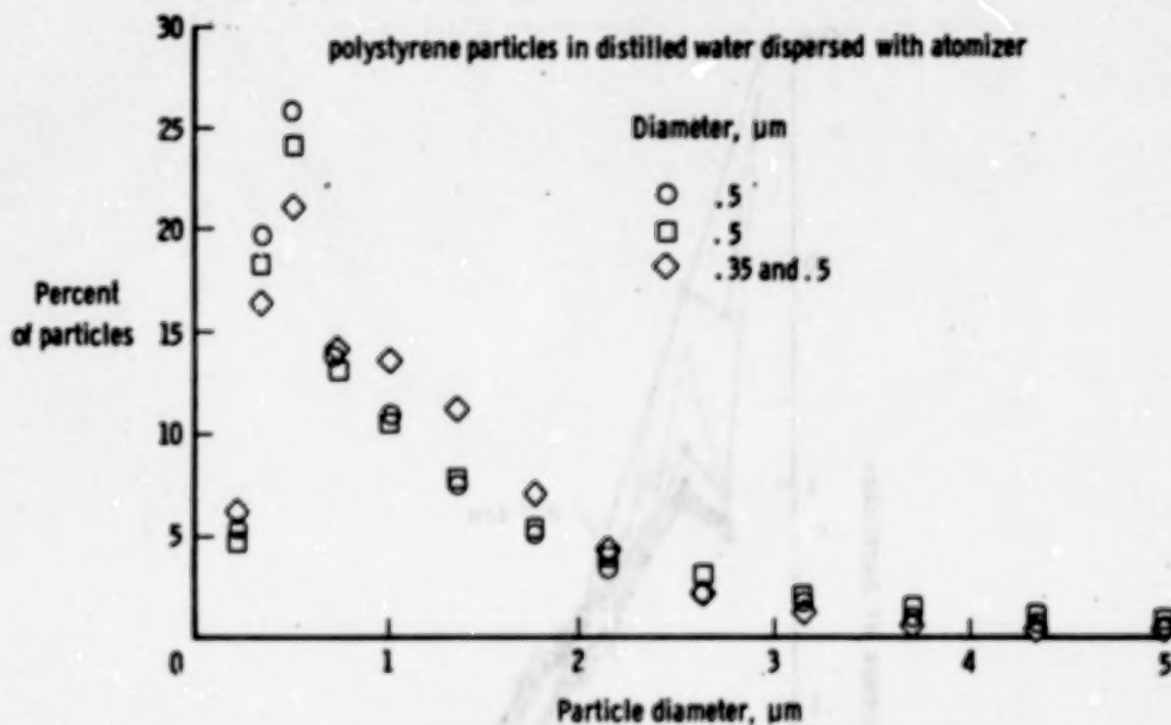
Figure 6

Particle Size Evaluation : Liquid Particles

The size of the liquid particles generally depends on seeder/nozzle characteristics and seeding-material characteristics. But, once generated, the particles can coagulate, evaporate or condense. These factors can and do affect the size of the generated particles after they leave the nozzle.

Kerosene, ethanol, dodecane, and tridecane were tested; an atomizer type generator was used to generate the particles. Kerosene particle distribution included a significant percentage of particles larger than one micron, whereas ethanol, dodecane, and tridecane were very nearly mono-dispersed with very small mean particle diameter. Fig. 7 shows the particle size distributions of dodecane and tridecane.

When dodecane was used as seeding material, it was found that the seeding rate and particle size could be controlled by varying the tunnel temperature.
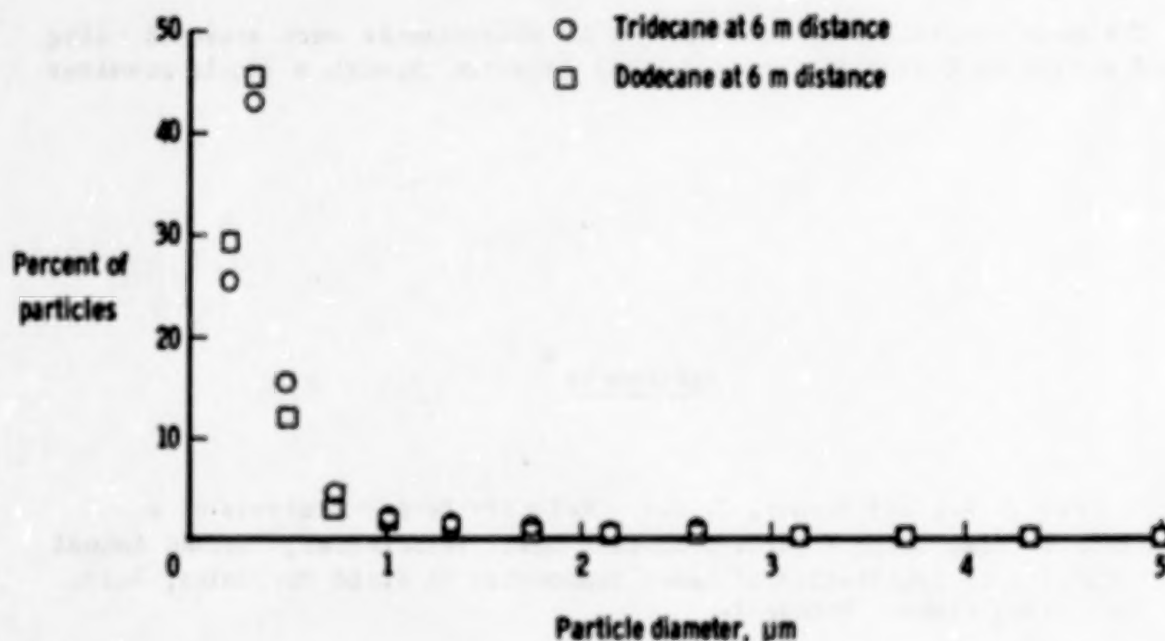
Figure 7

Conclusions

The desired seeding particles should be below 1 micron in diameter to minimize screen contamination.

Solid particles decay as a function of tunnel speed, resulting in 15% loss of particles/minute at a Mach number of 0.1.

Particle size analysis in the flow stream indicates the presence of particles larger than originally dispersed ones.

Kerosene leaves residue on the screens; its particle size distribution is poly-dispersed.

Ethanol, dodecane, and tridecane particles are nearly mono-dispersed.

Dodecane and tridecane evaporate completely, without leaving any residues on the screen, satisfying the tunnel requirement.

The most successful application and LV measurements were obtained using liquid particles (tridecane and dodecane) injected through a liquid atomizer.

References

1. Meyers, J. F.; and Hepner, T. E.: "Velocity Vector Analysis of a Juncture Flow Using a Three-Component Laser Velocimeter," Second Annual Symposium on Application of Laser Anemometry to Fluid Mechanics, July 2-4, 1984, Lisbon, Portugal.

2. Ormancey, A.; and Martinon, J.: Numerical Simulation of Particle Behavior in a Turbulent Flow. Rech. Aerosp. No. 1983-5, 1983.

3. Mason, B. J.: The Physics of Clouds. Clarendon Press, 1971.

SEEDING SUBSONIC, TRANSONIC AND SUPERSONIC
FLOWS WITH 0.5 MICRON POLYSTYRENE SPHERES

H. Lee Seegmiller
NASA Ames Research Center
Moffett Field, California

C-3

FACILITIES AND SEEDING MATERIAL

Polystyrene latex particles have been successfully used as laser veloci-metry seed material for flows in the Ames High Reynolds Channels (HR) I and II, the pilot channel, and the one-foot low speed tunnel (ref. 1-4). These facilities provide test flows with Mach numbers from 0.1 to 3.0 and test section sizes from 4"x6" to 18"x24". Tunnel mass flow in the HR-II channel can approach 1000 lb/sec. The latex particles have the following favorable characteristics:

size: 0.35 to 0.55 μm dia.
shape: spherical
specific gravity: 1.05
flow trackability: excellent (ref. 5)
toxicity: low
cost: low

They have the disadvantage of being packaged as an aqueous suspension which must be diluted and introduced into the test flow as an atomized mist. This occur sufficiently far upstream of the test section to minimize flow disturbances and permit the liquid mist to evaporate before reaching the model. Several techniques which have been developed to accomplish satis-factory seeding will be described.

SEEDING LOW-SPEED TUNNELS

Both the pilot channel and the one-foot low speed tunnel are open circuit designs using atmospheric inlets. These subsonic tunnels are seeded with an array of commercial air brushes mounted upstream of the inlet. To prevent migration of the seed material into the room, screened cages were mounted at the tunnel inlets and covered with several thickness of filter paper. The air brush array was mounted in an opening at the front of the cage and sprayed the liquid-seed aerosol into the enclosure at the front of the tunnel inlet. Tests were made to insure that evaporation of the liquid (alcohol) occurred before reaching the inlet.

Care must be taken to provide a uniform distribution of seed into all of the flow influenced by the test model to minimize spatial seeding bias. This is easily done for tunnel wall measurements because of the mixing in the turbulent tunnel boundary layer. Seeding in the core flow, however, is more difficult and requires experimentation in the positioning of the air brushes.

HONEYCOMB
AND SCREENS

FILTER PAPER

AIR BRUSH
ARRAY
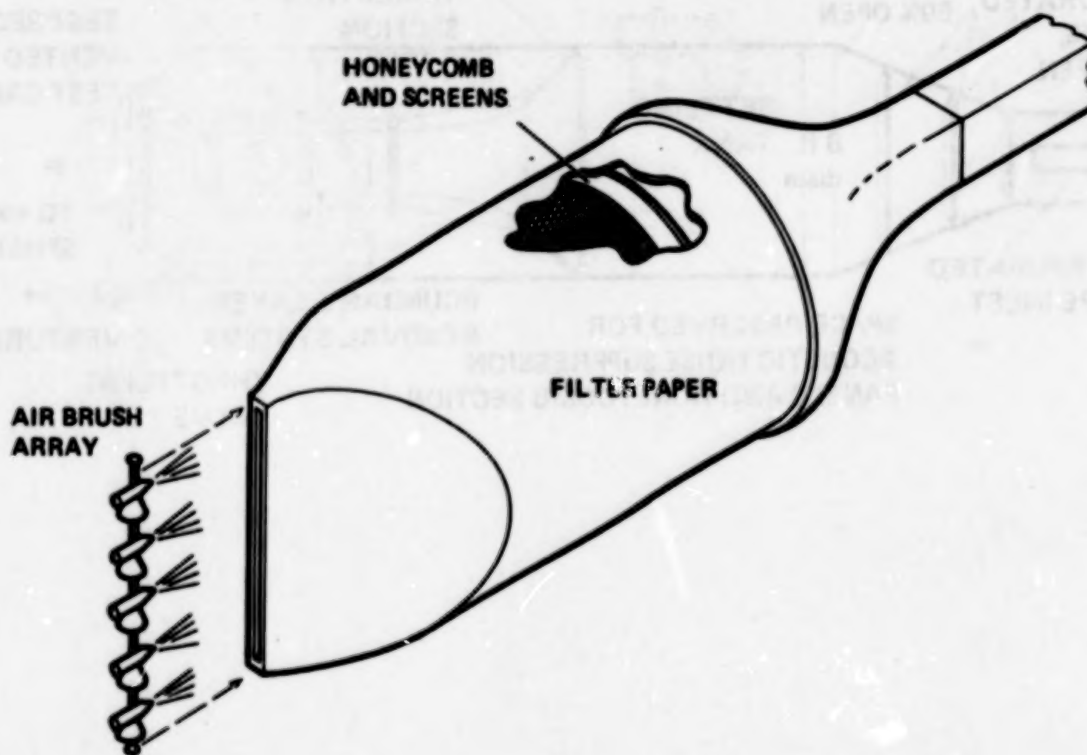
HIGH REYNOLDS NUMBER CHANNELS I & II

The High Reynolds Number Channels, I and II, are large transonic blowdown facilities with two-dimensional test sections adapted for airfoil testing. Additionally, HRC I can be used with fixed block supersonic nozzles for testing at M=2 and 3. The test section sidewalls of HRC II are fitted with porous metal suction panels which are used to thin the sidewall boundary layer and reduce airfoil interference effects. These porous panels, however, complicate LDV seeding because of the vulnerability to plugging with seed particles. The high pressure inlet piping and stagnation chamber arrangement of HRC II is shown below (ref. 6). HRC I is similar, but smaller in size. The high pressure air is first admitted to the tunnel through the perforated inlet pipe. Turbulence reduction occurs with flow through the three 40% open perforated plates and the 4 screens in the settling tank.

182
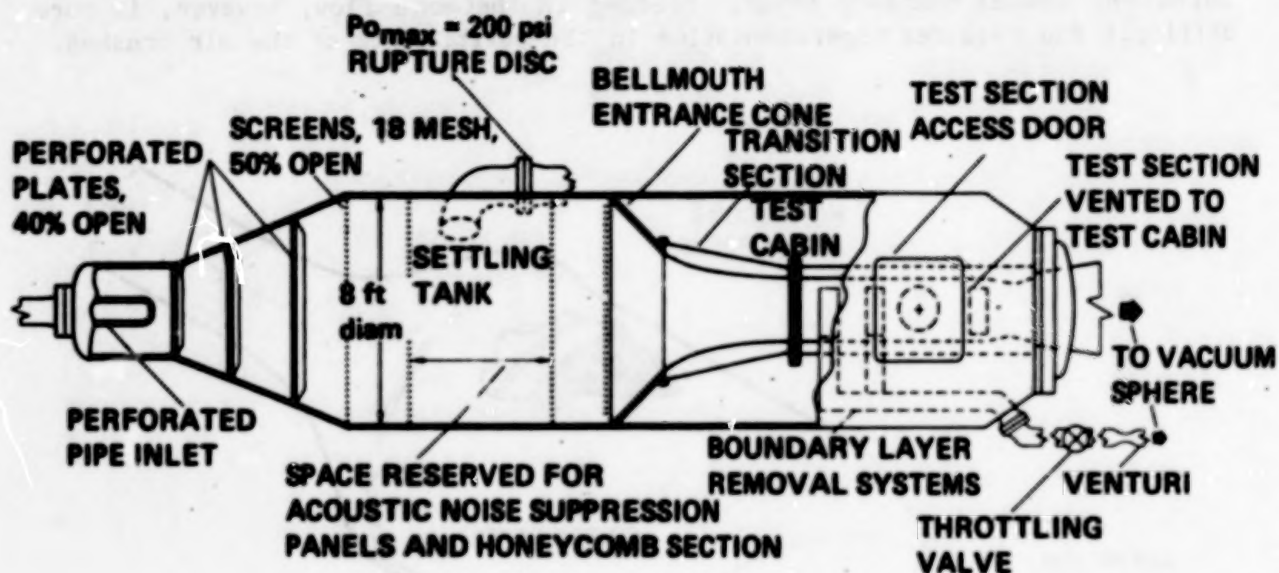
SEEDING THE HIGH REYNOLDS NUMBER CHANNELS

Several seeding arrangements have been used in these large blow-down facilities. The objective is to introduce a finely atomized aerosol of the polystyrene particles and the liquid diluent into the flow. This must be done at a location sufficiently far upstream to permit the liquid to evaporate, and to allow injection disturbances to be damped. Existing tunnel access port location and size were further limitations. Two locations have been tested: in the high pressure feed pipe upstream of the tunnel, and in the entrance chamber just downstream of the perforated pipe inlet.

Excellent mixing and distribution were obtained with the first location. Seed deposits on the test section walls and windows, however, indicated that this location could cause the porous boundary layer removal panels to become plugged with seed material. Despite the turbulence at the tunnel inlet caused by the perforated inlet pipe, tests indicated that injection here could be done without filling the tunnel sidewall boundary layer.
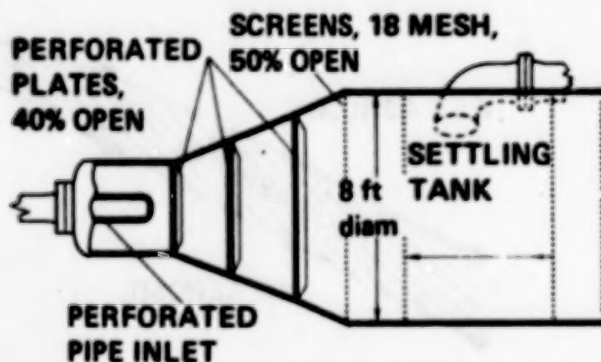
COMMERCIAL SEEDING INJECTORS

Several commercial atomizing nozzles were tested with generally poor results. The "airless" types produced a coarse, wet spray for a variety of pressures and orifice sizes and had an unsatisfactory geometric pattern. The air-liquid types that were tested were found to have a very limited range of usable pressures. The performance of one of the better types is graphed below.

Observations were made of the mist droplet size captured on a lucite sheet 3 feet from the nozzle during bench tests and from the quality of the Doppler signal observed during a tunnel run.
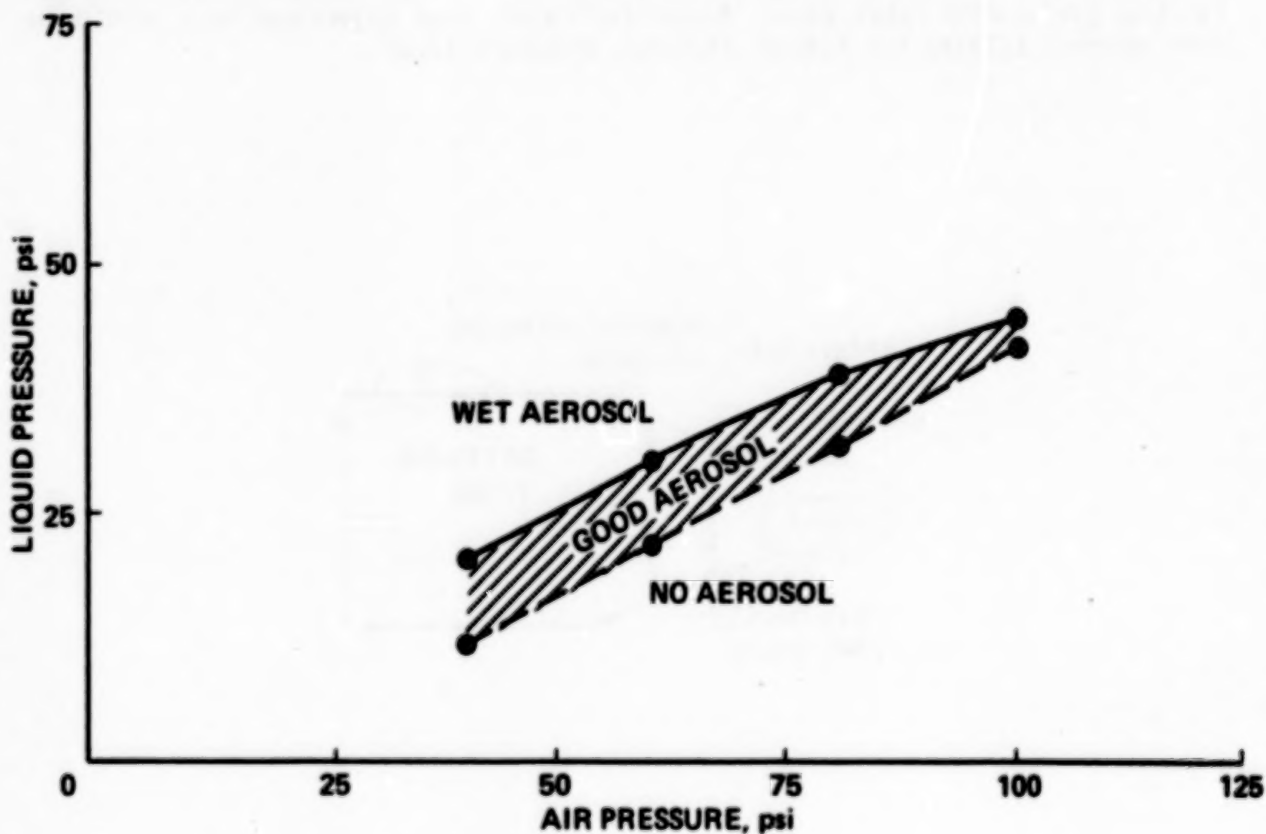
AMES DESIGNED INJECTORS

Three types of seeding injectors using air-liquid mixing have been successfully used in the High Reynolds facilities. Good atomization was obtained with all three designs for a wide range of pressures.

Type A was used in HRC I for several tests which did not require seeding of the entire flow. Wake surveys planned for HRC II, however, required more extensive seeding distributions. Multiple liquid nozzles at a throttling orifice in the high pressure air supply were used as shown at B. This arrangement provided a finely atomized spray with excellent distribution and uniformity. Previously mentioned concerns abut plugging of the porous boundary-layer removal panels in the test section side walls, however, eliminated this approach.

AIR SUPPLY

LIQUID (SEED) MIX

LIQUID (SEED) MIX

HIGH PRESSURE AIR LINE

A

B
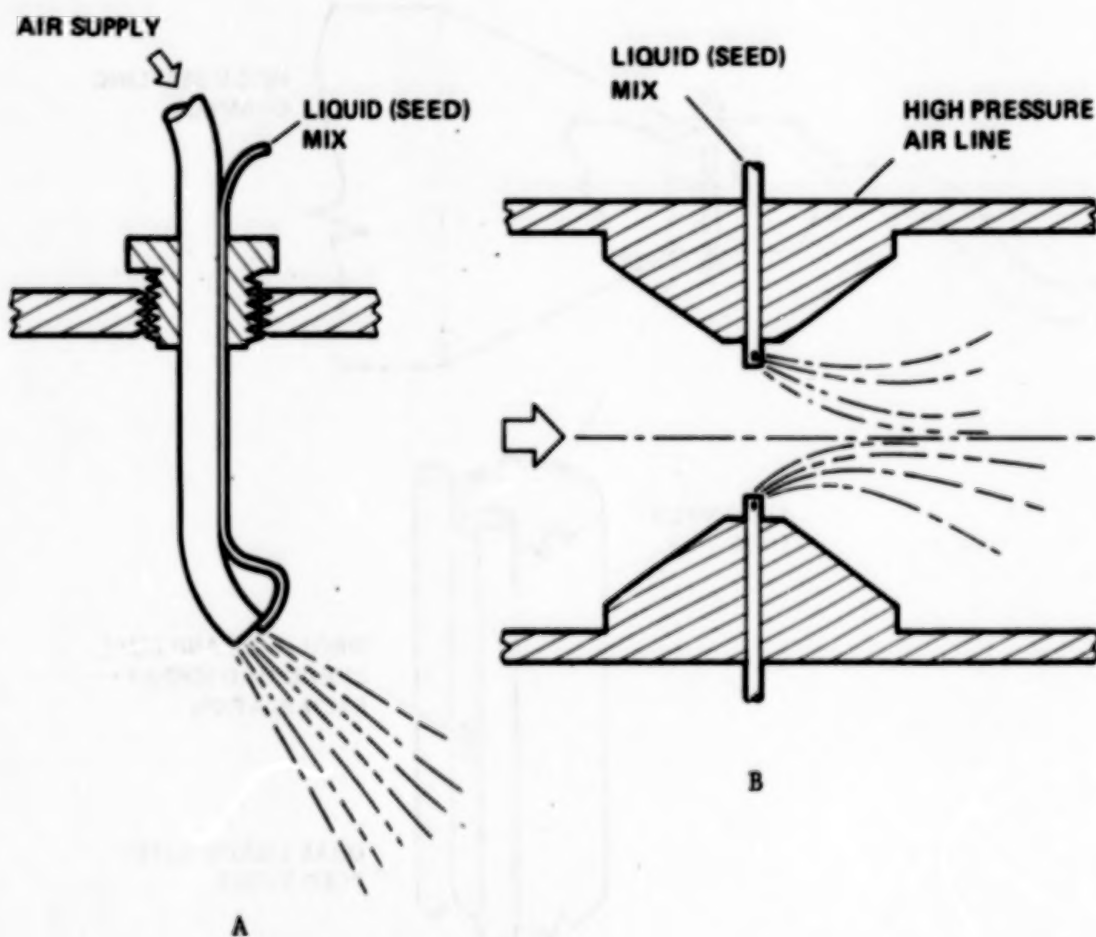
AMES TYPE C INJECTOR

The injector configuration shown at C was devised to provide a good distribution in the central "core" flow without filling the side boundary layers. This design has been used in both HRC I and II with excellent results. It is located in the tunnel entrance section on the plane of symmetry and spans the tunnel from top to bottom. It can be installed through the available 1-1/4"NPT threaded openings and can accommodate an arbitrary number and location of injection stations. Provision is made in the mounting for thermal strain relief and easy removal for cleaning. The opposing liquid jets are well atomized by the sonic air jet and the impingement of the air jet on the liquid supply tubes promotes a fan-shaped spray. Adjustment of the injection pressure and number of stations has provided the desired uniform distribution of seed material in the test section core without seeding the sidewall boundary layers.

HRC II SETTLING
CHAMBER

AIR SUPPLY
TUBE

SINGLE AIR AND DUAL
LIQUID ORIFICES AT
EACH STATION

DUAL LIQUID (SEED)
FEED TUBES

C

186
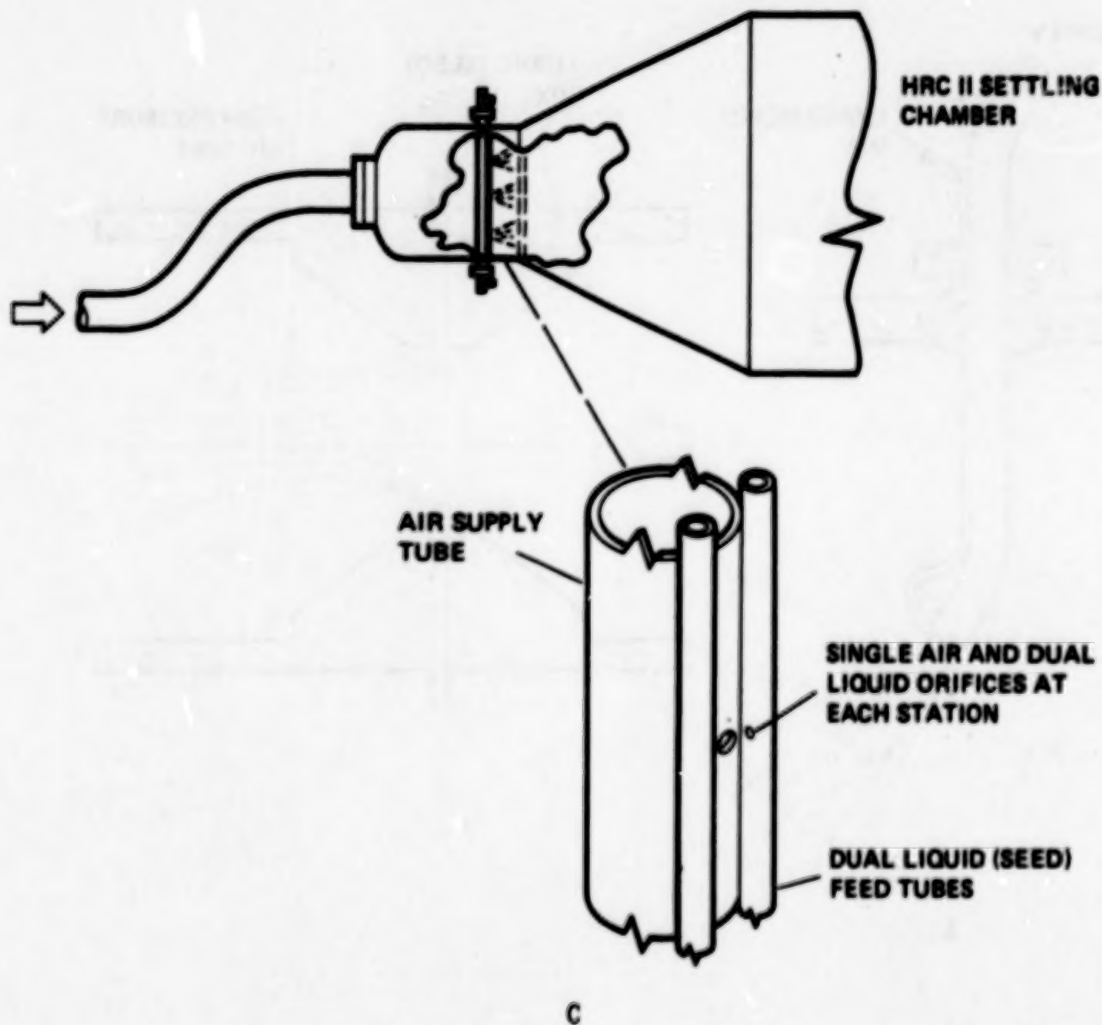
REFERENCES

1. Seegmiller, H. L.; Marvin, J. G.; and Levy, L. L., Jr.: Steady and Unsteady Transonic Flow. AIAA J., vol. 16, no. 4, December 1978, pp. 1262-1270.

2. Seegmiller, H. Lee; Marvin, J. G.; Harrison, D. R.; and Kojima, G.: Application of Laser Velocimetry to an Unsteady Transonic Flow. ICIASF '79 Record, September 1979, pp. 284-293.

3. Driver, D. M.; and Seegmiller, H. L.: Features of a Reattaching Turbulent Shear Layer Subject to an Adverse Pressure Gradient. AIAA 82-1029, June 1982.

4. Robinson, S. K.; Seegmiller, H. L.; and Kussoy, M. I.: Hot-wire and Laser Doppler Anemometer Measurements in a Supersonic Boundary Layer. AIAA 83-1723, July 1983.

5. Maxwell, Barry R.; and Seasholtz, Richard G.: Velocity Lag of Solid Particles in Oscillating Gases and in Gases Passing through Normal Shock Waves. NASA TN D-7490, March 1974.

6. McDevitt, J. B.; Polek, T. E.; and Hand, L. A.: A New Facility and Technique for Two-Dimensional Aerodynamic Testing. AIAA Testing Conference, AIAA-82-0608-CP, 1982.

DEVELOPMENT OF SEEDING TECHNIQUES
FOR SMALL SUPERSONIC WIND TUNNEL

W. R. Hingst
NASA Lewis Research Center
Cleveland, Ohio

and

R. M. Chriss
University of Toledo
Toledo, Ohio

NASA LEWIS 1FTx1FT SUPERSONIC WIND TUNNEL

The NASA Lewis 1x1 foot supersonic wind tunnel is used to experimentally verify computational methods. This tunnel, which is continuous running, operates from laboratory-wide high pressure air and vacuum systems. As such, the air does not recirculate but makes a single pass through the tunnel. The Mach number is varied with interchangeable nozzle blocks and has a range from Mach 1.6 to 4.0. Dry and filtered air is available up to pressures of 3 atmospheres. The air enters the tunnel system through a plenum having flow straighteners and 6 fine mesh screens. The exit of the plenum provides smooth contraction with an area ratio of approximately 20 that, along with the screens, provides a uniform flow for the nozzle. (See fig. 1.)
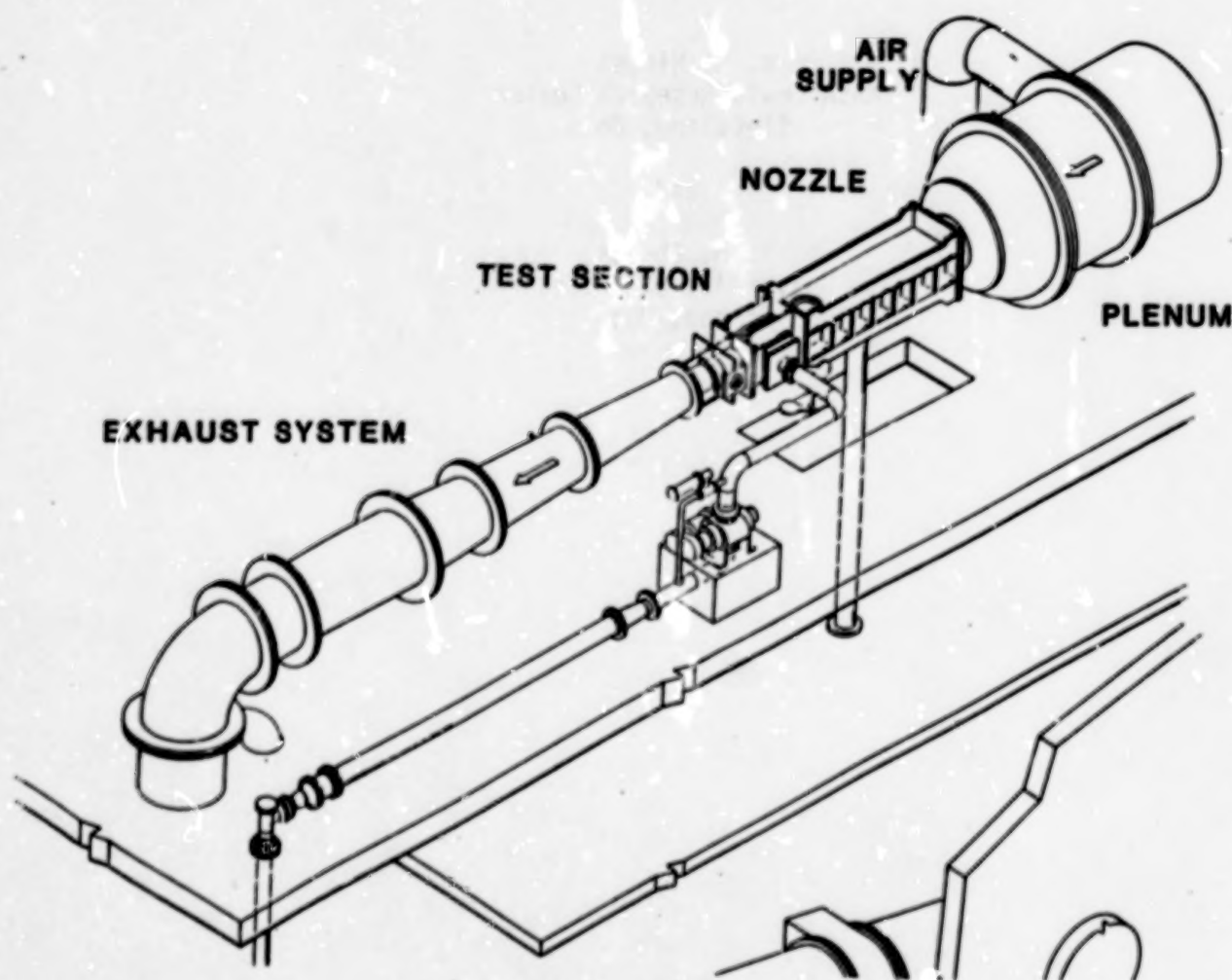
Figure 1

TUNNEL TEST SECTION

A test section downstream of the nozzle blocks is available for studies. This section, which is .65 m long, has two ports of tunnel height and .5m in length that are used for windows, model installation and instrumentation. Downstream of this test section is a transition and diffuser section which ducts the flow into the vacuum exhaust system. In the test described here, a flow blockage cone was installed in the transition section to stabilize a normal shock in the test section. This cone could be actuated axially to position the shock at the desired location. (See fig. 2.)
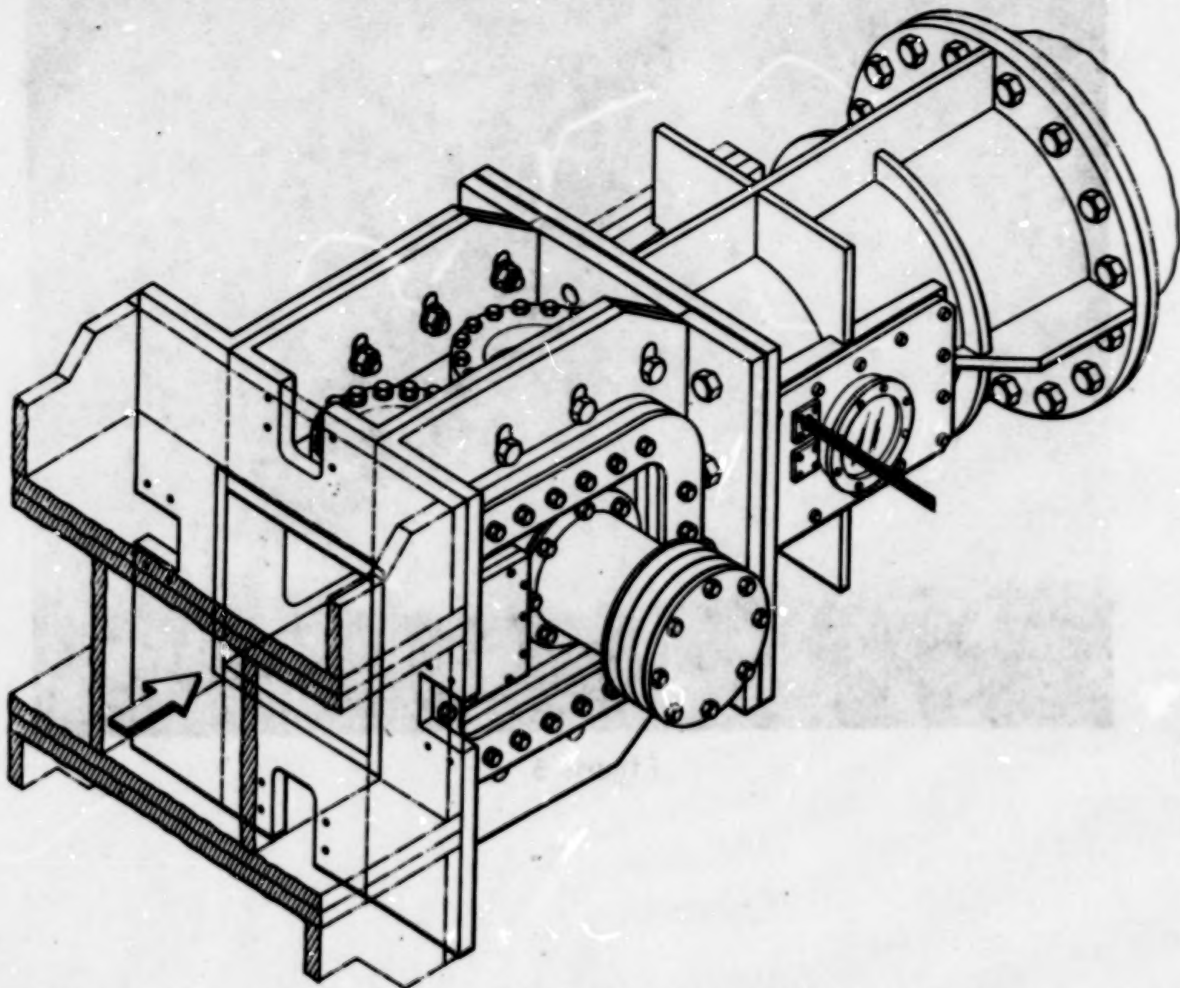
Figure 2

SCHLIEREN-FLOW VISUALIZATION

The normal shock-tunnel wall boundary layer interaction was investigated
at Mach number 1.6. Figure 3 shows the results of a Schlieren flow
visualization of the shock-boundary layer interaction. This photograph,
which extends approximately 10 cm from the tunnel floor, shows the
bifurcated or "lambda" shock structure. In this photograph the flow is
from right to left.
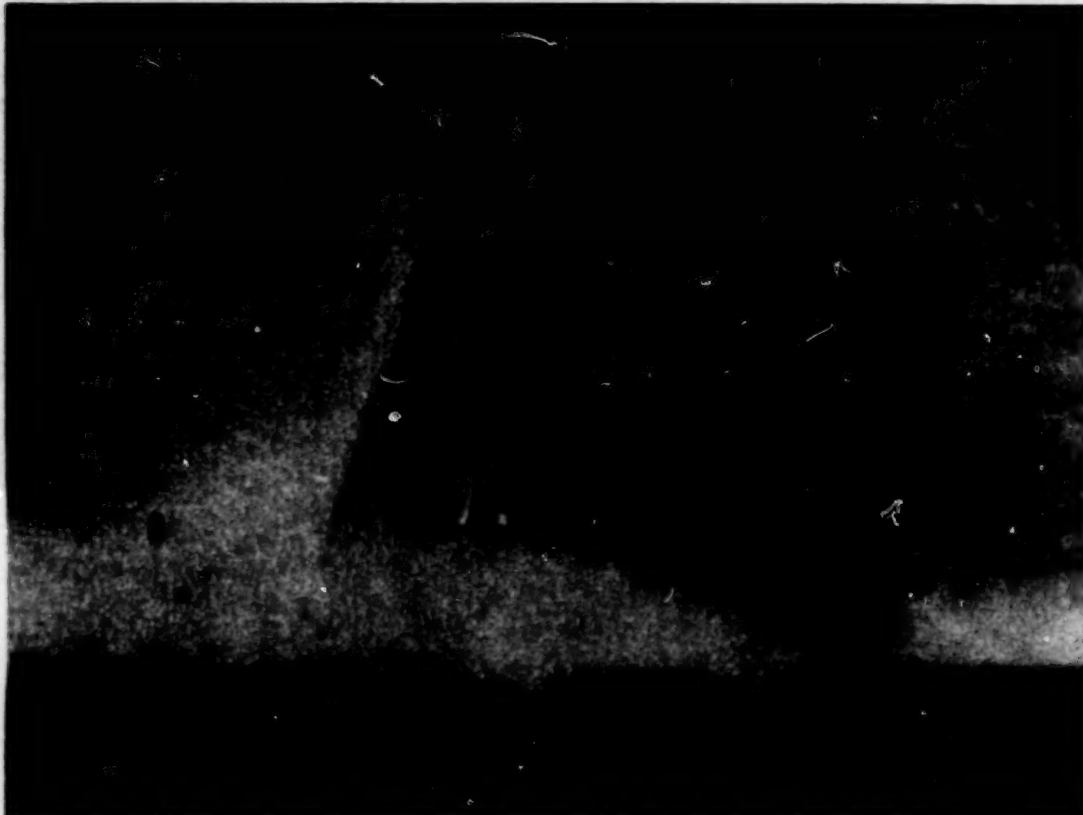
Figure 3

The pressure gradient from the shock at the relatively high Mach number of 1.6 causes substantial flow separation in the wind tunnel. In figure 4 surface oil flow visualization is used to define the three-dimensional separated regions produced by the shock interacting with the tunnel boundary layer. In this figure, an oil-fluorescent dye mixture was applied upstream and allowed to flow downstream through the interaction region. The results were photographed through the Schleiren window. The oil clearly defines a large separation bubble in the corner of the test section at the location of the shock.
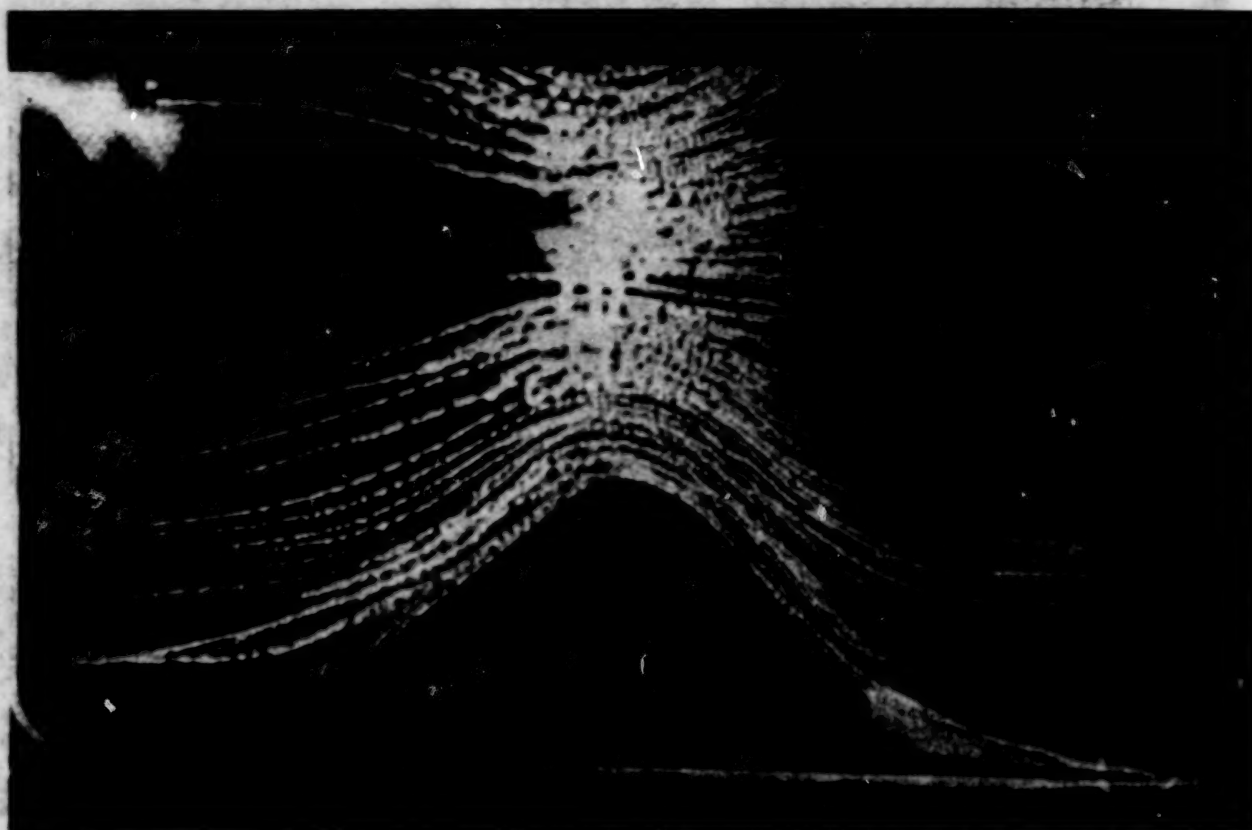
Figure 4

SURFACE OIL FLOW VISUALIZATION

In figure 5, a photograph of a slightly different surface oil flow
visualization technique was used. Here the oil is applied over the entire
surface of the tunnel and then the normal shock established in the test
section. Using this technique, the surface flow structure in the
separated region is defined. The surface oil flow shows the reverse flow
in the separated region.
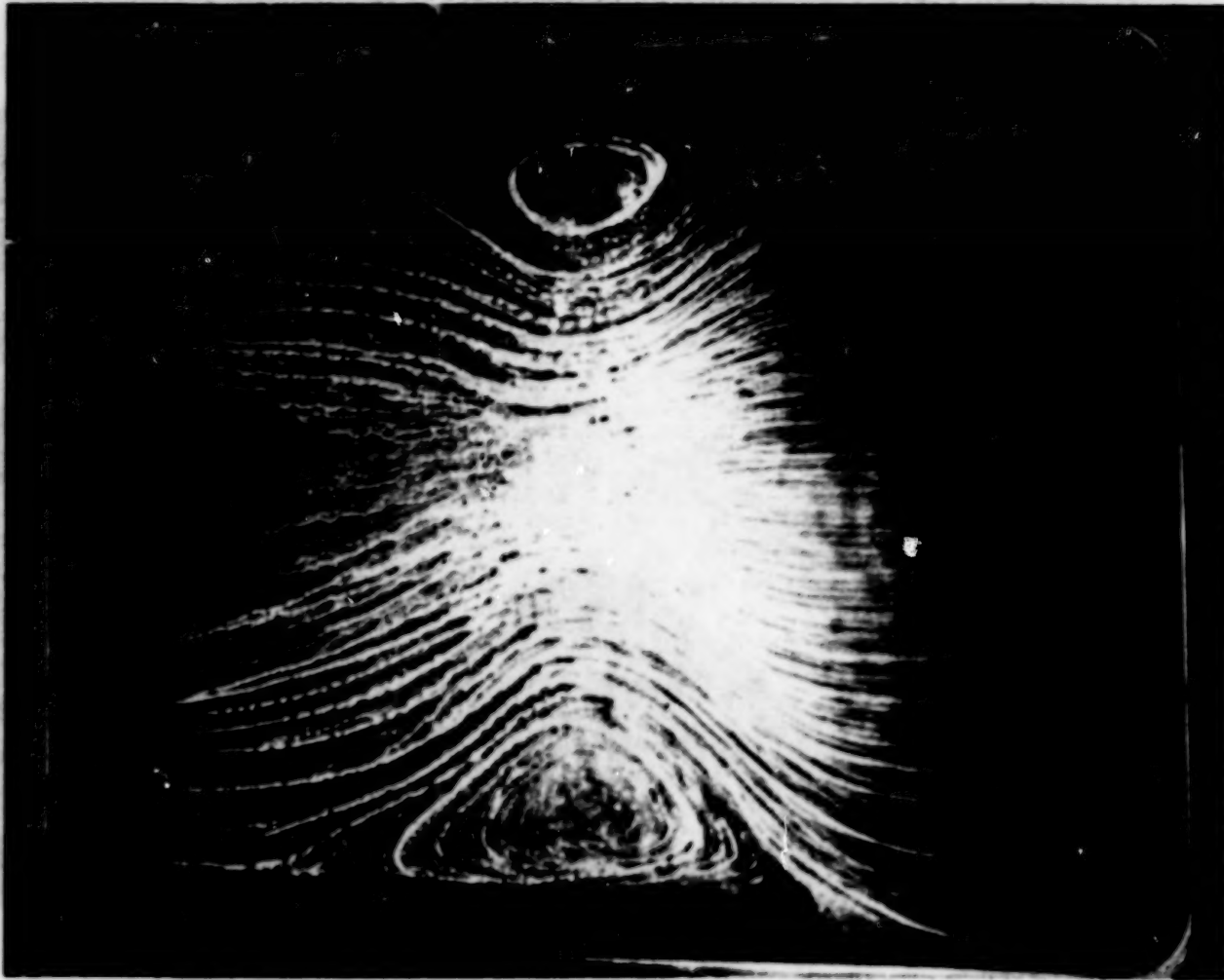
Figure 5

The three-dimensional nature of the separation is shown in figure 6. In
this photograph, the results of a surface oil flow visualization are shown
from an upstream location. This view was taken after the tunnel was shut
down and the tunnel nozzle block removed. In the mid-floor region, the
oil flow was disrupted by the line of an access port blank. The separated
region on the floor defined by the oil flow is nearly identical to that on
the side wall. These results give a picture of a quarter section of an
axisymmetric separated flow region in the corner.

Figure 6

PARTICLE GENERATOR

A schematic of the particle generator used in this experimental investigation is shown in figure 7. The design is based on a technique presented in Ref. 1 and is referred to as a evaporation - condensation generator. In this design, the seed material, DOP, is introduced along with a diluting gas through an atomizing nozzle. This mixture passes through a heating section that vaporizes the DOP. The vapor is then slowly cooled, allowing the oil to condense on residue nuclei. This creates a monodisperse aerosol. The mean diameter can be controlled by using an oil-alcohol mixture and varying the concentration of this mixture. For the tests described here, the oil concentration was maintained at 20% by volume.
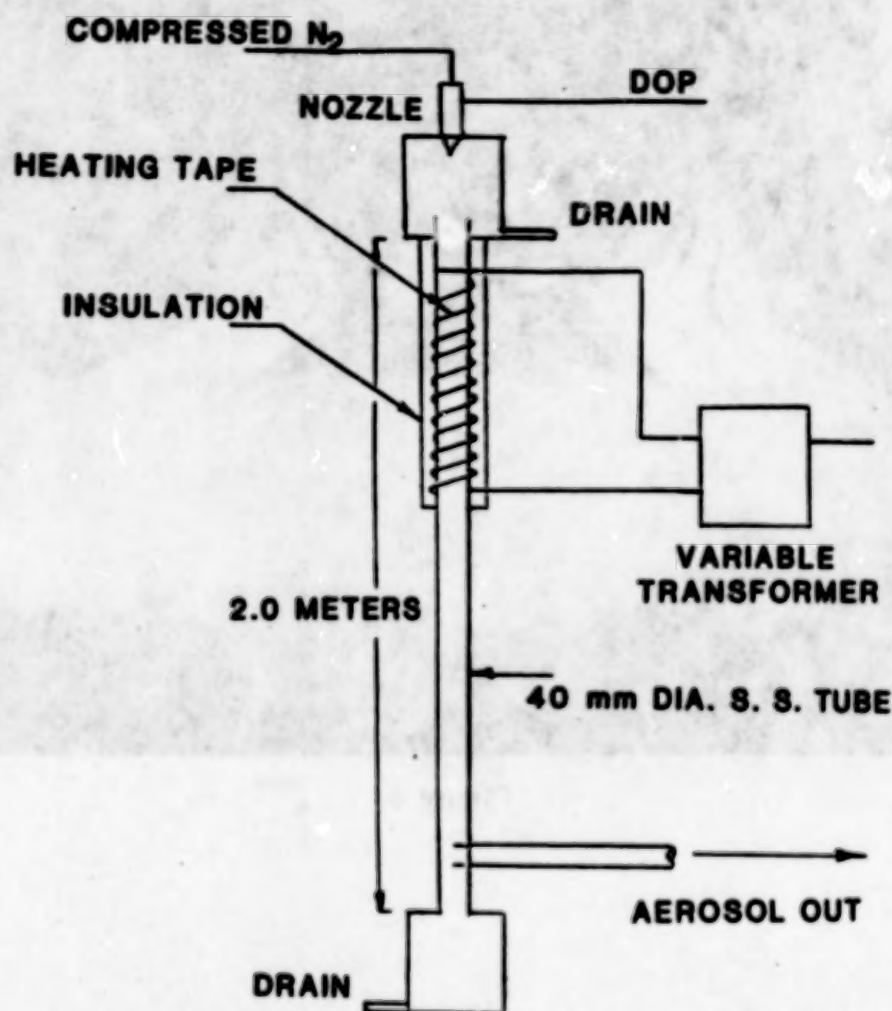
Figure 7

PARTICLE GENERATOR

Figure 8 is a photograph of the evaporation - condensation particle
generator. The generator is located approximately 10 meters upstream of
the tunnel plenum. The seed is injected into the flow at a location where
the air has passed through a pair of parallel filters and the two streams
are combined into a single pipe. This location provides for good mixing
of the seed with the flow. This technique seeds the entire tunnel flow
and does not provide a means for directing the seed material to any
location in the tunnel flow.
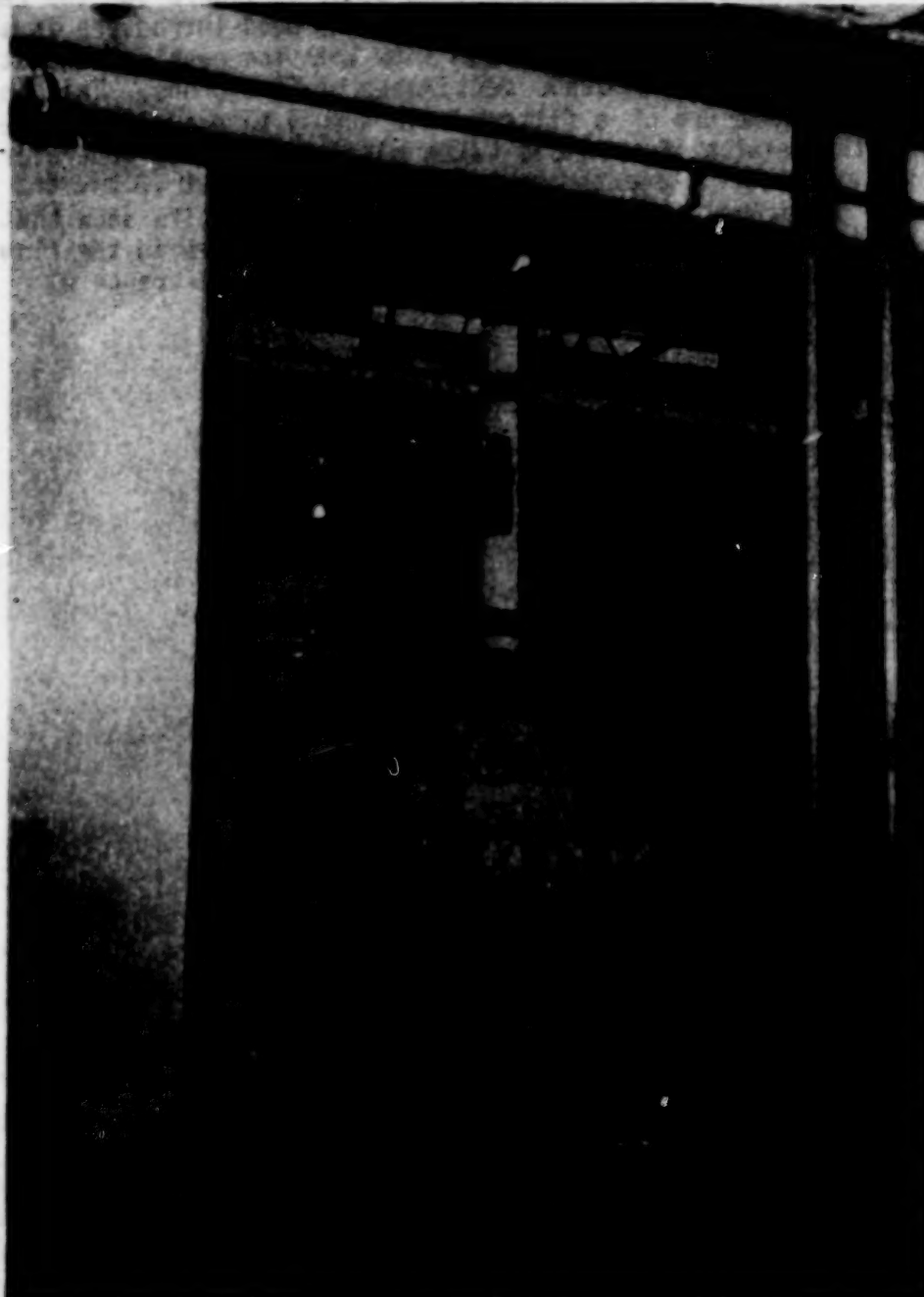
Figure 8

PARTICLE SIZER RESULTS

Since this experiment involves large pressure gradients in high speed
flow, the goal of the seeding technique was to produce sub-micron seed
particles to follow the flow. In addition, the number density of the
particles present should be sufficient to allow useful data rates over the
region of measurements. The tunnel flow was sampled in the test section
using a 10 mm dia. impact probe. These air samples were analyzed with a
TSI Inc. Aerodynamic Particle Sizer (APS 33). In figure 9a the results
of the sample for the tunnel operating with no seed introduced is shown.
These results show a relatively clean flow with the peak concentration of
less than 10 particles per cubic centimeter at .8 microns. This is
consistent with the use of a filtered air supply to drive the tunnel. In
figure 9b the results of a sample taken with the particle generator
operating are shown. Here the peak concentration is at .8 microns at
nearly 400 particles per cubic centimeter. These results show that the
seed clearly dominates the naturally occuring particles in the flow.
Additional information on the generator is given in reference 2.
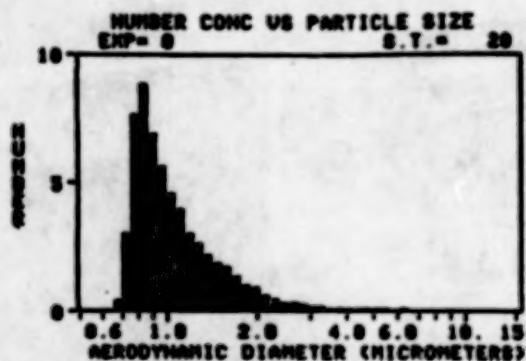
a) Particle concentration with no seed
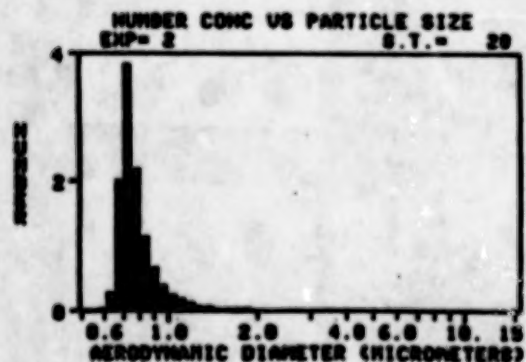
b) Particle concentration with seed added

Figure 9

LV SYSTEM

For the normal shock experiment described here, an independent check on
the seed material's ability to follow the flow is available. Away from the
influence of the wind tunnel boundary layers, the normal shock provides
essentially a step change in the axial velocity of the flow. By using a
Laser Velocimeter (LV) system to measure this velocity change, an idea of
the ability of the seed and LV system to resolve the high velocity
gradients present can be determined. Figure 10 is a schematic of the LV
system used in this experiment. The system is a dual beam configuration
using on-axis forward scatter. This system produces a good
signal-to-noise ratio that allows use of the smallest possible seed. The
focal length of the transmitting lens was 250 mm with a 22 mm beam
spacing. A focal length of 600 mm was used for the collecting lens. The
LV system including the laser was mounted on a 3-axis table that could be
remotely controlled.
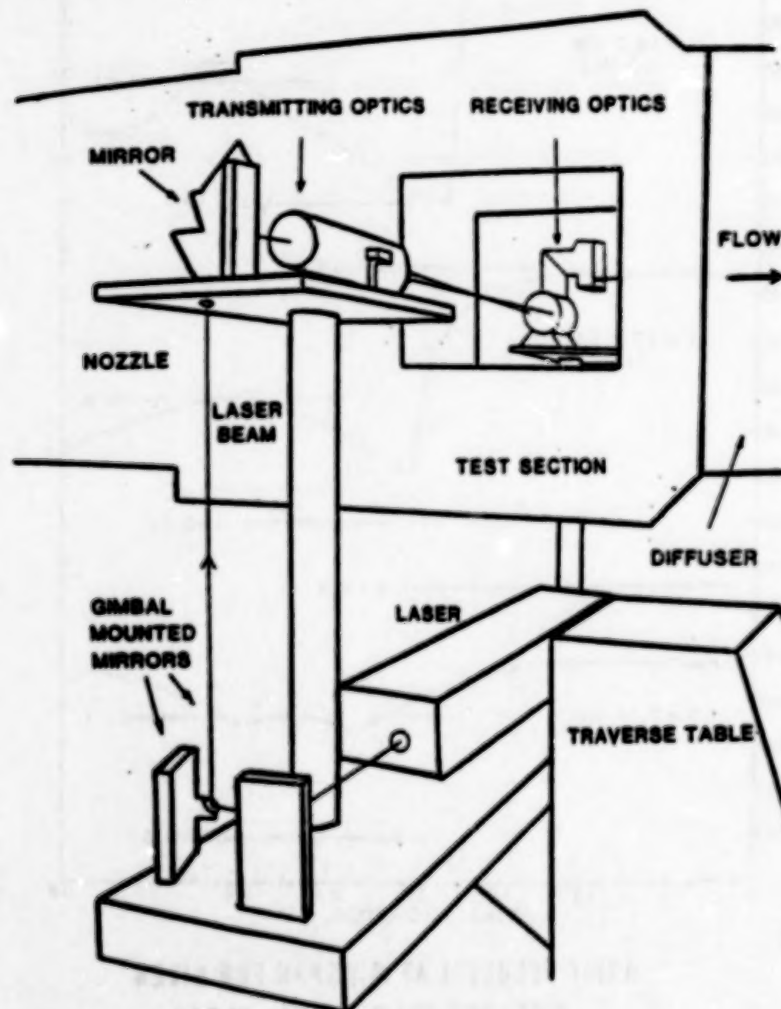
Figure 10

LV RESULTS

Some results of the LV measurements are shown in figure 11. The top
plot represents the velocity along the tunnel centerline along with the
one-dimensional normal shock results for the tunnel Mach number. The
results show good agreement. The increase in velocity after the shock is
a result of the separation bubbles, which produce an area change and
cause a deviation from the one-dimensional flow. The bottom plots
represent the velocity along lines that are progressively closer to the
tunnel side wall. These plots show the effect of the bifurcated shock and
boundary layer on the velocity. That is, the axial gradients are
substantially reduced.
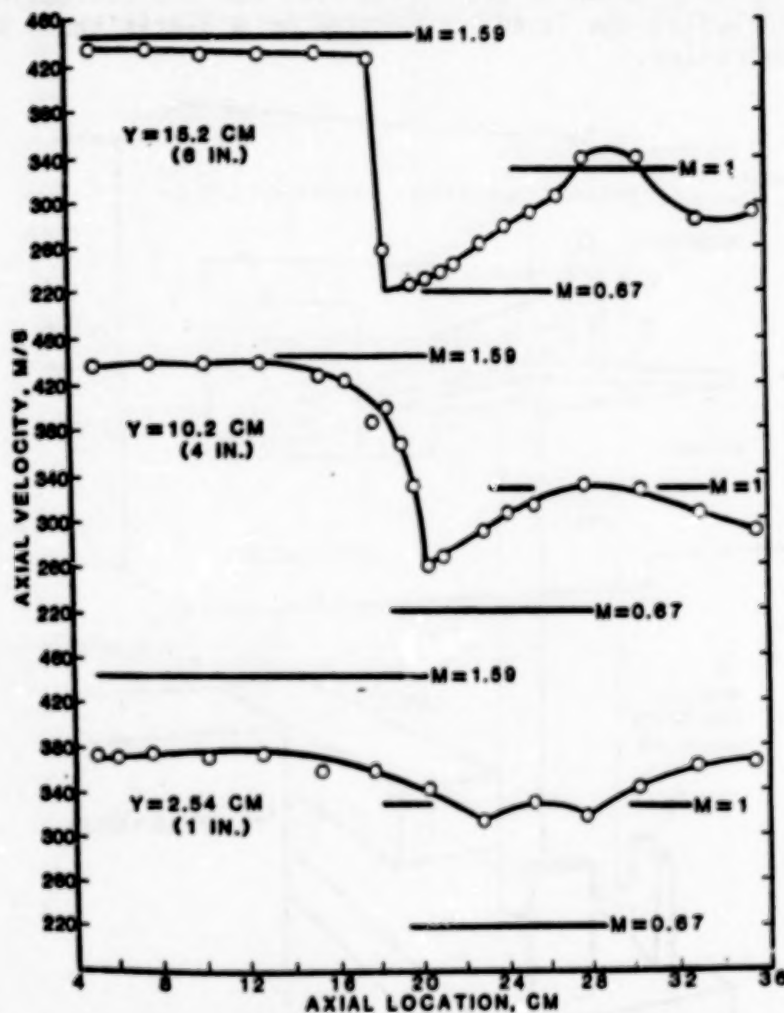
**AXIAL VELOCITY AT MIDSPAN FOR GIVEN
DISTANCE FROM TUNNEL FLOOR**

Figure 11

LV RESULTS

A Mach number contour has been constructed from the velocity measurements
and is shown in figure 12. This plot represents the flow through the
bifurcated shock-boundary layer interaction. These measurements were
taken at the mid-tunnel plane and represent the most nearly
two-dimensional interaction in the tunnel. These results are similar to
those of reference 3.
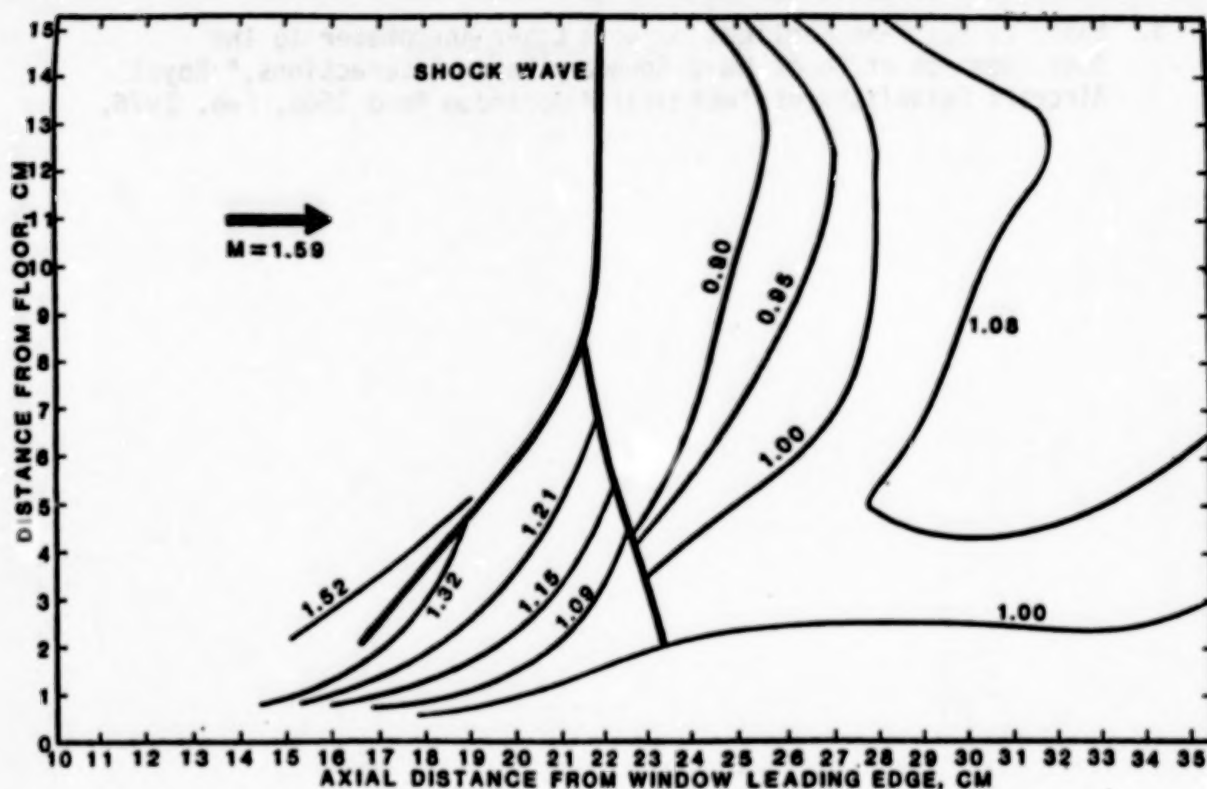
MACH NUMBER CONTOUR AT MIDSPAN FOR 3-D FLOW

Figure 12

REFERENCES

1. Liu, Y. H., Whitby, K. T., Yu, H. H. S., "A Condensation Generator for Producing Monodispersed Aerosols in the Size Range .036 μm to 1.3 μm," Journal De Recherches Atmospheriques, PP. 397-406, 1966.

2. Chriss, R. M., An Investigation of the Interaction of a Normal Shock Wave with a Turbulent Boundary Layer by Laser Anemometry, M. S. Dissertation, University of Toledo, 1984.

3. East, L. F., "The Application of a Laser Anemometer to the Investigation of Shock Wave Boundary Layer Interactions," Royal Aircraft Establishment Technical Memorandum Aero 1666, Feb. 1976.

AEROSOL SEEDING SYSTEMS FOR THE NSWC WIND TUNNELS

William J. Yanta
Timothy S. Smith
Arnold S. Collier

Naval Surface Weapons Center
Silver Spring, Maryland 20903-5000

AEROSOL GENERATOR LASKIN NOZZLES

Shown below are four types of Laskin nozzles which are used to generate the primary aerosol "mist". This mist may be used directly as LDV particles; however, in general, a wide range of particle size exists at this stage and requires the use of some type of mono-dispersion refinement technique. These techniques will be discussed later.

These nozzles rely on the shearing action of high speed air near a column of seeding liquid. Typically, olive oil or dioctyl phthalate (DOP) is used, but within the past year solid polystyrene particles in an alcohol suspension have been used with great success. Air, at a typical pressure of five psig, is supplied to the top of the nozzle which is merely a hollow tube. This air issues radially from one or more small jets located near the collar close to the bottom of the tube. When the collar is submerged in the seeding liquid, the hollow columns located in the collar become filled with liquid. The air from the jet shears the liquid into the fine mist.

Shown from left to right is the "true Laskin" (Reference 1) followed by the four-hole and eight-hole nozzles (Reference 2). A new-version one-hole nozzle which utilizes a submerged particle impactor is also shown along with its impactor. The units of the scale are inches.

VAPORIZATION-CONDENSATION GENERATOR

One way to produce mono-disperse aerosols from the course primary mist is to use a vaporization-condensation generator, shown here. Located inside the seeding liquid reservoir (lower right corner of the figure) is the Laskin nozzle and an amount of seeding liquid sufficient to submerge the nozzle collar. Air is supplied to the nozzle and poly-disperse mist is forced along with the air up the copper tube on the right side of the generator to the top where a manifold is located. There, the mixture is supplied to four vertical stainless steel tubes which are heated at the top by electrical heater tapes up to roughly nine hundred degrees Fahrenheit. This high temperature causes the walls of the tubes to radiate enough energy to the mist droplets to vaporize them. Solid impurities in each droplet do not vaporize but remain intact. These condensation "seeds" along with the vapor travel down the tubes to a region which is at approximately room temperature. Condensation takes place in a uniform manner which produces a mono-disperse aerosol. This aerosol is then collected by another manifold located at the bottom of the generator and passed on to the wind tunnel via a large diameter flexible hose.

One item that makes this generator rather unique is that it can be used to seed flows which have local static pressures of up to ten atmospheres. Also, the large size of this generator facilitates production of relatively large amounts of highly mono-disperse aerosol continuously. The units of the scale are inches. This is a scaled version of the generator described in Reference 3.

MINIATURE AEROSOL NOZZLE

Particle generators can be characterized using a miniature aerosol nozzle such as the Mach 3 nozzle shown here. By measuring the velocity lag which a particle experiences as it flows through a calibrated, rapidly accelerating flowfield, and comparing this lag to numerical predictions (Reference 4), a mean particle size can be determined.

This particle aerosol nozzle is actually a complete wind tunnel test section. It consists of a nozzle, diffuser, pitot probe and test cell with optical ports and can be used with a variety of gas supply and dump tank configurations. It is capable of sizing liquid particles (with a specific gravity of one) as large as 15 microns in diameter. Larger particles are subject to shattering. The diameter of the windows is approximately 1.25 inches.
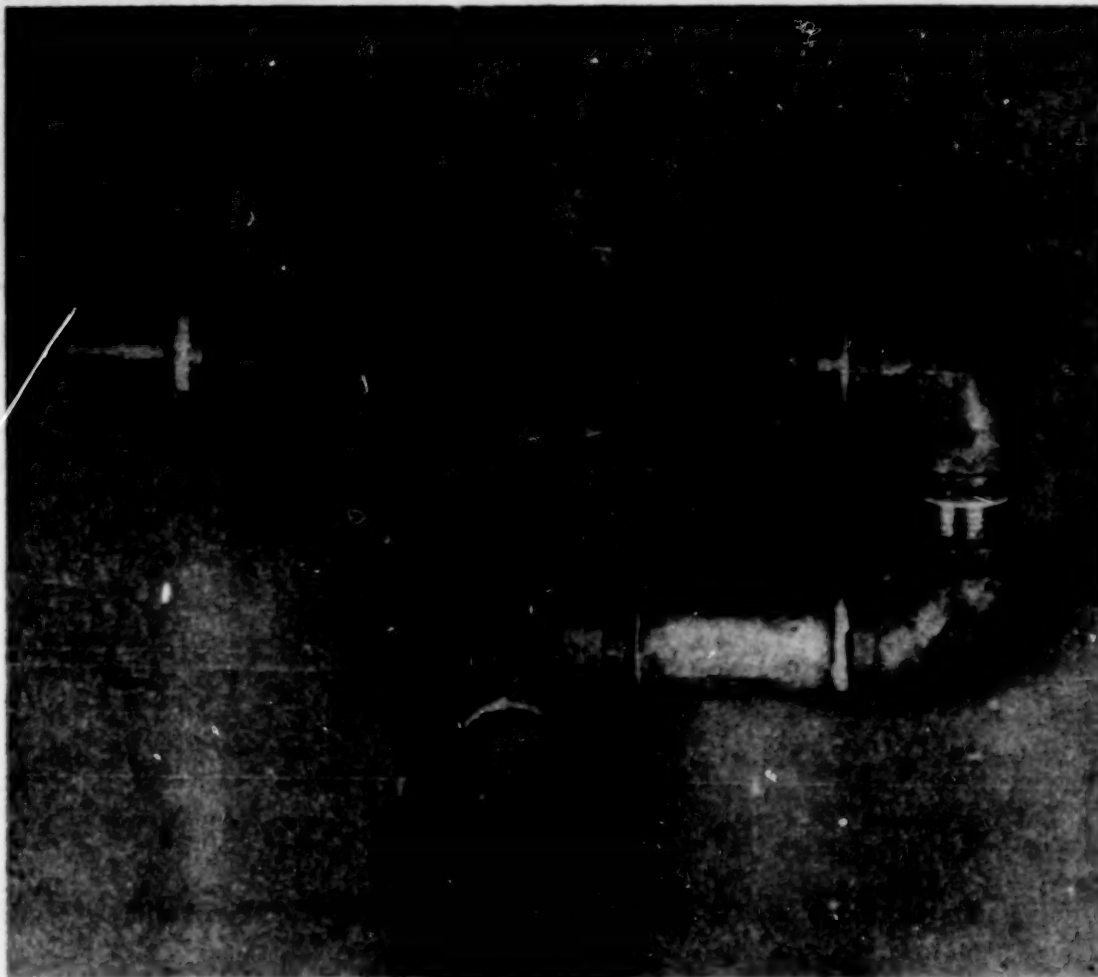
Shown below are two histograms of particle size distributions from a particle generator. The histogram on the left shows the particle size distribution of the coarse aerosol from a Laskin nozzle. By employing the Vaporization Condensation Generator shown previously to refine the coarse aerosol, passing the resulting particles through the miniature aerosol nozzle and measuring the particle velocity at a known distance downstream of the throat along the nozzle centerline, the particle size distribution was determined. The histogram on the right shows these results. Note the disappearance of the doublet peak at d = 3.0 microns.

Solid particles of uniform diameter are available commercially in a variety of diameters, materials and properties. When solid particle seeding in gas flows is desired, the simple particle generation scheme shown here can be used. In this generator, house air is sent through a Laskin nozzle and generates a coarse aerosol from a solution of solid particles in a volatile solvent. By adjusting the concentration of solids in solution such that the probability of having more that one particle in an aerosol droplet is small, the resulting seed will consist of only one particle. The optimum concentration was experimentally determined to be 0.25% by volume. The only limitation of this particle generating scheme is that the size of the coarse aerosol be large enough to contain the solid particle.

LARGE PARTICLE GENERATION

Below is a photograph of a Berglund-Liu Vibrating Orifice Monodispersed Particle Generator (TSI Model 3050). One noteworthy characteristic of this unit is its ability to produce a monodispersed aerosol with a droplet diameter of 0 to 400 microns.

The syringe pump shown on the left forces liquid at a constant feed rate through an orifice located in the generator shown in the center. A piezo-electric ceramic driven by a signal generator, shown on the right, induces a vibration on the orifice. The vibration causes the orifice to shear off a particle from the liquid stream at each cycle. Air is mixed at two stages in the system to disperse the individual droplets and therefore reduce agglomer-ation (see Reference 5 for a detailed description of operation).

The size of the aerosol droplet can be changed by varying the diameter of the orifice, the concentration of solute in the liquid solution, the orifice vibrating frequency or any combination of three. By using a dissolved sub-stance as a solute, solid particles may be generated.
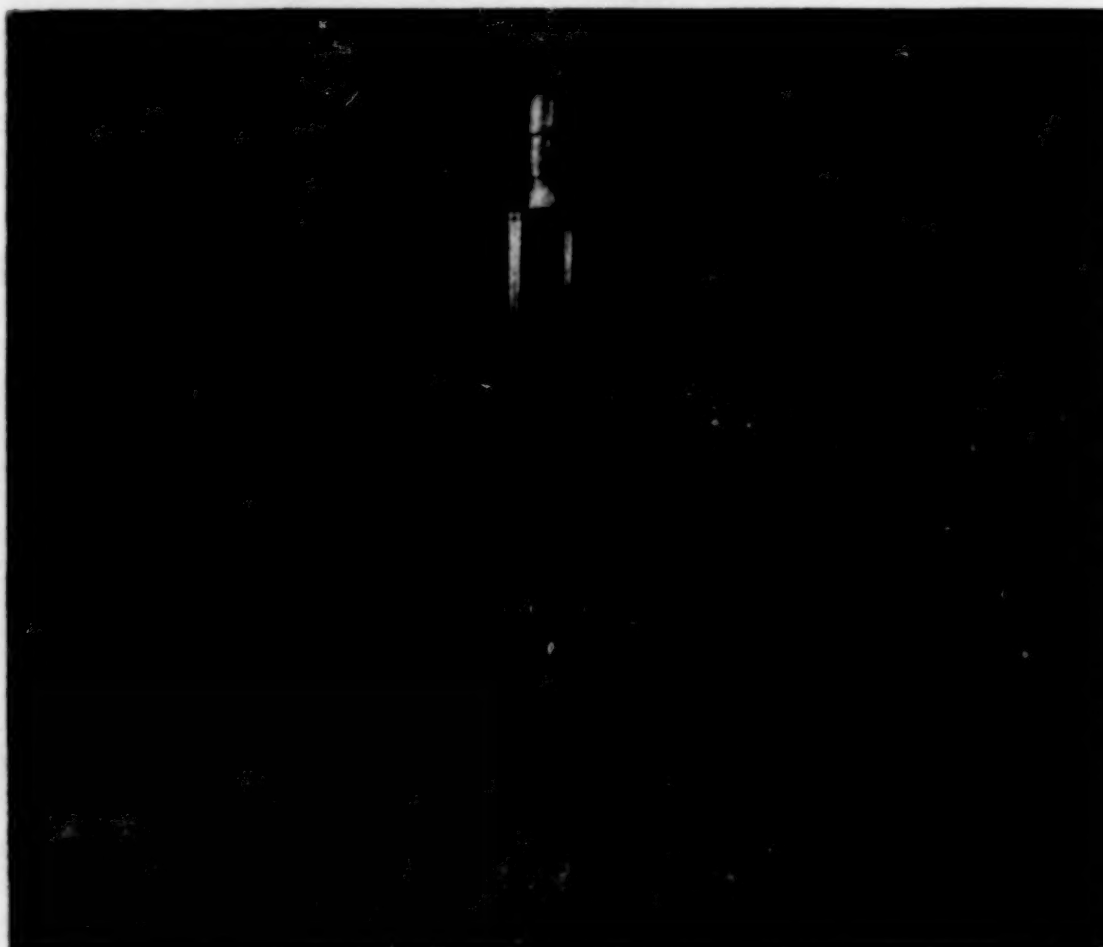
REFERENCES

1. Drew, R. T. and Bernstein, D. M. The Laskin Aerosol Generator. Journal of Toxicology and Environmental Health, 4:661-670, 1978.

2. Echols, W. H. and Young, J. A. Studies of Portable Air-Operated Aerosol Generators. NRL Report 5929, Naval Research Laboratory, Jul 1963.

3. Liu, Y. H., Whitby, K. T., and Yu, H. H. S. A Condensation Aerosol Generator for Producing Monodispersed Aerosols in the Size Range, 0.036μm to 1.3μm. Journal De Recherches Atmospheres, pp. 397-406, 1966.

4. Yanta, W. J. Measurements of Aerosol Size Distributions With a Laser Doppler Velocimeter. Aerosol Measurements, National Bureau of Standards Special Publication No. 412, Oct 1974.

5. Berglund, R. N. and Liu, B. Y. H. Generation of Monodisperse Aerosol Standards. Environmental Science and Technology, Vol. 7, pp. 147-153, Feb 1973.

SEEDING MATERIALS - HEALTH AND
SAFETY CONSIDERATIONS

R. D. Brown
Kelsey-Seybold Clinic, P.A.
NASA Langley Research Center
Hampton, Virginia

The choice of a proper seeding material for laser velocimeters must include health and safety considerations. Failure to do so can lead to catastrophic results.

All materials are toxic, and laser velocimeter seeding materials are no exception. Toxicity may be considered an inherent property of a given material. The manifestation of that property or the physiological response to the material is dependent on dose and exposure conditions. An approximate, physiological classification of toxicity is given in Table 1. It is only approximate because the same material can produce more than one response.

Table 1. Physiological Classification of Toxic Materials

Class	Examples
Irritant	Ammonia, Sulphur Dioxide
Asphyxiant	Nitrogen Dioxide, Carbon Monoxide
Anesthetic	Aliphatic Hydrocarbons, Ethyl Alcohol
Systemic Poison	Heavy Metals, Carbon Tetrachloride
Sensitizer	Isocyanates, Formaldehyde
Fibrotic Agent	Silica, Coal Dust
Mutagens & Carcinogens	Arsenic, Asbestos
Nuisance	Alumina, Kaolin

Toxicity in some situations is not necessarily the most restrictive factor in selection of materials. It is also very important to consider how the material is used so that actual exposure to the material in a damaging form can result. For example, nickel and cadmium are both extremely toxic as systemic poisons and in the case of nickel as a carcinogen. However, a nickel-cadmium battery is relatively harmless primarily because the materials are safely packaged. Seeding materials, however, seem to be used in a manner that maximizes the hazard potential.

Seeding materials are dispersed in air under conditions that favor personnel exposure. Dispersal equipment is frequently if not normally manned, and personnel are often required to make frequent adjustments to assure proper operations.

To be useful, seeding materials must be of a particulate nature, typically on the order of one to two microns or less in diameter. A respirable dust is defined by the American Conference of Governmental Industrial Hygienists (ACGIH) (1) as having the size distribution shown in Table 2. Particulates used as seeding materials therefore can be seen to be almost completely respirable, again maximizing the hazard potential.

Table 2. Respirable Particulate Size Distribution

Aerodynamic Diameter of Unit Density Sphere	% Respirable
<2	90
2.5	75
3.5	50
5.0	25
10	0

At this point it is probably obvious to conclude the most desirable laser velocimeter seeding material should lie within the nuisance classification. More toxic materials could be used but additional exposure controls would be required in order to reduce exposure. ACGIH has published the list of nuisance particulates shown in Table 3. It should be emphasized that "nuisance" does not necessarily mean inert. As used by ACGIH, exposure to a nuisance particulate under reasonable controls does not produce significant organic disease or toxic effect and has little adverse effect on the lungs. "Little adverse effect" is specifically defined as follows: 1. The architecture of the air space remains intact; 2. Scar tissue is not formed to a significant degree; and 3. Any tissue reaction is potentially reversible.

Table 3. Nuisance Particulates

Alumnia	Plaster of Paris
Calcium carbonate	Portland Cement
Calcium silicate	Rouge
Cellulose (paper fiber)	Silicon
Emery	Silicon Carbide
Glycerin Mist	Starch
Graphite (synthetic)	Sucrose
Gypsum	Titanium Dioxide
Kaolin	Vegetable oil mists
Limestone	(except castor, cashew nuts
Magnesite	or similar irritant oils)
Marble	Zinc Stearate
Mineral Wool Fiber	Zinc oxide dust
Pentaerythritol	

Regardless of the seeding material used, personnel exposures must be controlled so as not to exceed certain limits. Recommendations for exposure limits have been published by ACGIH and the National Institute for Occupational Safety and Health (NIOSH), a governmental agency located with the Department of Health and Human Services. Legally enforceable standards for exposure limits are promulgated by the Occupational Safety and Health Administration (OSHA) within the Department of Labor. In some situtations ACGIH or NIOSH recommendations may be legally enforced by OSHA. Generally, the ACGIH and NIOSH recommendations should be used as they are more conservative and are updated on a more frequent basis. The exposure limits are most commonly defined as the time weighted average concentration for a normal eight hour workday in a forty hour work week to which nearly all workers may be repeatedly exposed without adverse effect.

Personnel exposures for comparison with the exposure limits are determined by air sampling in breathing zones with methods demonstrated to meet accuracy and precision standards established by NIOSH. As the exposure limit is usually expressed as a time weighted average, extended sampling times or a series of measurements is often necessary. In any case, exposure for the entire workday must be determined. An assumption of no exposure for major portions of the day may be acceptable, however, if supportable. The eight hour, time weighted average exposure may be expressed as

$$C_{TWA} = \frac{\Sigma C_n T_n}{8}$$

where C_{TWA} = The 8 hour, time weighted average in ppm or mg/m3

C_n = The concentration during a given time period, n, in ppm, or mg/m3

T_n = The duration of the time period in hours

The units of concentration usually are given as volume per unit volume in parts per million parts of air (ppm) when dealing with a gas or vapor and or as mass per unit volume in milligrams per cubic meter of air (mg/m3) when dealing with a particulate.

When exposures do not extend over the entire work day, levels to which personnel may be exposed may be increased proportionately with corresponding reduction in exposure time. However, there is a limit to the truncating process, and it should not be carried to extremes. Clearly, exposure to an average ethyl alcohol concentration of 1,000 ppm for 8 hours would not produce the same response as exposure to 32,000 ppm for 15 minutes even though the 8 hour time weighted average exposure,

1,000 ppm, would be the same.

Another major area of concern is that of flammability. The most commonly referenced property of a material for assessment of flammability hazard is lower explosive limit (LEL). The LEL may be considered the same as the expression lower flammable limit. The LEL is defined as the minimum air concentration at which a homogeneous mixture can be burned when subjected to an ignition source of adequate temperature and energy. Health hazardous concentrations of any material other than a simply asphyxiant which simply displaces oxygen are always considerably less than lower explosive limits, generally by several orders of magnitude. The LEL for a gas or vapor is usually expressed as volume per unit volume in parts per hundred or percentage.

The volume per unit volume estimate for vaporization of a solvent dispersed into a test chamber of known volume can be calculated as follows:

$$C = \frac{(M)(24.45)}{(MW)(V)} \times k$$

where C = Concentration in ppm for k = million
and % for k = hundred
M = Mass of solvent in grams
MW = Molecular weight
V = Test Volume in liters

Ignition hazards from carbonaceous, chemical, plastic and miscellaneous dusts are reported in numerous Bureau of Mines publications. A single number describing the lower explosive limit for combustible dusts is sometimes available, but it may not be applicable to a given situation because of uncertainties. For examples, it is well recognized flammability increases with decreasing particle size. However, it is difficult to fully quantitate this because of inherent difficulty in maintaining dust laden atmospheres, both spatially and temporally. Other uncertainties include relative humidity of the air and temperature and energy of the ignition source. Generally speaking, however, dust concentrations need to be on the order of grams per cubic meter to be at the LEL.

A summary of health and safety considerations for some commonly used or proposed seeding materials is presented in Table 4. The exposure limits are those recommended by ACGIH (1) except for kerosene where the NIOSH recommendation (2) is given. The data for LEL are found in numerous references. Several entries

Table 4. Properties of Seeding Materials

Name	Exposure Limit	Health Effects*	LEL
Aluminum Oxide	10 mg/m^3	Nuisance, Carcinogen (!?)	
Kaolin	10 mg/m^3	Nuisance	
Silicon Carbide	10 mg/m^3	Nuisance	
Polystyrene Latex	10 mg/m^3	Nuisance, Carcinogen (!?)	15 g/m^3
	50 ppm	Anesthetic, Irritant	1.1%
Vinyl Toluene	10 mg/m^3	Nuisance	
	50 ppm	Irritant, anesthetic	0.1%
Propylene Glycol		Nuisance, slight irritant	2.6%
Kerosene	14 ppm	Irritant	0.9%
Ethyl Alcohol	1,000 ppm	Anesthetic, Irritant, Systemic	3.3%
Methyl Alcohol	200 ppm	Systemic, anesthetic Irritant	6.7%

* Varies with concentration, exposure conditions

deserve comment. A carcinogenic effect is given for both aluminum oxide and polystyrene latex even though these materials are generally considered to be only of nuisance hazard. In both instances, the materials were reported by NIOSH (3) to have equivocal tumorogenic properties. It is highly improbable these materials could be carcinogenic under any conceivable exposure conditions that would result from use as seeding materials. Curently no regulatory agency considers them as posing anything other than a potential nuisance hazard.

Use of polymeric materials such as the polystrene or vinyl toluene can also pose a hazard from the unreacted monomer. The monomer will always be more hazardous. Polymeric materials, therefore, should be used only after careful consideration of possible presence of unreacted monomers.

A final consideration in the choice of material is that of availability of or willingness to implement necessary controls. Hazard control generally falls into three categories: engineering, administrative, or use of personal protective equipment. There is a great latitude in the choice of controls, and discussion must be limited to a few examples.

Probably the simplest control is the administrative control of substitution with a less hazardous material. Use of a nuisance particulate such as kaolin instead of a heavy metal dust such as lead is an obvious example. Limitation of personnel exposure time has been alluded to previously.

An example of an engineering control could be to incorporate an exhaust system into the test chamber so the area can be periodically purged with fresh air to dilute the contaminated air volume. The effect of dilution ventilation is given by the equation:

$$C_F = C_0 e^{-RT/V}$$

where C_F = Final contaminant concentrations
C_0 = Originial concentrtion
R = Ventilation rate
T = Ventilation Time
V = Test Chamber Volume

Personal protective equipment includes respirators, rubber gloves, goggles, faceshields and the like. These devices are not failsafe and depend upon individual acceptance and attention for proper utilization. Peronal protective equipment, particularly respirators, should be used only when other controls are not effective or while they are being implemented.

REFERENCES

1. American Conference of Governmental Industrial Hygienists:
   Threshold Limit Values for Chemical Substances and Physical
   Agents ·in the Work Environment with Intended Changes for
   1983-84, ACGIH, Cincinnati, OH (1983-84).

2. National Institute for Occupational Safety and Health:
   Criteria for a Recommended Standard - Occupational Exposure
   to Refined Petroleum Solvents - 1977. HEW (NIOSH)
   Publication Number 77-192, Washington, DC (1977).

3. National Institute for Occupational Safety and Health:
   Registry of Toxic Effects of Chemical Substances. HEW
   (NIOSH) Publication Number 83-107-4, Washington, DC (1985).

GENERATING AEROSOLS FOR LASER VELOCIMETER SEEDING

Jugal K. Agarwal
TSI Incorporated
P.O. Box 64394
St. Paul, Minnesota 55164

INTRODUCTION

The laser velocimeter (LV) is a unique tool for fluid flow measurements. In such measurements, even though the fluid velocity is of primary interest, the LV signal originates from seed particles present in the fluid and the LV actually measures the velocity of these particles. Thus it is important that a sufficient number of seed particles be present in the fluid and they scatter sufficient light to produce LV signals. Also, the seed particles should follow the fluid with high fidelity.

Aerodynamic diameter is the true measure of a particle's ability to follow the flow. The aerodynamic diameter of a particle is defined as the diameter of a unit density sphere with same settling velocity as the particle in question. It is affected by geometric diameter, density and shape of the particle. For LV seeding, particles with smaller aerodynamic diameter are desirable because they follow the flow more readily. On the other hand, in general, the particle's ability to scatter light increases with its geometric diameter and its refractive index.

Monodispersity is a measure of the uniformity in particle size. It is represented by geometric standard deviation, σ_g. The σ_g of an aerosol could be calculated by using the equation:

$$\sigma_g = \frac{d_m}{d_1} = \frac{d_2}{d_m} = \sqrt{\frac{d_2}{d_1}} \tag{1}$$

where d_m is the mean diameter of the particles. The d_1 and d_2 are defined so that 15.87 percent of the aerosol particles have a diameter smaller than d_1 and 87.13 percent of the aerosol particles have a diameter smaller than d_2. The σ_g of a perfectly monodisperse aerosol (all particles have identical size) is 1.0.

For a given LV application, monodisperse aerosol containing particles of a particular optimum size is desirable. The particles of optimum size must be large enough to scatter sufficient light, but small enough to follow the flow. Once this optimum size is established, particles that are either smaller or larger than this size are undesirable. Smaller particles do not produce a useful LV signal, but they do scatter light which adds to the noise. The large particles produce signals which are not representative of fluid velocity.

In the past, very little attention has been paid to selecting the right particles for a given application. This is partly because not very many seeders were available, and partly because LV users had not realized the importance of seed particles and were not paying reasonable attention to the seed particles. This has often led to expensive trial and error of the various seeds in the actual facility. The cost of particle generation should be reviewed with respect to the total cost of the project. A reliable, well-characterized particle generator capable of producing large numbers of monodisperse particles of optimum size may actually save thousands, even tens of thousands of dollars in facility running cost. In some applications, a good particle generator may enable one to use a less expensive laser or signal processor, thereby reducing the total cost of the LV system.

Today it is possible to design the right seed particle for a given application. The first step would be to decide what aerodynamic diameter particle will follow the flow with sufficient fidelity. The next step would be to decide on a seed particle material considering its refractive index, toxicity and errosion properties. Then the optical system should be designed which is capable of giving measurable LV signal from the seed particles (refs. 1, 2). Finally, a seeder that will give monodisperse particle of the selected size in right number should be developed. The point is that now tools are available to evaluate and control parameters independently and one does not have to depend on trying various seeders in the facility and seeing what works. A detailed description of the various seeders available from TSI is given in reference 3.

223
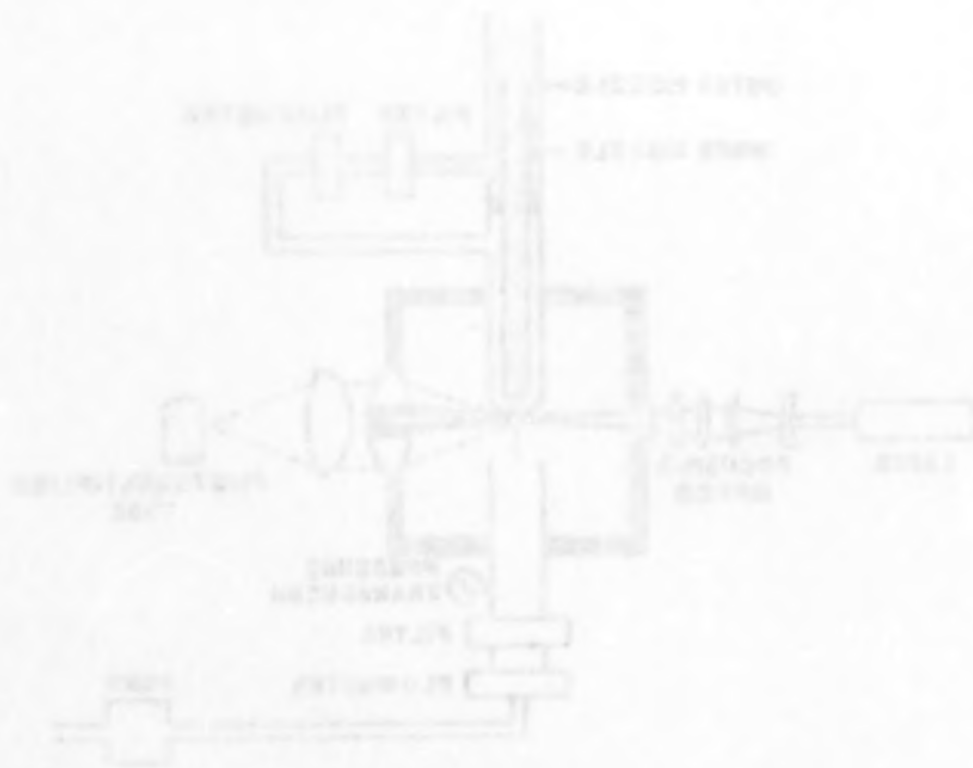
The first instrument that we found very useful in characterizing seed particles is the Aerodynamic Particle Sizer (TSI Model APS 33, ref. 4).

In this instrument the velocity of the particles accelerating from a thin plate orifice is measured using laser velocimetry.

The accelerating orifice assembly consists of a 0.8-mm inner nozzle and a 1.0-mm outer orifice. The inner nozzles receive 20% of the sampled flow, while the remaining 80% passes through a filter and flowmeter and is reintroduced as sheath air. This confines the sampled aerosol particles to the center portion of the accelerating jet.

The beam from a 2-mW He-Ne laser is split by a calcite plate, producing two beams. These beams are then focused to produce two parallel beams with rectangular cross sections just downstream of the accelerating orifice. The light scattered by the particles passing through the beams is collected and focused onto a photomultiplier tube. A particle passing through the two beams produces a pair of pulses. The particle velocity is determined by measuring the time between the two pulses. A microcomputer system converts the velocity data to size distributions and displays the data.
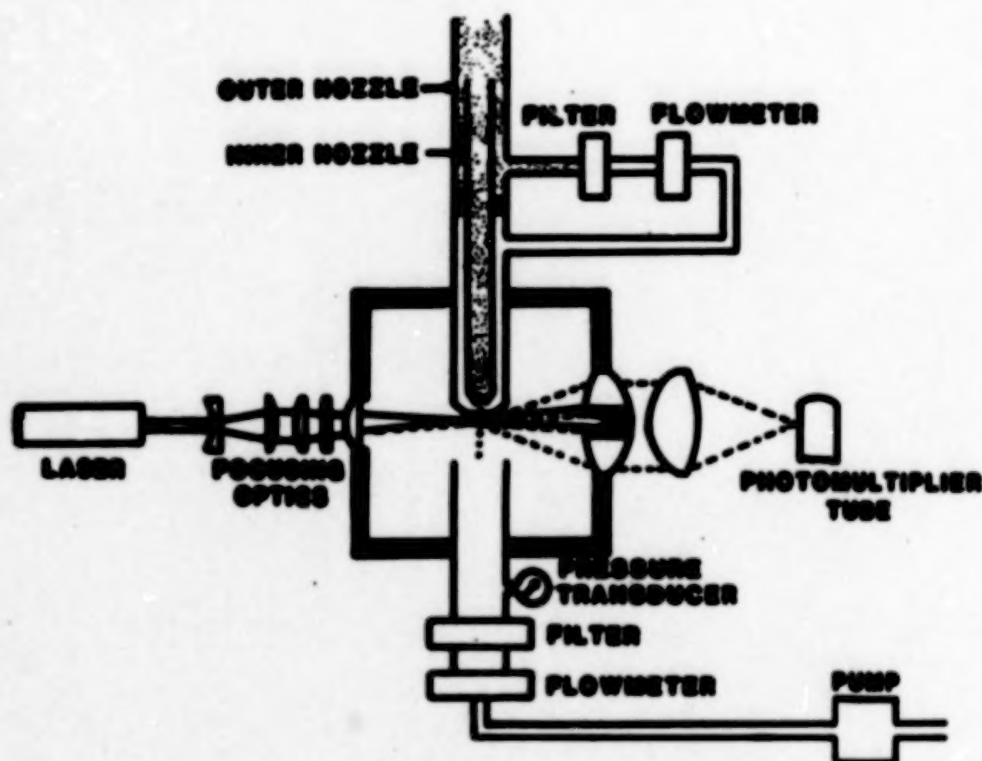
SCHEMATIC OF SENSOR

DIFFERENTIAL MOBILITY ANALYZER

The Differential Mobility Particle Sizer (DMPS, TSI Model 3932, ref. 5) is a unique submicrometer particle instrumentation that offers the fastest, easiest method of obtaining high resolution particle data in the 0.01-1.0 micrometer range. Electrical mobility, which is inversely proportional to particle diameter, is a measurement of how rapidly an electrically charged particle responds to an electric field. Aerosols entering the Electrostatic Classifier acquire a known charge level by passing through a Kr-85 neutralizer. The particles are then passed on to a Differential Mobility Analyzer that consists of two concentric cylindrical electrodes. A high voltage supply controlled by the computer maintains the center electrode at a precise negative potential. The outer electrode is at ground potential.

Inside the DMA is a core of particle-free sheath air surrounded by an annular ring of aerosol. The sheath air and aerosol both flow laminarly downward between the electrodes with no mixing of the two air streams. Particles with positive charges are attracted toward the negative-charged center electrode. The trajectory of the particle is a function of flowrate, analyzer geometry, electric field, particle diameter and the number of charges on the particle. Only those particles within a narrow, predictable mobility range pass through a slit near the bottom of the center electrode. The number concentration of these particles is measured with a Condensation Nucleus Counter. A microcomputer takes the data and presents the particle size distribution.

225
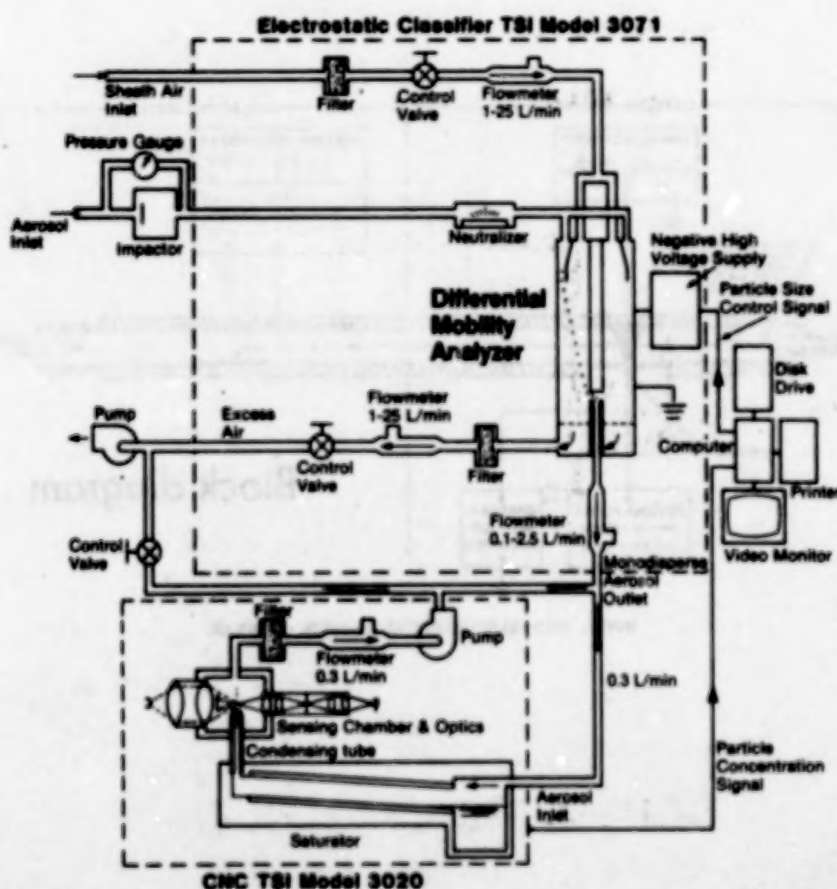
ELECTROSTATIC SAMPLER

Another instrument that is quite useful in evaluating seed particles is the Electrostatic Aerosol Sampler (TSI Model 3100, ref. 6). It consists of a charging section and a collecting section. A vacuum pump draws the aerosol through the system at a constant rate. As the aerosol passes through the charging section, the particles are subjected to alternating pulses of positive ions generated by a corona discharge from a fine wire. The positively charged particles then flow through the collecting section. A positive voltage periodically applied to the upper plate drives the particles to the lower surface. After sufficient time to deposit all charged particles, the voltage on the upper plate is shut off. The continuous aerosol flow through the chamber again fills it with charged particles. The unique separation of the charging section and the collecting section, together with the pulsed precipitating voltage, produces a uniform, representative sample, which may be evaluated without bias due to particle characteristics.

The instrument allows precise determination of the sampled aerosol quantity because this volume is completely independent of the flow rate through the instrument. Volume depends only on the number of precipitating pulses or cycles and the volume directly above the sample surface. This instrument is used to collect samples of seed particles on a microscope slide. The microscope slide is then examined under an electron or optical microscope. The geometric size of the seed particles can be obtained by visual examination of the collected sample. Also, the number concentration of the seed particles can be calculated by counting the number of particles per unit area of the microscope slide.

Block diagram

MODEL 3100—ELECTROSTATIC AEROSOL SAMPLER
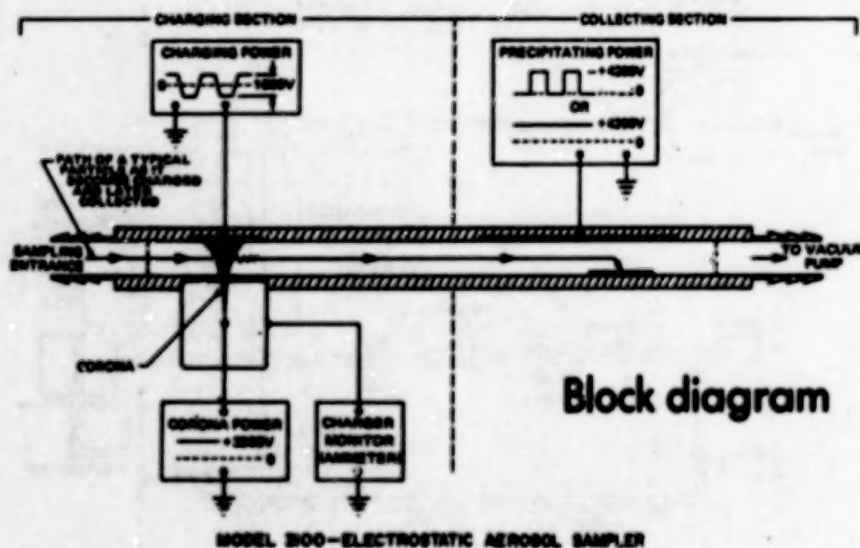
ATOMIZATION

Atomization is the most commonly used method to generate seed particles. Atomization is a process in which a high velocity air jet produces a fine spray of droplets by shearing off a liquid film. This process is simple and reliable. The most wide-spread use of atomizers is in medicine for inhalation therapy. Atomizers of various kinds are also used for lubrication in machining operations, dust suppression, and aerosol generation for filter testing. An atomizer can be used to produce seed particles in one of three ways:

1) Generate liquid droplets - In LV seeding, atomizers are often used to produce an aerosol from liquids such as DOP (dioctyl phthalate) or silicon oil. The particle size and number concentration depend on the surface tension and viscosity of the liquids as well as the design of the atomizer.

2) Generate solid particles from a solute - Solid particles of material such as salt can be generated by first atomizing a solution of the material in water and then drying the droplets. After the evaporation of the solvent, an aerosol of solute is obtained. The size of the particles can be varied by varying the concentration of the solute.

3) Generate monodisperse PSL particles - A monodisperse aerosol can be generated by atomizing a dispersion of uniform particles (such as Dow Diagnostic's polystyrene latex (PSL) particles) in a liquid. When the atomized droplets are dried, the size is reduced to that of the original solid particles. However, it is important that the concentration of solid particles in the dispersion be low enough so that the probability of having more than one particle per droplet is low (ref. 5). Normally, 5 drops of dispersion (10% solid) per liter of distilled water give the right dilution for LV seeding applications.

1. Atomizer Jet
2. Liquid Tube
3. Pressurized Air In
4. Spherical Impactor
5. Dilution Air In
6. Aerosol Outlet Tube
7. Drain
8. Atomizer Liquid
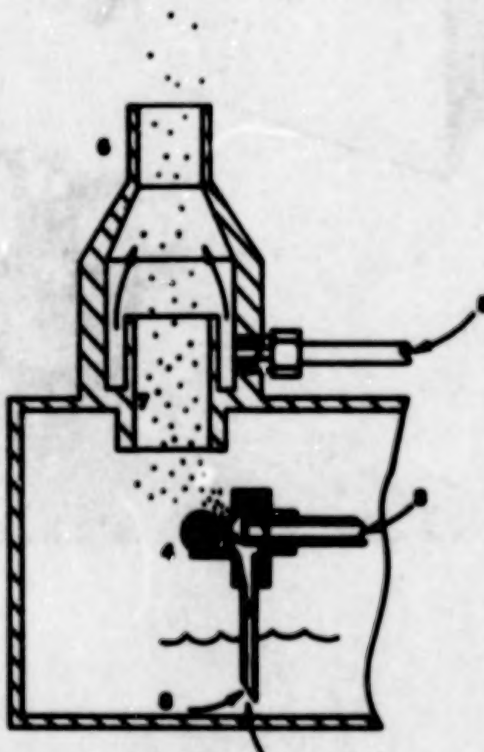
SEEDERS BASED ON ATOMIZATION PRINCIPLE

1.   Model 9302

The Model 9302 atomizer was specifically designed as a set-up tool for LV systems. The aerosol exits through a 1.0 mm black Delrin nozzle in the form of an aerosol stream. The aerosol stream can be easily directed toward the LV measuring volume by positioning the flexible steel aerosol outlet tube. When the black Delrin nozzle is moved in or out, a bypass slit is partially covered or uncovered, thereby increasing or decreasing the velocity of the aerosol stream.

2.   Model 9306

The Model 9306 atomizer has six atomizer jets. The atomizer is designed to introduce aerosol into a system under pressure (up to 400 kPa or 60 psi). Since any number of jets (1 through 6) can be selected, it provides the flexibility of changing the particle number concentration. The built-in dilution air system makes this atomizer ideal for generating dry monodisperse PSL aerosol as well as salt aerosol.
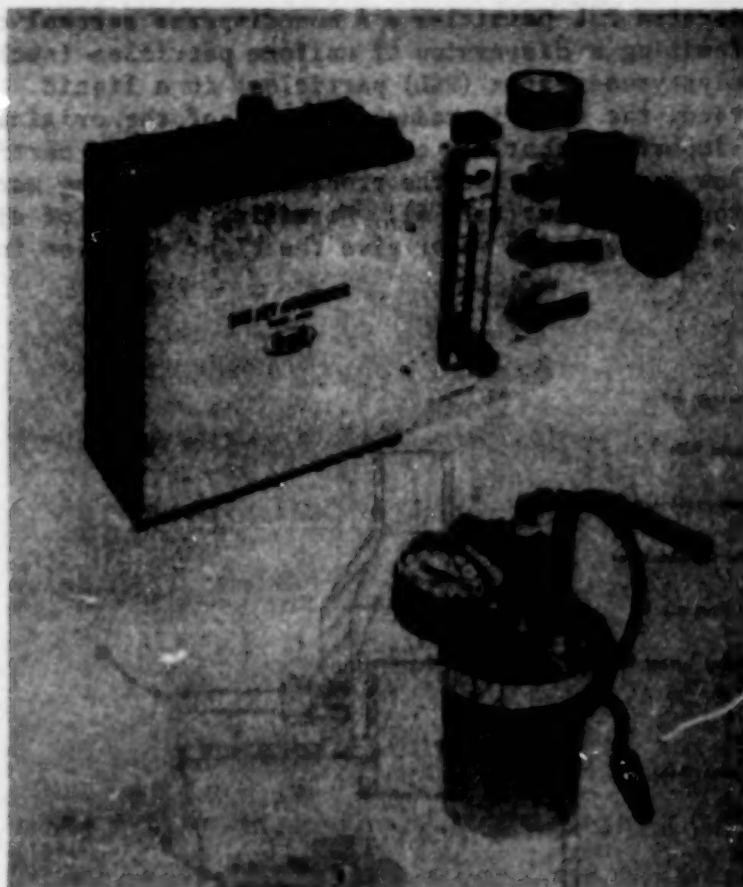
PARTICLE SIZE DISTRIBUTION OF SEEDS GENERATED BY 9302/9306 ATOMIZER

The particle size distribution of the corn oil aerosol generated by the
MOdel 9302 or 9306 is shown below. This size distribution was measured by the
Differential Mobility Analyzer. The operating parameters for the atomizer are
compressed air pressure (input) = 35 psi. Aerosol flow rate = 3 LPM per jet.

```
          TSI DIFFERENTIAL MOBILITY PARTICLE SIZER
          RFT1   CORN OIL PARTICLE SIZING
          AEROSOL FLOW RATE: .3 LPM         MEAS. MODE: 1
          MAXIMUM DIA. MEASURED: .886 UM    START: 00:00:00
          MINIMUM DIA. MEASURED: .017 UM    END: 00:00:00
```

NUMBER CONC VS PARTICLE SIZE
EXP= 4   N.M.= 1
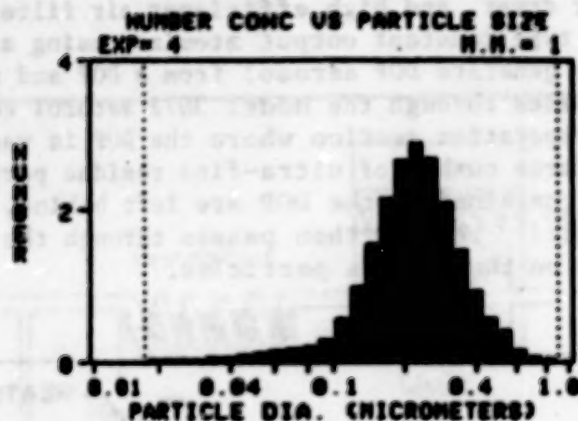
This is the process of evaporating an oil and allowing the vapor to recondense on ultra-fine nuclei particles under controlled conditions. Once the condensation process begins, the particles grow until all the oil vapor is consumed. Thus, if the condensation on the nuclei can be controlled to begin at the same time, all the particles will grow to the same size. This technique is widely used for filter testing (the particle generators are generally called hot DOP generators). Even though the principle is simple and well proven, the need for precise control of vapor feed rate, nuclei feed rate, and other parameters introduces several practical problems. This method is also limited to oil droplets. The advantage of this technique is that the generated aerosol is very monodisperse ($\sigma_g = 1.2$).

TSI markets a system based on this principle which consists of TSI Models 3074, 3075, and 3072. The Model 3074 is an air supply system consisting of a pressure regulator, air dryer, and high efficiency air filter. The Model 3075 is a non-recirculating type constant output atomizer using a syringe pump feed. The atomizer is used to generate DOP aerosol from a DOP and alcohol solution. The DOP aerosol then passes through the Model 3072 aerosol conditioner. It consists of a heated evaporation section where the DOP is vaporized. After the evaporation of DOP, a large number of ultra-fine residue particles made of nonvolatile impurities contained in the DOP are left behind, which subsequently act as condensation nuclei. The air then passes through the cold section where the DOP vapor condenses on the residue particles.
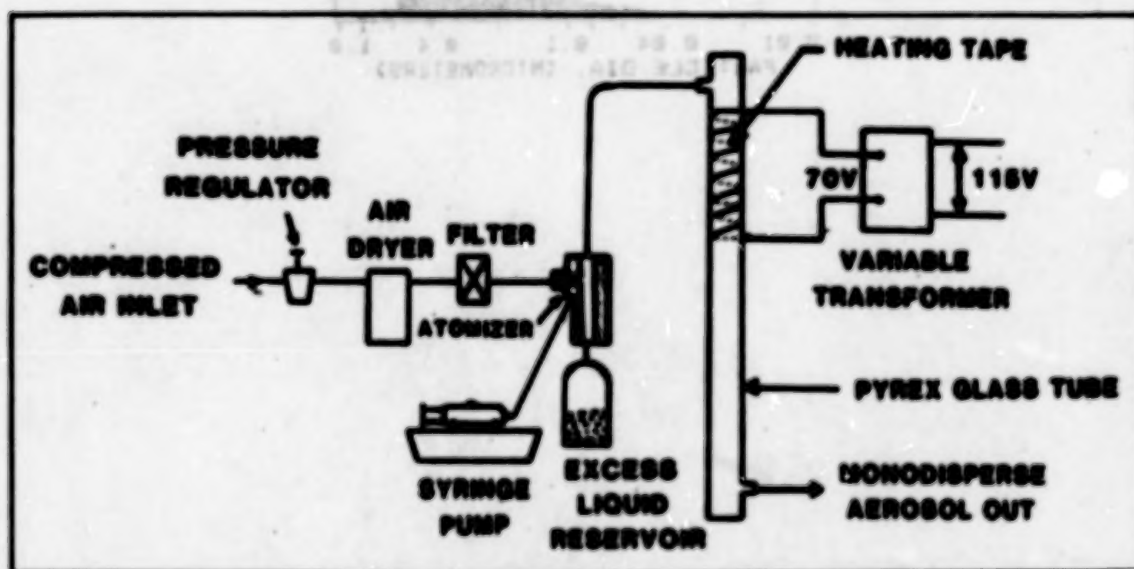
EVAPORATION/CONDENSATION SEEDER USING NaCL NUCLEI

Another type of evaporation/condensation generator is schematically shown below. Even though no standard commercial product is available at this time, such a seeder is available from TSI built on a custom order basis. It consists of an atomizer, a syringe pump, a heating coil and a cooling chamber. NaCl particles generated by the atomizer provide the condensation nuclei, and the DOP introduced by the syringe pump provides the aerosol material. The condensation nuclei and DOP mixture pass through a heating coil, where the DOP is vaporized. The mixture is then cooled in a chamber located immediately after the heating coil. The DOP vapor condenses on the NaCl particles causing the submicron NaCl particles to grow. The particle growth stops when the DOP vapor is consumed. Since the number of nuclei generated by the atomizer is constant, the particle size can be controlled by the DOP feed rate.

The main advantage of such an aerosol generator is that it produces reasonably monodisperse aerosol in large quantity.

Evaporation/Condensation Seeder
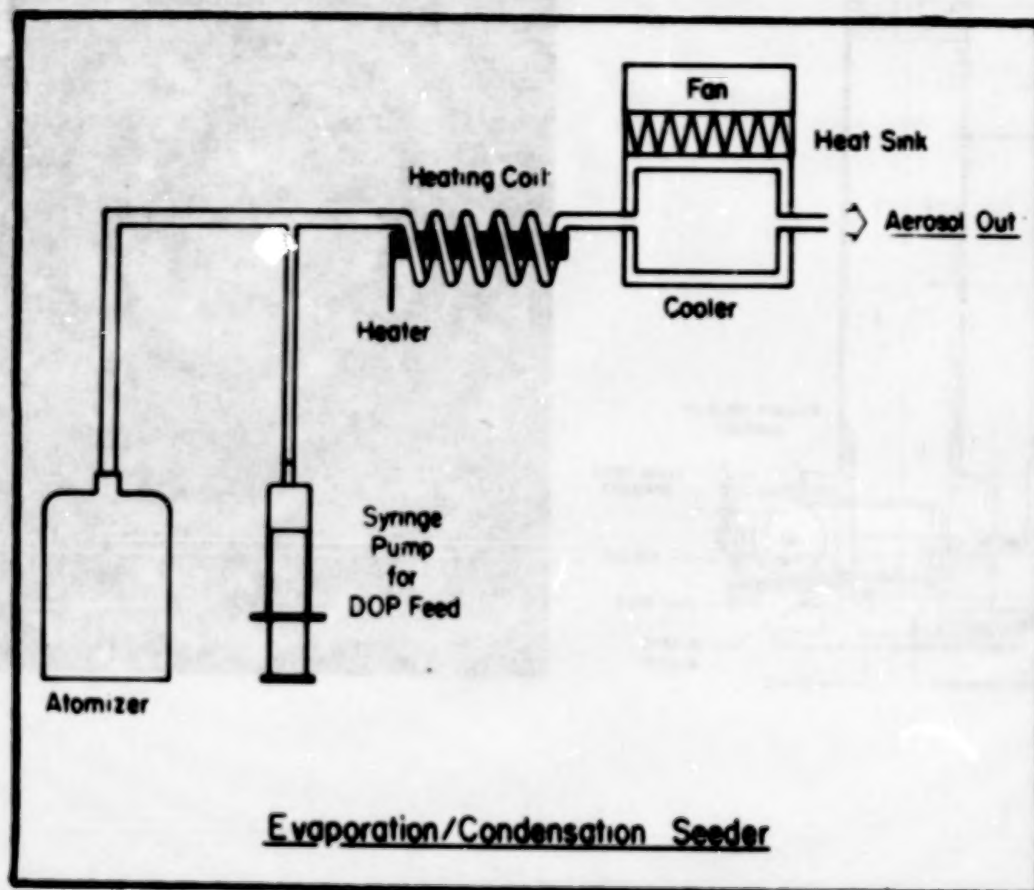
SEEDERS BASED ON THE PRINCIPLE OF DISPERSING SOLID PARTICLES:

MODEL 3400

The Model 3400 fluidized bed aerosol generator shown below is a dust generator designed to disperse any kind of non-sticky powder. The powder to be dispersed is stored in the powder chamber and is constantly fed into a bed of bronze beads by a variable speed bead-chain drive. The powder mixes with the bronze beads and coats them with a single layer of particles. An air stream then strips the particles from the beads and carries the particles with it in the form of an aerosol. By this process, an aerosol consisting of deagglomerated particles is obtained.

The adjacent micrograph shows the titanium dioxide particles dispersed by this seeder. The sample was collected by the electrostatic sampler described earlier.
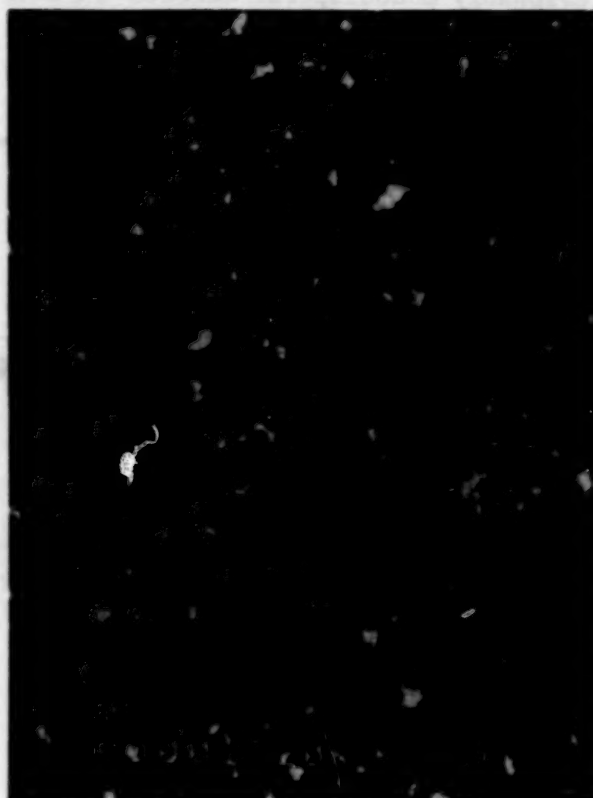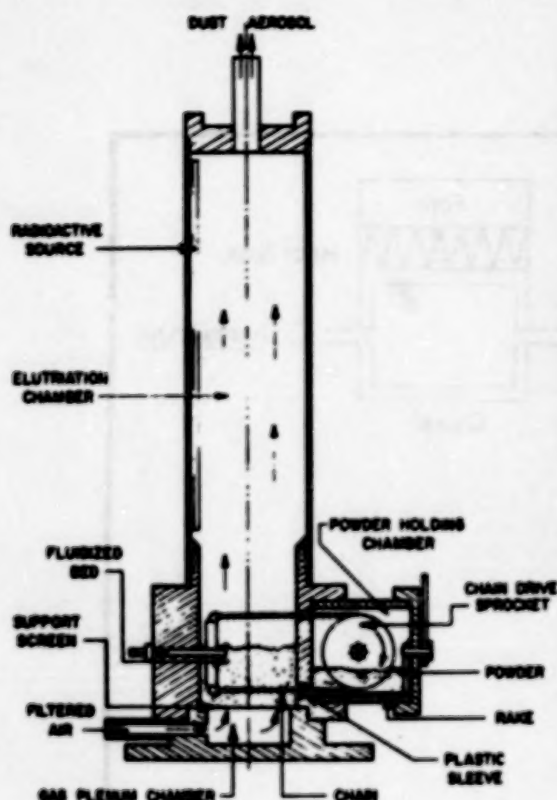
SEEDERS BASED ON THE PRINCIPLE OF DISPERSING SOLID PARTICLES:
MODEL 9310

This dust generator shown below is similar to the Model 3400, but it was designed to disperse much larger amounts of dust. The powder to be dispersed is stored in a powder chamber. The powder is continuously transported from the powder chamber to the bronze bead bed through a rotating spring. A stream of air strips the powder material from the bronze beads and carries the particles with it. As in the Model 3400, the aerosol output is constant and nearly complete deagglomeration is achieved.

MIXER

AEROSOL OUT

IMPACTOR

POWDER RESERVOIR

POWDER FEED

BRASS BEADS

MOTOR (C.S.)

COMPRESSED
AIR IN

MOTOR (C.S.)

MOTOR (V.S.)

DRY POWDER DISPERSER: MODEL 3410

The Dry Powder Disperser is a power dispersion system using mechanical abrasion from a bulk of densely packed powder by a rotating brush. The bulk powder is contained in a metallic cylinder and is continuously pushed towards the rotating brush by a piston moving at a specified velocity. Particles are broken out of the top surface of the bulk and are swept away by air passing through the brush. The seeding rate can be varied by varying the piston speed. When the cylinder is empty, it can be conveniently replaced by a filled one and the seeding can be resumed in a few minutes. To fill a cylinder, the powder is poured into the cylinder and compressed manually to give constant bulk density to the powder compound. Any dry and non-sticky powder can be dispersed by the Model 3410.

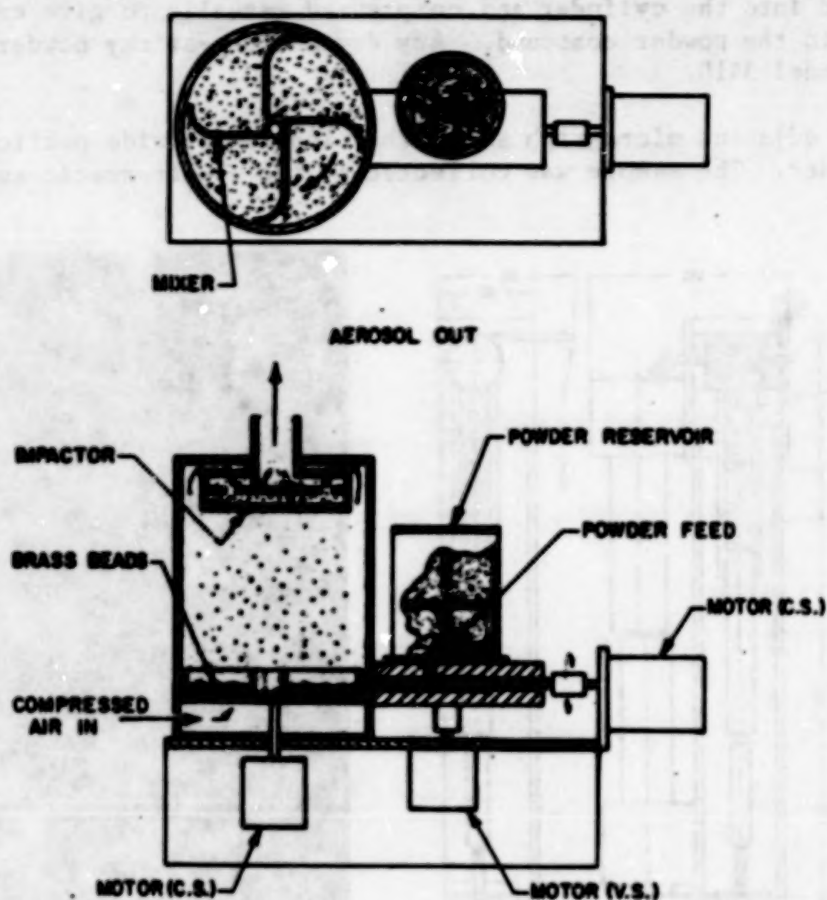The adjacent micrograph shows the titanium dioxide particles dispersed by this seeder. The sample was collected by the electrostatic sampler described earlier.
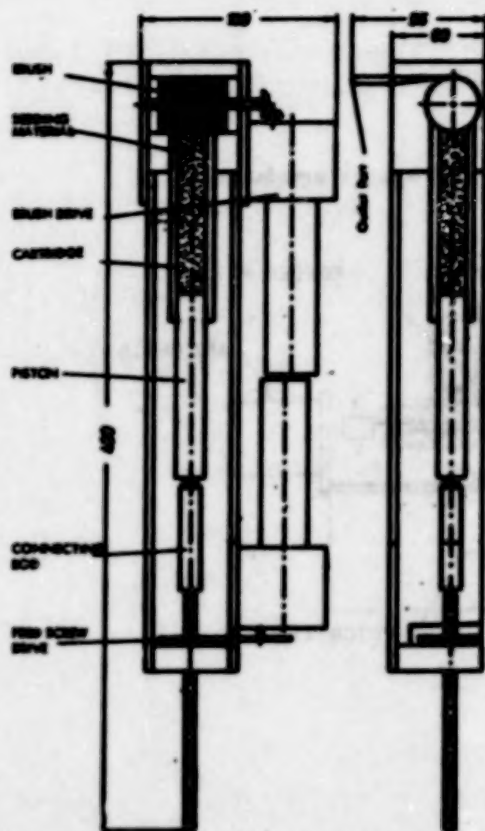
REFERENCES

1.   Adrian, R.J. and W.L. Earley; "Evaluation of LDV Performance Using Mie
     Scattering Theory", in Proc. of Minnesota Symposium on Laser Anemometry,
     University of Minnesota, Dept. of Conferences, Minneapolis, 426-54 (1976).

2.   Agarwal, J.K. and P. Keady; "Theoretical Calculation and Experimental
     Observation of Laser Velocimeter Signal Quality", TSI Quarterly,
     February-March (1980).

3.   Agarwal, J.K. and E.M. Johnson; "Generating Aerosol for Laser Velocimeter
     Seeding", TSI Quarterly, July-September (1981).

4.   Remiarz, R.J., J.K. Agarwal, F.R. Quant, and G.J. Sem, "Aerosols in the
     Mining and Industrial Work Environments - Volume 3", edited by V.A. Marple
     and B.Y.H. Liu, Ann Arbor Science (1983).

5.   Keady, P., F.R. Quant, and G.J. Sem; "Differential Mobility Particle Sizer:
     A New Instrument for High-Resolution Aerosol Size Distribution Measurement
     Below 1 µm", TSI Quarterly, April-June (1983).

6.   Liu, B.Y.H., K.T. Whitby, and H.H.S. Yu; "Electrostatic Aerosol Sampler for
     Light and Electron Microscopy", The Review of Scientific Instruments, Vol.
     38, No. 1, pp. 101-102 (1967).

PARTICLE PHASE FUNCTION MEASUREMENTS BY A

NEW FIBER ARRAY NEPHELOMETER: FAN I

W. M. Farmer, Edward J. Burlbaw, and A. Deepak*
Science and Technology Corporation
Las Cruces, New Mexico

ABSTRACT

A fiber array polar nephelometer of advanced design, the FAN I is capable of in-situ phase function measurements of scattered light from man-made or natural atmospheric particles. The scattered light is measured at 100 different angles throughout 360 degrees, thus providing a potential measurement of the asymmetry of irregularly shaped particles. Phase functions can be measured at 10 to 100 Hz rates and the range of measurable single particle sizes is from 5μm to as large as 8mm. For particles smaller than 5μm the ensemble average can be measured. The FAN I is microprocessor controlled and the data may be stored on floppy disk or printed out in tabular and/or graphical form. The optical head may be separated from the computer system for operation in field or adverse conditions.

Examples of laboratory measured scattering phase functions obtained with the FAN I for spherical particles is given to illustrate its measurement capabilities.

I. INTRODUCTION

The FAN I polar nephelometer is an atmospheric particle characterization system of advanced design. It is designed to measure, in situ, light scattered by atmospheric particles such as snow crystals and was initially developed for that purpose. The scattered light is measured at 100 different locations around a full 360 degree scattering direction at sample rates which can be set between 10 and 100 Hz. In its most sensitive mode of operation, the instrument can respond to single particles as small as 5μm diameter spheres or in its least sensitive mode it can respond to particles having maximum dimensions of approximately 8mm. The FAN I is controlled by a microprocessor, and the acquired data is permanently stored on floppy disks. Hardcopy of the data is provided by a computer printer with graphics capability. Software is supplied with the system for setup, calibration, and data display. The optical head can be separated from the computer system by 30 m or more for operation in adverse environments.

A description of the instrument is presented in Section II. In Section III is a comparison of measurements with theoretical calculations for glass beads. Section IV contains the conclusion.

II. FAN I DESCRIPTION

A. Optical System

A schematic of the optical head and associated electronics is provided in Figure 1. A corresponding photograph of the system with its protective covers removed is shown in Figure 2. A 5mW HeNe laser is the light source for the instrument. The system operator can adjust the output beam size from the laser's nominal 0.8mm beam size (which would be used for maximum instrument sensitivity and forward scatter angular resolution) to either 2.4mm or 8.0mm beam diameter [as measured to the exp(-2) intensity contour] using 3X or 10X beam expanders which screw directly into the output end of the laser. After leaving the beam expander, the output laser power is sampled during each sampling cycle for the phase function. This measurement will allow the system operator to make absolute radiometric scattered light measurements should he so choose. After leaving the input beam sampling system, the laser beam is transmitted across the 30.5cm diameter in situ sampling section. The beam is then reflected into a detection system which can be used to measure transmission across the sampling section. Scattered light is collected in a plane centered about the beam in which 100 gradient index lenses have been placed in a circle of constant radius. The lenses have fields of view of approximately 1 degree. Beginning at the transmission detector, which is defined as the position of zero scatter angle, and proceeding counterclockwise, the first collecting lens is placed at a 1.5 degree scatter angle, followed by 11 lenses spaced at 1.5 degree intervals up to 18 degrees. Next, lenses are placed at 5 degree intervals from 20 to 165 degrees and then at 1.5 degree intervals from 167.5 to 176.5 degrees. Using this arrangement, increased resolution is obtained in the forward and backscatter directions. The lens array between 180 and 360 degrees follows that for 0 to 180 degrees. (See Figure 3 for forward scatter positions.)

Scattered light collected by the gradient index lenses is transmitted to the Output Array Block by optical fibers as indicated in Figure 1. The scattered light outputs from the fibers are imaged to a 1024 element detector array. Only every third detector in the array is used in the FAN I. Because the detector elements must be precisely aligned with the elements of the output array block, the array is mounted on a two-dimensional micropositioner that is used to initially align the array during construction. The entire detection system is housed in a self-contained box which is shock-mounted in the main optics housing. Also included in the main housing is the instrument control and signal processing electronics and a data buffer computer memory as well as the laser power supply. Besides making this part of the FAN I capable of operating in a stand-alone mode, the electronics provide sufficient heating for the optical head during cold weather operation.

B. Signal Processing Electronics

The signal processing electronics begins at the detector array. The detector array is a two-dimensional serially scanned optical sensor array consisting of 1024 silicon photodiodes in a 32 x 32 matrix. The detector elements are located on 100µm centers. The detector element

outputs are scanned at a nominal rate of between 10 and 100 Hz which is set by the system operator. During the time between detector scans, the outputs from the detectors are capacitively stored thus effectively integrating the signal between scans. The scan rate therefore sets the integration time for the detectors. Signal integration is used to achieve high signal-to-noise ratios from low levels of scattered light. The detector elements have solid state reliability for rugged field applications and the elements have fast recovery times after reaching saturation.

The detector array and integrating electronics are controlled by a Z80 microprocessor. The microprocessor is used to control the diode sample rate and the 'frame rate' or the rate at which the array is periodically sampled. Scattering conditions and instrument setup parameters are controlled from a computer terminal by the system operator. As the detector scan begins, the detector elements are sampled serially into a 12 bit analog to digital converter. The first element sampled corresponds to the scatter magnitude at 90 degrees. A threshold comparator circuit is used to determine if sufficient signal exists from a particular scan to save the data. The signal level threshold is set by the system operator and can be one of 256 different levels. If the signal output at 90 degrees is below the designated threshold level, the array output is dumped and the detector array is reset to acquire data. When the required threshold is exceeded, the detector outputs are stored in a buffer memory configured on the Z80 microprocessor. If the data acquisition system is ready to receive data, the buffer memory immediately transmits the acquired scan to the data acquisition memory which is much larger than the Z80 memory. The data acquisition memory has been given software instructions on how to accumulate the data and store the data in floppy disk files for post experiment analysis. Should the data acquisition memory be busy at the time the buffer memory has acquired a scan, the buffer memory can acquire as many as 128 scans of data before it becomes full and must be unloaded before data acquisition can continue. The buffer memory thus allows considerable flexibility in how the data are acquired and stored, and allows the user many options in system operation that would not be possible otherwise.

C. Data Acquisition System

The data acquisition system supplied with the FAN I polar nephelometer consists of a computer terminal, a computer printer with graphics capability, and a microcomputer having 256K of RAM, and two 8 inch diameter floppy disk drives. The computer memory can be expanded to 1Mb. A 12 slot card cage is provided with the computer to allow ease of memory expansion and the inclusion of specialized hardware should the need arise. 'C' software is used in the data reduction routines. It is a language particularly suited to the polar nephelometer since one of its major uses is in the manipulation of data arrays.

Supplied with the data acquisition system is basic data reduction software. The basic function of the data reduction software is to average the recorded scans according to the user defined groupings or ensembles and display the phase function data as plots and/or listings.

Calibration and weighting factors may be applied to the raw data. Provisions are made for creating averaged background scans and subtracting them from the raw data. Every scan may be reduced individually or ensembles can be created which reduce as much as the entire data file onto one plot. Ensemble averaging is done on an angle by angle basis very much like a multichannel analyzer. In principle, the multiple scan ensemble reduction represents a second integration of the data. The first integration occurs at the signal detector and represents the integration of the scattered light as a particle passes through the incident beam. This integration should represent a single orientation of an asymmetric particle. The second integration should represent an integration over numerous particle orientations assuming that the particles are randomly oriented as they pass through the incident laser beam. The data in the histogram are displayed in a typical phase function format where relative histogram magnitudes are displayed as a function of angle. With the FAN I, however, it must be recalled that the full 360 degree scatter angle is recorded. It should be expected that for asymmetric particles, the 0 to 180 phase function will not be congruent with the 360 to 180 degree phase function. Differences in the two phase functions should reflect particle asymmetry. Therefore, the two halves of the full 360 degree phase function are displayed separately for the user's convenience.

III. PERFORMANCE

In order to check the performance of the FAN I, spherical particles of known refractive index and diameter (range) were dropped through the scattering volume. These results were then compared with Mie scattering calculation results for single particles. Figures 4, 5, and 6 show the results for 58, 193, and 650μm beads and the theoretical calculations. The scale factor of the calculations has been adjusted to make them coincide with the measurements. The difference in scattering between the 0 to 180 and 360 to 180 measurements can be attributed to the asymmetry and imperfections of the beads, within the limit of the measurement errors. Figure 7 shows a slightly different representation of the same data as in Figure 4 for the 58μm beads. Here the data has been plotted with equal spacing between the data points which emphasizes the forward and backward scattering resolution.

IV. CONCLUSIONS

The FAN I is a state-of-the-art instrument capable of measuring the relative scattering intensities throughout 360 degrees. We have shown the results of measurements for spherical (or nearly so) particles and have compared them to Mie calculations and shown good agreement.

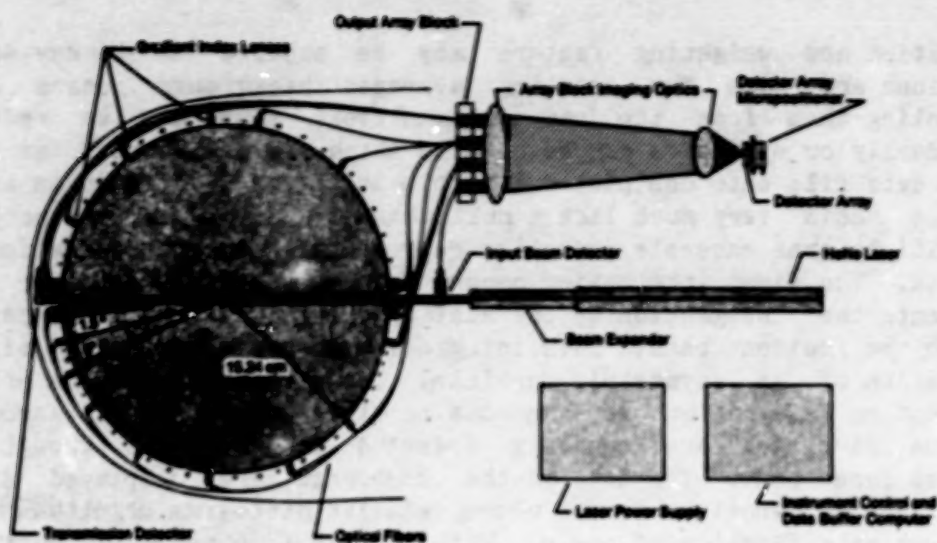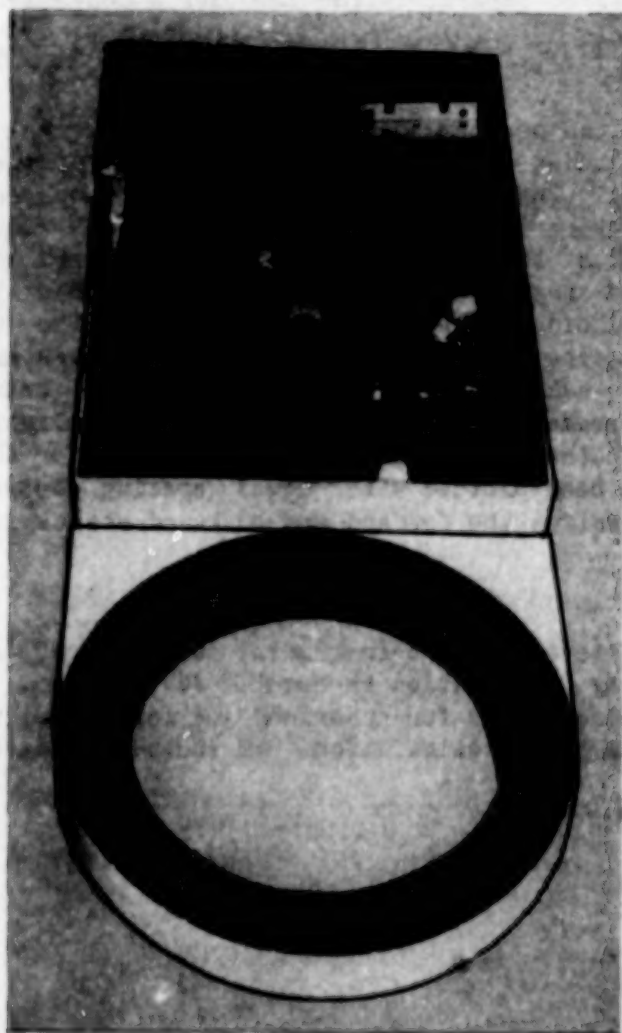**Figure 1. Schematic of optical arrangement of FAN I nephelometer.**

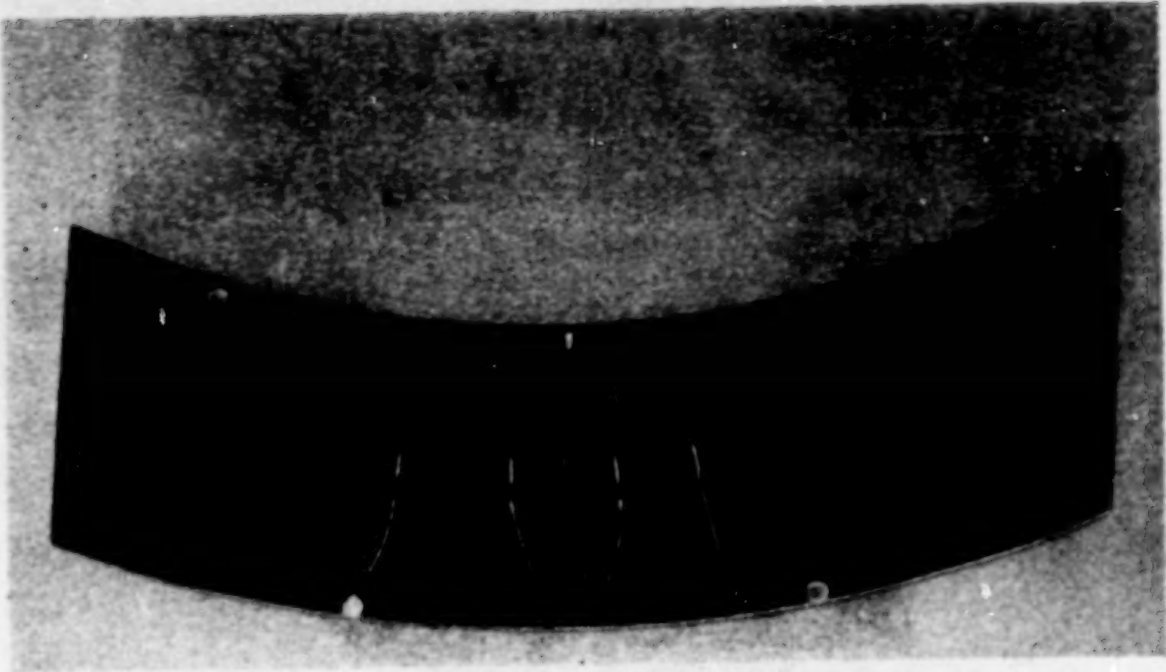
Figure 2. Photograph of FAN I nephelometer optical system.

Figure 3. Forward scattering lens positions for FAN I nephelometer.

A TECHNIQUE TO MEASURE THE SIZE OF PARTICLES
IN LASER DOPPLER VELOCIMETRY APPLICATIONS*

C. F. Hess
Spectron Development Laboratories, Inc.
Costa Mesa, California

245

ABSTRACT

A method to measure the size of particles in LDV applications is discussed. Since in LDV the velocity of the flow is associated with the velocity of particles to establish how well they follow the flow, in the present method the interferometric probe volume is surrounded by a larger beam of different polarization or wavelength. The particle size is then measured from the absolute intensity scattered from the large beam by particles crossing the fringes. Experiments using polystyrene particles between 1.1 and 3.3 μm and larger glass beads are reported. It is shown that the method has an excellent size resolution and its accuracy is better than 10% for the particle size studied.

NOMENCLATURE

b_0	waist radius
d	particle diameter
G	gain function of instrument
I	intensity
K	scattering cross-section
n	particle relative index of refraction
P	parallel polarization
S	perpendicular
x,y,z	coordinates
V	particle visibility

Greek Symbols

$a = \pi d/\lambda$	size parameter
γ	intersection angle of small laser beams
θ	angle between laser beam and axis of collecting lens
μ	laser wavelength
Ω	solid angle of collection

Subscripts

1   **refers to small beams**

2   **refers to large beam**

3   **center of beam**

INTRODUCTION

A technique to measure the size of particles in laser Doppler velocimetry (LDV) systems is described here. In typical LDV applications the velocity of the flow is inferred from the measurement of the velocity of very small particles seeded in the fluid. These particles are chosen to be small (0.5 μm to 1 μm) and when possible neutrally bouyant to insure that their velocity is the same as the velocity of the flow. There are, however, many situations of interest where large particles might be generated, and since they don't necessarily follow the flow they will introduce an error in the velocity measurement. Examples of these situations are flows with very large accelerations, sooting environments, wind tunnels with large amounts of oil droplets, and in general, two phase flows where it is of interest to distinguish the velocity of the two phases. Many LDV electronic processors have built-in saturation circuits to reject signals with excessive amplitudes. This, however, will not prevent large particles from being measured. Since the intensity profile of the laser beams is typically Gaussian, large particles moving through the edge of the beams will scatter light with an acceptable signal level. Therefore, the saturation circuits mentioned above will only accept large particles when they cross through the edge of the Gaussian laser beams. This will not eliminate velocity bias but it might introduce additional errors since the large particles are detected over a different volume which could have a different velocity. The method discussed here eliminates the above limitation and provides for a mechanism to obtain the size distribution of the measured particles. In its simplest form this method can be used to produce a velocity histogram of small particles and one of large particles where the separation can be arbitrarily selected.

In this method two small laser beams of a given wavelength and polarization are crossed in the middle of a large laser beam of the same wavelength but normal polarization. The two small beams interfere where they cross, and this interference pattern identifies the center of the large beam. This defines a region of almost uniform intensity within the large beam where the light scattered by the individual particles can be related to their size. Only particles crossing through the interference pattern are measured and their velocity is obtained from the Doppler signal. Their size is obtained from the absolute scattered light since the incident intensity is known.

The method which is referred to as Polarization Intensity Maximum (PIMAX) was described in Reference (1) where it was used to measure the size and velocity of droplets in a spray. For LDV applications it is necessary to show that the PIMAX technique can also discriminate the size of particles down to a

fraction of a micron. Numerical and experimental studies were conducted to demonstrate such ability and they are reported here.

The method could also be implemented in two-color LDV systems. Here two small beams of one color cross in the middle of two crossing large beams of another color forming two fringe patterns perpendicular to each other. As before, the small beams identify the center of the large beams from which the size information is obtained.

The model presented here is for spherical particles with a diameter of the same order as the wavelength of the incident beams. Therefore, the full Mie solution (2) is necessary to analyze the scattering patterns. Results are presented for flows seeded with known size particles.

DESCRIPTION OF OPTICAL TECHNIQUE

The method discussed here bases the size measurement on the absolute intensity scattered by the particle crossing the probe volume, and the velocity measurement on the classical Doppler signal. A similar method could be described for a single beam velocimeter but the approach used here is for LDV. In situ single particle counters are limited because of the nonuniform profile (typically Gaussian) of laser beams. Under this condition a particle crossing the middle of the beam will scatter more light than a similar particle crossing through the edge. Therefore, the relationship between size and scattered light is not unique.

To circumvent this problem, two small beams of a given wavelength or polarization are crossed in the middle of a larger beam of different wavelength or polarization identifying a region of almost uniform intensity and, therefore, removing the Gaussian ambiguity. The crossing beams will interfere and a fringe pattern will be formed in the middle of the large beam (Figure 1). Signals exhibiting a sinusoidal modulation correspond to particles that cross the fringe pattern and therefore the middle of the large beam. Both size and velocity of individual particles can be extracted from this signal. The method and results reported here correspond to the two-polarization (PIMAX) system.

If we refer to the small beam as 1 and the large beam as 2, the intensity profiles in the probe volume can be separated by their polarization and given by:

$$I_1 = 2I_{o_1} \exp\left(\frac{-2}{b_{o_1}^2}\right)[x^2+y^2+z^2\gamma^2/4] \cdot \left[\cosh\left(\frac{2x\gamma y}{b_{o_1}^2}\right)+\cos\frac{4\pi x \sin\left(\frac{\gamma}{2}\right)}{\lambda}\right] \quad (1)$$

and

$$I_2 = I_{o_2} \exp\left[-\frac{2}{b_{o_2}^2}(x^2+y^2)\right] \quad (2)$$

248

where I_o is the center intensity, γ is the intersection angle, b_o the waist radius, λ the laser wavelength, and x,y,z the coordinates. The z dependence of the large beam is negligible. If we also assume that $\frac{z\gamma}{2} = 0$ (which is an excellent assumption since a pinhole in the receiver will limit the value of z), the intensity scattered by a spherical particle is given by:

$$I_{s_1} = 2I_{o_1} K_1(d,n,\theta,\Omega,\lambda,,P)G_1 \exp\left[\left(-\frac{2}{b_{o_1}^2}\right)(x^2+y^2)\right]\left[1 + \cos 2\frac{\pi\gamma x}{\lambda} \cdot V\right] \quad (3)$$

and

$$I_{s_2} = I_{o_2} K_2(d,n,\theta,\Omega,\lambda,S)G_2 \exp\left[\left(-\frac{2}{b_{o_1}^2}\right)(x^2+y^2)\right] \quad (4)$$

where K is the scattering cross-section as obtained by the Lorentz-Mie theory (3). It is a function of a complex size function d, the index of refraction n, the collection angle θ, the solid angle of collection Ω, the wavelength λ and the polarization. Here it is assumed that the small beams have a polarization parallel to the scattering plane while the polarization of the big beam is perpendicular. G is the gain function of the instrument, and V is the visibility of the measured particle.

It should be pointed out that the visibility of the particle is not an adequate parameter to obtain the size, given that many of the particles of interest are below 3 μm, and in general, many of the particles will be submicron.

Equation (3) gives the signal response of the laser Doppler velocimeter which will establish the detectability of the signal. The processing logic will be the following: signals exhibiting sinusoidal modulation will have crossed the fringe pattern which is located in the middle of the large beam. Therefore, signals validated by the laser velocimeter correspond to particles crossing the middle of the large beam and their scattered light can be inverted to size since the Gaussian ambiguity is removed. In Equation (4) the exponent can therefore be approximated as unity and we get

$$I_{s_2} = I_{o_2} K_2 G_2 \quad (5)$$

The K_2 coefficients will be obtained from Lorentz-Mie scattering using a modified version of the numerical program developed by Dave (4). Equation (5) can then be solved for the particle size which is contained in K_2 $(d,n,\theta,\Omega,\lambda,S)$.

NUMERICAL COMPUTATIONS OF THE SCATTERING FUNCTIONS

To obtain the particle diameter, d, it is necessary to know the functional relationship of K_2 $(d,n,\theta,\Omega,\lambda,S)$ as given by Equation (4). This function can be quite complex and it is necessary to find the conditions under which the ambiguities, if any, are within tolerable error margins. The computations were made in a PDP11 computer. Parametric studies were conducted to establish optimum experimental conditions. These parameters include the angle of collection (θ), the solid angle of collection (Ω), and index of refraction $(n_1 - Im(n_2))$. The results show that the best optical characteristics are near forward scattering angles of collection ($\theta < 5°$).

Since the index of refraction of the particles present in LDV applications may be quite different, it is important to establish conditions which are less sensitive to these variations. Both real (n_1) and imaginary (n_2) parts of the refractive indices were varied to check the sensitivity of these parameters. Figures 2 and 3 show the scattered intensity as a function of the particle size parameter α for different values of n_1 and n_2 at different scattered angles.

It can be concluded from these calculations that shallow angles of collection ($< 5°$) offer the most favorable conditions.

The calibration of the system was conducted with known size polystyrene particles, therefore the scattering function corresponding to these particles was also evaluated. The results are shown on Figure 4 and, as before, the shallow angles offer the best conditions.

APPARATUS AND EXPERIMENTAL FACILITY

Figure 5 shows a schematic of the optical system used in the experiments. The system consists of a transmitter and a receiver positioned 5° off axis. The transmitter uses a 7 mW He-Ne laser. The laser beam is focused on a diffraction grating (DG) by lens L_1, and the three major orders are collimated by lens L_2. The zero order beam goes through a beam compressor formed by L_4 and L_5 and its polarization is rotated by PR. Lens L_3 focuses and crosses all three beams to form a probe volume like the one shown in Figure 1. The light scattered by particles crossing the probe volume is collected by L_6 and focused onto the photomultipliers by L_7. A cube polarizer (CP) efficiently divides the scattered light into its two polarization components. In addition, a polarization filter was placed in front of the PMT which looks at the big beam (BPMT) to reduce the crosstalk between the two polarizations.

The size of the probe volume was typically 600 μm for the large beam and 86 μm for the small ones. The fringe spacing was 10.7 μm. To reduce the size of the probe volume we used a slit in front of the BPMT. The width of this slit was typically equal to the diameter of the small probe volume (100 μm) and its length was about four times longer to avoid signal masking. Thus, the probe volume was about 10^{-5} cm^{-3} which in general is quite adequate for LDV applications.

The outputs of the photomultipliers are input to an electronic breadboard which measures the Doppler period and the peak intensity of each scattering center. A description of the electronics can be found in Reference (5).

THE PARTICLE GENERATOR

The particle size of interest is that corresponding to typical LDV applications. We used polystyrene particles of 1.1 µm, 1.7 µm, 2.7 µm and 3.3 µm in diameter. These are latex particles made by Dow Chemicals of good size uniformity and of spherical shape. The particles come suspended in water with a concentration of 10% by weight. A few droplets of the particle suspension were introduced and diluted in a nebulizer. An air compressor provided the air flow to produce a mist carrying the polystyrene particles out of the nebulizer and into a heated chamber. There the water was evaporated and the particles were sprayed over the probe volume.

Different size particles could be introduced into the nebulizer thus producing monodisperse, bimodal, trimodal and quadrumodal distributions. The compressor was also used to trap the particles after they passed through the probe volume to avoid contaminating the surrounding environment. Figure 6 shows a photograph of the optics and the particle generator.

An alternative apparatus was also constructed to introduce glass beads into the probe volume. The glass beads come in dry containers and their size distribution was reasonably broad. A test tube with a stopper was used to contain the glass beads. Two glass tubes protruded through the stopper and flex tubing was connected at the end of each glass tube. One of the flex tubes was connected to a nitrogen tank via a pressure regulator and a flow meter. The other flex tube discharged the glass beads into the probe volume. The flow rate of nitrogen could be regulated very carefully and thus the flow velocity at the exit of the flexible tube could be reproduced.

EXPERIMENTAL RESULTS

The system was calibrated and tested with polystyrene latex particles of uniform and known size distributions. The size and uniformity of the particles were checked with a microscope and agreed with the manufacturer's specifications.

Size and velocity distributions of the polystyrene particles flowing out of the heating chamber were obtained with the optical system described above. Figure 7a shows the distributions corresponding to 1.74 µm and 3.3 µm. The calibration high voltage of 500V was established based on the 1.74 µm. The arrow with the 3.3 µm mark indicates the value predicted by the Mie calculations. In Figure 7b an intermediate size of 2.7 µm was added and the calibration high voltage was changed to 550V to decrease the size range. As before the calibration was based on the 1.74 µm, and the arrows point at the numerically predicted values. The 3.3 µm was measured very accurately, but the measurement of the 2.7 µm particles was off by two bins. This error was consistent and very repeatable. We attribute it to the oscillations found in the scattering function. Figure 7c shows the distributions corresponding to four different latex particles. As before the calibration was obtained with

the 1.74 μm particles. The calibration high voltage is 550V. It must be pointed out that the size histograms are divided into 53 equal size bins. Therefore, distributions on the large diameter end will appear broader than those in the small diameter end.

These results indicate that the technique and instrument can accurately discriminate the particles by their size in LDV applications. Unfortunately, since all the particles are rather small and the flow velocity is also small and constant, all the particles moved at about the same velocity. Therefore, no velocity/size discrimination could be established. To illustrate this last point we used very large glass beads which would not follow the flow. Two different size classes were simultaneously introduced into the test tube and entrained into a constant nitrogen flow. These particles were sprayed over the probe volume and their size and velocity histograms are shown on Figure 8. Notice the bimodal size distribution and the corresponding bimodal velocity distribution. Although not obvious from this figure the small particles are moving faster than the big ones. This is better illustrated in Figure 9 which shows a velocity/size distribution of the entrained small and large glass beads. It can be deduced that the small glass beads are moving at about 13 m/s while the large ones are moving at about 8 m/s.

This particle size range is not expected in LDV applications but the experiment illustrates the kind of error that can be incurred in the flow velocity measurement if no consideration is given to the particle size.

An aspect of the PIMAX technique that needs to be considered is the crosstalk between the two polarizations. To establish this crosstalk a series of tests were conducted. First, the polarization ratio of the transmitted laser beams was measured with and without particle extinction. To produce a substantial particle interference a fuel spray was used to attenuate the laser beam by 10%. Very little change in the polarization ratio was measured which is of no surprise since the light scattered in the forward direction carries the same polarization as the incident radiation. A second set of tests was also conducted. Monodisperse droplets produced by a Berglund-Liu generator scattered light which could be analyzed by the receiving optics. One PMT measured the S-polarized light while the other measured the P-polarized light. We blocked the large beam which is S-polarized and illuminated the particles with the small P-polarized beams. The scattered light was measured in the PMT intended for the S-polarized light. The crosstalk was about 4% at large (20°) angles and smaller at shallow angles. This crosstalk could be virtually eliminated by placing a polarizing filter in front of the PMT. It should be noted that the intensity into the small and large beams may not necessarily be the same and, therefore, the crosstalk will be proportional to the intensity ratio. For the small particles of interest in LDV and at shallow angles of collection this crosstalk is negligible.

Obviously the two-color system (IMAX) is not subject to this crosstalk. In general, it is easier to separate the different colors of the scattered light than it is to separate the different polarizations. Yet budget constraints may impose the use of single color lasers in which case PIMAX is a viable technique.

CONCLUSIONS

A method has been presented and results discussed to measure the size of particles in LDV applications. The accuracy and resolution of the method were illustrated by measuring polystyrene particles between 1.1 μm and 3.3 μm in diameter. The effect of crosstalk between the two polarizations was measured and established to be very small.

It was shown, using large glass beads, that different size particles move at different velocities and, therefore, the velocity of the flow cannot be established from the particle velocity unless consideration to the particle size is given.

ACKNOWLEDGEMENTS

REFERENCES

1. Hess, C. F., "Spray Characterization with a Nonintrusive Technique Using Absolute Scattered Light," Optical Engineering, Vol. 23, No. 5 (1984).

2. Mie, G., "Beiträge zu optik trüber Medien; Speziell Koloidaller Metallösungen," Ann. Physik, 25, 377 (1908).

3. van de Hulst, H. C., "Light Scattering by Small Particles," Wiley, New York, 1962, Chapter 9.

4. Dave, T. V., "Subroutine for computing the parameters of the electro-magentic radiation scattered by a sphere," IBM Scientific Center, Report No. 320-3237 (1968).

5. Hess, C. P. "Nonintrusive optical single-particle counter for measuring the size and velocity of droplets in a spray," Applied Optics, Vol. 23, No. 23 (1984).
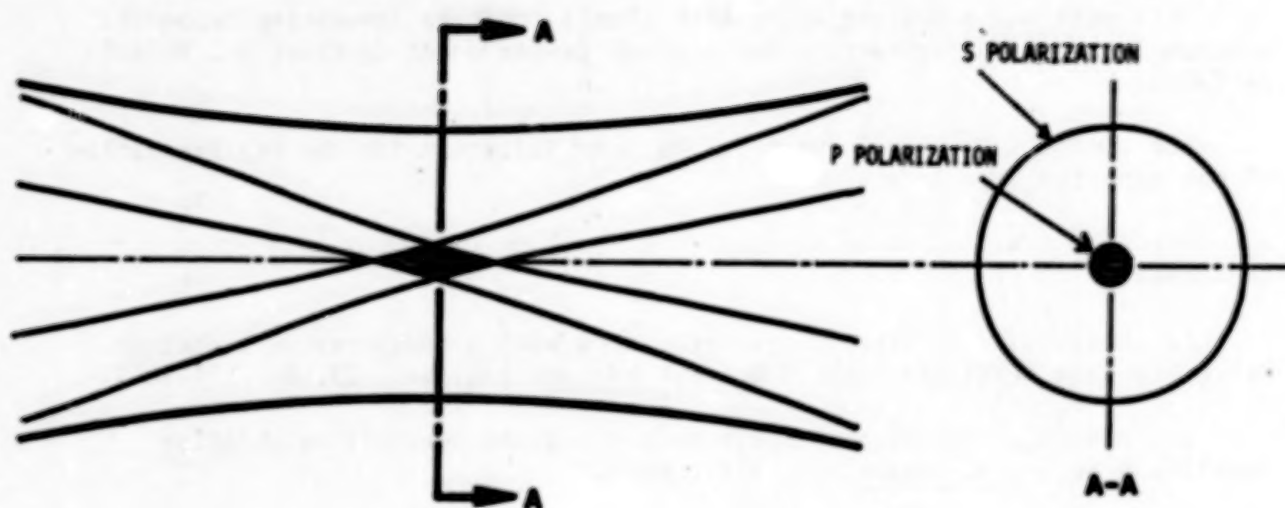
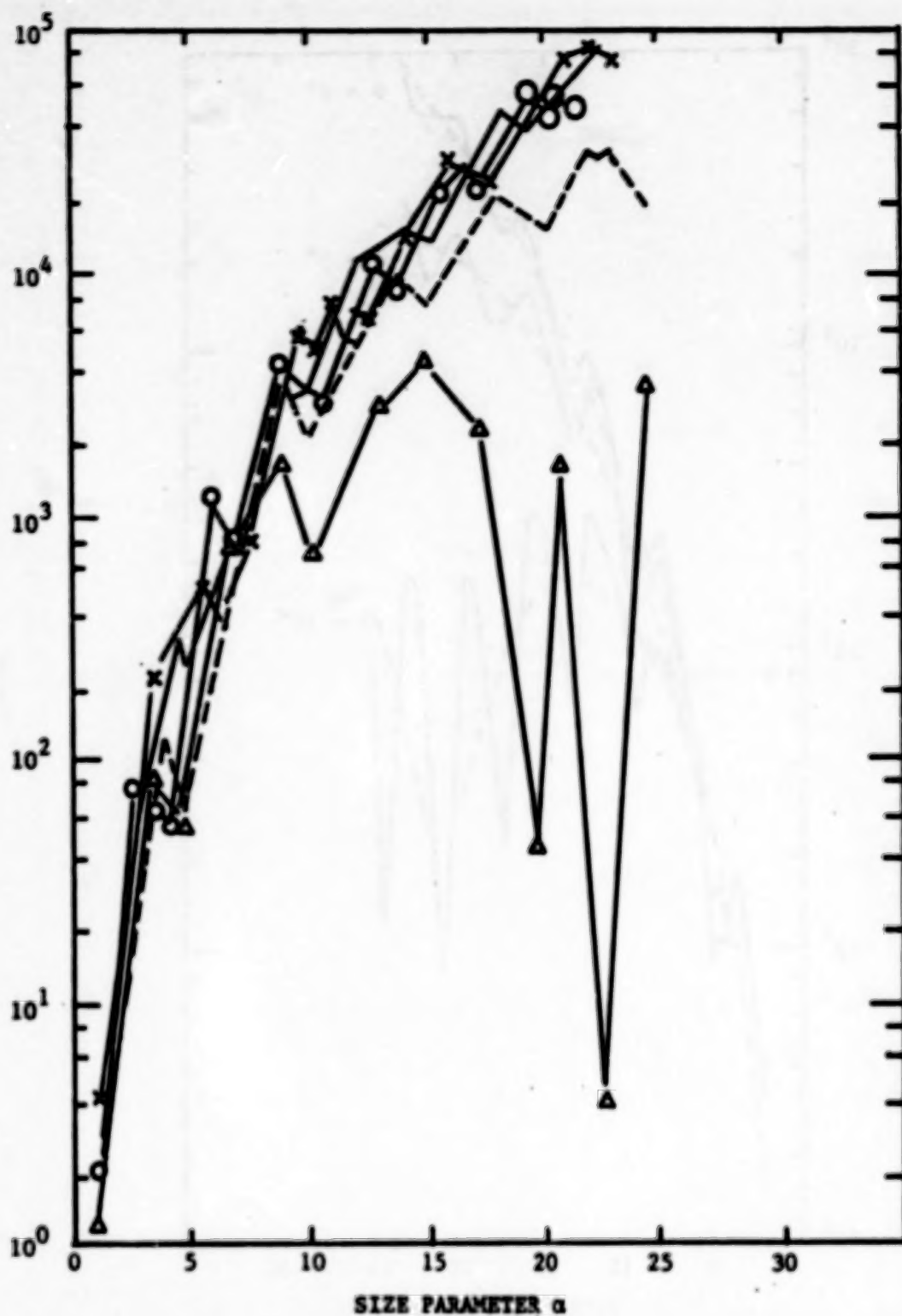Figure 1. Probe volume of two polarization PIMAX technique.

Figure 2. Perpendicularly polarized scattered light intensity as a function of the size parameter α

$\theta = 0°$: (x-x-x ($\tilde{n} = 1.56 - 12.9 \times 10^{-7}$), ———
($\tilde{n} = 1.66 - 12.9 \times 10^{-7}$), 0 - 0 - 0
($\tilde{n} = 1.96 - 12.9 \times 10^{-7}$) $\theta = 5°$: (----- $\tilde{n} = 1.66$),
$\theta = 10°$: ($\Delta - \Delta - \Delta$ $\tilde{n} = 1.66$)
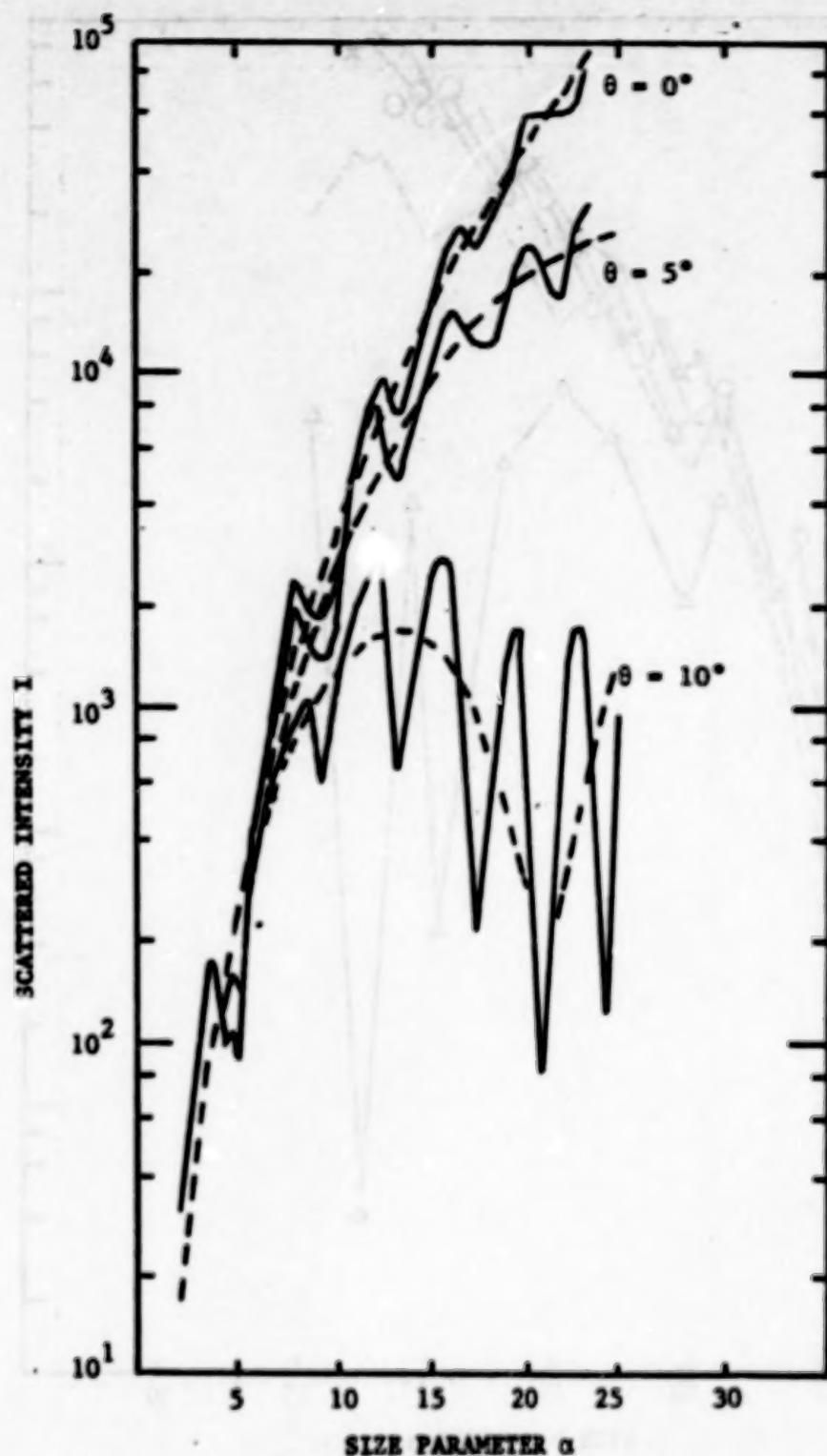
Figure 3. Perpendicularly polarized scattered light intensity as a function of the size parameter α for different refractive indices (———— ñ = 1.75, —————— ñ = 1.75 - 10.29) at angles 0°, 5° and 10°.
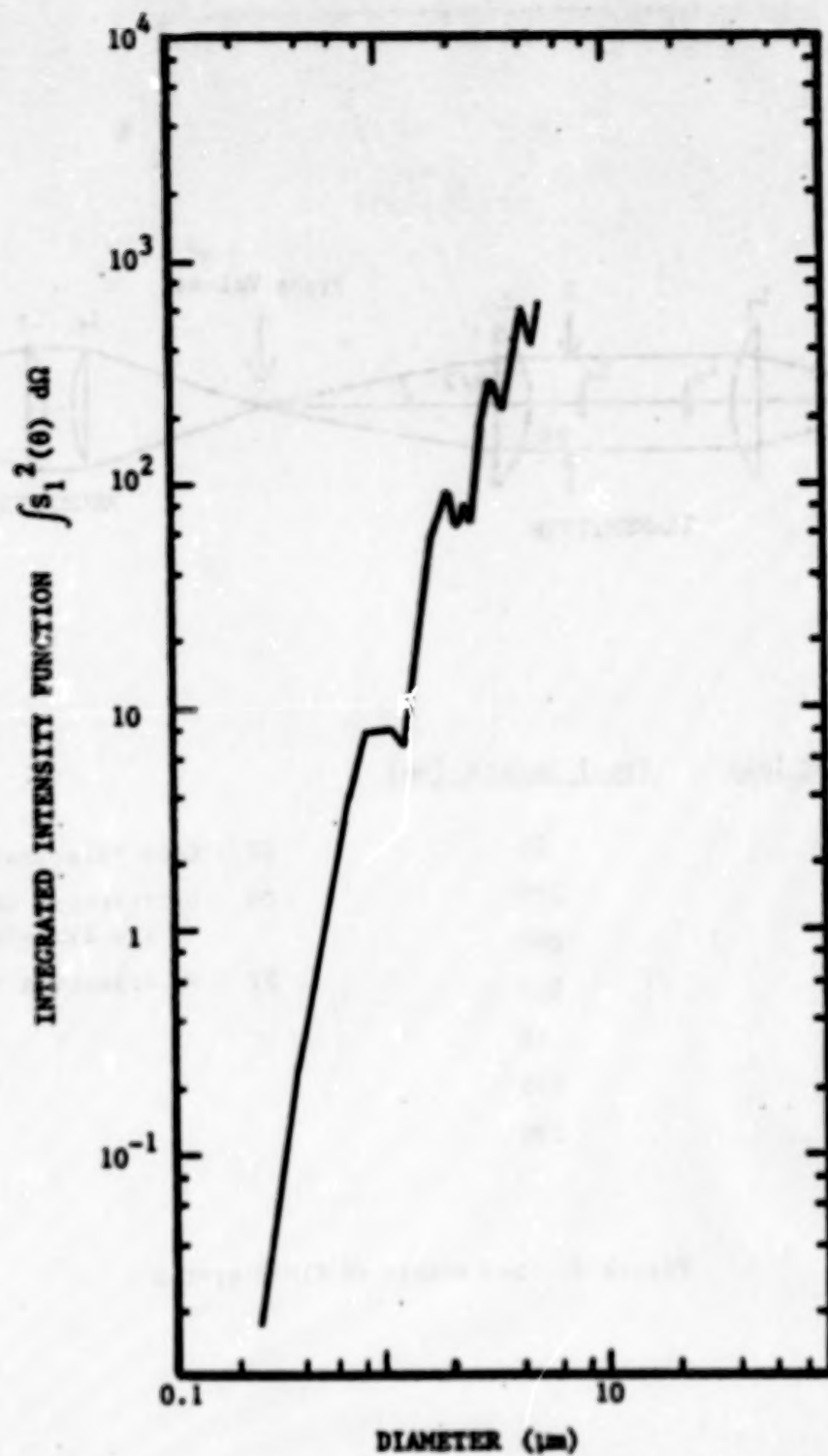
Figure 4. Integrated intensity function for θ = 5°
and F/5 lens for polystyrene microspheres (n = 1.59)
as a function of diameter.
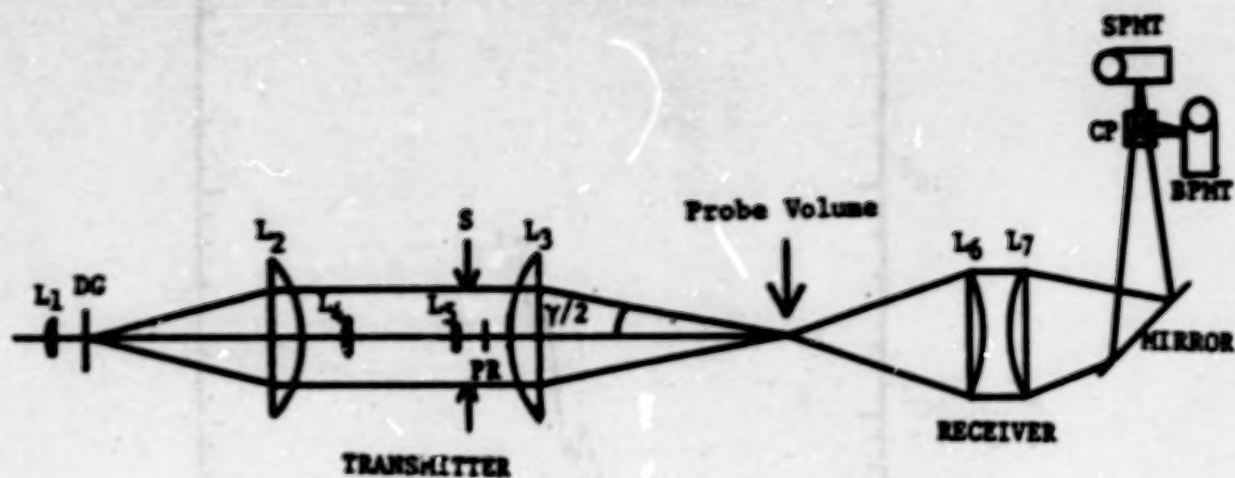
Achromatic Lens	Focal Length (mm)	
L_1	35	CP : Cube Polarizer
L_2	220	DG : Diffraction Grating
L_3	200	100 lines/mm
L_4	112	PR : Polarization Rotator
L_5	16	
L_6	300	
L_7	500	

Figure 5. Schematic of PIMAX system

Figure 6. Photograph of PIMAX transmitter and particle generator.
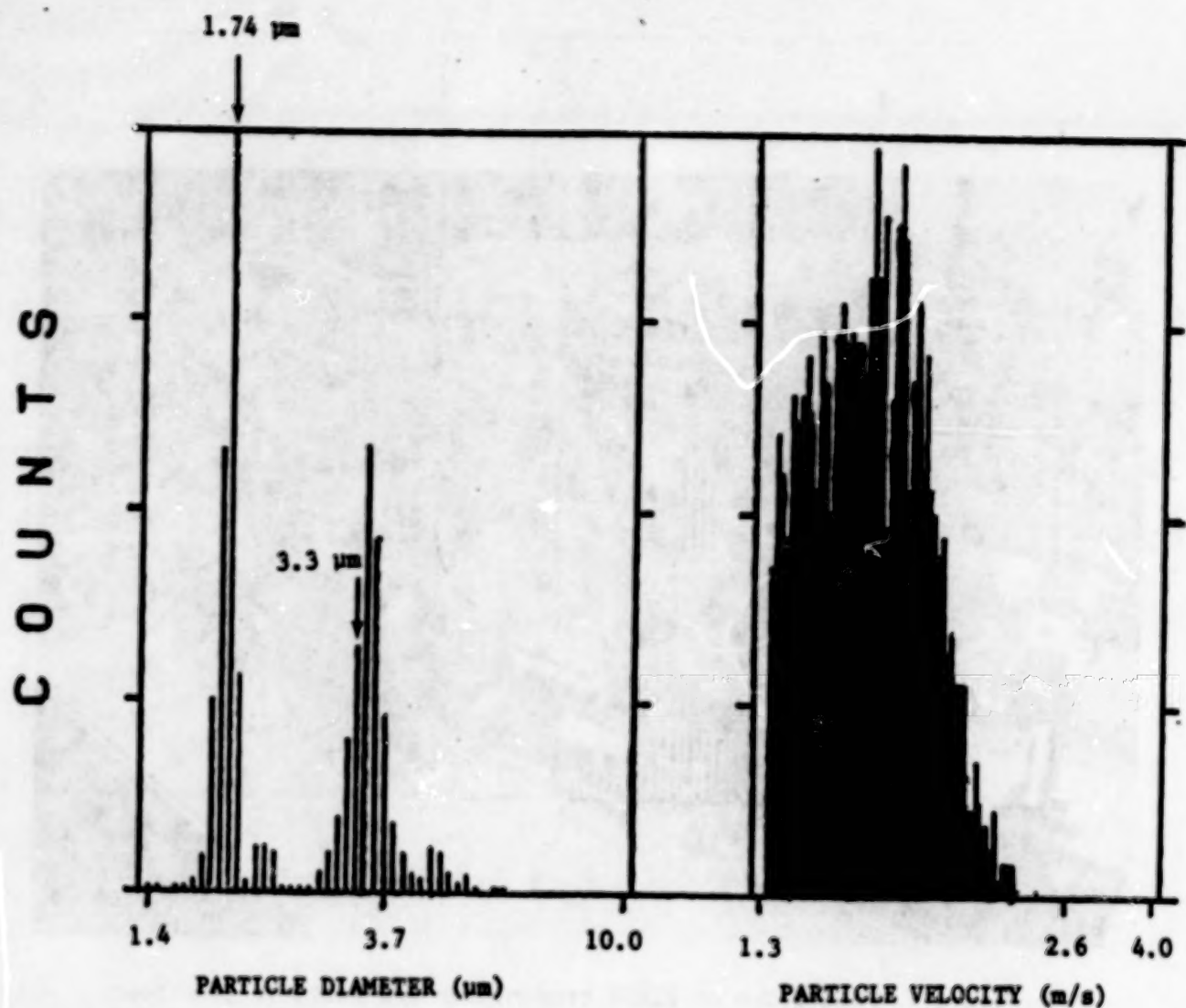
Figure 7a. Size and velocity histogram of 1.74 μm and 3.3 μm polystyrene
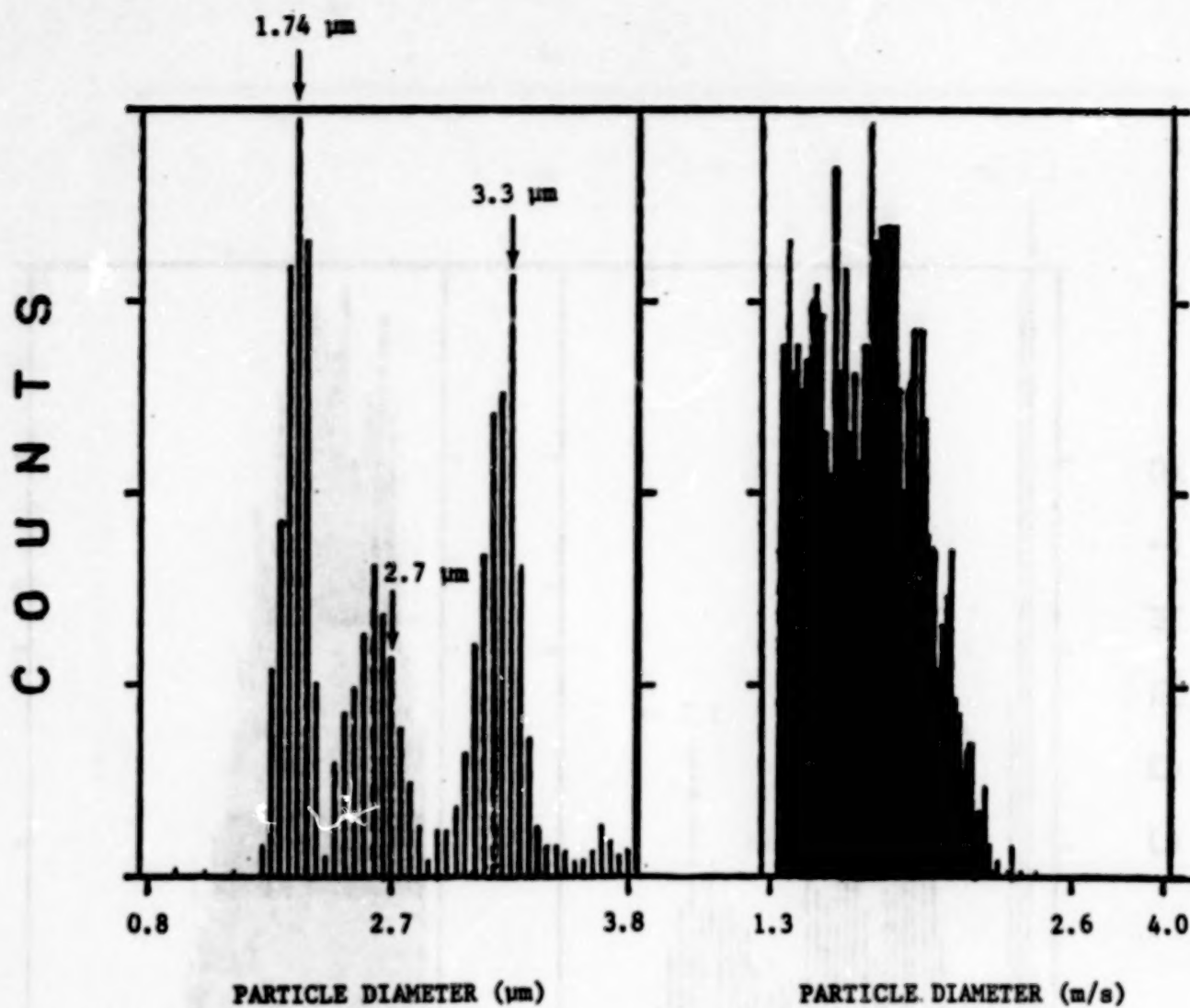spheres in air. Photomultiplier tube high voltage = 500 V.

Figure 7b. Size and velocity histogram of 1.74 μm, 2.7 μm, and 3.3 μm polystyrene spheres in air. Photomultiplier high voltage = 550 V.
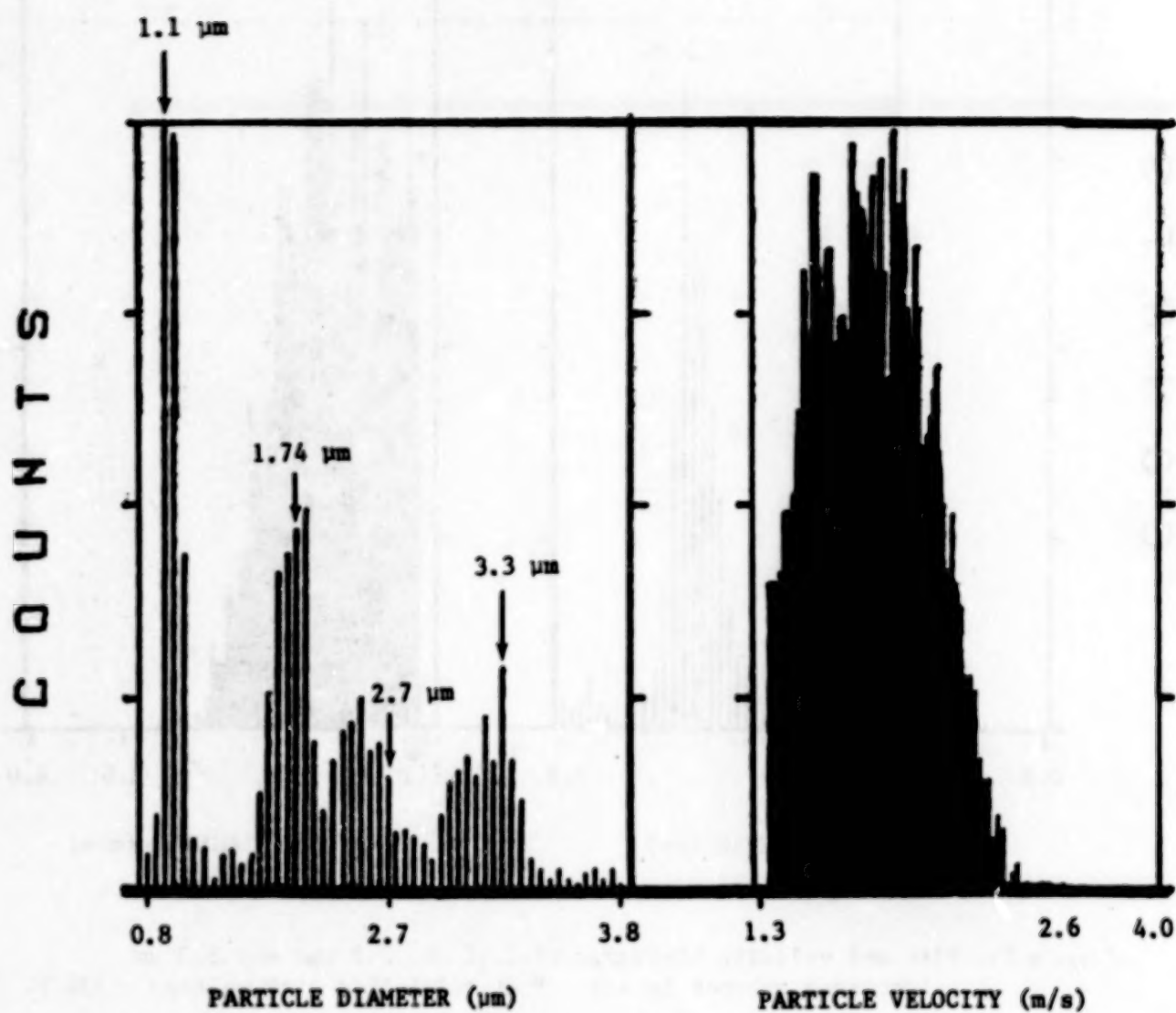
Figure 7c. Size and velocity histogram of 1.1 μm, 1.74 μm, 2.7 μm, and 3.3 μm polystyrene spheres in air. Photomultiplier high voltage = 550 V.
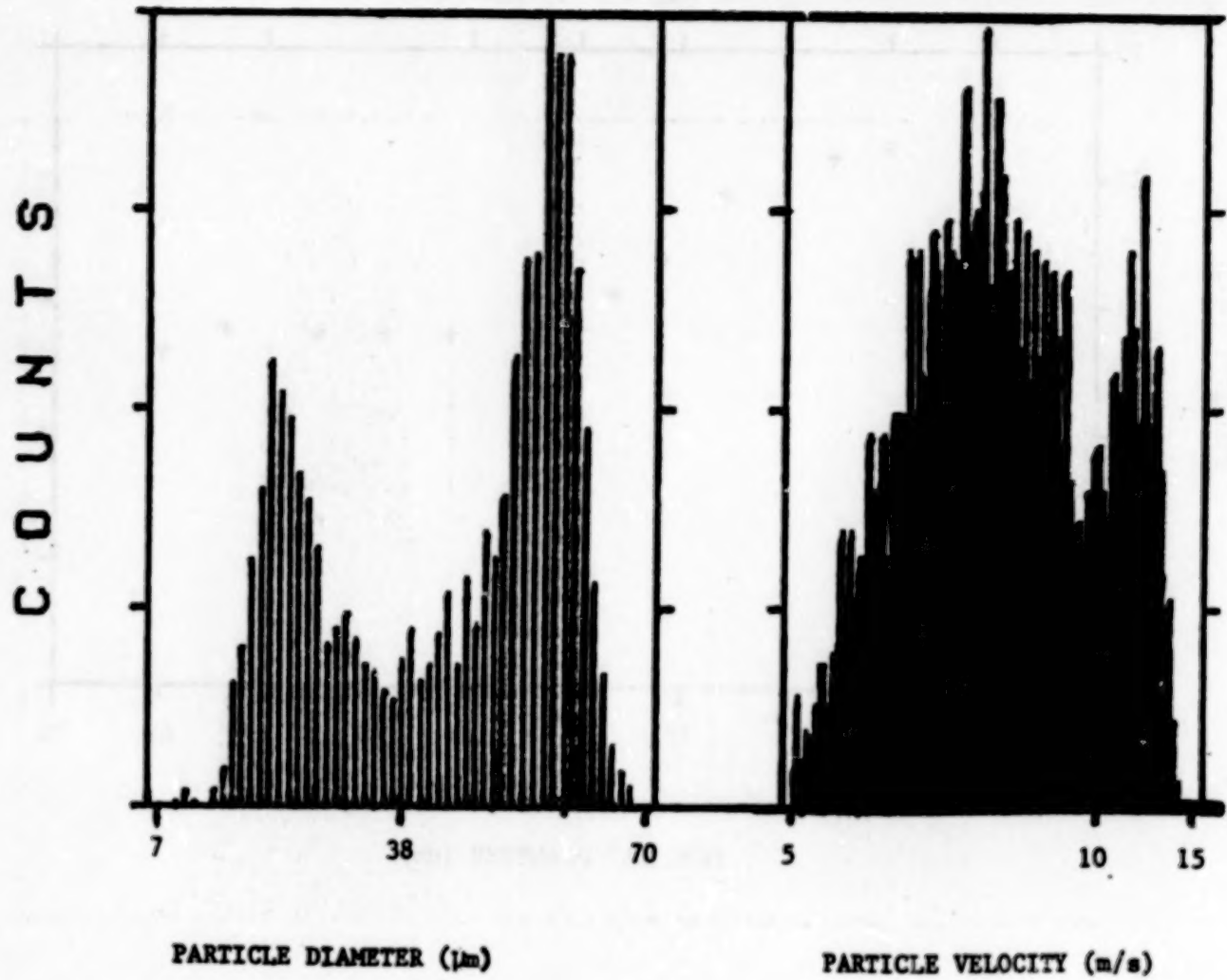
Figure 8. Size and velocity histogram of small and large glass beads
entrained in an air jet.

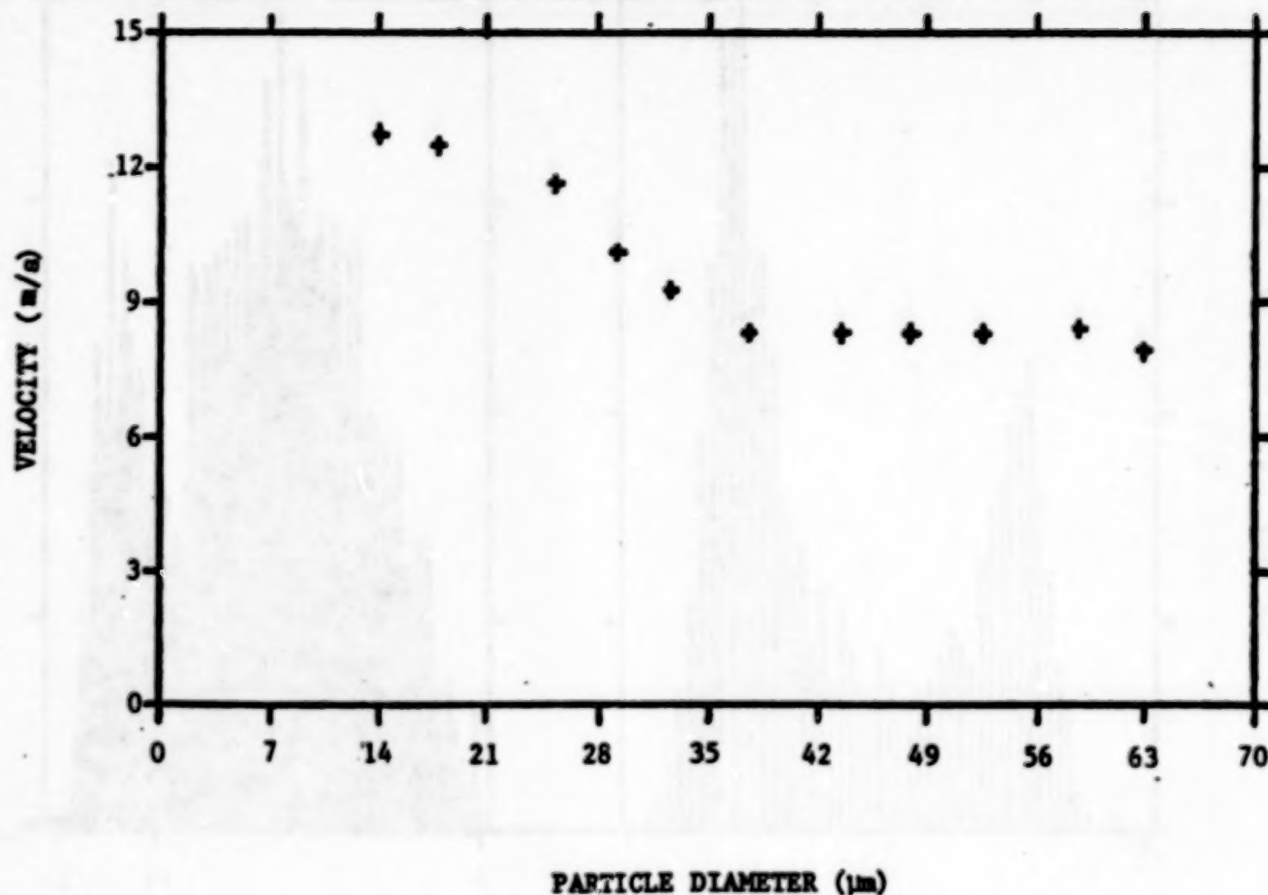Figure 9. Velocity distribution of small and large glass beads entrained in an air jet.

1. Report No.	2. Government Accession No.	3. Recipient's Catalog No.
NASA CP-2393		

4. Title and Subtitle	5. Report Date
WIND TUNNEL SEEDING SYSTEMS FOR LASER VELOCIMETERS	October 1985
	6. Performing Organization Code
	505-31-53-13

7. Author(s)	8. Performing Organization Report No.
William W. Hunter, Jr., and Cecil E. Nichols, Jr., Compilers	L-16013
	10. Work Unit No.

9. Performing Organization Name and Address	
NASA Langley Research Center Hampton, Virginia 23665	11. Contract or Grant No.
	13. Type of Report and Period Covered

12. Sponsoring Agency Name and Address	
National Aeronautics and Space Administration Washington, DC 20546	Conference Publication
	14. Sponsoring Agency Code

15. Supplementary Notes

16. Abstract

This report is a compilation of papers presented at the Workshop on Wind Tunnel Seeding Systems for Laser Velocimeters, held March 19-20, 1985, at the NASA Langley Research Center. Papers presented fundamental particle response to local flow field characteristics, calculations, seed particle generation schemes, and particle characterization techniques. The papers covered a range of wind tunnels including subsonic, transonic, and supersonic.

17. Key Words (Suggested by Author(s))	18. Distribution Statement
Laser velocimetry Wind tunnels Seeding	Unclassified - Unlimited
	Subject category 35

19. Security Classif. (of this report)	20. Security Classif. (of this page)	21. No. of Pages	22. Price
Unclassified	Unclassified	273	A12